(NASA-TM-103510) RESEARCH AND TECHNOLOGY, 1990 Annual Report (NASA) 268 p CSCL 05B
N92-19537
Unclas
G3/99 0075451

RESEARCH AND TECHNOLOGY 1990

The Annual Report of the Marshall Space Flight Center

Research and Technology 1990

ORIGINAL CONTAINS
COLOR ILLUSTRATIONS

Annual Report of the Marshall Space Flight Center

NASA TM – 103510

NASA

National Aeronautics and
Space Administration

George C. Marshall Space Flight Center
Marshall Space Flight Center, Alabama 35812

ORIGINAL PAGE
BLACK AND WHITE PHOTOGRAPH

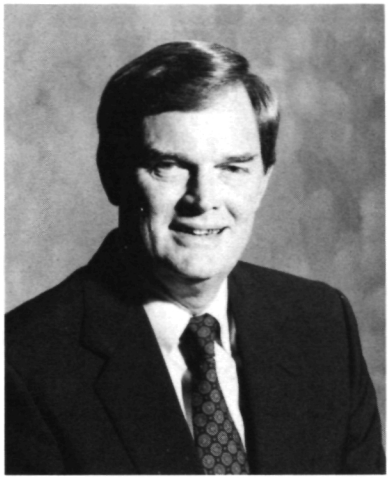

Living The Dream . . .

This is a milestone year for the Marshall Space Flight Center, a year in which we celebrate our 30th Anniversary. During those 30 years, we have seen many early dreams come to reality—men on the Moon, a first space station in progress, worldwide communications by satellite, astronomy from space, global monitoring of the Earth, and many more. The Marshall Space Flight Center is proud to have been a key element in these adventures. Many of our accomplishments would not have been possible without the research conducted, and the technology developed, by our Center over these years.

At Marshall Space Flight Center, where the German rocket team eventually settled, we are especially cognizant of the role played by Dr. Wernher von Braun in our dream of space exploration. In this issue of Research and Technology 1990, we pay a small tribute to Dr. Von Braun in recognizing that his dreams of yesterday are the realities of today. While Dr. Von Braun's technical accomplishments are documented in other publications, we want to share with you some of the thoughts and philosophies upon which his dreams were built.

The dreams are continuing—a permanent space station; low-cost, highly reliable launch and space vehicles; an outpost on the Moon; and finally, the human exploration of Mars. The technologies for these adventures are being developed today. You will find many of these efforts, and more, in this report.

T.J. Lee
Director

Acknowledgements

The point of contact and coordinator at MSFC for this report is P.Y. Potter [ER01/(205) 544-5723]. She was assisted by an editorial committee consisting of S.H. Morgan, G.R. Wallace, G.F. McDonough, C.R. Chappell, and W.C. Snoddy. Detailed editorial support and production assistance was provided by MSI, a Division of The Bionetics Corporation. The work at MSFC is a cooperative effort, but, because of space restrictions, it is impossible to list all those involved in the projects described in this report.

To assist the reader, the MSFC contact, office code, telephone number, and sponsoring agency are included at the end of each article. An alphabetical index of all contacts is presented at the end of this report.

Table of Contents

Key Words ix

***The Dream*, Wernher von Braun** xiv

Advanced Studies

Introduction	C.R. Darwin	1
Transportation Systems		
Advanced Recovery Systems	G.W. Johnson	2
Integrated Earth-To-Orbit Transportation	U. Hueter	5
Space Exploration Initiative	J.P. Sumrall	8
Advanced Launch System	J.T. Watkins	10
Advanced Launch System Propulsion Advanced Development	J.L. Taylor, Jr.	11
Space Transportation Main Engine	H.A. Cikanek	14
Space Systems		
Gravity Probe-B	R. Ise	16
Gamma-Ray Imaging Telescope	M.E. Nein	17
Space Station Advanced Programs	J.M. Butler	20
Geostationary Earth Observatory Program	J.M. Butler	21
Controls, Astrophysics, and Structures Experiment in Space	J.R. Dabbs	23
Pinhole Occulter Facility	J.R. Dabbs	23
Electral Power System Fault Study	N.R. Dugal-Whitehead	24
Tether Applications in Space	J.K. Harrison	26
Tumbling Satellite Retrieval	J.R. Turner	27
Long Duration Exposure Facility Dose Predictions and Measurement	J.W. Watts	28
Future Lunar Science Missions	C.L. Johnson	30
Aeroassisted Orbital Transfers	A.W. Deaton	31
Superconducting Gravity Gradiometer	C.L. Johnson	32
Data Systems		
The TOPO Plot: A Data Reduction/Graphics Routine for Tracking Spectral Trends in Vibration Data	J.E. McBride	34
WetNet: An Interdisciplinary Information and Research Data System	H.M. Goodman	37
Interannual Variations of Thunderstorms and Lightning Activity at Global and Regional Scales	S.J. Goodman	38
Computer Accessibility for the Visually Impaired	G. Higgins	41
Compiling Knowlege Bases	G. Higgins	42
Four-Dimensional Man-Computer Interactive Data Access System Technology	P.J. Meyer	43

Research Programs

Introduction	E.A. Tandberg-Hanssen	45
Microgravity Science		
Introduction		46
Optimization of Measurement to Determine Crystal Strain State	L. Kiefling	46
Microgravity Activities	J.F. Stone	47
Model Immiscible Systems	D.O. Frazier	51
Advanced Technology Materials	M. Vlasse	52
Solution Crystal Growth	R.L. Kroes	54
Protein Crystal Growth	D.C. Carter	55
Astronomy and Astrophysics		
Introduction		57
Gamma-Ray Burst Studies	G.J. Fishman	57
Induced Radioactivity Analysis of the Long Duration Exposure Facility	G.J. Fishman	59
Superconducting Magnetic Suspension Systems and Bearings	P. Peters	61
X-Ray Astronomy Research	M.C. Weisskopf	62
Expert System Reasoning	W.J. Selig	64
Infrared Astronomy and Cometary Research	C.M. Telesco	65
Solar Physics		
Introduction		66
Electron Irradiation of GaAs Solar Cells	D.L. Edwards	67
Coronal and Interplanetary Physics	S.T. Suess	69
Solar Magnetic Fields	M.J. Hagyard	70
Magnetospheric Physics		
Introduction		72
Neutral Environment With Plasma Interactions Monitoring System	W.T. Roberts	73
Plasma Waves and Ion Heating at the Earth's Magnetic Equator	D.L. Gallagher	74
Superthermal Ion Composition Spectrometer Double-Focusing Electrostatic Analyzer	V.N. Coffey	76
The Statistical Behavior of Hydrogen Ion Temperatures From Dynamics Explorer 1/Retarding Ion Mass Spectrometer	P.D. Carven	77
Imaging of Magnetospheric Energy in the Vacuum Ultraviolet	M.R. Torr	79
Interplanetary Magnetic Field Influences on the Polar Wind	M.O. Chandler	81
Atomic Physics and Aeronomy		
Introduction		83
Development of a Microchannel Plate-Based Low-Energy Electron Spectrometer	C.J. Pollock	83
Infrared Spectroscopy of the Stratosphere	M.M. Abbas	85

Earth Science and Applications

Introduction		88
Intelligent Protection System for Space Power Applications	N.R. Dugal-Whitehead	88
Trace Atmospheric Carbon Monoxide Sensor	A. Hafner	90
Habitable Atmosphere Contaminant Monitoring	A. Hafner	90
The Geophysical Fluid Flow Cell	F.W. Leslie	91
Thermosphere Model Verification Studies With the Long Duration Exposure Facility	R.J. Suggs	92
Revised Gust Model for Space Vehicle Performance Assessments	S. Smith	93
Mars-Global Reference Atmosphere Model	B.F. James	94
Aerosol Physicochemistry and Backscatter Modeling	J. Rothermel	96
Global Backscatter Experiment	J. Rothermel	97
Aerosol Optical Properties Laboratory	J. Rothermel	98
Atmospheric Electricity Research	R.J. Blakeslee	99
Lightning Simulator and Sensor Calibration	M.W. James	100
Quick View System for Aircraft Data	M.W. James	102
MSFC Shuttle Lightning Research	O.H. Vaughan	103
Lightning/Rainfall Relationships	R.J. Blakeslee	104
Global Atmospheric Temperature Monitoring From Satellites	R.W. Spencer	105
The Advanced Microwave Precipitation Radiometer	R.W. Spencer	107
The High-Resolution Microwave Spectrometer Sounder	R.W. Spencer	108
Doppler Radar Wind Profiler	C. Carlson-Lapenta	109
Space Applications of Sensor Development	M.W. James	110
Organization of Cloud and Precipitation Patterns Within Extratropical Baroclinic Waves	F.R. Robertson	111
Atmospheric Laboratory for Applications and Science	T.L. Miller	113
Numerical Modeling of Nonlinear Baroclinic Fluid Systems	T.L. Miller	115
Remote Sensing Perspectives on the Global Hydrologic Cycle	F.R. Robertson	117
Global Atmospheric Modeling	F.R. Robertson	119
Aircraft Data Evaluation Workstation Development	G.J. Jedlovec	120
Geophysical Parameter Retrieval From Multispectral Aircraft Measurements for Geostationary Earth Observatory Science Applications	G.J. Jedlovec	122
Satellite Sensor Simulations	G.J. Jedlovec	123
Investigations of Atmospheric Moisture Variability	G.J. Jedlovec	124
Imaging of the Atomization Process	K.W. Gross	125

Technology Programs

Introduction	G.R. Wallace	129
Propulsion		
Computational Fluid Dynamics Flow Analysis of the Bearing, Seals, and Material Tester	G.A. Wilhold	130
Computational Fluid Dynamics Methodology for Fast Transients	G.A. Wilhold	132
Velocimetry With Refractive Index Matching	J.P. Heaman	133
Combustion Chamber Analysis Code	G.A. Wilhold	134
Cold Flow Aerodynamic Turbine Testing	W.J. Bordelon, Jr.	135
Adaptive High Order *h-p* Finite Element Method for Complex 3-D Flows	P.K. McConnaughey	137
Verification of Internal Flow Analysis in 3-D Geometries	G.A. Wilhold	138
Development of Unsteady Aero/Heat Transfer Experimental Data Base for Axial Turbines	G.A. Wilhold	139
Three-Dimensional Turbopump Flowfield Analysis	G.A. Wilhold	142
Turbine Stage Computational Fluid Dynamics Analysis and Data Base for Unsteady Aero/Heat Transfer	G.A. Wilhold	144
Plume Temperature Measurements	R.H. Eskridge	146
Injector Diagnostics Development	R.H. Eskridge	147
Completion of Forbidden Orbit Transfer Study	R. Burns	149
Space Shuttle Main Engine Preburner Temperature Profiler	W.T. Powers	149
Space Shuttle Main Engine Exit Diagnostics	W.T. Powers	152
Vortex-Shedding Flowmeter for Space Shuttle Main Engine	W.T. Powers	153
Space Shuttle Main Engine Propellant Path Leak Detection, Real Time	M.L. Johnson	155
Optical Leak Detection for Ground-Based Operations	M.L. Johnson	156
In-Flight Optical Leak Detection	M.L. Johnson	157
Solid Rocket Motor Propellant and Polymer Materials Structural Test Program	V. Richard	159
Analysis of Static and Dynamic Nonlinear Viscoelastic Response	V. Richard	160
Formed Platelet Combustor Liner Construction Feasibility	F. Braam	161
Turbine Blad-Tip Seal Force Interaction—"Alford" Forces	G.E. Wilmer	163
Bipropellant Two-Phase Flow Simulation in a Rocket Thrust Chamber	K.W. Gross	165
Propellant Atomization Simulation of Coaxial and Impinging Injection Elements	K.W. Gross	168
Materials and Processes		
Weld Process Modeling	A.C. Nunes	170
Feasibility of Atomic Oxygen Interactions Accelerated Testing	R. Carruth	171
Long Duration Exposure Facility Experiments and Orbital Materials Interaction Studies	A. Whitaker	172
In Situ Contamination Effects Study	R. Linton	173
Atomic Oxygen Ion Beam Neutralizer	J.M. Reynolds	174
Advanced Low Earth Orbit Atomic Oxygen Simulation System	J.A. Vaughn	175

Portable Spectroreflectometer	J.K. Norwood	177
Optically Stimulated Electron Emission for Bonding Surface Cleanliness Inspection	H.D. Burns	178
Impact Damage Tolerance of Composite Laminates	A. Nettles	179
Development of Low Thermal Conductivity PAN-Based Carbon Fibers for Solid Rocket Motor Nozzle Applications	R.G. Clinton	181
Alternate Ablative Material Development for Solid Rocket Motor Nozzle Applications	R.G. Clinton	183
Diamond Film Production Using an Oxyacetylene Torch	F. Roberts	185
Industry Advisory Committee Established for Carbon Phenolic Constituent Test Methodology and Specifications	L.A. Fikes	187
Prepreg Properties and Process Relationships to Microstructure in Carbon-Phenolic Laminates	R.G. Clinton	188
Mechanical Property Testing of Tag Ends	S.W. Tillery	189
High Heat-Flux Testing Using the Plasma Torch Test Bed	T. Lawrence	191
The Temperature Variation of Hydrogen Diffusion Coefficients	M.D. Danford	192

Structures and Dynamics

Adaptive Computational Methods for High Reynolds Number Internal Flows	P.K. McConnaughey	194
An Algorithm for Periodic Waveform Recovery from Space Shuttle Main Engine Vibration Measurements	J.E. McBride	196
Deployable Aerobrake Structural Development	M.L. Tinker	199
Novel Composites for Protection Against Orbital Debris	J.R. Horn	201
Slit Digital Radiography for Analysis of Bondline Defects in Solid Rocket Motors	M.W. Suits	201
An Analytical Formulation for a Design Technology for Multiphase Structures	R.M. Sullivan	202
Generalized Failure Criteria for 2-D Carbon-Carbon	R.M. Sullivan	203
Thermal Degradation Tests of Damaged Multilayer Insulation From Hypervelocity Impacts	P.E. Thompson	204
Probabilistic Model for Fracture Mechanics Service Life Analysis	R. Stallworth	205

Automated Systems

WELDSMART: A Vision-Based Weld Quality Assurance System	K. Fernandez	207
Development of ROBOSIM for Academic/Industrial Use	K. Fernandez	209
Robotic Eddy Current Inspection System	C.C. Bryson	210
Artificial Intelligence as Applied to Flight Mechanics	R. Burns	211
Fully Automated Variable Polarity Plasma Arc Welding	K. Lawless	212
Autonomous Rendezvous and Docking	R. Howard	213
Advanced Telerobotic Concepts Using Neural Networks	R.R. Kissel	215
A Perception System for Object Recognition, Acquisition, and Tracking in Cluttered Environments	R.R. Kissel	216
Active Detection and Tracking Sensor for Passive Targets	R. Howard	217
The Environmental Control and Life Support System Advanced Automation Project	B.S. Dewberry	218

Space Systems

Welding in Space	C. Kurgan	220
CO_2 Laser Research and Development	J.W. Bilbro	221
Coherent Doppler Lidar Research and Development	J.W. Bilbro	222
Advanced X-Ray Astrophysics Facility's Technology Mirror Assembly	J.W. Bilbro	223
Expendable Lightweight Composite Intertank	D.B. Ford	225
Pathfinder Mechanical Joints for In-Space Assembly and Construction	F.P. Thomas	226
Space Station Low-Temperature Portable Cooler for Biological Samples	C. Horan	228
Assessment of Materials in Solid Rocket Motors by Near Real-Time Computed Technology	M.W. Suits	229
Space Station Module Power Management and Distribution	L.F. Lollar	230

Avionics

Nickel-Cadmium Battery Expert System-2	Y.B. Johnson	232
Optical Plume Anomaly Detector	W.T. Powers	234
Nonintrusive Flowmeters for Rocket Engines	W.T. Powers	235
Nonintrusive Hot Gas Temperature Sensor	W.T. Powers	237

Index of Key Words

"Alford" Force(s) 163, 164
2-D Carbon-Carbon 203
Ablative Materials 181, 182, 183, 184
Abstract Time Slice (ATS) 64
Accelerometer 32, 33
Acquired Immune Deficiency Syndrome (AIDS) 55
Across-Ply Tensile (APT) 189, 190
Active Cavity Radiometer (ACR) 114
ADA 42
Adaptive Grids 194
Advanced Atomic Oxygen Simulation System (AAOSS) 175, 176, 177
Advanced Development 20
Advanced Launch System (ALS) 6, 10, 14, 15, 147
Advanced Very High Resolution Radiometer (AVHRR) 124
Advanced X-Ray Astrophysics Facility (AXAF) 223
Aeroassist 31
Aerobrake 226
Aerosol Optical Properties Laboratory (AOPL) 98
Aerosols 96, 97, 98
Anisotropic 202
Artificial Gravity 27
Artificial Intelligence (AI) 42, 211
Atmosphere Trace Molecules Observed by Spectroscopy (ATMOS) 86
Atmospheric Laboratory for Applications and Science (ATLAS) 113, 114, 115
Atomic Oxygen 171, 172, 173, 174, 175, 176, 177
Atomic Oxygen Simulation (AOSS) 174
Atomization 125
Auroral Oval 79, 80
Automated 88, 89, 212, 213
Autonomous Rendezvous and Docking (AR&D) 213
Autonomously Managed Power Systems (AMPS) 24
Backscatter 96, 97, 222
Battery (ies) 232, 233
Biaxial Propellant Testing 160
Bit Pattern 217
Block Grids 195
Bondline Defects 201
Braille 41
Burst and Transient Source Experiment (BATSE) 57, 58, 59
Bursts 57, 58, 59
C-Language Production System (CLIPS) 64
Carbon Fiber(s) 179, 181, 182
Carbon Monoxide (CO) Sensor 90
Carbon Phenolic 183, 187, 188
Carbon-Phenolic Composite 187
Cellular Structure 125
Charring and Erosion 202
Chemical Release and Radiation Effects Satellite (CRRES) 85
Coaxial or Impinging Injection 168
Coherent Doppler Lidars 222
Combustion 134
Community Climate Model (CCM1) 119, 120
Composite 225
Composite Materials 180
Computational Fluid Dynamics (CFD) 13, 132, 141, 142, 144, 165, 167
Computed Tomography (CT) 229
Computer Vision 207
Computing 102
Contamination 173
Control 209
Controller 212, 213
Controls Structures Interaction 23
Convection 91, 92, 119, 120
Convective Storms 104
Cooler 228
Cooling Liner(s) 161
Crack(s) 205, 206
Cryogenic Infrared Spectrometers and Telescopes for the Atmosphere (CRISTA) 114
Crystal(s) 46, 47, 48, 54, 55
Crystal Growth Furnace (CGF) 48
Crystal Growth Solutions 54
Crystallographic Axis 46
Crystallography 56
Damage 225
Data Analysis 102
Data Base 141
Decentralized Controller 215
Deployable Aerobrake 199, 200
Detection 217

Diagnostics 152
Diamond 185
Directional Solidification 51, 52
Doppler Radar 109
Double-Notch Shear (DNS) 189, 190
Droplet(s) 125, 165, 166
Earth Observing System (EOS) 39, 100, 108
Earth Science 37
Electron Irradiation 67
Electrons 83, 84, 85
Electrostatic Analyzer 76
Electrostatic Angle Analyzer 76
Electrostatic Deflection Analyzers 76
Energy Analyzer 76
Engineering Analysis and Data System 124
Environment 73
Environmental Control and Life Support System (ECLSS) 20, 21, 218, 219
Ethanol 51
Experiment for Rapidly Intensifying Cyclones Over the Atlantic (ERICA) 111
Expert System 64, 207, 232
External Tank (ET) 17, 18, 19
Failure Criteria 203
Fast Atmospheric Signature Code (FASCOD) 124
Fiber-Optic Raman Thermometer (FORT) 150, 151
Films 51, 52, 185, 186
Finite Element Code 137
Flares 70, 71
Flight Mechanics 211
Flow(s) 130, 133, 153, 154, 155
Flowmeter 154, 235, 236
Flux 61
Gallium Arsenide (GaAs) 67
Gamma-Ray 57, 58, 59
Gamma-Ray Bursts (GRO) 57, 58, 59
Gamma-Ray Imaging Telescope (GRIT) 17, 19
Gas Chromatograph with Mass Spectrometer (CG/MS) 90
Gas Tungsten Arc Welding (GTAW) 220, 221
Geophysical Fluid Flow Cell (GFFC) 91, 92
Geophysical Fluid Flow Simulation (GEOSIM) 116, 117
Geophysical Parameters 122
Geostationary Earth Observatory (GEO) 122
Geostationary Earth Observatory Program 21, 22
Geosynchronous Operational Environment Satellite 99
Global Backscatter Experiment (GLOBE) 96, 97, 98, 222, 223
Globally Averaged 106
Gradiometer 32, 33
Graphics 209
Gravity 32, 91
Gust 93
Gyroscopes 16
H-P Adaptive 137
Hand-Held 177, 178
Heliopause 69
Heliotail 69
High Heat-Flux 191
High T_c Superconductors (HTSC) 52, 53
High-Resolution Microwave Spectrometer Sounder (HIMSS) 108
Hot Gas 237, 238
Human Immunodeficiency Virus Type I (HIV-I) 55
Hybrid Mosaic on Stacked Silicon (HYMOSS) 110
Hydrogen Diffusion 192
Hydrologic Cycle 37, 117
Hyperbaroclinic Zones 111
Hypercoherence Filter 197, 198
Hypercoherence Function 196
Hypervelocity Impact 201, 204
Impact Testing 179
Impulsive Transfer 149
Incompressible Flow 137
Induced Radioactivity 60
Infrared (IR) Astronomy 65
Infrared (IR) Detector System 146
Infrared 90
Infrared Space Observatory Spectra Photometer (ISOPHOT) 65
Infrared Spectroscopy 85
Infrared Telescope Facility (IRTF) 65
Injectors 134
Instruments 84
Interactive Hydrology 119, 120
Interfaces 41
Internal Flow 138
Interplanetary Space 81
Intertank 225
Ion Beam 171, 172, 174
Ion Temperature 77
Ionosphere 83, 85
Ions 74, 75
Isotropic 202

Keplerian Orbits 149
Knowledge Bases 42
Knowledge Engineering Environment (KEE) 42
Knowledge-Based Management System (KBMS) 231
L-Arginine Phosphate (LAP) Crystals 52
Large Autonomous Spacecraft Electrical Power System (LASEPS) 24
Large Lunar Telescope (LLT) 30
Laser 149, 156, 221, 222
Laser Atmospheric Wind Sounder (LAWS) 97, 221, 222
Laser Doppler Velocimeter (LDV) 133
Launch Systems Evaluation Advisory Team (LSEAT) 109
Leak 155
Leak Test 156
Lidar 98
Lightning 38, 99, 103, 104, 105
Lightning Imaging Sensor (LIS) 100
Lightning Mapper Sensor (LMS) 100
Limited Area Mesoscale Prediction System (LAMPS) 111, 116, 117, 118
Limited Capability System (LCS) 109
Local Interstellar Medium (LISM) 69
Long-Duration Exposure Facility (LDEF) 28, 29, 59, 60, 92, 93, 172
Low Earth Orbit (LEO) 171, 175, 177
Low Gravity 47, 49
Lowest Level Processor (LLP) 230
LOX/LH_2 Engine 11
Magnetic Bearings 61, 62
Magnetic Equator 74, 75
Magnetic Fields 28, 29, 70, 71
Magnetopause 30, 31
Magnetosphere 77, 79, 80, 81, 82
Man-Computer Interactive Data Access (McIDAS) 43
Mars 8, 9, 94, 95
Mars Global Reference Atmosphere Model (Mars-GRAM) 94, 95
Marshall Engineering Thermosphere (MET) Model 92
Mass Spectrometer and Incoherent Scatter (MSIS) Model 92
Mechanical Joint 226
Mechanical Property Tests 189
Mesoscale Lightning Experiment (MLE) 103, 110
Microgravity 54
Microstructure 188, 189
Microwave 37, 107
Microwave Sounding Unit (MSU) 105, 106
Millimeter-Wave Atmospheric Sounder (MAS) 113, 114
Mirror(s) 223, 224
Moisture 124
Molecular Contamination 173
Moon 8, 9
Multilayer Insulation (MLI) 204
Multispectral Atmospheric Mapping Sensor (MAMS) 120, 121, 122, 123, 124
Network 37
Neural Network 215, 216
Nondestructive Evaluation 189
Nonintrusive 235, 236, 237, 238
Nonlinear (Large Deformation) 160, 161
Nonlinear Analysis Codes 159
Nonlinear Optical (NLO) 52
Nozzle Assemblies 229
Nozzle(s) 181, 182, 183
Nucleation 54, 55
Observatory 21
Optical Plume Anomaly Detector (OPAD) 234, 235
Optically Stimulated Electron Emission (OSEE) 178
Optimal Trajectories 31
Orbital Debris 201
Ozone 85, 86
Parafoil 3, 4
Particles 28
Path Plan 209
Perception 216
Performance 135
Peroxyacetylnitrate (PAN) 181, 182, 183
Personnel Launch System (PLS) 7
Photomultiplier Tube (PMT) 158, 159
Piezoelectric 235, 236, 237
Plasma 73, 74, 75, 81, 175
Plasma Arc 170
Plasma Heating 83
Plasma Torch 191, 192
Plasma Torch Test Bed (PTTB) 191, 192
Plasmasphere 77, 78
Platelet Fabrication 162
Plume 234
Plume Temperature 147
Polarimetry 63

Polychromator 234, 235
Portable 228
Potable Water 218
Potable Water Processing Assembly (PWPA) 218
Power 88
Power Spectral Density (PSD) 34, 36
Preburners 149, 151
Prepreg 187, 188, 191
Propellant 155
Propellant Atomization 168
Propellant Grain 159
Propulsion/Avionics Module (P/A Module) 2, 3
Protection 88
Pulsed Laser 158
Pyrometer 47
Q-Switch 158
Quick-View System (QVS) 120, 121
Radiometer 107, 108
Rain 107
Rainfall 38, 39, 104, 105
Raman Scattering 152
Raman Spectroscopy 148
Recovery 2
Relativity 16
Remote Manipulator System (RMS) 177, 178
Retrieving 27
Robot Compatible 226
Robotic Eddy Current Inspection 210
Robotics 209
Rotating Cavities 130
Satellite Sensors 123
Satellites 105
Secondary Flow 142
Sensor(s) 212, 213, 214
Shuttle 103
Shuttle Solar Backscatter Ultraviolet (SSBUV) 114
Shuttle-Derived Vehicle (SDV) 5, 6
Signature 34
Simulation 209
Slit Digital Radiography 201, 202
Small Expendable Deployer System (SEDS) 26
Solar Cells 67, 68
Solar Constant (SOLCON) 114
Solar Spectrum (SOLSPEC) 114
Solar Ultraviolet Spectral Irradiance Monitor (SUSIM) 114
Solid Propulsion 11, 13
Solid Rocket Motor (SRM) 183, 201, 202, 203, 229
Solid Rocket Motor (SRM) Nozzles 187
Space Exploration Initiative (SEI) 8, 9
Space Shuttle Probabalistic Optimization Code (SSPOC) 205, 206
Space Station 20, 73, 228
Space Station Freedom 228
Space Station Module Power Management and Distribution (SSM/PMAD) 24, 230, 231
Space Transportation Main Engine (STME) 14, 15
Spacecraft 27
Special Sensor Microwave/Imager (SSM/I) 37, 111, 112, 119
Spectral Elements 137, 138
Spectrometer 110, 234
Spectroreflectometer 177, 178
Split Window Variance Ratio (SWVR) 124, 125
Spray (s) 134
Stellar X-Ray Polarimeter (SXRP) 63
Storage 228
Storm 99
Stratosphere 85, 86, 87
Sun 70
Superconducting Gravity Gradiometer (SGG) 32
Superconductor 61, 62
Systems Studies 20
Tag Ends 189, 190
Tailorable Advanced Blanket Insulation (TABI) 199, 200
Tandem Mass Spectrometer (MS/MS) 90
Tangential Impulse 149
Telerobotic (s) 215
Temperature 105, 106
Temperature Variation of the Diffusion Coefficients 192
Tether Applications Atmospheric Research 27
Tethers 26
Thermochemical Decomposition 202
Thermopile Detector 238, 239
Thermosetting Polymer Matrix Composites 202
Timelag Method 192
Tolerance 225
TOPO (Topographic Plot) 35, 36
Tracker 216
Tracking 217
Transfer Orbit 149
Transient Analysis 133
Tumbling 27
Tumbling Satellite Retrieval (TSR) 27

Turbine Blade 163, 164
Turbine(s) 135, 136, 139, 141, 142, 144, 145
Turbopumps 163
Turbulence 93
Two-Phase 165
Ultralow Temperature 17
Ultraviolet (UV) 178
Ultraviolet Imager (UV1) 79
Unsteady 139, 141, 145
Vacuum 220
Variable Polarity Plasma Arc (VPPA) 170, 171
Variable Thrust Engine (VTE) 165, 166
Vector Magnetograph 70, 71
Vibration 34
Viking 94, 95
Visible-Infrared Spin Scan Radiometer
(VISRR) Atmospheric Sounder (VAS) 124, 125
Visually Impaired 41
Voice Synthesis 41
Vortex Shedding 153, 154
Weld Inspection 207
Welding 170, 171, 220
X Ray 223, 229
X-Ray Astronomy 62, 63
X-Ray Imaging 23

ORIGINAL PAGE
BLACK AND WHITE PHOTOGRAPH
©

The Dream . . .

Wernher von Braun

Born
March 23, 1912, in Wirsitz, Germany; son of Baron Magnus and Emmy von Braun

Family
Wife Maris Louise von Quistrop; children Iris Careen, Margrit Cecile, and Peter Constantine.

Education
B.S. in mechanical engineering, Berlin Institute of Technology, 1932; Ph.D. in physics, University of Berlin, 1934.

Early Career
While pursuing his undergraduate degree, assisted in Dr. Hermann Oberth's early liquid-fuel rocket experiments. Accepted research grant from the German Ordnance Department in 1932 to develop liquid-fuel rocket engines. Began full-time work as a rocket development engineer for the Ordnance Department after completing his doctorate.

Named army technical director of the Rocket Center at Peenemünde, Germany, in 1937.

Over the next 8 years, led the team which developed the A-5 rocket, the V-2 ballistic missile, and the Wasserfall antiaircraft guided missile.

In 1945, brought the majority of the Peenemünde rocket specialists out of east Germany to establish contact with the Western Allies.

Von Braun Chooses America

Excerpt from speech prepared for: Alabama Legislature
Date: June 20, 1961

"As you may recall, some of my former German colleagues and I came to Alabama from Fort Bliss, Texas, some 10 or 11 years ago, and 6 years ago this past spring, we were awarded our American citizenship."

Von Braun's Team at Fort Bliss Before Moving to Huntsville, Alabama

Excerpt from speech prepared for: Memphis Executive Club
Date: January 12, 1960

"I suppose that most of our people know today—as we of the South have known for several years—that there is an Army installation called Redstone Arsenal in northern Alabama. That is the place where the Army centered its rocket development programs beginning in 1950. Here, a unique collection of people and facilities has been assembled to conduct any long-range missile or space project. I say 'unique' advisedly. There is nothing quite like it anywhere in the Free World. Here, at one place, under one roof so to speak, are the people, the equipment, and the know-how with which to create things the like of which never before existed."

Excerpt from speech prepared for: Memphis Executive Club
Date: January 12, 1960

"In a few weeks, my team will be largely relieved of the responsibility for weapons development. Late in October, the President decided, in view of earlier decisions related to service roles and missions, that the development organization at Redstone Arsenal should be transferred from the Army's management to the National Aeronautics and Space Administration. NASA, as we call it, was created in 1958 to carry forward the country's space exploration program. The intent was to separate, not to divorce, the military from the scientific effort to learn more about and eventually to master the environment beyond the sensible atmosphere."

MSFC Ground Breaking

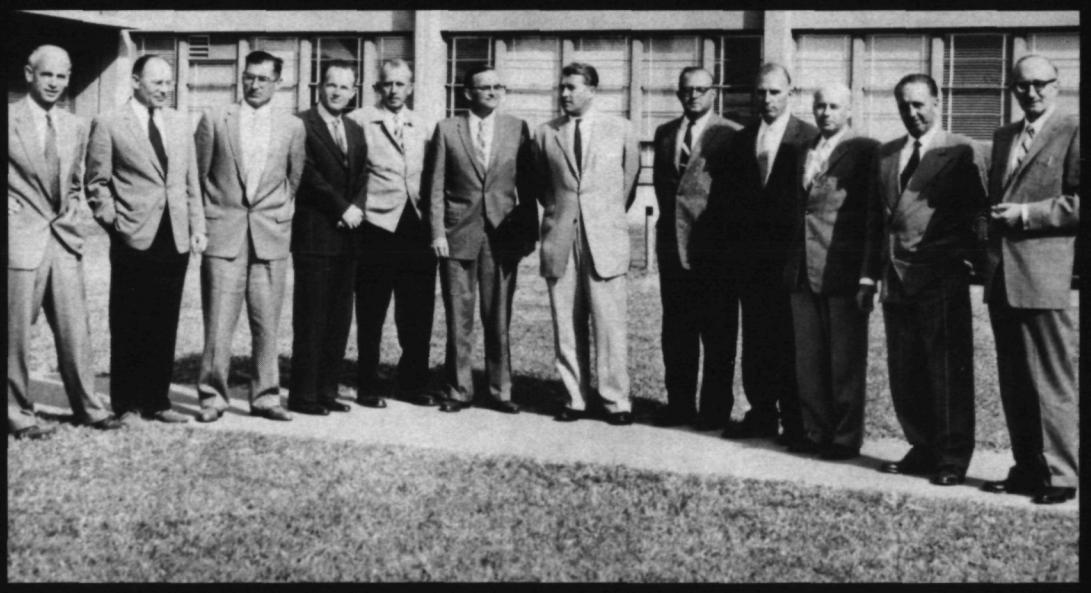

Dr. Von Braun and the Original German Rocket Team at Building 4488, MSFC

Excerpt from speech prepared for: Huntsville–Madison County Chamber of Commerce, Dr. Von Braun quoting Mr. Webb, NASA Administrator
Date: December 8, 1964

"Second, let's take a realistic and discerning look at what Mr. Webb said. I quote: 'For you who are concerned with the future of Huntsville, it is most important to keep in mind that the Marshall Space Flight Center is both the research and development and the management center for the Apollo vehicles...
" 'We have given the Marshall Center the job,' Mr. Webb said, 'and we want it to continue to have the job, here in Huntsville, of research and development on the giant vehicles required for the Apollo manned space flight missions.
" 'We have also given the Marshall Center the job of managing the contractors who will assemble, test, and launch giant vehicles, and much of this work is handled here in Huntsville.' "

Rocket Development for U.S. Army

Came to United States with colleagues in 1945 under contract to the U.S. Army; named project director for the rocket office of the Research and Development Service, U.S. Army Ordnance Corps, at Fort Bliss, Texas; simultaneously directed high-altitude V-2 firings at the White Sands Missile Range in New Mexico.

In 1950, moved with rocket team to Redstone Arsenal in Huntsville, Alabama, serving first as technical director of the Guided Missile Development Group and, later, chief of that division; began research and development of the Redstone ballistic missile.

Became a U.S. citizen on April 14, 1955.

Named development operations director for the Army Ballistic Missile Agency in Huntsville; the Jupiter, Jupiter C, Juno II, and Pershing missiles were developed during this period.

America's first satellite, Explorer I, successfully launched into orbit by the Agency's Jupiter C rocket on January 31, 1958.

Director, Marshall Space Flight Center

Appointed founding director of NASA's Marshall Space Flight Center, established in 1960 to provide launch vehicles for the newly formed space Agency.

Excerpt from speech prepared for: Alabama Legislature
Date: June 20, 1961

"The Marshall Center is now in the process of hiring more than 1,600 new employees. Most of the people we need so urgently are graduate engineers and scientists. In other words, highly skilled and educated men and women."

Excerpt from speech prepared for: Missouri State Teachers Association
Date: November 3, 1960

"Today, more than ever before, education must be more than instruction and the absorbing of facts. A college degree should be a jumping off place rather than a curbstone to sit on. Education should be a live and stimulating thing. Mere knowledge does not spark the imagination. At the same time, if you don't know anything, how can you think?

"Imagination: Here is one commodity that's always in short supply. Imagination points the way. It's the stuff that has changed man from a cave dweller to a man who inhabits libraries and class rooms."

Excerpt from speech prepared for: Alabama Legislature
Date: June 20, 1961

"Even now a lot of people still ask me, 'Why do you want to go to the Moon?' I like to remind them about one of this country's most famous scientists.

"When wise old Ben Franklin sent up his kite that day in the thunderstorm, he got his knuckles singed by electricity. What did Franklin learn by this experiment? Not much. Only that electricity from the clouds would shock him. But because Ben was curious about the world around him, his simple research—plus a few other experiments conducted elsewhere—stirred up a lot of interest. A burst of attention was then focused on electrical research, and as a result, old Ben Franklin's kite sparks flew around the world. Today, we can't drive a tractor, fly an airplane, light a house, or send a satellite into space without electricity.

"My point here is that as wise as Ben Franklin was, he didn't have the faintest idea of the great benefits that were in store for mankind as a result of the first faltering experiments that he and others about that time carried out. But Franklin did have scientific curiosity. It was curiosity that made him go fly a kite that day, not some mysterious, prophetic knowledge that he was about to help pave the way for vast new benefits for all mankind.

"So when somebody tells you to go fly a kite, don't punch him in the nose. Who knows? You, too, might discover electricity.

"It is curiosity that sets man apart.

"It is curiosity that makes him learn.

"This has been true throughout history...first curiosity; then learning; then advancement.

"But the guy who is curious—the restless searcher for new knowledge—never knows where his curiosity will lead him. All he knows is that some time, in some way, the knowledge he digs up will better the lot of his fellow man.

"For instance, the great bacteriologist, Sir Alexander Fleming, found, one day, that certain bacteria were killed by a mold. This accidental discovery—which happened because Fleming was curious about mold—gave us penicillin.

"He didn't have the faintest idea that what he saw under his microscope that day would end up by saving many, many thousands of human lives. It's always that way.

"We just never know what the next bit of information will bring forth.

"That's why we want to—and why we must—explore space. It's our next frontier, our newest challenge, and the greatest unknown today."

Excerpt from speech prepared for: Guideposts
Date: October 1960

Dr. Von Braun at Age 12 (center) With His Two Brothers

Question: "I believe you received your first real telescope when you were 12?"

Answer: "Yes. When I was growing up in Germany, it was the tradition for Lutheran parents to give their children a rather splendid gift when they were confirmed. Every boy in town, it seemed, asked for a pair of long pants and a watch. Except me. The other boys went to church in long trousers, and every one of them needed to know what time it was everyfew steps. But I didn't care. I got my telescope."

Question: "When was it that you first seriously considered trying to get a rocket into space?"

Answer: "Well, I'm glad you used the word 'seriously.' Because I guess I've always *daydreamed* about space flight. When I was in my early teens, I used to slip off to an old World War I munitions dump and pick up odd parts to use in my home-made rockets. I'd try out the rockets in a field near our house. I would kneel down at a safe distance and dream that I was sending another Von Braun Super Space Ship out to a faraway galaxy, and then I'd push the ignition button. Usually the rockets wobbled a little way into the air and fell back again. They were really just a lot of smoke and noise."

Question: "Your dreams weren't very practical, then?"

Answer: "Not at all."

Excerpt from speech prepared for: Missouri State Teachers Association
Date: November 3, 1960

"Ideas, imagination, education, action...these equal happiness. There is nothing in the world more fun than to come up with a new idea and see it put to use.

"And where—except from our schools and colleges—is the stimulation of the minds of our young people to come?

"Training, yes. Instruction, yes. Learning, by all means.

"But if the young men and women of today are going to be equipped to meet the responsibilities that lie ahead of them in the remainder of this century...[they] are going to have to move swiftly to provide the broad, deep, and stimulating education that will be so sorely needed.

"I am confident that our educators and the American people will do just that."

America's first two astronauts launched into suborbital space flight in 1961 by Marshall's Mercury/Redstone boosters.

Saturn I, Saturn IB, and Saturn V launch vehicles—the first designed specifically for manned space flight—developed by the Marshall Center; the first unmanned Saturn I launched on October 27, 1961. Later Saturn I flights placed Pegasus micrometeoroid detection satellites into Earth orbit.

Five Saturn IB's launched in Project Apollo, with the fifth—Apollo 7 on October 11, 1968—the first manned flight of the Apollo spacecraft.

The powerful Saturn V escaped Earth's gravity to take the Apollo 8 crew into lunar orbit in December 1968. Two missions later, the crew of Apollo 11, launched July 16, 1969, by the sixth Saturn V, accomplished the historic first manned landing on the Moon on July 20, 1969.

Von Braun also led Marshall in development of the Lunar Roving Vehicles used during the last three Moon missions and in planning for Skylab, America's first space station, launched in 1973. Studies on advanced space transportation systems leading to the space shuttle were also begun during this era.

NASA Deputy Associate Administrator

Transferred in 1970 to NASA Headquarters to lead the Agency's planning for future

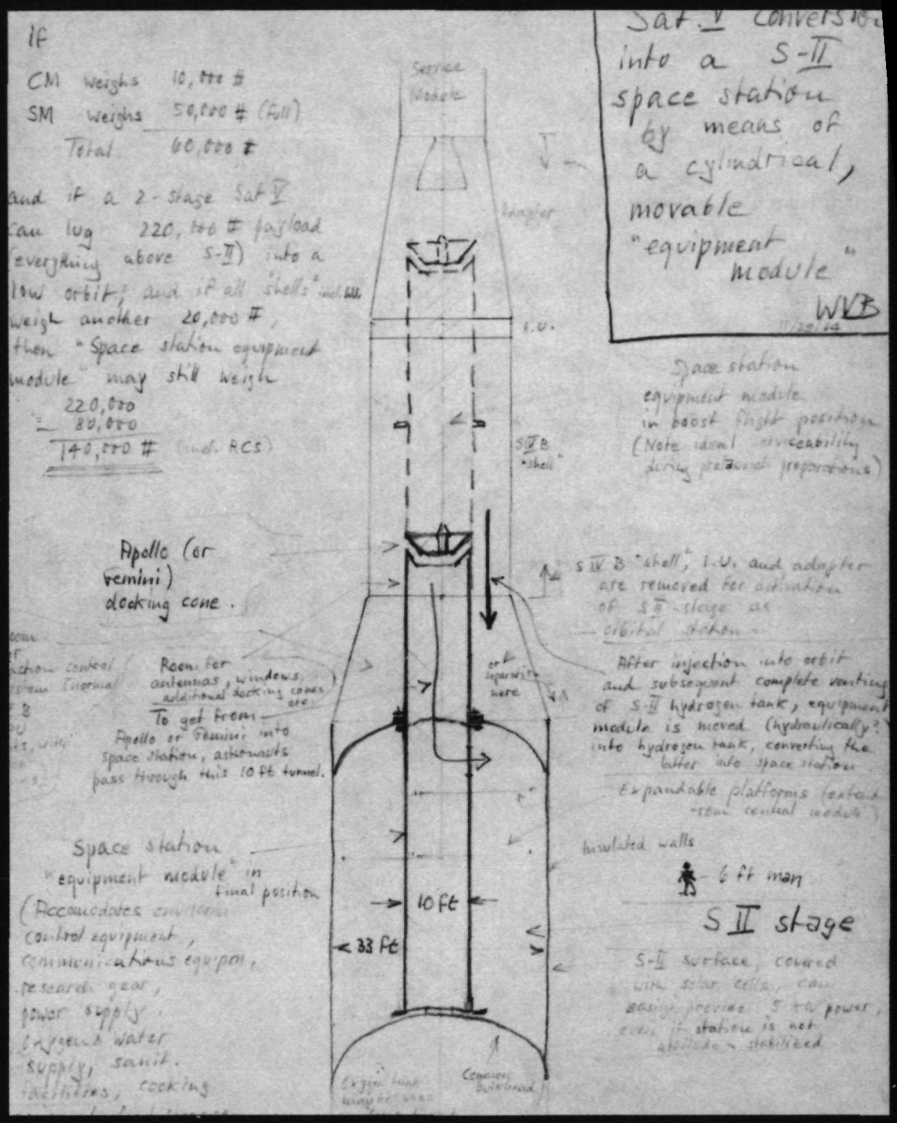

Dr. Von Braun's Sketch of Early Space Station, 1964

Excerpt from speech prepared for: United States Senate Committee on Aeronautical and Space Sciences
Date: August 5, 1969

"The space shuttle, a chemically powered hydrogen-oxygen reusable airplane-type engine which can be flown from the surface to the orbit, would require a go-ahead in 1971. I forgot to mention that the money for this NERVA flyable engine is actually in our 1970 budget request. So this is entirely feasible provided the present budget request passes the House and Congress.

"We would need a go-ahead on this reusable Earth-to-orbit space shuttle, the backbone of all our NASA future endeavors, in 1971. We can have a first flight, as I say, in 1975 if we get the go-ahead here.

"Further on, we need a space station module which is actually a correlative to this mission module, this living room where the astronauts will live during the months of interplanetary voyage. This kind of mission module will also be used in the space station and on the lunar surface. We need a go-ahead for that in 1971 also."

Excerpt from speech prepared for: Huntsville–Madison County Chamber of Commerce
Date: December 8, 1964

"In order to put a man on the Moon in this decade, we must be able to fly unmanned Saturn V vehicles as early as 1967. This means that the peak of our effort in design, procurement of hardware, manufacturing, and testing will probably occur in 1966. From that point onward, our total effort in the Apollo program is expected to decrease.

"Since it normally takes from 2 to 3 years to build up a capability for new programs, NASA is now trying to determine what projects should follow Apollo.

"Three major possibilities are being considered. The first is to put more emphasis on Earth orbital operations. The brilliant successes of communications and weather satellites show that these programs will yield many very handsome payoffs. Earth orbital operations could be extended to include large manned space stations, shuttle vehicles from Earth to orbit, and, possibly, launching platforms from Earth orbit to outer space.

"The second field being studied is further lunar exploration. Methods for living, working, and moving about the Moon's surface would be developed if this area is pursued.

"The third field under consideration is planetary exploration. First attempts would probably be made at exploring Mars and Venus with unmanned devices, to be followed later with manned exploration.

"The selection of any one of these three fields for major emphasis would not eliminate all of the work on the other two. Regardless of the field to be selected, the hardware developed in the 20 billion dollar Apollo program would be used to the maximum."

Mission Officials Relax in the Launch Control Center Following the Successful Apollo 11 Liftoff

Dr. Von Braun With Apollo 11

space missions as Deputy Associate Administrator. Also served as senior NASA representative to other Government Agencies, the science community, and private industry.

Fairchild Industries

Left Government service in 1972 to become vice president, Engineering and Development, for Fairchild Industries in Germantown, Maryland. Retired from Fairchild in 1977, due to ill health, and died on June 16 of that year.

Awards

Numerous awards for pioneering role in rocketry and space exploration included: Department of Defense Distinguished Civilian Service Award, 1957; Department of Army Decoration for Exceptional Civilian Service Award, 1957; U.S. Chamber of Commerce Award for Great Living Americans, 1958; Dr. Robert H. Goddard Memorial Trophy, 1958; Distinguished Federal Civilian Service Award, 1959; The Notre Dame Patriotism Award, 1959; Daughters of the American Revolution Americanism Medal, 1959; British Interplanetary Society Gold Medal Award, 1961; The Hermann Oberth Award, 1961; Order of Merit for Research and Invention, 1962; NASA Medal for Outstanding Leadership, 1964; Diesel Medal in Gold, 1965; Engineer of the Century, 1966; Galabert International Astronautical Prize, 1967; The American Society of Mechanical Engineering "Man

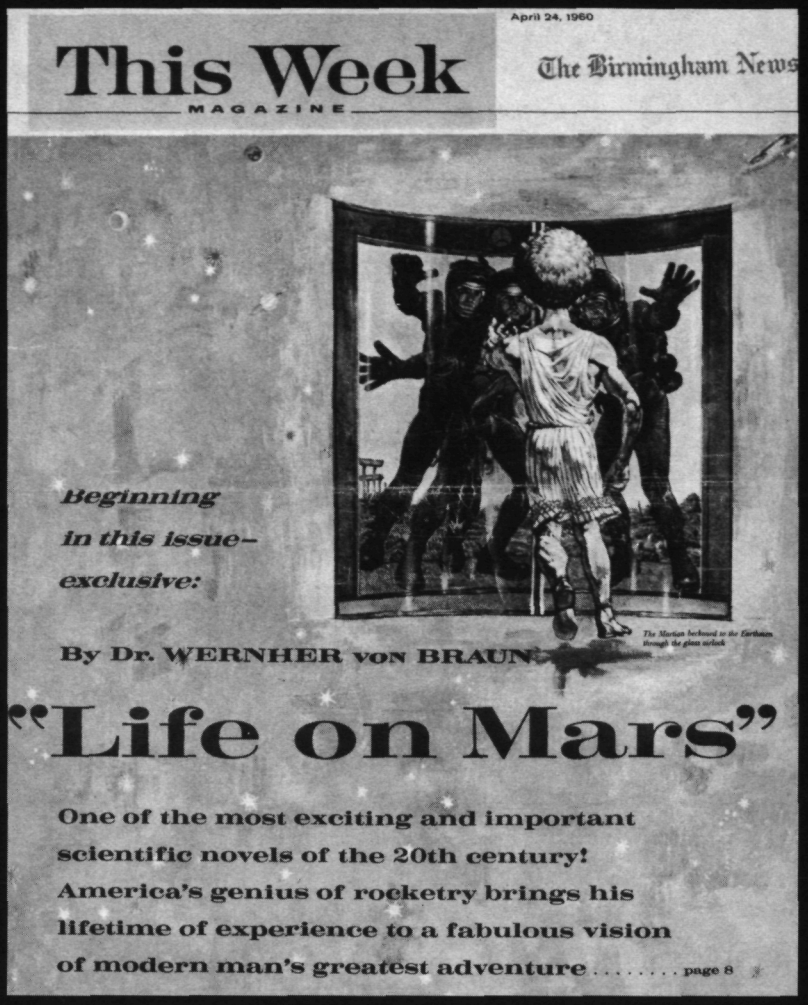
April 24, 1960

This Week
MAGAZINE

The Birmingham News

Beginning in this issue– exclusive:

By Dr. WERNHER von BRAUN

"Life on Mars"

One of the most exciting and important scientific novels of the 20th century! America's genius of rocketry brings his lifetime of experience to a fabulous vision of modern man's greatest adventure ..... page 8

Excerpt from speech prepared for: United States Senate Committee on Aeronautical and Space Sciences
Date: August 5, 1969

"Mr. Chairman, as Dr. Paine has pointed out, we have conducted a feasibility study on a manned mission to the planet Mars as a possible followup to the present series of unmanned Mars flights, both the Mariner and the subsequent Viking family. This is, of course, only one of the possible options available to us as a logical follow-on in the manned space flight area in the post-Apollo period. Now, it is in the nature of planetary missions that the windows do not occur as frequently as with flights to the Moon. We can go to the Moon once every month but to the planet Mars, we can go only approximately every 2 years.

"It is for this reason that my mission description includes some hard departure and arrival dates, but I ask you not to construe this to mean that this is a hard sales proposal, so to speak. It is only necessary in this case to tie a complete mission analysis to hard departure dates in order to make the story consistent all the way through. So what you are going to hear now is a presentation of a typical manned Mars mission involving a total of 12 crew members departing to the planet Mars in November 1981 and returning to Earth in August 1983."

Excerpt from speech prepared for: Alabama Legislature
Date: June 20, 1961

"To make Huntsville more attractive to technical and scientific people across the country—and to further develop the people we have now—the academic and research environment of Huntsville and Alabama must be improved and improved immediately. As many of you know, the University of Alabama has a University Center in Huntsville, which is definitely a step in the right direction. In addition, they have just opened a small Research Institute closely affiliated with this Center. As this institute grows, large corporations will be encouraged to establish research organizations nearby to form an industrial research park as a part of the university complex, which, in turn, will give birth to major new industries throughout the State."

Excerpt from speech prepared for:
Alabama Legislature
Date: June 20, 1961

"Let's be honest with ourselves about it: It's not water, or real estate, or labor, or power, or cheap taxes that brings industry to a State or city. It's brainpower. Nowadays, brainpower dumped in a desert will make it rich. Right now, you could run a profitable electronics firm on the Moon, if the company liked the climate. Educational climate, that is."

Excerpt from speech prepared for: Memphis Executive Club
Date: January 12, 1960

"Are you familiar with the definition of an executive written by Elmer Frank Andrews? He said that 'if a man has an office with a desk on which there is a buzzer, and if he can press that buzzer and have somebody come dashing in response, then he's an executive.'

"Looking out over this assemblage I see a number of men who, like me, have become buzzer pushers by force of circumstance. I am not at all convinced that it was the executive who first created the buzzer. I suspect it was a shrewd electronics manufacturer who developed the product and then sold it to our secretaries. If the truth were known, I think it would be something like this—an executive is a man who walks into his office one morning and finds a buzzer on his desk and then is instructed by his secretary how to use it."

Dr. Von Braun With Secretary, Bonnie Holmes

of the Year" Award, 1967; Smithsonian Institution, Langley Medal, 1967; Associated Press "Man of the Year in Science" Award, 1967; NASA Distinguished Service Medal, 1969; National Space Hall of Fame, 1969; Freedom Foundation National Recognition Award, 1970; Medal of Honor, 1977. In addition, Von Braun was awarded more than 20 honorary doctorate degrees.

Fellowships/ Memberships

American Institute of Aeronautics and Astronautics, American Astronautical Society, British Interplanetary Society, Norwegian Interplanetary Society, Hermann Oberth Society, Hellenic Astronautical Society, International Academy of Astronautics, I.A.F., Austrian Astronautical Society, and the National Academy of Engineering.

Founding president of the National Space Institute.

Publications

Authored or coauthored hundreds of articles and many books including: Across the Space Frontier, 1952; Conquest of the Moon, 1953; The Mars Project, 1953; History of Rocketry and Space Travel, 1966, 1969, 1975; Space Frontier, 1967, 1971; Moon, Man's Greatest Adventure, 1971; The Rocket's Red Glare, 1976; and New Worlds, 1979.

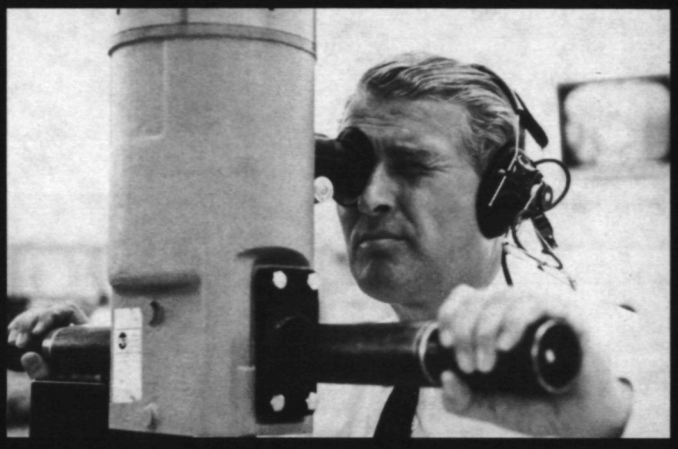

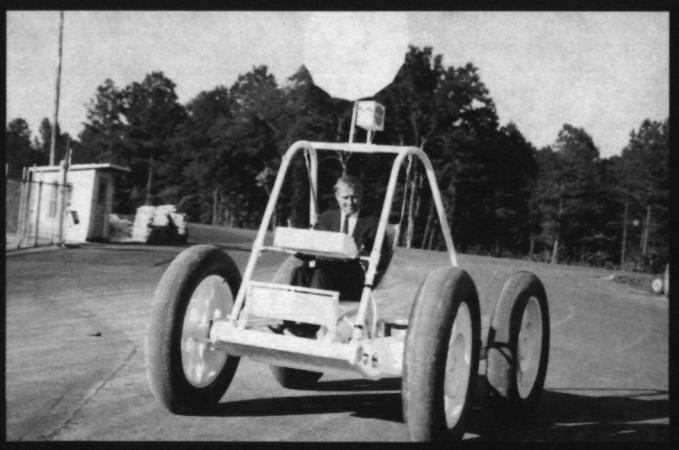

Excerpt from speech prepared for: American Newspaper Publishers Association Meeting at Waldorf-Astoria
Date: April 28, 1960

"Certainly, the space program will make a lasting contribution to the cause of human progress if it becomes the means by which to attract youth to science. A basic understanding of scientific discipline will be essential to the informed citizen in the years ahead because technology will inevitably dominate civilization to an even great extent."

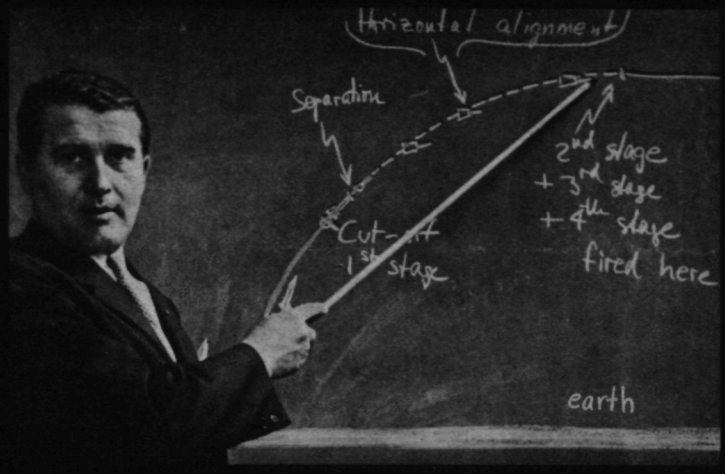

Excerpt from speech prepared for: Missouri State Teachers Association
Date: November 3, 1960

"We must recognize individual abilities at the earliest possible ages and then cultivate and encourage them through the years of preparatory education to make it possible for them to achieve their greatest potential in adult life."

Excerpt from speech prepared for: Missouri State Teachers Association
Date: November 3, 1960

"Incidentally, there is a fellow on my staff at the George C. Marshall Space Flight Center who works in his spare time as head of the math department of a small college nearby. And I want you to know that in this little liberal arts college every student...regardless of his or her major course of study...is required to take calculus. Not just 1 year of business arithmetic or trig, but calculus. He says it's good for the students. I don't know what the students, particularly the English majors, say about him."

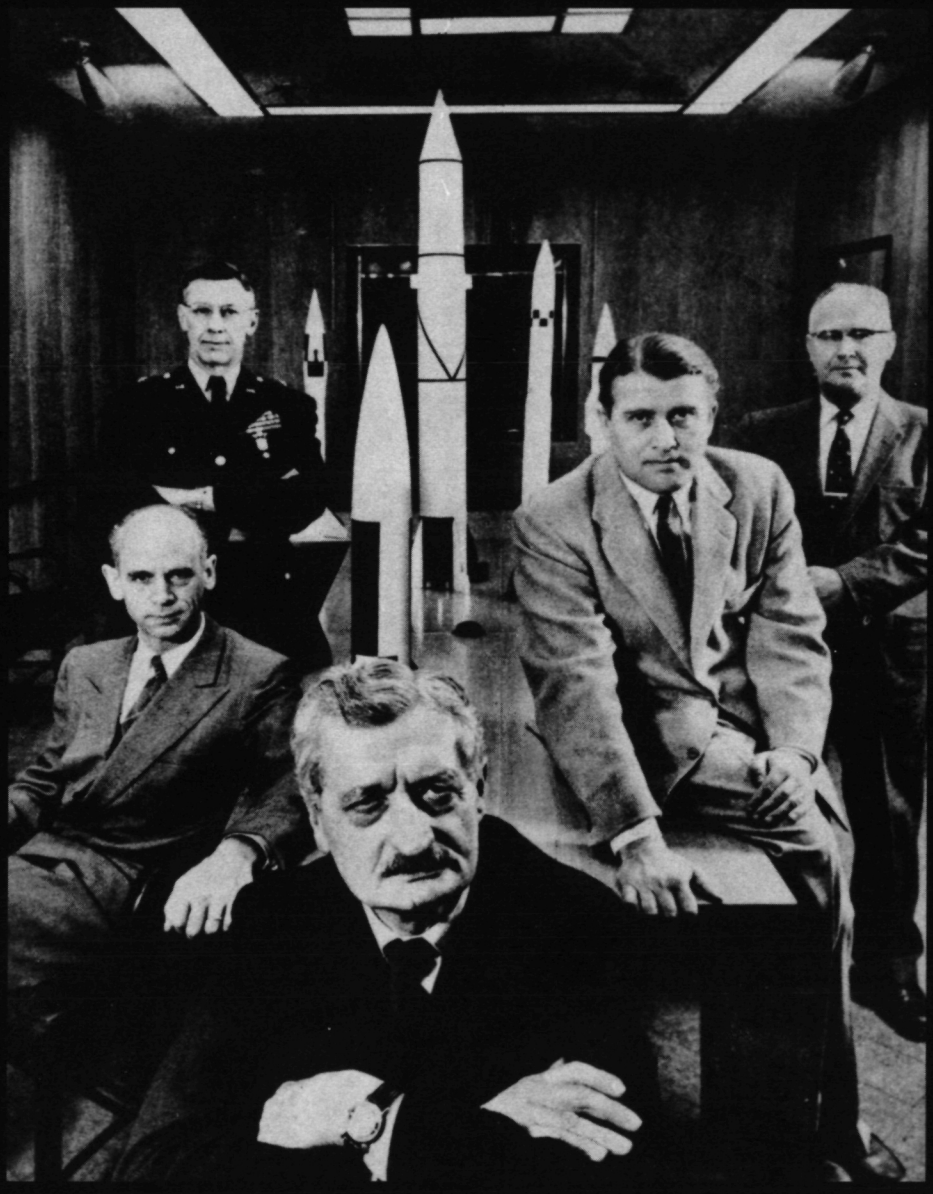

Dr. Von Braun With Associates Including Dr. Oberth (center), Mathematician and Physicist, and Dr. Von Braun's Mentor in Germany.

Excerpt from speech prepared for: Missouri State Teachers Association
Date: November 3, 1960

"...the future of America in an age dominated by technology will depend largely upon the quantity and quality of engineers and scientists available to carry the Nation forward. Thus, we must face up to the situation and ensure that adequate recognition and reward are provided to them and to the teaching profession which prepares them."

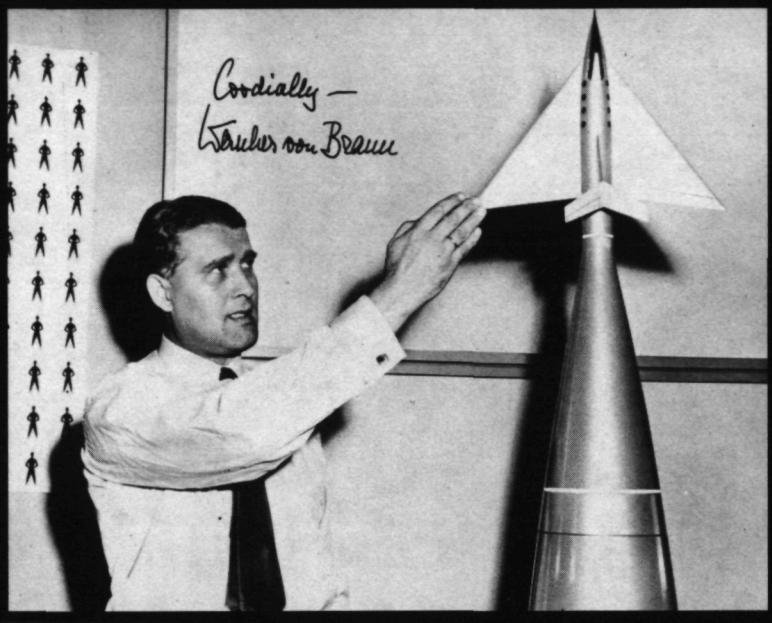

Excerpt from speech prepared for: Missouri State Teachers Association
Date: November 3, 1960

"Here I'd like to interject a comment on something I feel very strongly about. So many of us harp so strongly on the need for high-quality technical training that we overlook something equally important. We should, by all means, stress the study of humanities also.

"Any college graduate who hopes to carve out a fully rounded lifetime of success and happiness must know how to read a good book and maybe play a piano as well as manipulate a slide rule.

"More and more in today's complex society, it behooves a student to study history, government, geography, economics, sociology, and foreign languages.

"It wouldn't hurt him either to study a little politics.

"I believe, too, that we need to ponder carefully another thought: Money has become too much the measure of success and achievement, to the people of my generation. And that attitude echoes in the things which interest our children. I doubt if the great discoveries have derived from efforts directed solely towards the profit side of the ledger—many of them resulted from the labors of researchers and inventors interested only in knowledge and not the ups and downs of the stock market. There is virtue and reward in achievement for the sake of achievement, which may be an old saw but one which needs resharpening and more use.

"It is not financial reward, certainly, which motivates the rocket developer—yet he is constantly asked 'Why do we do these things? Will they ever pay off?' Can you imagine anyone asking that of an Einstein or a Pasteur? There will be payoffs, of course, as we advance into space, but the most important, the reward of greatest lasting value, is our increased understanding of the spatial environment and of its influence upon our earthly existence. You cannot put a price upon such a discovery as that of the Van Allen Radiation Belt, made possible through the launching of several artificial Earth satellites of relatively small weight. We have opened the door into the limitless reaches of the universe by such modest beginnings and we can see just far enough ahead to know that man is at the threshold of a momentous era. Here is opportunity, challenge, adventure so tremendous as to beggar description. Here is the tomorrow which youth wants to embrace and for which we must provide whatever guidance and preparation we can."

"Dr. Von Braun worked with great determination to make his cherished dream of space exploration come true. One of his principal contributions to our world was his unfaltering belief in space exploration long before it became a reality. With singleness of purpose, he pursued that dream through many obstacles and adversities until his untiring efforts and genius, linked with those of many of you, gave it the substance of reality.

"The names of three men stand out in our memory as the pioneers who believed that a man could explore space: Goddard in America, Oberth in Germany, and Tsiolkovski in Russia. They were theoreticians, and their names will be well-known to students of history far in the future.

"But one name will stand out as a giant among men for the acutal beginning of space exploration, when the theories of those brilliant forerunners were put into practice. That is the name of Von Braun.

"Our space program—for which the name Von Braun, more than any other, became synonymous—has yielded many practical benefits; it has improved the quality of life; it has given a timely uplift to the American spirit and kindred spirits across the world; it enhanced man's appraisal of the universe; it increased his vision; it stimulated the economy, and it continues to force the development of science and technology.

"As Dr. Von Braun once wrote, and would say to you today: 'There can be no thought of finishing, for aiming at the stars—both literally and figuratively—is the work of generations, and no matter how much progress one makes, there is always the thrill of just beginning.'"

Excerpts of text of remarks by Dr. William R. Lucas, MSFC Director, to employees over closed circuit television in a memorial service for Dr. Wernher von Braun.

Advanced Studies

The challenges of future space accomplishments in science, applications, and exploration are almost unlimited. Advanced Studies light the pathway for human steps into the solar system in the 21st century, and they define the systems that will enable us to understand the Earth and the universe.

Expansion of human presence beyond Earth's boundaries will require a new generation of space transportation vehicles. Building on its heritage of engineering excellence, MSFC leads the Agency's efforts to conceptualize the transportation systems of the future, ranging from launch vehicles that boost to low Earth orbit to space transfer vehicles which traverse the great distances to the Moon, Mars, and beyond.

Future systems in near-Earth space will help us understand our own fragile planet better. A wide range of science data will be obtained from missions and orbiting platforms being studied. These systems and data will help us monitor and understand the processes that cause ozone depletion, global warming, and other threats to Earth and its atmosphere.

The Hubble Space Telescope, the first of the Four Great Observatories, is now returning a stream of scientific data. Advanced studies of other capable orbital facilities for this and the next century are being conducted. Studies are underway to determine how the Space Station *Freedom* could evolve to serve as a base of operations to support the Space Exploration Initiative.

Human expansion into the solar system and scientific research into the origins of the universe and the evolution of the planet Earth are noble endeavors, presenting the greatest challenges man has yet undertaken. Advanced Studies will unlock the door to this future.

C.R. Darwin
Director, Program Development

Transportation Systems

Advanced Recovery Systems

Numerous advanced launch vehicle studies of space shuttle derivatives, the joint U.S. Air Force/NASA Advanced Launch System, the Personnel Launch System (PLS), and others, have shown the potential economic and operational advantages of **recovery** and reuse of main engines and other high-cost systems. By incorporating the main **propulsion and avionics** into a single package, here referred to as the **propulsion/avionics (P/A) module**, the launch vehicle's most expensive and complex components become recoverable, refurbishable, and reusable. This approach enables rapid reuse of the components, maximizes launch vehicle payload performance, and minimizes development cost compared to a totally reusable manned vehicle. The **P/A module** is being considered in two basic configurations, shown in figure 1. The high lift-to-drag (L/D) version, shown in the landed, roll-out configuration, has the advantage of using wheels for a conventional aircraft-type runway landing, and offers increased landing opportunities upon return to the launch site from orbit. The ballistic or low L/D configuration, shown at touchdown, is relatively less complex, lighter in weight, and costs less. Weights range from about 25,500 kg (56,000 lb) for the ballistic configuration to almost 30,000 kg (66,000 lb) for the high L/D module.

The high L/D **P/A module** features a delta platform shape approximately 15 m (50 ft) long, 15 m (50 ft) wide, and 6 m (20 ft) tall. Advanced carbon/carbon material is needed for the short radius leading edge. Hypersonic wind tunnel tests at the NASA/Langley Research Center have been conducted to show the specific heating properties, select the carbon/carbon, and size the internal insulation. Shuttle thermal protection is adequate for the remaining surfaces of the vehicle. This shape provides a cross range of 2,897 km (1,800 mi), which allows more than 10 return orbit opportunities per day to Kennedy Space Center (KSC), Edwards, and Vandenberg Air Force Bases. The ballistic module has a blunt shape approximately 7 m (23 ft) in diameter and is 6 m

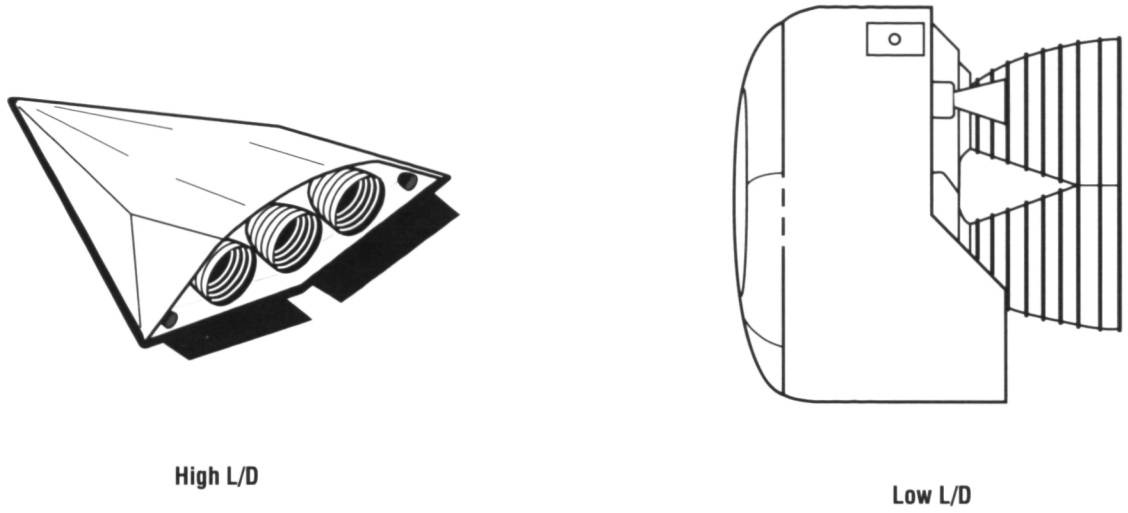

Figure 1. The P/A Module: High L/D and Low L/D Versions

(20 ft) long. Cork is the preferred ablator for the expendable nose shield. Heating rates for this selection have been confirmed by high-speed wind tunnel tests. Also, the shuttle thermal protection system is used for the remaining areas of the body, including the base. This vehicle has only two return landing opportunities per day to KSC due to the limited cross range provided by the low L/D. It lands on a circular, grass-covered site 1 to 2 km (0.6 to 1.25 mi) in diameter, depending on whether a lifting or ballistic parachute is used. Final impact attenuation is provided by airbags.

Vehicle application, onorbit stay-time properties, entry and landing control, landing site features, and optimization of subsystem design features are the primary study areas at this time. Vehicle application studies address integration of the **P/A** into specific vehicles, the facility impacts, and the cost-benefits of reuse. Cost payback for the added **P/A module** development on a specific launch vehicle can be as early as three flights, depending on engine and other cost estimates. Control studies are producing entry control algorithms, attitude thruster/propellant sizing, flap effectiveness, and control limits. With a 15-minute update on landing wind conditions, landing site targeting for the ballistic **P/A** is estimated to within 213 m (700 ft) with a 95-percent certainty. Drop tests have been completed confirming the expected attenuation of the airbags on landing impact for the ballistic module.

For recovery of **P/A modules**, and potential applications to other programs, including Space Station *Freedom* crew return, cargo return, and the PLS, a precision recovery gliding parachute system for soft touchdown on land is being developed. This system, termed the Advanced Recovery System (ARS), has a target landing capacity of more than 27,000 kg (60,000 lb) which represents a significant increase in the weight capability of **parafoils**.

The ARS began in 1986 with phase I study contracts to define a system for the safe land recovery of large, high-cost launch vehicle components. The result was a ram-air gliding parachute, also known as the parafoil (fig. 2). The **parafoil** required for a 27,000-kg (60,000-lb) payload was defined to be a 985-m^2 (10,600-ft^2) system.

Phase II extended the effort to include a scaled demonstration of the concept. This program is currently underway and is scheduled to end after FY90. Plans are to continue with phase III after this time if funds are made available. Phase II included two series of wind tunnel tests at the NASA/Ames

ORIGINAL PAGE
BLACK AND WHITE PHOTOGRAPH

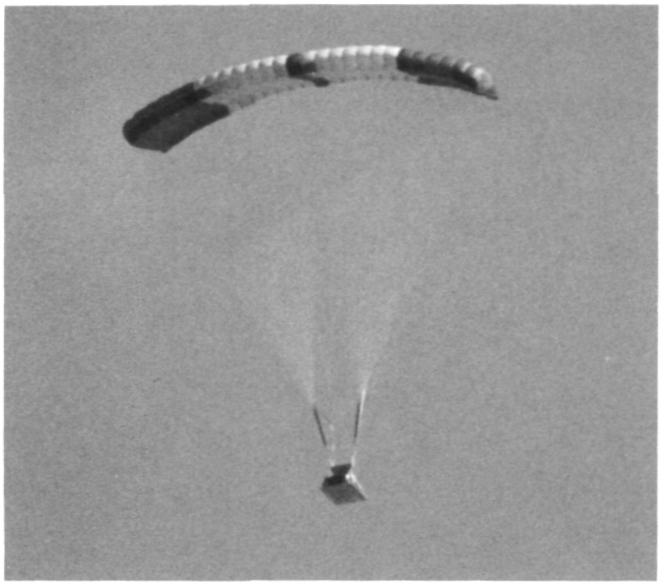

Figure 2. The Ram-Air Gliding Parachute (Parafoil)

Research Center's National Fullscale Aerodynamics Complex. The first series was conducted in September 1988, and the second series was completed in April 1990. Several different scaled-parafoil models were tested, using various aspect ratios and two different airfoil sections. These tests have aided in establishing steering control methods, rigging angles, and loads for the drop test program, as well as establishing a **parafoil** aerodynamics data base under controlled conditions, therefore greatly contributing to the state-of-the-art.

The other portion of the program includes a series of 11 aircraft drop tests with weights ranging from 4,500 to 9,000 kg (10,000 to 20,000 lb). The **parafoil** and weights being used are about one-third scale, so the tests present wing loadings representative of a full-scale payload. Man-in-the-loop steering controls have been incorporated for turns and flared landings.

To date, nine drop tests have been attempted with eight of the tests being totally successful. Deployment of the large **parafoil**, using a unique midspan reefing technique developed by Pioneer Aerospace Corporation, has been demonstrated reliably. Steering has been incorporated on the last three tests and works as planned. The largest weight tested to date has been about 6,400 kg (14,000 lb), which represents almost triple the weight successfully flown before. Unfortunately, the last test ended in failure because of a nonstandard extraction from the aircraft; this was not a failure of the **parafoil**, but rather was due to problems with associated test equipment. The failure will delay resumption of the test for about 4 months.

Upon completion of phase II, a third phase is planned to further increase the tested weight and to incorporate autonomous steering into the system. This phase is scheduled to continue for about 3 years.

G.W. Johnson/PT01
(205) 544–0636
Sponsors: Office of Space Flight, Advanced Launch Systems Joint Program Office

Integrated Earth-To-Orbit Transportation

NASA is currently analyzing alternatives to establish the desired path for future unmanned and manned launch vehicles. This activity considers the civil needs over the next 20–30 years and is attempting to match vehicles and supporting operational concepts to meet these requirements. Requirements include the Space Exploration Initiative (SEI) which will dictate the need for a new, unmanned, heavy-lift capability. Studies will be conducted over the next several years to ascertain the best path to follow from both a technical and programmatic point of view. Specific areas of focus will be safety, resiliency, assured access, cost, and availability. The results of the studies will formulate an integrated Earth-to-orbit infrastructure, including vehicles and supporting facilities, needed to satisfy both unmanned and manned civil space requirements.

The unmanned systems generally fall into one of the following three categories: concepts primarily derived from existing space shuttle concepts—**Shuttle Derived Vehicle (SDV)**; concepts as defined

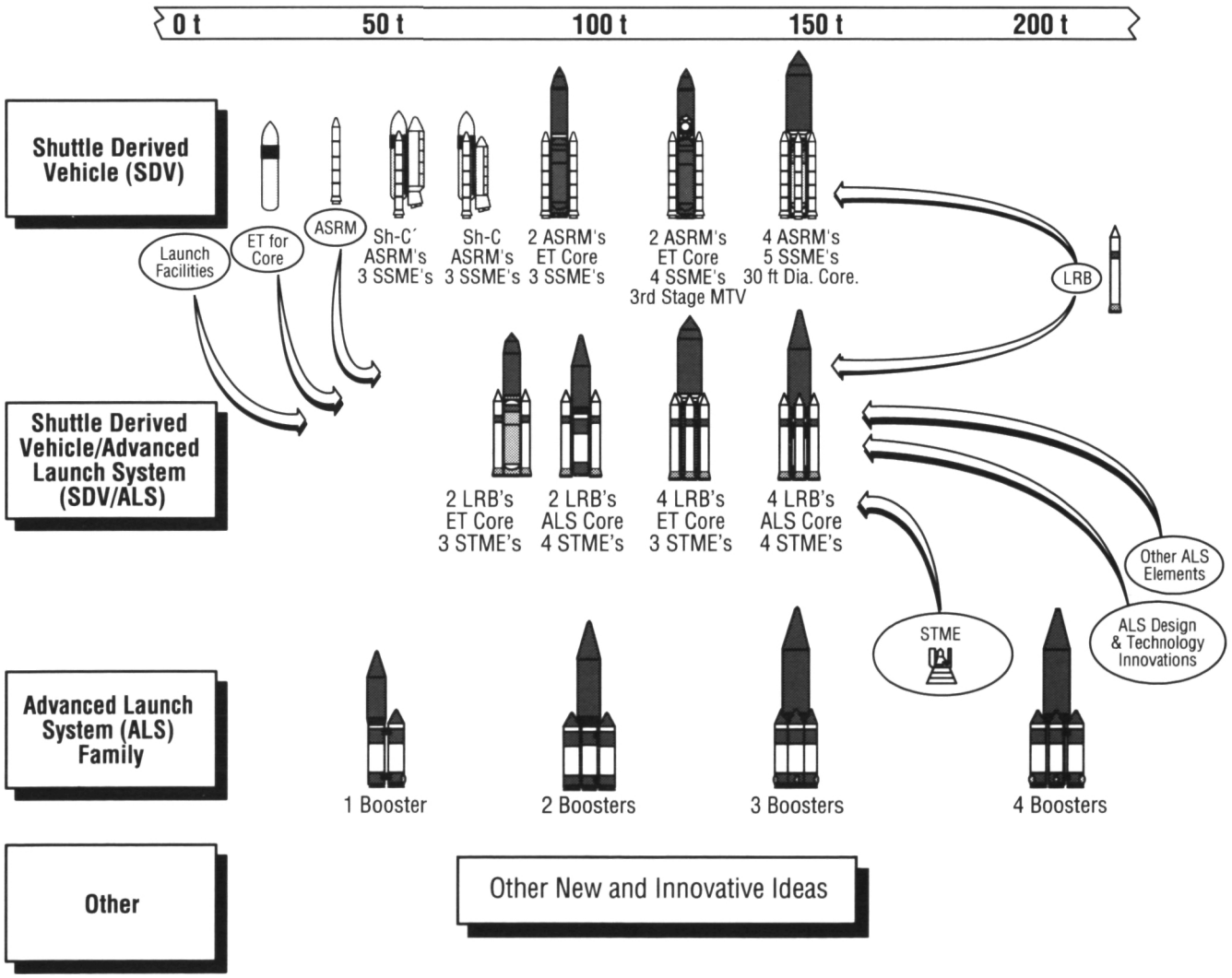

Figure 3. SEI Candidate Unmanned Vehicles

in the **Advanced Launch System (ALS)**; and concepts that draw heavily from existing hardware and facilities, but incorporate new technologies, processes, and select hardware from the **ALS** program. This latter option is labeled the **SDV/ALS** approach. Figure 3 shows some conceptual configurations for each of these approaches.

The **SDV** approach takes maximum advantage of existing hardware elements, such as the solid rocket motors, the external tank, the space shuttle main engine, as well as existing processing and launch facilities. Vehicle options defined from these elements include the reference Shuttle-C and numerous inline shuttle-derived concepts.

The **ALS** concept is characterized as a clean sheet approach which takes maximum advantage of new technologies, processes, and facilities in order to minimize recurring launch vehicle costs. This approach offers several long-term advantages, but it does require a greater nonrecurring investment to put these new systems in place.

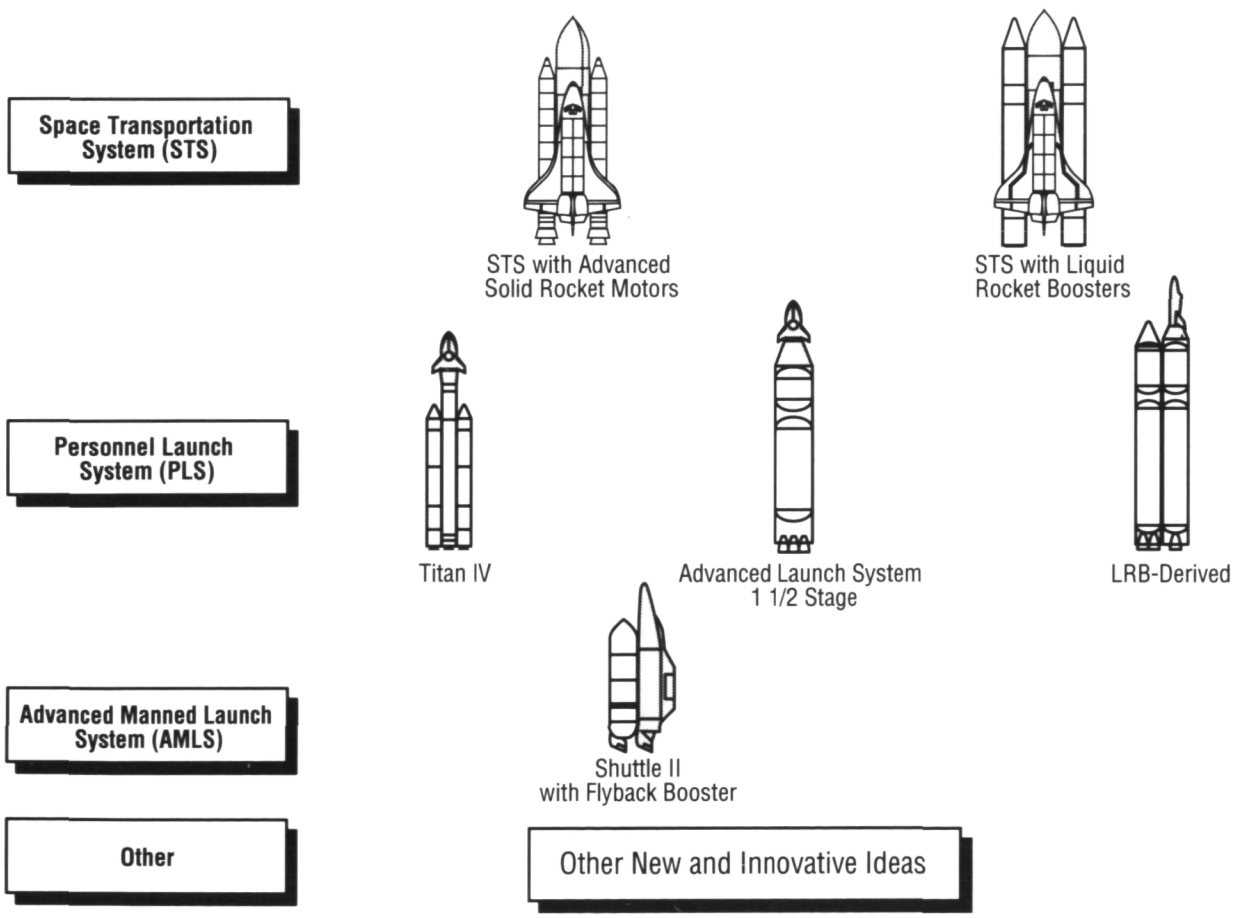

Figure 4. Candidate Manned Vehicle Concepts

The **SDV/ALS** approach selectively draws from the **SDV** and **ALS** approaches. The goal is to achieve the ALS efficiencies and lower recurring costs, but in an incremental manner rather than all at once. This would spread the development and facilities costs over several years and result in lower peak-year funding requirements.

The manned systems generally fall into one or more of the following three paths: space shuttle evolution; the **Personnel Launch System (PLS)**; and the Advanced Manned Launch System (AMLS). Figure 4 shows some conceptual configurations for each of the different paths.

Shuttle evolution deals with major block changes to the National Space Transportation System (NSTS), as opposed to the shuttle improvements underway. A near-term block change is the planned incorporation of the advanced solid rocket motors (ASRM's). Another potential block change under consideration is liquid rocket boosters (LRB's). The LRB would improve reliability by providing engine-out capability and improve emergency escape capability for the crew by permitting booster throttling and/or engine shutdown. Additionally, the LRB's would provide an increase of 9,000-kg (20,000-lb) lift capability over the current solid rocket boosters (SRB's).

The **PLS** study is assessing the feasibility of separating man from cargo. The potential of launching a manned capsule or a cargo return vehicle (CRV) on existing and/or new launch vehicles is being studied. The vehicle options include the Titan IV (requiring man-rating), the **ALS** 1.5-stage vehicle, an external tank-derived 1.5-stage, and a concept derived from shuttle-compatible LRB's.

The AMLS, formerly known as Shuttle II, will be the next generation reusable manned transportation system to replace the existing space shuttle. The vehicle will be capable of transporting both crew and cargo to low Earth orbit. However, its cargo-carrying capability may be less than the current shuttle since alternate unmanned vehicles will be available for heavier payloads.

U. Hueter/PT21
(205) 544–8492
Sponsor: Office of Space Flight

Space Exploration Initiative

On July 20, 1989, President Bush called for a long-range, continuing commitment to space exploration, specifically to a sustained program of manned exploration of the solar system. He announced three major space policy objectives. First, to have Space Station *Freedom* up before the century is out. Second, for the new century, to build a permanent lunar base. And, third, to launch a manned expedition to **Mars**.

On May 11, 1990, President Bush provided not only a goal but a timetable. He stated that before Apollo celebrates the 50th anniversary of its landing on the **Moon**, the American flag should be planted on **Mars**. This now gives us a timetable for planning; return to the **Moon** in the first decade of the new century and an expedition to **Mars** before the end of the following decade.

To support this endeavor, NASA Administrator Richard Truly created a task force in the fall of 1989 to conduct a 90-day study of the main elements of a **Space Exploration Initiative (SEI)**. The results were documented in a report that provided several reference approaches, built upon past programs and recent studies to reflect wide-ranging strategies that incorporated varied program objectives, schedules, technologies, and resource availabilities.

The MSFC prime responsibility in the **SEI** is to analyze and provide concepts for the integrated transportation systems, which include launch vehicle options, lunar transportation system concepts, and Mars transportation system concepts. Additionally, MSFC supports the lunar and **Mars** science definition activities and the planetary surface system areas for habitation modules and manned surface rover vehicles.

The launch vehicle options for the **SEI** under investigation at MSFC include shuttle-derived approaches, the joint NASA/DOD Advanced Launch System, and new heavy-lift launch vehicles.

Figure 5 depicts a typical concept for a lunar transportation system as it would appear leaving low Earth orbit. The system includes a lunar transfer vehicle, which operates to carry crew and cargo between Space Station *Freedom* and lunar orbit and utilizes aerobraking for Earth orbit capture upon return from the **Moon**. A lunar excursion vehicle which operates between lunar orbit and the surface, is also part of the system. This past year, MSFC continued to investigate the option of an earlier space transfer vehicle for unmanned planetary and geosynchronous missions. It could be a derivative of the lunar transfer vehicle from the **SEI**.

Figure 5. Concept for Lunar Transportation System

A typical **Mars** transportation system includes three elements: (1) a trans-**Mars** injection stage to depart Earth orbit; (2) a **Mars** transfer vehicle that provides a habitation module to support the crew during the transit from Earth orbit to **Mars** orbit and return to Earth orbit, an aerobrake for **Mars** orbit capture and later for Earth orbit capture, and a trans-Earth injection stage to depart **Mars** orbit; and (3) a **Mars** excursion vehicle, or lander, that provides transportation between **Mars** orbit and the surface. A typical excursion vehicle, or lander, is depicted in figure 6.

On May 31, 1990, NASA announced the beginning of a nationwide outreach process in search of ideas, concepts, and technologies which might benefit the **SEI**. This process is being implemented to ensure that all reasonable conceptual space exploration alternatives have been evaluated. Additionally, a synthesis group has been formed for synthesizing the inputs received from the outreach program into two or more strategies for how to go back to the **Moon** and then to **Mars**. At MSFC, a number of trade studies were conducted on the integrated transportation system to better understand alternative approaches and propulsion systems for implementing the initiative. These results are a part of NASA's input to the outreach/synthesis process.

J.P. Sumrall/PT41
(205) 544–8491
Sponsor: Program Development

Figure 6. Concept for Mars Excursion Vehicle (Lander)

Advanced Launch System

The **Advanced Launch System (ALS)** is a joint venture of the U.S. Air Force and NASA. It will consist of a family of unmanned cargo vehicles planned to meet the needs of the Nation's payload community into the next century. The family is conceived to provide optimal launch capability, at minimal cost over a range of payload weights from 18,000 to 100,000 kg (40,000 to 220,000 lb), to low Earth orbit with capabilities for growth. The design objectives of each member of the family of vehicles are low cost, high reliability, and operability. To meet the cost and robustness goals, tradeoffs will be made in the areas of weight and performance. One primary goal of the program is to reduce today's cost per pound of payload delivered to low Earth orbit by an order of magnitude. Overall responsibility for the program is vested in a joint NASA/Air Force Program Office.

The mission model for the **ALS** includes the mission needs of all authorized users (the Strategic Defense Initiative Organization, NASA, DOD, and universities). The two basic scenarios are the normal mission model and the expanded mission model. The normal mission model is based on DOD and civil payloads similar to those being launched by today's launch vehicles. The expanded model includes a deployment of either a Strategic Defense Initiative system or a Mars or lunar program being considered for the Space Exploration Initiative. Each of the scenarios involves different missions which drive the design of the **ALS**. Some other capability requirements are:

- Initial launch capability in 2000
- Initial operational capability in 2002
- Design reliability > 98 percent
- Launch call-up capability of 30 days or less
- Payload substitution within 5 days of launch
- Launch-on-schedule probability of 95 percent
- Surge capability of seven missions in 5 days
- Life-cycle cost competitive across 453,500–2,267,600 kg (1–5 million lb) per year
- Clean pad (no tower) and simple payload interfaces.

The phase II effort has been performed in a total quality management environment. The contractors have organized product development teams that utilize the principles of simultaneous engineering to develop design concepts that fully represent the requirements of the customer. Concurrently, the Government has employed similar processes to develop a consistent set of requirements. The first step toward developing a set of NASA level I requirements using quality functional deployment methods has been accomplished. A continuation has been scheduled for the fall of 1990.

J. T. Watkins/HA41
(205) 544–1750
Sponsors: Office of Space Flight, U.S. Air Force/Space Division, Strategic Defense Initiative Organization

Advanced Launch System Propulsion Advanced Development

Advanced development research and technology activities to support Advanced Launch System (ALS) propulsion definition studies were initiated in 1988. Efforts covered by the program are divided according to the nature of each task into the five following categories: liquid oxygen **(LOX)/hydrogen engine**, LOX/hydrogen, LOX/methane engine, liquid propulsion test facilities, and **solid propulsion**. The primary emphasis of the tasks is to support definition studies with demonstration and validation of design concepts, manufacturing processes, materials, and design techniques which will be employed to enable ALS propulsion to meet the program goals of high reliability, low cost, and operability. Particular effort is concentrated on producibility to allow dramatic cost reduction and quality increases compared to conventional propulsion systems. Testing is conducted at the MSFC Pressure-Fed Test Facility (test stand 116) and other test facilities at Stennis Space Center and the U.S. Air Force Astronautics Laboratory.

LOX/liquid hydrogen (LH_2) activities include conduct of detailed trade studies, detailed design, fabrication, and testing of major engine components to fully investigate low-cost manufacturing processes, low-cost/producible/high-quality design concepts, and advanced manufacturing techniques. Emphasis will be placed on materials and materials fabrication processes which will support the selected approaches. The total effort will include the design, fabrication, and test of an LH_2 turbopump (fig. 7),

ALS PROPULSION ADVANCED DEVELOPMENT PROGRAM			
Task#	**Description**	**Task Mgr.**	**Contractor**
1200	**LOX/LH_2 Engine**	**MSFC**	**N/A**
1201	LOX Turbopump	MSFC	Pratt & Whitney
1202	LH Turbopump	MSFC	Aerojet
1203	LOX/LH Combustion Devices	AFAL	Rocketdyne
1205	EM Propellant Flow Control	MSFC	Aerojet
1206	Controller/Sequencer	MSFC	Aerojet
1207	Subscale combustion devices	MSFC	Rocketdyne
1300	**LOX/LH_2 and HC Engine**	**MSFC**	**N/A**
1301	LH_2 Turbopump	MSFC	Rocketdyne
1302	Combustion Chamber	MSFC	Aerojet
1304	Combustion Stability Verification	AFAL	Rocketdyne/Aerojet/ Pratt & Whitney
1600	**Solids Development**	**MSFC**	**N/A**
1601	Clean Propellant	MSFC	TBD
1602	Nozzle/Case/Insulation	MSFC	TBD
1604	Integration and Verification	AFAL	Thiokol
1605	Non-Destructive Evaluation	MSFC	Martin-Marietta
1700	**Facilities Development**	**SSC**	**N/A**
1701	TS-116 (Thrust Chambers)	MSFC	Industrial/Amelco
1702	CTF (Turbomachinery)	SSC	Fluor
1703	2-A (Combustion Devices)	AFAL	EG&G

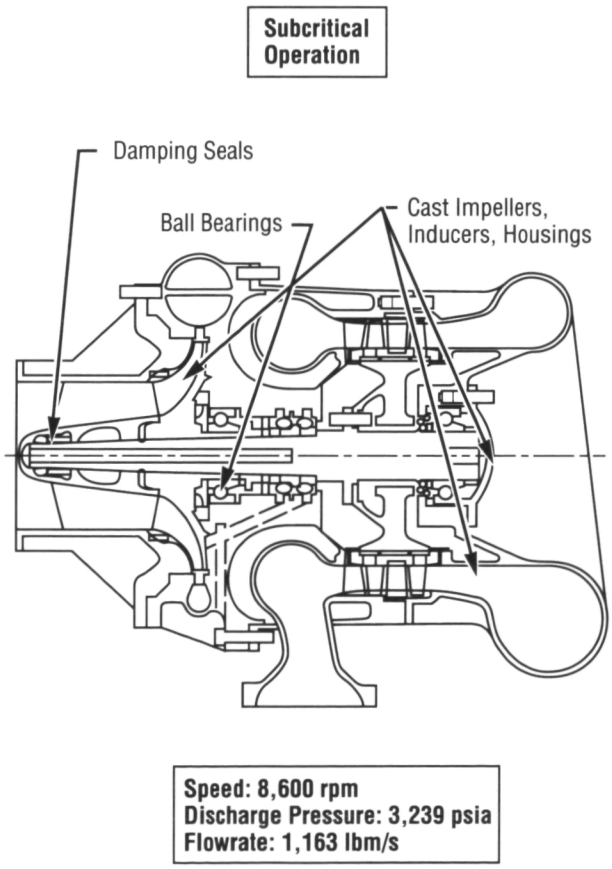

Figure 7. Liquid Oxygen Turbopump (Pratt & Whitney)

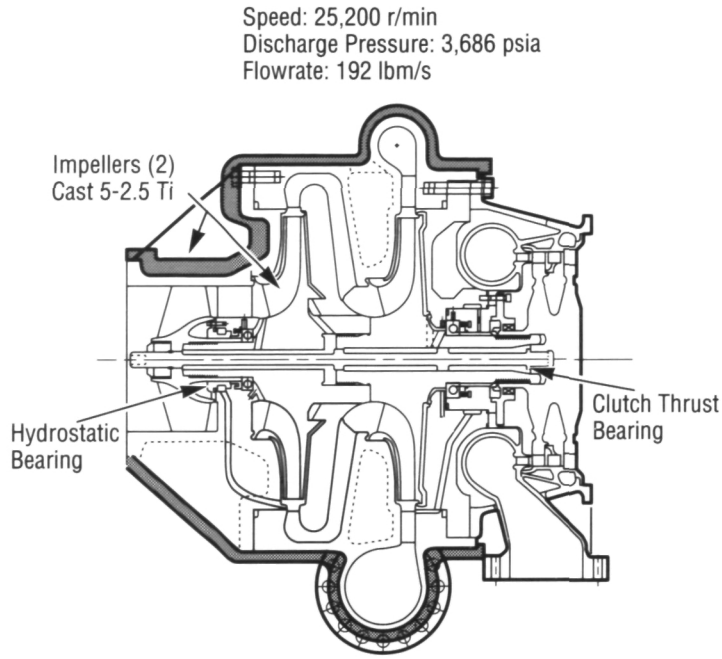

Figure 8. Liquid Hydrogen Turbopump (Rocketdyne)

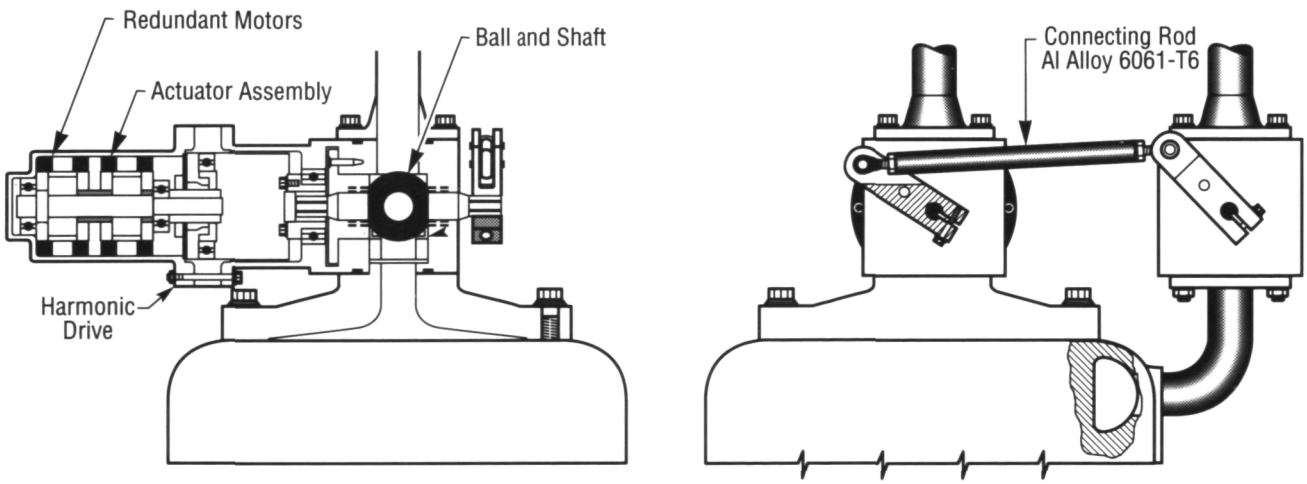

Figure 9. Electromechanical Propellant Flow Control (Aerojet Techsystems)

LOX turbopump (fig. 8), LOX/LH_2 thrust chamber assembly, LOX/LH_2 gas generator assembly, an electromechanical propellant valve flow control system (fig. 9), and a brass-board controller/sequencer.

LOX/LH_2-LOX/CH_4 activities include conduct of detailed trade studies, and design, fabrication, and testing of major engine components to fully investigate low-cost manufacturing processes, low-cost/producible/high-quality design concepts, and advanced manufacturing techniques. Emphasis will be placed on evaluation of materials and materials fabrication processes which will support the selected approaches. The total effort will include the design, fabrication, and test of the LOX/LH_2 turbopump, thrust chamber assembly, and gas generator assembly.

Many of the liquid propulsion tasks have reached significant milestones during the past year. For example, testing began in August 1990 on a 40-klb LOX/hydrogen injector at MSFC test stand 116. These test results will validate design concepts and provide data for stability verification prior to the start of manufacturing for the large-scale combustion devices (580 klb).

Booster/core propulsion subsystems technology activities will provide definition of system architecture for low-cost auxiliary propulsion systems, definition of ALS design requirements and criteria, design and validation of a prototype LOX tank pressurization system remote from the engine, and demonstration of control authority and stability.

Solid propulsion activities center on technologies that support a monolithic case, fixed nozzle, clean-propellant booster concept selected by ALS studies as the candidate to best meet ALS goals of high reliability and low cost. Specific tasks are grouped into the categories of clean propellants, nozzle/case technologies, and motor element integration technologies. Clean propellant work will demonstrate high-rate, low-cost processing of low hydrochloric-acid content propellants. To support the demonstration, a pilot-scale plant will be built, continuous processing methods will be operated, and moderately large-scale demonstration firings will occur. Hardware concepts which will improve the reliability and costs of nozzle cases, insulation, etc., will be selected, designed, and demonstrated on a small-scale basis to verify that the new concepts can meet ALS goals. A task investigating castable nozzles is also being pursued.

J.L. Taylor, Jr./HA31
(205) 544–8824
Sponsors: Office of Space Flight, U.S. Air Force/Space Division, Strategic Defense Initiative Organization

Space Transportation Main Engine

The **Space Transportation Main Engine (STME)**, shown in figure 10, will provide Earth-to-orbit main propulsion for the next generation of U.S. launch vehicles. **STME** phase A concept study began in 1986 to support joint NASA/U.S. Air Force space transportation architecture studies. Current **STME** phase A studies are providing engine designs and program plans to support the joint NASA/Air Force **Advanced Launch System (ALS)** phase II studies. The **STME** has followed a revolutionary approach to rocket engine concept definition leading to highly reliable, low cost, producible designs.

Results show that the **STME** is a key to the **ALS** family of vehicles building block approach which allows a broad range of economical payload capability. The **STME** building block will provide reliable, economical, core propulsion across the family. With the **STME** and other building block elements, various combinations of the **ALS** will be able to launch payload masses from 18,000 to 100,000 kg (40,000 to 220,000 lb) per mission with capabilities for growth. The versatile **STME** can also provide economical propulsion well into the Nation's future, and can be utilized in a variety of additional applications including shuttle liquid rocket boosters and Shuttle-C.

STME parametric cost and performance data have been developed for use in **ALS** design trades. Based on trade results, a baseline Gas Generator (GG) cycle engine configuration, which can be applied to either expendable or reusable vehicle configurations, was selected to allow thorough investigation

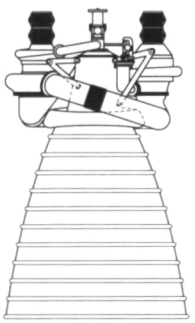

Space Transportation Main Engine (STME)			
	Gas Generator (GG)	**Closed Expander (CE)**	**Open Expander (OE)**
Propellants	LOX/Hydrogen	LOX/Hydrogen	LOX/Hydrogen
Demonstrated Reliability	99% @ 90% Confidence	99% @ 90% Confidence	99% @ 90% Confidence
Thrust	580 klb (VAC)	580 klb (VAC)	580 klb (VAC)
Specific Impulse (I_s)	431.5 (VAC)	427.5 (VAC)	431 (VAC)
Weight	7,560 lb	7,425 lb	7,975 lb
Application	Expendable or Reusable Core or Booster	Expendable or Reusable Core or Booster	Expendable or Reusable Core or Booster
Chamber Pressure	2,250 psia	1,100 psia	2,000 psia
Control	Open Loop	Open Loop	Open Loop

Figure 10. Space Transportation Main Engine

of design features and program plans. The baseline engine concept fits well within the reliability, cost, and performance guidelines required by **ALS** vehicle concepts. However, two other cycles have been under study as well. They are the closed expander (CE) and the open expander (OE). These cycles are being analyzed and compared with each other as well as with the baseline (GG). These studies were concluded in a Design Concept Review (DCR, July 1990), where the results of all conceptual and trade studies were presented. Government (USAF/NASA) and contractor teams are currently conducting a detailed assessment which will result in a cycle selection in late August or early September 1990.

The **STME** will set new standards for high reliability, low cost, and robust features in a high-performance liquid rocket engine system utilizing liquid hydrogen fuel and liquid oxygen. The revolutionary design approach embraces the best technology and management techniques to design high quality and producibility at the expense of conservative thrust, weight and I_{sp}. Engine features include dual-thrust capability to provide engine-out failure coverage throughout the mission. Total quality management techniques such as simultaneous engineering, quality function deployment, and variability reduction, combined with new processes such as investment, castings, plasma-spray metal application, automated joining, automated assembly, and advanced materials, exemplify technologies under consideration to help make program goals a reality.

To develop, verify, and validate these manufacturing and design technologies, an extensive advanced development (ADP) research and technology program has been established in support of **STME** studies. Full-scale turbopumps, a thrust chamber, and control hardware will be built and tested to provide confidence in the results of **STME** phase A and phase B studies. Test facilities at the Air Force Astronautics Laboratory and MSFC will be upgraded to perform thrust chamber firings, and a new Component Test Facility (CTF) is under construction at Stennis Space Center (SSC) to provide turbopump testing.

Development and testing of a prototype **STME** is planned to begin in mid-FY92. This program is planned to build and test approximately six equivalent sets of **STME** hardware. A rigorous component testing program is planned on the existing ADP facilities prior to engine systems testing. Initial engine systems testing will be performed on the second position at the Technology Test Bed (TTB) facility at MSFC. Engine system testing is planned in early-FY95. Engine system and major component testing during full-scale development and production will be performed at SSC. The SSC CTF will be expanded to meet full-scale development requirements, current propulsion test facilities will be converted for **STME** use, and a new dual-position single-engine stand will be constructed. The development program will be a 90-month effort which will include research and development testing of engine components and systems, followed by a complete, rigorous verification and certification program. Studies in support of **ALS** have identified nonengine propulsion hardware as a major contributor to reliability. Therefore, **STME** testing will include parallel development of many traditional vehicle hardware elements such as flexible interface lines, thrust-vector control hardware, heat shields, and flight-configuration feedlines. This integrated development approach will culminate in core and booster cluster tests at SSC, followed by two development flight tests. These development features, along with design concepts and management approaches defined in phase A, will give the program unprecedented confidence in reliability and cost as production and operation program phases are entered.

The full-scale development effort will culminate with one test flight in late FY2000 of an **ALS** vehicle and another in late FY2001. Initial operational capability (IOC) will be reached in FY2002, with full production of the **STME** beginning approximately 1 year prior to IOC.

H.A. Cikanek/HA31
(205) 544–1461
Sponsors: Office of Space Flight, U.S. Air Force/Space Division, Strategic Defense Initiative

Space Systems

Gravity Probe-B

The Gravity Probe-B (GP-B) (fig. 11) is the **relativity gyroscope** experiment being developed for NASA by Stanford University to test two extraordinary, unverified predictions of Albert Einstein's general theory of **relativity**. The experiment will determine how space and time are warped by the presence of the Earth, and more profoundly, by the Earth's rotation, by measuring tiny changes in the spin axis of four **gyroscopes** contained in an Earth satellite orbiting at a 644-km (400-mi) altitude directly over the poles. The gyroscopes are so free of disturbances that they will provide an almost-perfect space-time reference system. These effects, though small for the Earth, have far-reaching implications for the nature of matter and structure of the universe. To accomplish the experiment requires **gyroscopes** that drift less than 1 millionth of a degree in a year.

The project has been approved for an engineering demonstration phase consisting of two distinct but complementary efforts. One is the development and test of a GP-B system ground test unit (GTU), and the other is the development and flight of a shuttle test unit (STU).

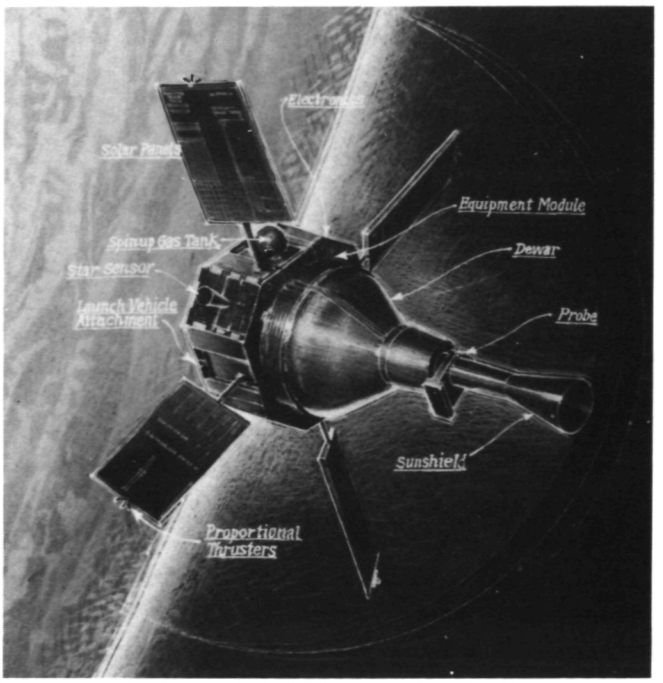

Figure 11. Gravity Probe-B

ORIGINAL PAGE IS
OF POOR QUALITY

The initial phase of the GTU activities is the first integrated system test (FIST), which includes two gyros mounted in a quartz block contained within a probe assembly. The probe assembly provides a high-vacuum environment with the necessary feed-throughs and thermal isolation. The probe fits into a liquid-helium dewar that provides the **ultralow temperature** required for superconductive and extremely stable mechanical properties. The system includes electronics for gyro suspension, spin speed, and spin-axis determination, as well as house keeping data. The design and fabrication of FIST is complete, and testing has started. The successful completion of FIST will be a major step in establishing the experiment's feasibility. The system will be upgraded to include ultralow magnetic shielding (FY91) and a science mission configuration probe and dewar (FY93).

An essential factor in gyro performance is the gyro suspension system which must be capable of operating both on the ground and in a near-zero-g environment. The shuttle test unit will test and establish the characteristics of the suspension system in the low-g environment. The STU will consist of two gyros and a section of the quartz block contained in an evacuated vessel. The unit will include the helium gas spin-up system, suspension, and other electronics necessary for experiment control and data processing. Design of the STU has been started, and a requirements review was completed in FY90. The preliminary design review is scheduled for early FY91 with the Critical Design Review in FY92.

In addition to the above activities, science mission studies have been initiated and results will be available in FY91. The studies are to identify the technology drivers and to establish the spacecraft design approach.

R. Ise/JA91
(205) 544–1962
Sponsor: Office of Space Sciences

Gamma-Ray Imaging Telescope

A potential follow-on mission to the Gamma-Ray Observatory (GRO) currently under study is a **Gamma-Ray Imaging Telescope (GRIT)** using the shuttle **external tank (ET)**. The telescope (fig. 12) will be configured on-orbit inside the LH_2 tank of the ET. A deployable 8.2-m (27-ft) diameter mirror that can fit through the 91-cm (36-in) diameter manhole will be used. Subsystems for telescope control and avionics will be mounted inside the intertank. The telescope, which could be launched in the late 1990's, has been under investigation at MSFC and the Ames Research Center. It would provide about 10 times the resolution of the GRO. MSFC has conducted extensive studies to solve technical problems which were identified during systems studies. These concerns include protection of the pressurized tank from micrometeoroid penetration and containment of secondary space debris caused by existing space debris and micrometeoroid impact with tank insulation, deorbit of the tank, thermal control, reboost, and packaging of subsystem components inside the intertank. These areas are now better understood.

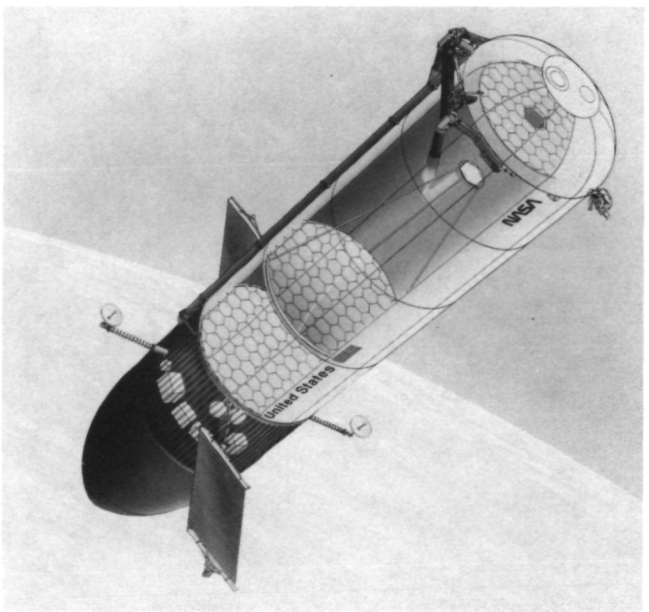

Figure 12. Gamma-Ray Imaging Telescope (GRIT)

Secondary gamma ray production in the entrance dome of the **ET** is of prime concern as a source of unwanted diffuse gamma rays. The aluminum end dome on the **ET** has a density of about 0.16 g/cm^2. This has a potential for production of a background many times that of the diffuse cosmic background, making measurements of the cosmic background impossible and reducing the signal-to-noise ratio for discrete source detection. In the present design, the trigger modules containing the anticoincident scintillators will be placed as close to the inside surface as possible, as a means of detecting either the charged primary or any charged secondaries. This should significantly reduce the background problem. A quantitative method of evaluating this background is offered by Monte Carlo programs, such as FLUKA-87, which have been developed to simulate hadronic cascades in matter. The results of an initial exploration of this problem for an idealized geometry are summarized in figure 13. This figure shows the probability of unvetoed gamma rays from proton interactions in a 0.16 g/cm^2 layer of carbon immediately adjacent and exterior to an anticoincidence shield. At each angle, a pencil beam

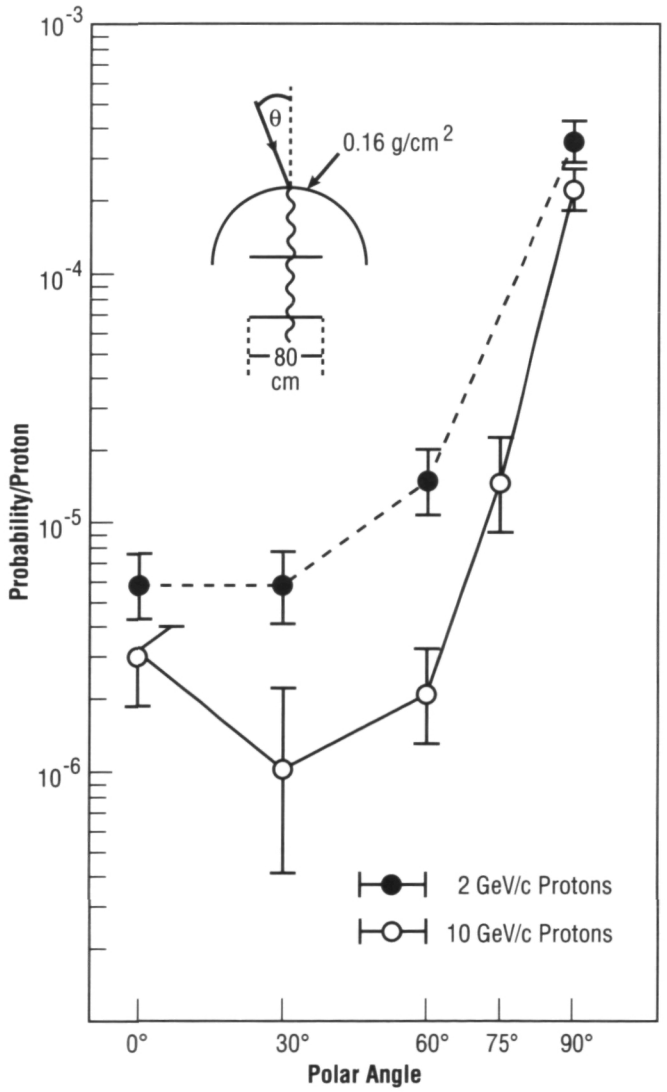

Figure 13. The Probability of Detecting an Unvetoed Background Gamma Ray as a Function of the Proton Arrival Direction for Two Proton Momenta. The Error Bars Relate to the Simulation of Between 5,000–10,000 Elastic Events Per Point and Correspond to the Detection of Between 6 and 45 Background Events Per Point.

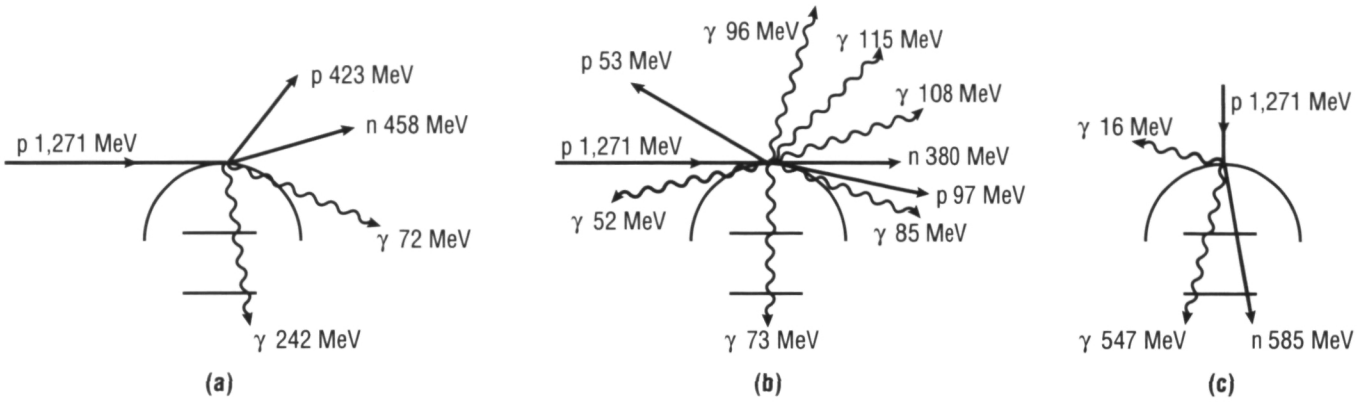

Figure 14. Examples of Unvetoed Inelastic Events for an Incident Proton Momentum of 2 Ge/Vdc (a-b) at Grazing Incidence and (c) at n or at Incidence. The Kinetic Energies of the Incident Proton and of the Secondaries Emerging From the Collision Are Indicated.

of protons is directed at the center point of the carbon layer at its apex. The background probability rises to a maximum at grazing incidence, as the chance that charged secondaries escape detection by the shield increases. Examples of two events at grazing incidence are shown in figures 13 and 14. At normal incidence, the probability is much reduced, but unvetoed gamma rays are still detected. One mechanism responsible for this charge exchange is illustrated by the event shown in figure 14c. The FLUKA-87 program has now been used by Stanford University, under a grant by MSFC, to optimize the **GRIT** design from the standpoint of minimization of unvetoed gamma-ray production. Preliminary results are quite encouraging and show that proper location of the anticoincident scintillator along the curvature of the **ET** aft dome will reduce the background count rate (at 100 MeV cutoff) to about 8 percent of the count rate, due to the extragalactic diffuse source. This is in great contrast to the predicted background rate of about 60 percent of the diffuse for the initial planar arrangement of the scintillator.

In FY90, MFSC continued the development of thin-film mirror technology, which will be required for development of this telescope.

M.E. Nein/PS02
(205) 544–0619
Sponsors: Office of Space Flight; Office of Space Science

Space Station Advanced Programs

Space Station *Freedom* advanced programs work covers the time period after the **space station** becomes operational and includes growth and/or evolution of the station. "Growth" generally implies increase in size or capability of an existing concept, whereas "evolution" connotes some change in the basic approach, direction, or broad use of a facility, including its growth. Some evolution options assume that only one **space station** is available, and evolution is accomplished by converting the original station to one having a greater capability and/or a different application. Other options involve multiple **space stations** (or derivatives) having different emphases.

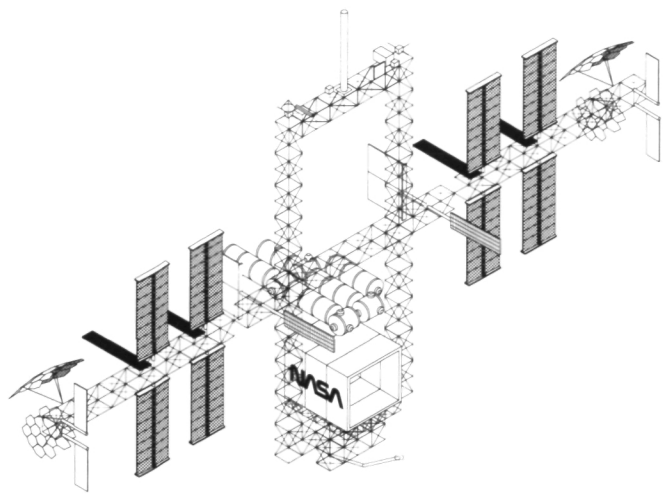

Figure 15. Time-Phased Space Station Growth

MSFC's 1990 activities in the space station growth/evolution area included **system studies** and **advanced development** tasks, as part of an intercenter effort sponsored by the Level I Space Station Engineering Office at NASA Headquarters. One principal thrust in this work has been to provide preliminary identification of potential "hooks and scars," which would have to be implemented early on the baseline Space Station *Freedom* to allow subsequent growth/evolution with minimum impact. This data was provided in time to support the appropriate S.S. *Freedom* preliminary design reviews which were in progress in FY90.

One concept of an evolutionary space station is provided in figure 15. This concept has some R&D capability, but other concepts have a transportation node emphasis. Other concepts emanating from the current overall effort have different mixes of R&D and transportation node emphasis. Each type of station is responsive to different types of user requirements, and it is not yet clear which trend will dominate in the early time frame after the initial Space Station *Freedom* becomes operational. Thus, one goal of the advanced programs activity is to identify the potential modifications to the initial station, which would allow maximum growth/evolution flexibility.

Systems studies in FY90 have examined logistic systems evolution and **environmental control and life support system (ECLSS)** evolution. In these studies, various concepts of each of the systems, encompassing a range of different sizes, technologies, and capabilities, were examined. Several versions of growth/evolutionary space

stations embodying increases in size, technology level, mission accommodation, capability, and/or quantity, were considered in these assessments, and implications of such evolution were defined. Potential hooks and scars were identified in each area of study.

Another area of study has been the evolution of manned **modules**. Various types of modules were examined, including attached and free-flying pocket labs and various concepts of **modules** having externally attached payloads. A limited assessment of potential pocket lab user requirements was made, and resource requirements for different concepts were determined.

Advanced development work was done in the areas of advanced automation of the **ECLSS** and the power management and distribution system, and in digital optical computer concepts. The work done in these advanced development tasks involved implementation of preliminary hardware/software concepts into test beds, models, and simulation equipment to verify concepts. Since the size and complexity of space systems is increasing dramatically, effective use of automation and robotics will be necessary for the Space Station *Freedom* program and other related projects to ensure effective systems management and to conserve scarce crew time and other resources.

J.M. Butler/PS04
(205) 544–4833
Sponsor: Office of Space Station

Geostationary Earth Observatory Program

The **Geostationary Earth Observatory (GEO)** program consists of multiple **GEO's** which will be used to track global environmental change and provide data concerning the complex interactions among the land, sea, and atmosphere. Geostationary orbit affords opportunity for obtaining excellent temporal coverage of these processes. The **GEO** program is an integral part of the Mission to Planet Earth (MPE) initiative, which calls for several large, new, Earth-monitoring spacecraft to be developed and launched by the late 1990's. Preliminary thinking is that three of the five **GEO's** will be developed by the United States, and the others will be provided by Japan and Europe. Each **GEO** will provide the advantage of continuous environmental data coverage of an entire Earth hemisphere, supplementing data from polar orbiters which can see only some parts of the globe at intervals of several days. Data collected from all MPE spacecraft will provide information necessary for an integrated model of the Earth to predict the future course of the global environment.

In 1990, MSFC continued in-house and contracted studies on the **GEO** program and initial **observatory**, in parallel with several instrument studies. Several concepts for the initial **observatory** were explored, based on preliminary "strawman" science instrument complements. These instrument complements allow the Earth to be viewed as a total system. Instruments are grouped into three classes, based on their application. The first class is facility instruments, which will provide observations that are multidisciplinary. Some of these instruments are similar in measurement capability to those on the Earth-observing system polar **observatory**. The second class of instruments will support operational requirements for Earth, atmospheric, and solar measurements. The third class consists of principal investigator instruments which will allow unique measurements of Earth-system processes.

Figure 16 shows a typical **GEO** concept in deployed on-orbit configuration that will accommodate the science instruments identified by the Science Steering Committee. This configuration weighs about 5,409 kg (11,900 lb), including 13 payload instruments with a total weight of 1,603 kg (3,527 lb). The **GEO** is sized for a 10-year life. Over the lifetime of the **observatory**, all of the instruments are assumed to operate continuously, while providing their own means of thermal control. As more details of the payload complement and the individual science instruments become known, **GEO** concepts will be refined. Since geostationary orbital emplacement and activation of the initial **GEO** will not require crew support, the **GEO** is a candidate for launch on an expendable launch vehicle. The Titan IV with Solid Rocket Motor Upgrade and Centaur G-Prime Upper Stage is the current baseline launch vehicle for the initial **GEO**. In the future, payload instruments may grow in weight and perhaps in dimension. Advanced launch vehicles, such as the Shuttle-C, could be used in place of the Titan IV, should they become available. The Shuttle-C, with an appropriate upper stage, would increase significantly both the volume and payload delivery capability.

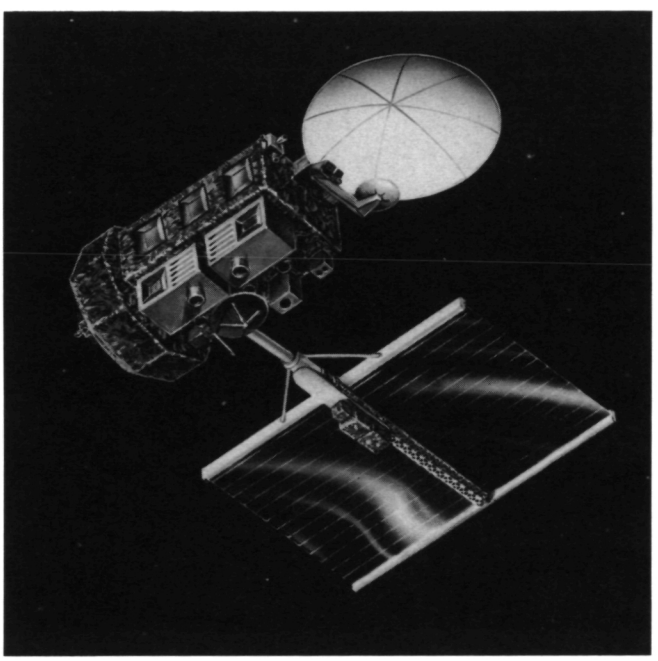

Figure 16. Earth Science Geostationary Platform Typical Concept

GEO pointing stability is a major design driver and has a significant effect on current stringent instrument pointing and stability requirements. **GEO** structures and guidance, navigation, and control (GN&C) system operation will determine whether some of the instruments must be equipped with their own pointing mounts or image motion compensation devices.

One of the major challenges of the MPE program is to integrate and manage the flow of data from all sources, such as the **GEO**, polar observatories, space station instruments, and Earth probes. Since this is an international program, information must be disseminated to scientists around the world in a timely manner. Concepts of the **GEO** data system capable of handling data rates of up to 100 megabits per second are being assessed. The **GEO's** may also be interconnected by optical communication data links to facilitate large data flows.

J.M. Butler/PS04
(205)544–5833
Sponsor: Office of Space Science Applications

Controls, Astrophysics, and Structures Experiment in Space

The Controls, Astrophysics, and Structures Experiment in Space (CASES) is an experiment in **controls structures interaction** that also provides accommodations for an important astro/solar physics experiment. CASES will provide a large flexible structure (32-m (105-ft) deployable boom) and instrumentation for characterizing its zero-gravity dynamic behavior. This information will be contrasted with math models and results from ground-based simulations. The deployable mast is equipped with a set of small cold-gas thrusters and two sets of angular momentum exchange devices (AMED's). The AMED's are sets of measuring devices (rate gyros) and actuators (momentum wheels) which are located on the boom tip and at approximately 30 percent of the boom length. The gas jets are very low thrust, less than one pound, but with the 32-m moment arm supplied by the boom, the attitude of the shuttle and boom can be controlled and pointed in any desired direction. The AMED packages control the flexible body-bending models.

CASES provides very accurate pointing of an astrophysics/solar hard **x-ray imaging** experiment. This experiment will address important issues in high-energy astronomy, such as the nature of the energy source seen at the galactic center and the energy release mechanisms in solar flares.

The MSFC inhouse preliminary definition study demonstrated feasibility of the CASES concept and, currently, two contracted phase B studies are being managed at MSFC. A CASES ground test facility (GTF) is under construction at MSFC and will be used to support design of the CASES experiment.

Significant accomplishments in FY90 include progress on the GTF and completion of a pair of contracted phase B studies.

J.R. Dabbs/PS02
(205) 544–0623
Sponsor: Office of Aeronautics and Space Applications

Pinhole Occulter Facility

The Pinhole Occulter Facility (POF) is a solar-oriented collection of instruments mounted on the Spacelab instrument pointing system (IPS) mounted in the shuttle cargo bay. It utilizes a long, deployable structure (50 m (164 ft)) to position an external occulter (also called a mask) to provide a "man-made solar eclipse" for white light and UV coronal telescopes. This optical geometry allows larger optics, lower stray light levels, and, therefore, a dynamic range very low and much farther out in the corona. This mask also contains x-ray apertures coupled with large, proportional counters to image hard-x rays to study high-energy processes on the solar surface. The large separation needed for these imaging techniques (uniform redundant array and fourier-transform imaging) require the use of the 32-m (105-ft) boom. The x-rays will be imaged to subarc-second resolution and in higher energies than previously possible. The coronal observations will be with higher spatial resolution, much greater dynamic range, and much nearer the solar limb than ever before possible. These observations, especially those closer to the surface, are of major importance in the modeling of energy-release mechanisms for solar flares, and also for studies of energy transport mechanisms in the low corona. The availability of the POF as a high-resolution **x-ray imaging** tool and as a high-resolution, wide-scale white light and ultraviolet coronal facility provides the technological advances necessary for the next generation of solar studies.

The POF has been proposed for additional study as an attached payload for Space Station *Freedom*. It is one of several solar instruments that will eventually make up the Advanced Solar Observatory (ASO).

During FY90, conceptual studies of the science instruments and science objectives as an attached Space Station *Freedom* payload were continued. In FY90, a computer simulation of the X-Ray Imaging Detector was developed as a testbed of the Fourier-Transform Imaging Experiment on the POF. The aspect sensor subsystem was breadboarded in FY90. An accommodation study of the POF as a space station-attached payload will be completed in FY91.

J.R. Dabbs/PS02
(205) 544–8668
Sponsor: Office of Space Science and Applications

Electrical Power System Fault Study

Marshall Space Flight Center proposes to implement computer-controlled fault injection into an electrical power system breadboard to study the reactions of the various control elements of this breadboard. Elements under study include the remote power controllers (RPC's), the algorithms in the control computers, and the artificially intelligent control programs which are resident in this breadboard. To this end, a study of electrical power system faults is being performed to yield a list of the most common power system faults. The results of this study will be applied to a multichannel high-voltage dc spacecraft power system called the **large autonomous spacecraft electrical power system (LASEPS)** breadboard (fig. 17).

The **LASEPS** breadboard is being created out of two existing breadboards: the autonomously managed power system (**AMPS**) breadboard and the space station module power management and distribution (**SSM/PMAD**) breadboard. The **LASEPS** breadboard will create a complete power system breadboard from the loads to the power generation and storage.

The data used in the electrical power system fault study has come from both terrestrial and aerospace sources. The fact that the terrestrial systems are ac and the aerospace systems are dc has made little difference in the type of faults experienced within the distribution systems, as long as the voltage level of the terrestrial system is below 20,000 Vac. Above this voltage level, the terrestrial systems mainly see hard faults or shorts. Within the lower voltage range of the ac systems, similar problems are seen with "soft" faults, as well as hard faults within the distribution systems and in the loads, as are seen in the space systems. A soft-fault condition is one where there is a small leakage current loss in the system that is not large enough to cause hardware circuit breakers to trip.[1]

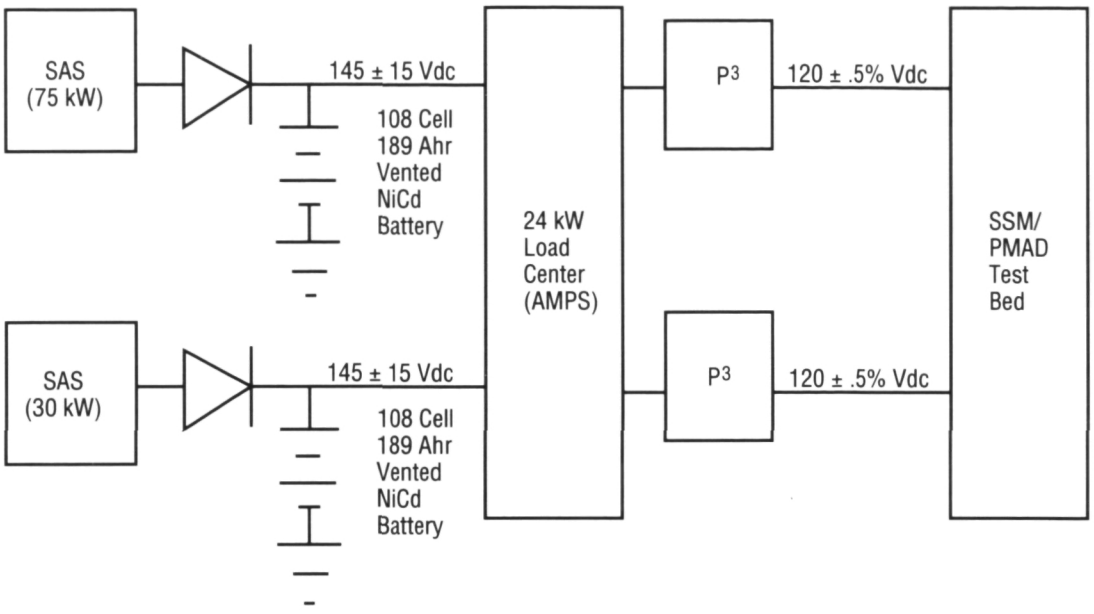

Figure 17. Large Autonomous Spacecraft Electrical Power System (LASEPS)

The most common fault which is recorded in electrical power systems is a fault in the terminal-end user load. Some of the other common faults found in electrical power systems are:

- Short of bus to neutral or return
- Short of one bus or line to another
- Soft shorts of bus or line to return or ground
- Loss of ground to neutral connections
- Multiple neutral to ground connections
- Bus switch short
- Bus switch open
- Short of load to neutral or return
- Short of load to chassis or earth ground
- Open circuit failure of load
- Soft short of load.

It was found during the study that an analogy can be made between the neutral of the three-phase ac power lines and the return of the dc lines, as well as the earth ground of the ac systems to the chassis ground in a dc system. Henceforth, the references to the neutral and return and the references to earth ground and chassis ground in the above list refer to these analogies.

In the power generation and storage, most of the data are still being collected. The source of these data is primarily from aerospace applications, although there are some limited terrestrial uses of

solar array and battery systems where information may be found. Some of the faults which may be implemented in the breadboard in this area include:

- Solar array degradation
- Solar array panel short
- Solar array panel open
- Solar array electromagnetic interference
- Solar array parasitic plasma current power loss
- Solar array corona discharge
- Isolation diode short
- Isolation diode open
- Battery undercharge
- Battery cell short
- Battery cell open.

Many of these faults will be implemented by software simulation or control since the solar arrays are simulated and the battery operation is computer controlled.

[1]Gholdstom, E. W., and Cecka, J. R., "Use of a Distributed Microprocessor Network for Control of the Space Station Electrical Power System," 1987 IECEC Vol. 1, pp. 522–527.

[2]Dugal-Whitehead, N. R., and Lollar, L. F., "Fault Analysis of Multichannel Spacecraft Power Systems," 1990 IECEC, in press.

N.R. Dugal-Whitehead/EB12
(205) 544–3304
Sponsor: MSFC Center Director's Discretionary Fund

Tether Applications in Space

Tether Applications in Space (TAS) studies and experiments are aimed at defining and developing ways to use **tethers** in space. These activities have been underway for a number of years and some, like the **Small Expendable Deployer System (SEDS)**, have reached the hardware stage.

SEDS is a lightweight, spinning-reel-type system designed to deploy a payload attached to the end of a 20-km (12-mi) long **tether**, which is cut and discarded after use. First flight objectives are to validate the design concept and study the dynamics of **tether** deployment. SEDS weighs about 39 kg (85 lb), including the tether weight of 7 kg (15 1b). The **tether** is made from a high-strength, low-density, polyethylene fiber called SPECTRA. **SEDS** will fly on a Delta II launch vehicle in late 1991. Hardware development was completed in 1989 on the mechanical systems. These were tested in early 1990. The electrical system was completed and tested in 1990. Analysis and planning leading up to the physical integration of **SEDS** into the Delta II began in 1989 and will continue until the launch.

During flight, the payload, weighing 23 kg (50 1b), will be deployed toward Earth. Payload instruments are an accelerometer, tensiometer, temperature sensor, and a magnetometer (for orientation information). The experiment will last about 2 hours, ending when the **tether** is fully deployed and has swung to a near-vertical position, pointing toward Earth. The **tether** is then cut, allowing it and the payload to re-enter Earth's atmosphere. The **SEDS** concept is shown in figure 18.

Numerous future applications of **SEDS** are being considered. One is the routine deorbiting of Space Station *Freedom* waste materials, packaged in

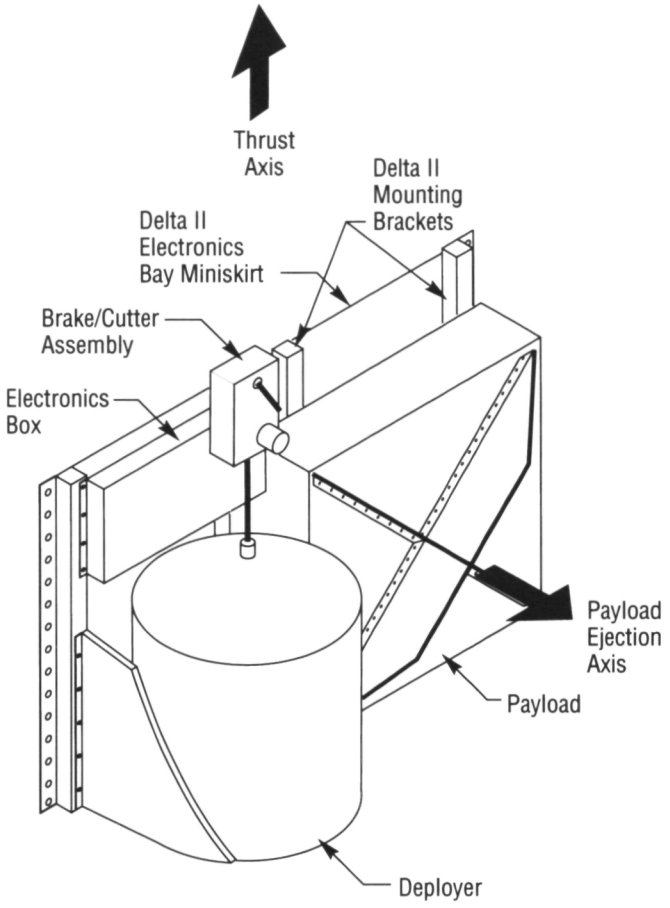

Figure 18. Small Expendable Deployer System Components and Configuration

lightweight containers that can be folded for easy storage during shuttle trips to the station. Another is the generation of **artificial gravity** in a small capsule at the end of the **tether**. This is done by slowly spinning the **tether** with masses at each end, i.e., the capsule and a propulsive device. The most obvious use of **SEDS** will be to place instruments in the 90- to 120-km (56- to 75-mi) altitude region for upper atmospheric research.

J.K. Harrison/PS04
(205) 544–0629
Sponsor: Office of Space Flight

Tumbling Satellite Retrieval

The high cost of NASA orbital assets requires the development of a system capable of recovering failed **spacecraft** for repair/servicing. The requirement for such a system also derives from the need to remove spacecraft at their end of life and to mitigate the propagation of orbital debris.

With the availability of an orbital maneuvering vehicle, the potential for **retrieving** satellites will be greatly enhanced. Such a vehicle would be capable of docking to relatively stable **spacecraft** with compatible interfaces and returning them to the shuttle. Recent studies identify the need for a **Tumbling Satellite Retrieval (TSR)** kit as a growth/delta capability configuration, which would facilitate the recovery of unstable/failed **spacecraft** and orbital debris without predetermined interfaces.

The work performed to date has resulted in the design, fabrication, and initial testing/evaluation of the **TSR** ground demonstration hardware. The ground test series has demonstrated the feasibility of the **TSR** satellite capture and provided data which will aid in the resolution of technical issues necessary for proceeding to a high-fidelity ground demonstration and, ultimately, to a flight demonstration.

Test activities are continuing in MSFC's robotic laboratory to further refine system controls, sensors, pilot display, and control input requirements.

The **TSR** ground demonstration system is pictured in figure 19. Figure 20 is an artistic representation of the **TSR** as it might appear supported by an orbital maneuvering vehicle/space tug approaching a disabled **spacecraft**.

J.R. Turner/PS01
(205) 544–0617
Sponsor: Office of Space Flight

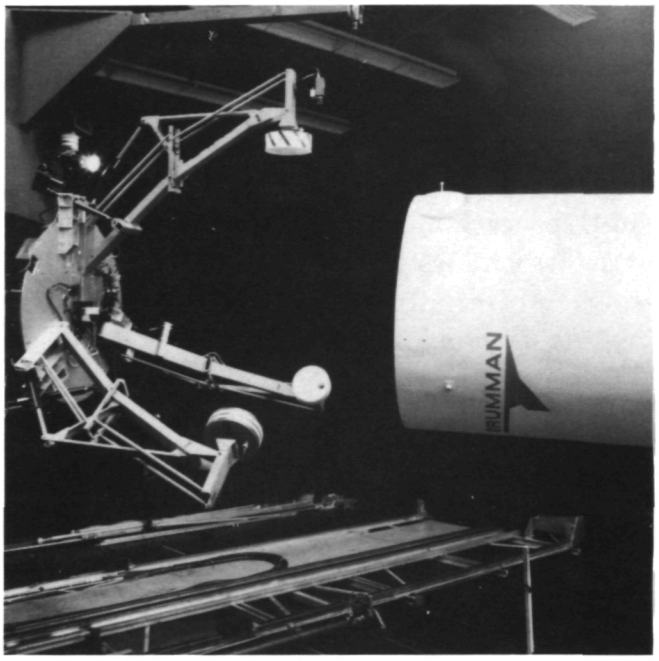

Figure 19. TSE Ground Demonstration System

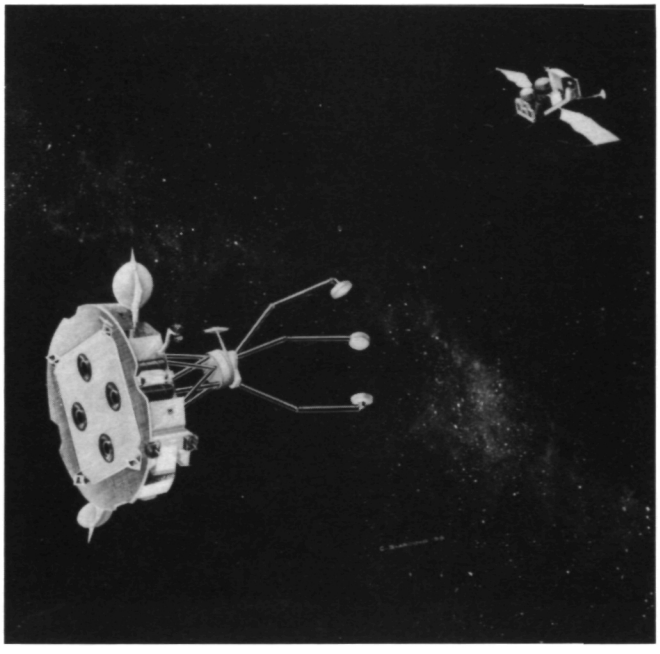

Figure 20. TSR Integrated With an Orbital Maneuvering Vehicle/Space Tug

Long Duration Exposure Facility Dose Predictions and Measurement

Over the last several years, MSFC has had an ongoing effort modeling the high-energy radiation environment for spacecraft in low Earth orbit. Experimental results of measured radiation doses are currently becoming available from the **Long Duration Exposure Facility (LDEF)** spacecraft for comparison with the model predictions. The LDEF spacecraft flew in a 28.5° inclination circular orbit with an altitude in the range of 175 to 258.5 nmi. It was gravity-gradient stabilized and oriented so that one side always pointed along the velocity vector. Both the altitude and orbit are similar to those planned for Space Station *Freedom*. For this orbital altitude and inclination, two components contribute most of the penetrating charge **particle** radiation encountered—the galactic cosmic rays and the geomagnetically trapped Van Allen protons, but the protons contribute the majority of the dose deposited. Where shielding is less than 1.0 g/cm^2, geomagnetically trapped electrons also make a significant contribution. All three sources are strongly modulated by Earth's **magnetic field**. Almost all the trapped flux will be encountered in the region called the South Atlantic Anomaly, produced because Earth's **magnetic field**, though approximately dipolar, is not centered on Earth. The particles follow a helical path about a **magnetic field** line. As the field intensity increases, both the diameter and the pitch of the helix decrease until the pitch becomes zero. The point with zero-angle is called the mirror point, and the center of the helical path is called the guiding center. From here, the helix reverses direction and **particles** travel up the field line toward decreasing field intensity and away from Earth. In the South Atlantic Anomaly, almost all the **particles** observed are near their mirror points. Most of the flux is arriving from a narrow band perpendicular to the local geomagnetic

field direction. The current environment model in use is the "Vette" model[1,2] together with the associated **magnetic field** models. Given an orbital trajectory, the field models yield the **magnetic field** coordinates B and L. Given the B and L along the trajectory, the Vette model yields the omnidirection flux along the trajectory as a function of energy. The proton environment used was AP8MIN[2], the electron environment was AE8MIN[2], and the **magnetic field** model was the IGRF 1965.0 80-term projected to 1964, the epoch of the environmental model. The Vette proton models have a large uncertainty (a factor of two in values of flux). The electron models have an even larger uncertainty (a factor of six). To obtain the **LDEF** mission fluences, we calculated long-term average fluxes for five circular orbits at 258.5, 255.0, 249.9, 230.0, and 172.0 nmi altitude, which occurred on mission days 0, 550, 1,450, 1,950, and 2,105, respectively, and did a numerical integration over time, assuming a straight line between time points.

The mission proton doses were obtained from the mission fluences using the Burrell proton dose program, which is based on the "straight-ahead" and "continuous-slowing-down" approximations for transporting the protons. Two simple geometries were used—a point tissue receiver material at the center of a spherical aluminum shell, and a point tissue receiver material behind a plain aluminum slab with infinite shielding behind the receiver. For the electron and Bremsstrahlung dose, we used the MSFC electron dose program which is based on fits to data from the ETRAN electron Monte Carlo program. It only performs the slab geometry. As an estimate for the spherical shell geometry we doubled the slab results, which underestimates the actual result.

In figure 21, the calculated results are compared to preliminary measurements from experiment P0006 by Dr. Gene Benton[3] of the University of San Francisco. At each depth, there are two measurements

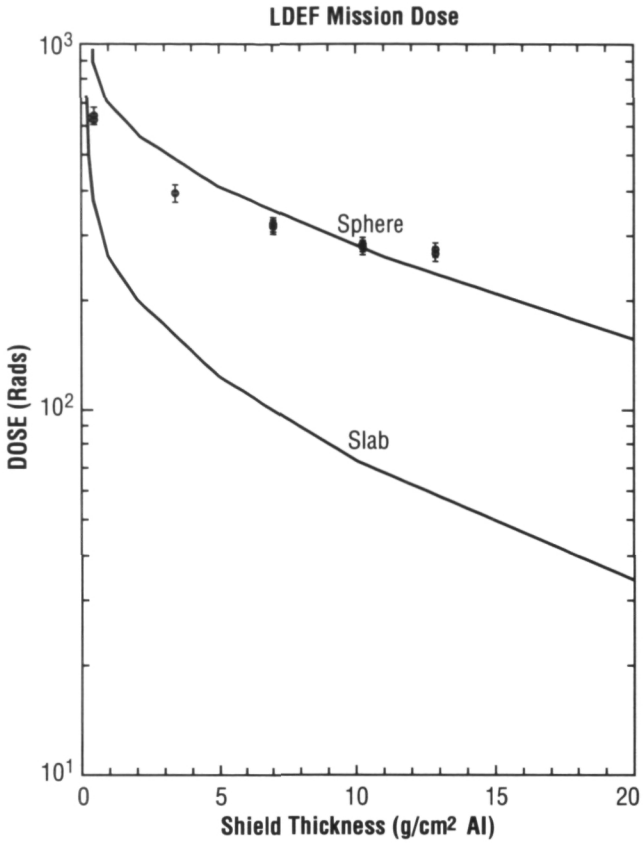

Figure 21. LDEF Mission Doses

with type-200 and type-700 thermoluminescent detectors (TLD's). The P0006 packages were located on the western side of the spacecraft where the east-west effect should produce the highest doses. (The calculations assume an isotropic angular distribution of the flux.)

[1]Sawyer, D.M., and Vette, J.I., "AP–8 Trapped Proton Environment for Solar Maximum and Solar Minimum," National Science Data Center, Goddard Space Flight Center, *NSSDC/WDC-A-R&S 76–06*, 1976.

[2]Teague, M.J., and Vette, J.I., "A Model of the Trapped Electron Population for Solar Minimum," National Science Data Center, Goddard Space Flight Center, *NSSDC 74–03*, 1974.

[3]Benton, G., Private Communication, 1989.

J. W. Watts/ES62
(205) 544–7696
Sponsor: Office of Space Science and Applications

Future Lunar Science Missions

The lunar surface provides a stable base for large science projects that cannot be otherwise accomplished either on Earth or in space. The absence of an atmosphere makes it ideally suited for cosmic-ray, space physics, neutrino experiments, ultraviolet (UV), optical, and infrared (IR) astronomy research. Its location relative to Earth is ideal for magnetospheric imaging and sounding. Several missions being studied by MSFC utilizing this unique science environment are discussed below.

The combination of high resolution, low background, wide bandwidth, wide field, stable operation platform, and excellent viewing provide a compelling scientific basis for developing a **large lunar telescope (LLT)** with an aperture of about 16 m, operating in the UV/visible/IR wavelength regime. A 10–16-m filled-aperture, passively cooled, diffraction-limited telescope placed on the Moon would have unprecedented powers to address a wide range of the most fundamental astrophysical problems, including the detection of planets around neighboring stars.

An in-house study is defining a baseline **LLT** design and identifying critical issues relating to its fabrication and placement on the lunar surface. Key technology enabling areas with impact on telescope design are being identified. FY91 Research and Technology Objectives and Plans (RTOP's) have been submitted to define the studies required to resolve the complex interfaces between the **LLT** observatory, the lunar base, and other Space Exploration Initiative (SEI) elements.

The lunar calorimeter mission has two objectives of importance to the cosmic-ray physics community: (1) exploration of the composition of cosmic-ray nuclei with energies in excess of 10^{15} eV, and (2) determination of the sources and acceleration mechanisms of the high-energy cosmic rays. The measurements necessary to achieve these objectives can be accomplished only on the Moon for two reasons. First, the cosmic rays of interest do not interact with Earth's atmosphere, thus losing their character, and second, the mass required for efficient operation of the detector can be obtained from the lunar regolith, eliminating the need to transport tons of material through space from Earth.

The neutrino telescope will search for a diffuse flux of heavy neutrinos, a directional flux of weakly interacting massive particle annihilation products from Earth and the Sun, and for discrete sources of cosmic neutrinos. The detection of these neutrinos would have exceedingly important implications for particle physics and cosmology. For reasons similar to that of the lunar calorimeter, the neutrino measurements can best be performed on the Moon. Existing neutrino detectors in large Earth-based underground caverns are extremely inefficient and may not even be capable of measuring the neutrino flux of interest due to the cosmic-ray-induced background.

A lunar-based magnetospheric imaging system would be able to study the high-temperature plasma of Earth's magnetosphere, the structure and dynamics of the magnetospheric plasma boundaries, geotail plasma and plasmoids, and would allow investigations of the Sun-Earth interaction regions and their dynamics. The Moon provides excellent geometry for plasmasphere, ring current, and geotail viewing, and is stable enough for very high-resolution measurements that would be difficult to obtain under other conditions (free-flying satellite, etc.).

The scientific goals of a lunar-based **magnetopause** sounder include active soundings of the **magnetopause** boundary using dipole transceiver arrays

with pulse/coded outputs. These soundings would allow the determination of the plasma gradients in the **magnetopause** boundary layer, boundary motions, the waveguide propagation characteristics of the magnetosphere, and the changes in the magnetospheric tail configuration and magnetic flux caused by external forcing and internal processes.

A lunar solar observatory would include a variety of instrumentation to investigate the basic plasma physics processes responsible for the metastable energy and impulsive energy release in solar flares. More fundamental research would be conducted into the cause of the solar activity cycle and the factors that control the structure and behavior of the solar magnetic field, photosphere, chromosphere, and corona. A most useful capability for the lunar solar observatory would be flare alert and warning for the lunar base.

C.L. Johnson/PS02
(205) 544–0614
Sponsor: Office of Space Science and Applications

Aeroassisted Orbital Transfers

A research study into using the upper regions of Earth's atmosphere to slow down (**aeroassist**) a spacecraft returning from geosynchronous orbit, the Moon, or Mars has been conducted by Rice University (Dr. Angelo Miele) and sponsored by the Aeroassisted Flight Experiment (AFE). The research study results are summarized in a report.

In the report, optimal trajectories for the AFE vehicle are derived and suggestions made to implement a guidance system for the atmospheric phase of flight.

The results were surprising in that only one reversal of the lift vector was required of the **optimal trajectory**. A series of four reports was published from this research effort. The research has direct application to the Lunar/Mars Initiative program.

Miele, A., Wang, T., and Lee, W.Y., "Optimization and Guidance of Trajectories for Coplanar, Aeroassisted Orbital Transfers," 1989.

A.W. Deaton/EL58
(205) 544–2247
Sponsor: Small Business Innovation Research

Superconducting Gravity Gradiometer

Precise knowledge of Earth's global gravity field is essential to geophysics, oceanography, and geodesy. In addition, such information will play a key part in addressing those scientific and environmental questions which concern the integrated functioning of Earth as a system. The acquisition of this knowledge is being supported through NASA's geodynamics program, which strives to understand the structure, composition, and dynamics of the solid Earth through the use of satellite technology. The **Superconducting Gravity Gradiometer (SGG)** is an instrument which holds great promise for making sensitive gravity measurements to meet these needs. Figure 22 demonstrates the evolution of this device.

The **SGG** instrument, being developed at the University of Maryland, will measure the global **gravity** field to 2–3 mgal ($1\ gal = 10^{-2}\ ms^{-2}$) precision and 50-km (31-mi) resolution. Newton's inverse square law of gravitation and the Lense-Thirring effect of general relativity might also be tested by the **SGG**. This advanced **gradiometer** has been under development since 1980 through NASA, Air Force, and Army sponsorship.

The flight instrument will consist of a three-axis **SGG** integrated with a superconducting six-axis **accelerometer** (SSA). The SSA is required to measure the linear and angular accelerations of the

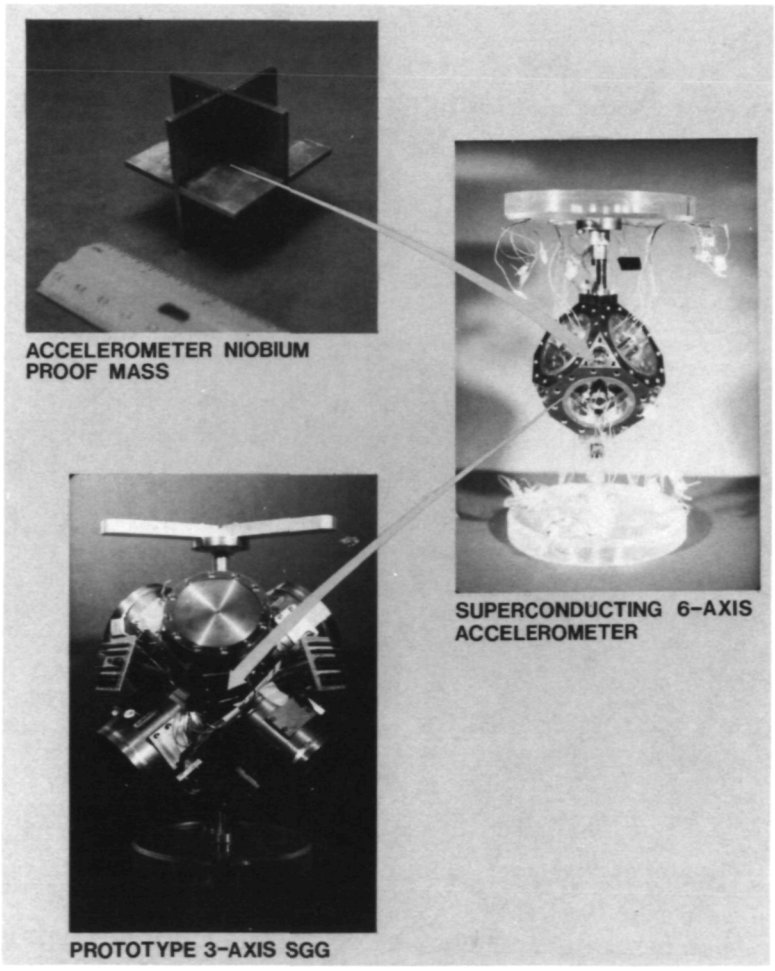

Figure 22. Superconducting Gravity Gradiometer Evolution

ORIGINAL PAGE
BLACK AND WHITE PHOTOGRAPH

instrument platform. The SGG gravity gradient design goal sensitivity is 3×10^{-4}E Hz $^{-1/2}$ (*where* E = 10^{-9} cm^{-2}).

Testing was completed on the single-axis **gradiometer** unit after an extensive effort to reduce laboratory background noise. The noise reduction effort has led to a magnetic suspension technique, and the instrument has been shown to exhibit a fundamental sensitivity approximately two orders of magnitude beyond that of conventional room temperature **gradiometers**. Based on the single-axis results, the construction of a three-axis unit was completed and is undergoing extensive laboratory tests. The six-axis superconducting **accelerometer** was constructed and dynamic error analysis obtained.

The performance of the three-axis model II **gradiometer** around 0.2 Hz has been improved an order of magnitude by applying three-axis residual balance techniques. The model III single-axis system has been operated and integrated with the model III six-axis superconducting **accelerometer**.

MSFC has led a study in the preliminary definition of a free-flying **SGG** science mission. A low-altitude orbit (160 km (99 mi)) must be selected for the mission to provide the desired measurement accuracy. A feasibility study is currently underway to determine if the European Space Agency's (ESA's) Eureca spacecraft will provide a suitable environment for a short-duration flight test of the instrument at a higher altitude.

Moody, M.V., Chan, H.A., and Paik, H.J., "Superconducting Gravity Gradiometer for Space and Terrestrial Applications." *J. of Appl. Physics*, Vol. 60, No. 12, pp. 4308–4315, 1986.

Morgan, S.H., and Paik, H.J., "Superconducting Gravity Gradiometer Mission." Vol. I, Study Team Executive Summary. NASA TM-4091.

C.L. Johnson/PS02
(205) 544–0614
Sponsor: Office of Space Science and Applications

Data Systems

The TOPO Plot: A Data Reduction/Graphics Routine for Tracking Spectral Trends in Vibration Data

In support of space shuttle main engine (SSME) development and advanced technology test programs, a number of sophisticated diagnostic algorithms have been integrated into the Operator Interactive Signal Processing Systems (OISPS) operational on MSFC's Structures and Dynamics Laboratory computers. These include nonlinear spectrum analysis, adaptive filtering, envelope detection, and other analytical methods applicable to specific SSME mechanical symptom detection and identification investigations. For quick-look data assessment, the (linear) **power spectral density (PSD)**, isoplot, and root-mean-square (rms) time history of a measurement are the most basic and valuable computational tools. When viewed in the context of empirical statistical data representing SSME component measurements obtained under similar operating conditions, these analyses can provide a quick, qualitative indication of component "health" (from a dynamics standpoint) and signal any gross deviations from nominal operation.

The most fundamental "**signature**" used to characterize an SSME **vibration** (acceleration, pressure, strain, etc.) measurement is the mean-square density spectrum, or power spectral density. Figure 23a illustrates an isoplot, or family of spectra, from a strain gauge measurement representing 450 seconds during a hot-firing test. The **PSD** provides a detailed snapshot of conditions over an interval of (usually) constant power operation. In contrast, the isoplot yields a more qualitative indication of amplitude/frequency trends over a complete hot-firing test or powered flight. These plots are particularly useful for detecting the *time* of any significant deviations in the **vibration signature** and correlation with engine operating parameters (power profile, programmed venting, etc.). Figure 23b shows an alternate format.

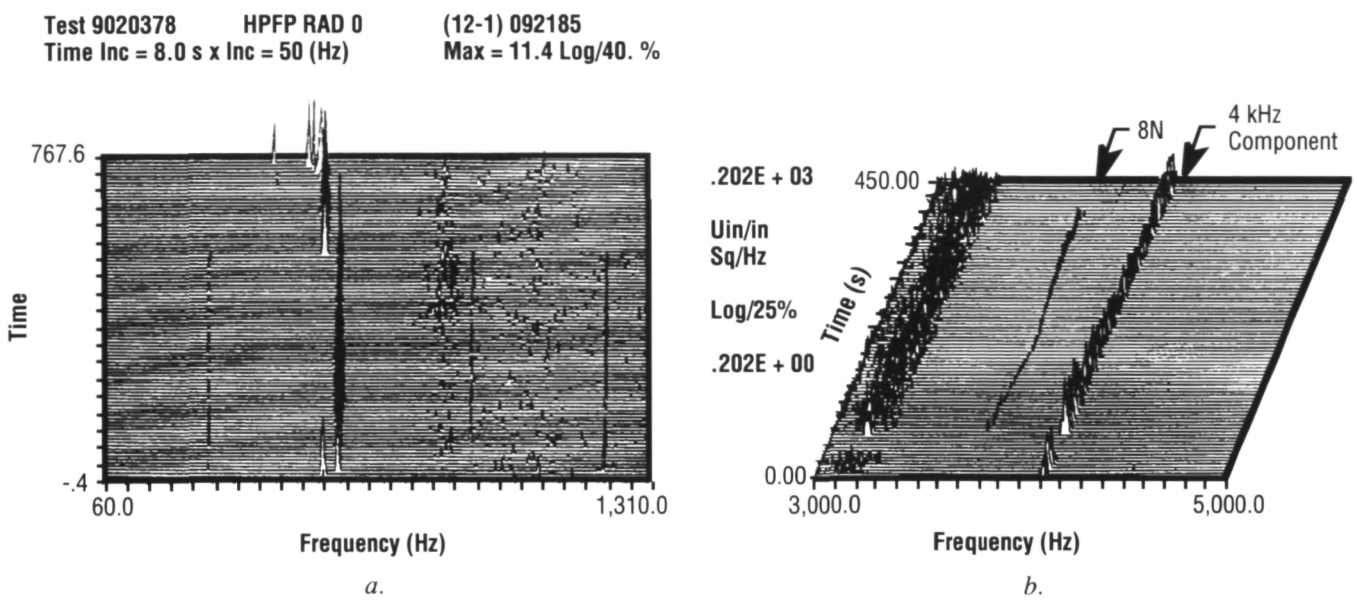

Figure 23. Illustration Isoplot Format

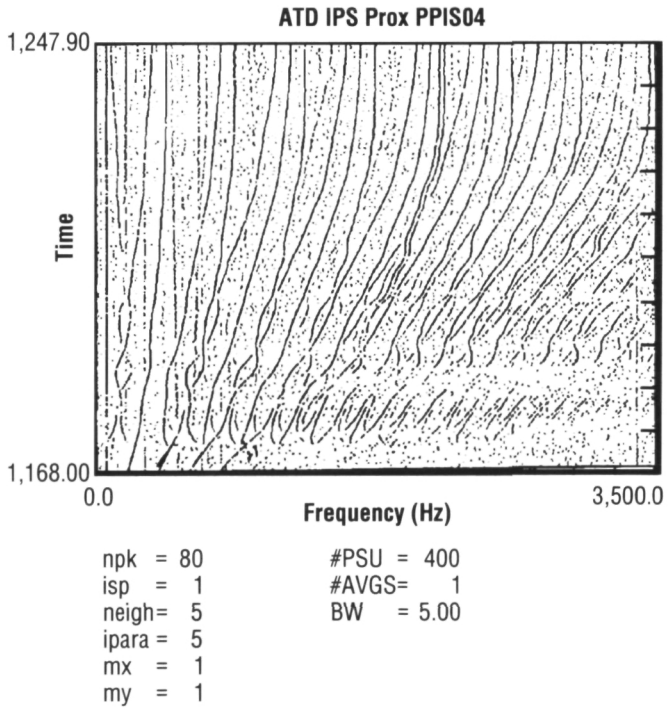

Figure 24. TOPO Plot of Bearing Displacement During Speed Change

The **PSD** isoplot has been used extensively to display spectral components in a frequency/time/amplitude format. This display is especially useful for nonstationary data, which allows one to trace any particular frequency component as a function of time. However, there are several limitations to the procedure.

- For clarity, a threshold level has to be chosen when plotting an isoplot in which some possibly significant peaks with **PSD** amplitude lower than the threshold are excluded.
- For a nonstationary case, when manned **PSD** peaks are crowded together, or crossover occurs, it is difficult to identify the trace of some peaks. Then, it is necessary to subdivide the entire frequency range into several smaller ranges and plot the results separately.
- The number of **PSD's** which can be legibly displayed in an isoplot is limited to approximately one hundred.

To provide improved tracking of spectral trends, a new method called "**TOPO**" (for Topographic Plot) was developed and programmed. The method uses a novel peak-identifying routine to pick out all meaningful peaks in each **PSD** and assign a "peakyness" parameter for each identified peak. Each peak is then plotted on a **TOPO** plot as a dot whose width is proportional to the "peakyness" parameter associated with the peak. Figure 24 is an example of bearing test data during ramp-up. Four hundred **PSD's** are plotted in this figure, and the non-stationary and crossover can be clearly visualized.

The **TOPO** plot technique has been integrated in the OISPS program and is in routine use for SSME data evaluations. For computerized data base application, the technique provides significant data compression since only spectral peak values need be stored. Enhancements in the graphic output format, to aid in data interpretation, are presently under evaluation, including color coding of amplitude ranges.

Coffin, T., Swanson, W.L., and Jong, J.Y., "Data Analysis Methods and Signal Processing Techniques for Space Shuttle Main Engine Diagnostic Evaluation," Wyle Laboratories Final Report Under Contract NAS8-36549, October 1989.

J.E. McBride/ED23
(205) 544–1523
Sponsor: Space Shuttle Main Engine Office

WetNet: An Interdisciplinary Information and Research Data System

WetNet is an **Earth science** information and data analysis system. The WetNet system is oriented towards the acquisition, management, archival, distribution, analysis, and display of meteorological data relevant to the study of the global moisture cycle. The name "WetNet" was formulated from two primary aspects of the system. The first is the emphasis on the study of the water cycle, i.e., "Wet," while the "Net" is an abbreviation of the word **network**, which implies the linking of the remotely based scientists. The goal of WetNet, therefore, is to provide a data analysis system which will enhance the research environment in the Earth's **hydrologic cycle** and promote a collegial atmosphere for algorithm development among a diverse group of interdisciplinary Earth scientists.

Remote sensing, from space, of all phases of the water cycle has become more sophisticated as more advanced instruments are placed into operation. One of the more recent instruments is the **Special Sensor Microwave/Imager (SSM/I)** on a polar orbiting Department of Defense satellite. The **SSM/I** is a passive **microwave** imaging radiometer which remotely senses Earth's environment through four polarized frequencies (19, 22, 37, and 85 GHz). WetNet is using the **SSM/I** as its primary data source for the development of new Earth science algorithms. Algorithms to measure precipitation, atmospheric water vapor, total precipitable water, marine wind speed, land use classification, snow, sea ice, and other **Earth science** parameters are currently under development at NASA/MSFC, NASA/Goddard Space Flight Center, NASA/Jet Propulsion Laboratory, and many universities and research institutes. WetNet is providing not only the data but also the analysis capabilities to the scientists. To achieve this goal, each WetNet science investigator (over two dozen) has been provided with a workstation, special display and analysis software, and a continual data distribution of the **SSM/I** data. The software permits the contouring, animation, and analysis of the satellite images, while the interactive nature of the system permits the sharing of algorithms for verification, intercomparison, and modification among the scientists. A more detailed description of the WetNet system may be found in the FY89 Research and Technology Report.

In 1989–90, the workstation user interface, mainframe data processing, and data distribution procedures were developed. In 1990, WetNet entered into the operational phase. The WetNet scientists are being phased in through three separate workshops at MSFC. The first group received training and instruction in February, the second group in May, and the last group in August 1990. In the spring of 1991, the workstations will be distributed throughout the year as all investigators are brought online. The data and archive distributions began in June with a retrospective look at January 1990 data. Further data processing and distributions will occur on a regularly scheduled basis throughout the year. Additional functionality and improved features of WetNet will be developed throughout the life of the project.

H.M. Goodman/ES44
(205) 544–8006
Sponsor: Office of Space Science and Applications

Interannual Variations of Thunderstorms and Lightning Activity at Global and Regional Scales

Figures 25a and 25b show the global distribution of **lightning** at midnight for May–June 1986 and May–June 1987, observed by the Optical Linescan System on the Defense Meteorological Satellite Program (DMSP) Block 5D satellite. This period is notable for the 1986–1987 El Niño-Southern Oscillation (ENSO) episode. It is of particular interest that ENSO events since the 1940's have been responsible for above-normal **rainfall** and increased discharge of the Magdalena River at Calamer, Colombia (10°15′ N, 74°55′ W) during the period May–June. Indeed, there was also more midnight **lightning** activity in this region in 1987 than in 1986. Within a 10° latitude×10° longitude region in northern Colombia (centered at 6° N, 73° W), there were 30 days (346 flashes) during May–June 1987 with observed **lightning** at midnight in comparison to only 23 days (240 flashes) during May–June 1986. It thus appears that a substantial increase in organized thunderstorm activity can be expected in this region during ENSO episodes.

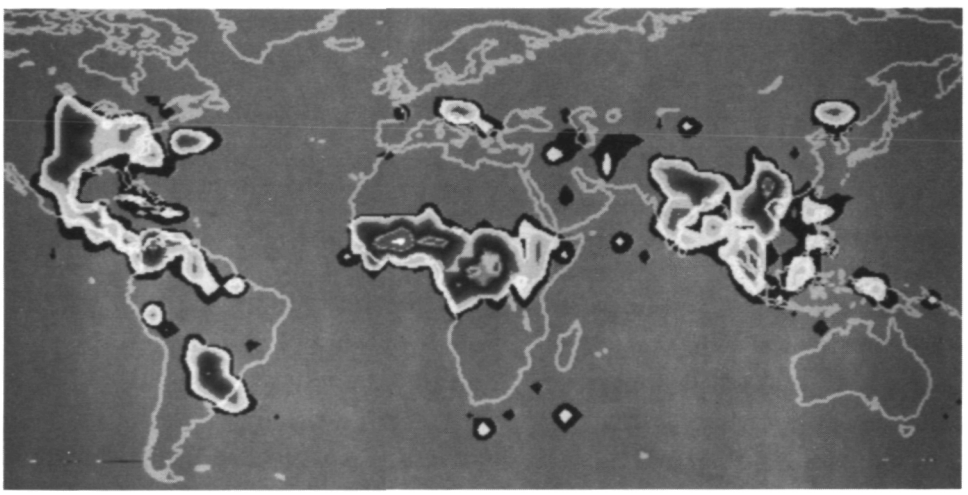

Figure 25a. Global Lightning Distribution—May–June 1986

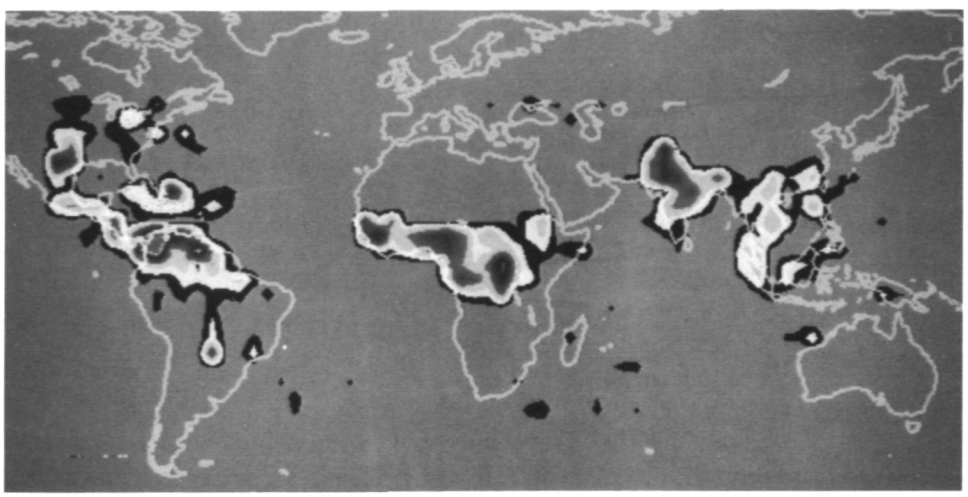

Figure 25b. Global Lightning Distribution—May–June 1987

ORIGINAL PAGE
BLACK AND WHITE PHOTOGRAPH

Data acquired since 1986 by a ground-based, continuously operating **lightning** network located in the Tennessee Valley further illustrates how the interannual variability of **lightning** activity can be addressed (fig. 26). This period is particularly noteworthy as north Alabama experienced its driest and wettest summers on record, respectively, in 1988 and 1989. **Lightning** and **rainfall** data have been analyzed within a 2° latitude×3° longitude area (33.8–35.8° N, 86–89° W) during June 1986–1989 (fig. 27).

Observations from low Earth orbit are better suited to address the global **lightning** distribution than the **lightning** activity in specific storms, which can be sampled only for short periods. Detailed observations of **lightning** activity at the storm scale will be possible in the late 1990's, with optical **lightning** sensors being developed as scientific payloads for the National Oceanic and Atmospheric Administration (NOAA) Geosynchronous Operational Environmental Satellite (GOES)-Next, and the NASA **Earth Observing System (EOS-A)** polar platform, Earth probe missions, Space Station *Freedom*, and geostationary platform. At that time, the **lightning** characteristics of individual clouds will be obtained simultaneously with measurements from visible and infrared imagers, passive microwave radiometers, and perhaps active rain radars. Such **lightning** observations can be readily associated with the thunderstorms that produced them, and the detection of even a single discharge is significant, providing important information on storm location, storm height, the presence of ice, and electric current generation.

Goodman, S.J., and Christian, H.J., Lightning, Global Change Atlas, Gurney, R. ed., Cambridge University Press, New York, NY in press 1991.

S.J. Goodman/ES44
(205) 544–1683
Sponsor: Office of Space Science and Applications

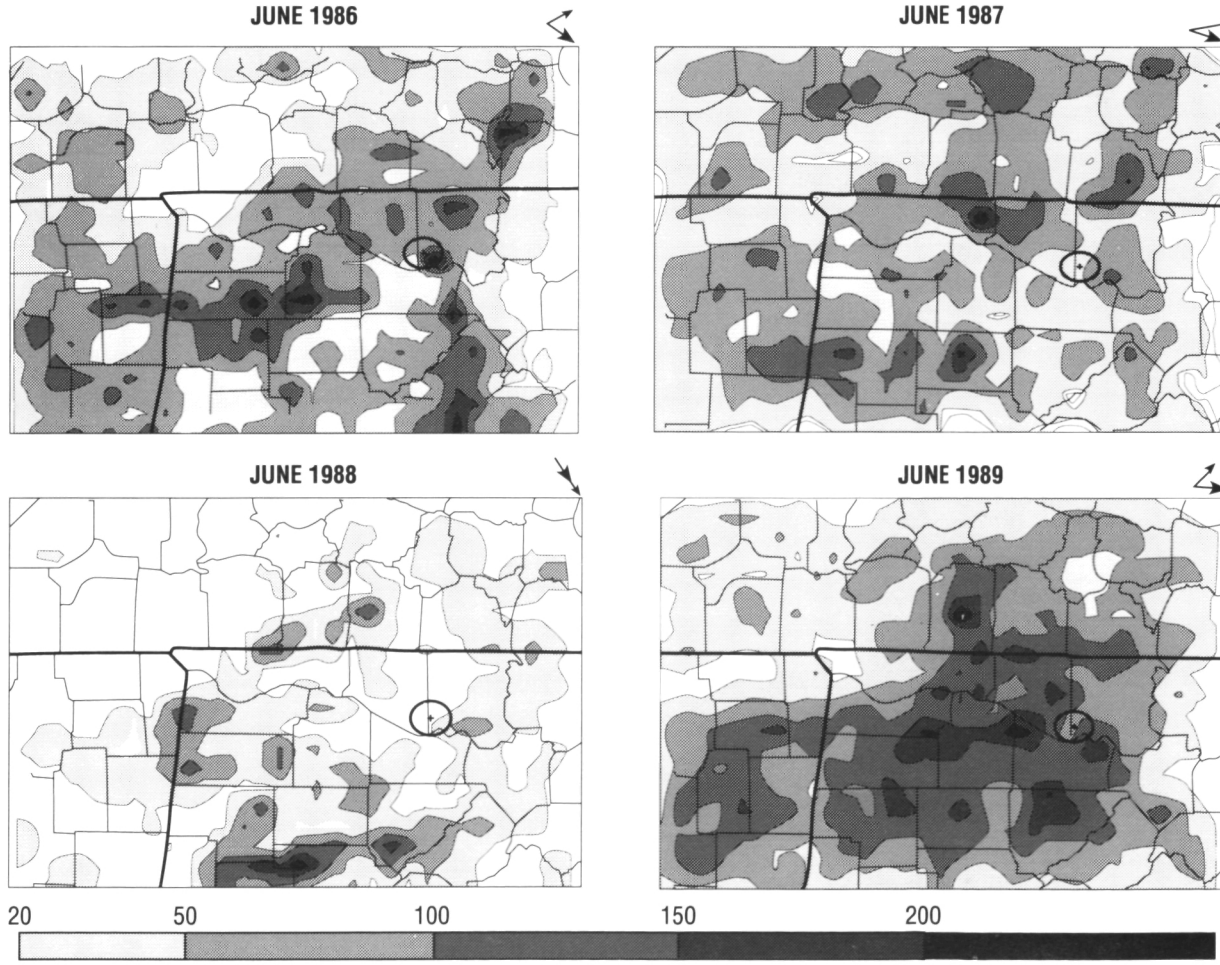

Figure 26. Cloud-to-Ground Lightning in the Tennessee Valley, June 1986–1989

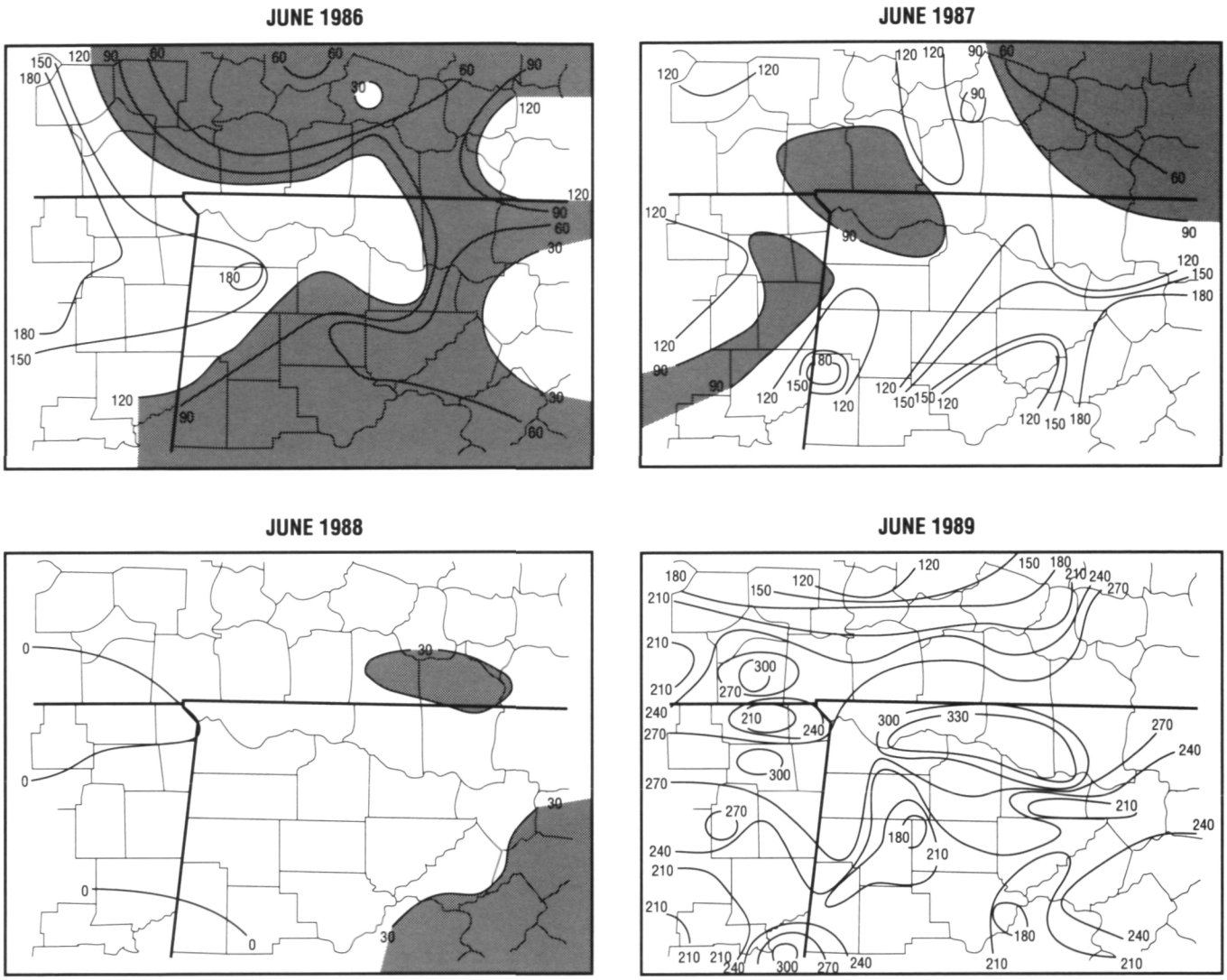

Figure 27. Minimal Precipitation in North Alabama, June 1986 – 1989

Computer Accessibility for the Visually Impaired

Computer technology is applied throughout NASA in widespread areas such as science, engineering, administration, procurement, and training. Computers are not only used to derive new pieces of information but also are used to warehouse existing information. Access to computing information is a key element of many jobs. **Visually impaired** individuals who work for NASA require the same access to information in performance of their jobs as sighted employees. This requirement adds new demands on methodologies used in computer interfaces and other input/output technologies.

The research project on computer accessibility for the visually impaired is funded through the Center Director's Discretionary Fund. The research involves evaluation of some existing technologies in **voice synthesis**, screen reading programs, **braille** hardcopy output, **braille** display, raised graphics, **braille** input, and optical character recognition are being combined to provide a high quality **interface** that is robust and highly flexible. The **interface** will provide an alternative that works equally well with word processors, data base programs, spreadsheets, communications, schedulers, orbital analysis programs, and other scientific applications. Optical character recognition technologies allow the user to incorporate printed materials into the computing environment for use with the other adaptive technologies. This printed material, as well as any other electronic data, can be output via **voice synthesis** or **braille**. The user can also work interactively with the data through the screen-reading application or a **braille** display device.

Graphical interfaces that are found in engineering work station environments, Macintosh systems, and X-Windows preclude use of some off-the-shelf adaptive products. Data in the graphical environments is bit-mapped, whereas most adaptive technologies rely on character-based memory maps. One of the goals within the project is to determine how these advanced graphics-based systems can be made available to **visually impaired** users. This may be implemented as raised images to be touched. It may also be implemented by extracting the textual information from within protocols such as X-Windows for output through voice or **braille** devices.

Research is also being done in ways to influence development of future standards that make computer-based information more accessible to the **visually impaired**, while not limiting the display capabilities of sighted peers. These standards may be in areas such as screen attributes, cursor tracking, color designations, and standard methods for acquiring the textual information behind bit-mapped displays.

The intended result of this project is to advance the capabilities on NASA's **visually impaired** personnel by making new computing environments more accessible. It is hoped that some of the uses of **voice synthesis** and optical character recognition technologies will improve **interfaces** for the entire NASA community.

G. Higgins/EO41
(205) 544–5462
Sponsor: Center Director's Discretionary Fund

Compiling Knowledge Bases

Artificial intelligence (AI) techniques have become an important technology for the solution of some of the most difficult programming tasks. The dominant and most effective technology for developing such applications is at work in a multimechanism, integrated **knowledge-based** system development environment. Unfortunately, systems developed in environments such as these are inappropriate for delivering many applications, particularly applications germane to space systems—they are not real-time, carry the overhead of the entire list processing (LISP) environment, and, particularly in the light of space station requirements, are not written in **ADA**.[1]

Research into a mechanism for compilation of **knowledge bases** into standard **ADA** is being done for NASA through a Small Business Innovation Research (SBIR) contract with IntelliCorp. In phase I, a prototype system was completed by the principal investigator, Bob Gilman, and other IntelliCorp associates. The prototype transforms knowledge bases written in **KEE (Knowledge Engineering Environment)** to **ADA** language syntax. As a sample case for the prototype, the diagnostic portion of the CS-1-FIXER system (an Environmental Control and Life Support System-(ECLSS-)related space station application) was compiled from **KEE** to compilable **ADA** code. In the process, key elements of the **KEE** core were rehosted in **ADA** packages for inclusion in compilation of stand-alone executable **knowledge bases**.

Several key issues that characterize **knowledge-base** systems are being explored during development of this system. These include data typing within languages, functional objects, and automatic storage or memory management. The first two issues have been addressed in the prototype, and the third is part of the research that will be carried on under a Phase II SBIR contract with IntelliCorp.

The final system will consist of **ADA** packages that contain **KEE** functionality. A **KEE** knowledge base will be transformed from the native LISP code to **ADA**. This transformed code can be compiled, along with the **KEE** core, and mixed with other **ADA** code to produce stand-alone executables. The transformation process is restricted in a large degree to the functionality of **KEE**, excluding the graphics-based user interface. This means that the rules, frames, and other **KEE** mechanisms will be transformed to **ADA**, but the sophisticated development environment, with its associated baggage, will not be moved to the **ADA** environment. Processes, some of which were developed for the prototype, will provide a means to test the translated code in the **ADA** environment. There will be procedures that evaluate **knowledge bases** during development.

This research is very important in the continuing effort to field real-time and onboard systems with **AI** components. The development environments are very attractive and useful for code creation but often impede movement of the application into a more standard operations environment. Transforming **knowledge bases** to **ADA** for inclusion in these systems offers a powerful new alternative.

[1]*Compiling Knowledge-Based Systems Specified in KEE to ADA, Phase II Proposal*, IntelliCorp, Inc., Aug. 1989.

G. Higgins/EO41
(205) 544–5462
Sponsor: Center Director's Discretionary Fund

Four-Dimensional Man-Computer Interactive Data Access System Technology

The **Man-Computer Interactive Data Access System (McIDAS)** has been under development at the Space Science and Engineering Center (SSEC) of the University of Wisconsin-Madison for 20 years. During this period, its software and **data bases** have grown extensively. It has been used for the analysis and display of two-dimensional meteorological data, e.g., satellite imagery, temperature contours, etc. Under support from MSFC during FY90, SSEC has been developing a four-dimensional (4-D) analysis and display tool. Since the Earth-atmosphere system is a volume which is evolving in time, a tool is needed that will allow the scientist to visualize multiple parameters from varied viewing geometries.

The eventual goals of this effort are to design and implement a 4-D data management system within **McIDAS** and design and develop the software and hardware necessary for interactive display of Earth systems data. This should provide tools which will render complex 4-D fields of environmental data sets on an interactive basis, allowing rapid integration of interdisciplinary Earth science data sets into one display. The system will be used for qualitative and quantitative interpretation.

Toward these goals, the following tasks have been accomplished during FY90. The Stardent graphics supercomputers have been upgraded to the Stardent 2000 series, which offers twice the computational power of the Stardent 1000 machines. Geometric remaps have been incorporated as part of the display software. Figure 28 illustrates the ability to view a global data set on the sphere of the Earth. Work has been done at MSFC to view model output from the Geophysical Fluid Flow Cell (GFFC) experiment. The GFFC numerical model visualization corroborated the dish-pan experiments conducted at MSFC. The SSEC has decided to begin development of a UNIX version of the **McIDAS** system. The 4-D technology work was instrumental in that decision.

ORIGINAL PAGE
BLACK AND WHITE PHOTOGRAPH

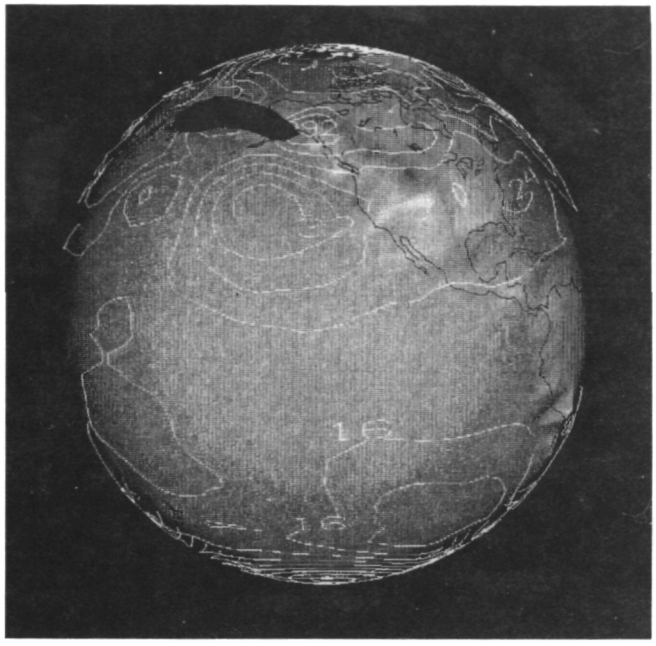

Figure 28. McIDAS Global Hemispheric Depiction

Planned activities for FY90 include greater generalizations of **McIDAS** software to operate under the UNIX and X-Windows environment. Improved use of the GS-2000 may allow for the blending of real-world versus modeled results in one display. A generalization of the coordinate spaces used for both input and output will be developed, along with more generic remapping. Signal processing work will be done to operate with large climatological **data bases**. Work still remains to obtain a quantitative understanding of these data volumes. The project will explore porting the **McIDAS** code to the CRAY supercomputer at MSFC.

P.J. Meyer/ES43
(205) 544–1654
Sponsor: Office of Space Science and Applications

Page intentionally left blank

Research Programs

One of mankind's greatest adventures is expansion of the frontiers of discovery and understanding through scientific research. During the past 30 years, MSFC has been at the forefront of that adventure. In support of the Center's research and development mission, selected centers of excellence have been established in Earth science, solar-terrestrial physics, astrophysics, and microgravity science. Through ground-based research and flight experiments, Center scientists are developing scientific instruments and analyzing data to study the Earth system on a global scale; to investigate the Sun, the geospace environment, and the effects of solar processes on the Earth; to study the universe in infrared, x rays, gamma rays, and cosmic rays; and to utilize the unique capabilities of the space environment to study the nature of physical, chemical, and biological processes in low gravity to advance knowledge in fluid physics, materials science, and biotechnology.

E.A. Tandberg-Hanssen
Director, Space Science Laboratory

Microgravity Science

MSFC has become a Center of excellence for Microgravity Science and Applications. Combining this Center of excellence with developing programs in regional universities (i.e., The University of Alabama in Huntsville; Alabama A&M University; The University of Alabama, Birmingham; and Vanderbilt University), this area has become a focus for microgravity research. In an effort to study the influence of weightlessness on basic physical processes, a number of ground-based microgravity research and flight programs are continuing at a high level of activity. MSFC scientists and engineers are utilizing suborbital flight vehicles such as the KC-135 aircraft, the MSFC Drop Tube, rocket flights, etc., to conduct research and checkout of potential flight hardware and experiments. More than 20 Principal Investigators have had proposals selected as a result of peer reviews in MSFC-managed microgravity ground-based disciplines. Our scientists and engineers are preparing state-of-the-art experiments for a number of flight programs aimed at the U.S. Microgravity Laboratory (USML), the International Microgravity Laboratory (IML) -1 and -2, the U.S. Materials Pallet (USMP), Space Station Freedom, *and other shuttle flight opportunities. The result of these efforts has been the selection of 14 MSFC scientists as experiment Principal Investigators and 8 MSFC scientists selected as flight hardware development project scientists or assistant mission scientists for these flights commencing in 1991. Such experiments will clarify how the absence of gravity-driven convection, for example, can beneficially influence solidification and crystallization processes.*

Optimization of Measurement to Determine Crystal Strain State

Single-**crystal** alloys are being used more and more extensively in the construction of turbine blades, primarily due to their superior mechanical properties as compared with multigrain materials. These alloys are characterized by strongly anisotropic properties, which require special methods of analysis and design. An important issue in the analysis of anisotropic materials is the calculation of material constants. Due to the large number of independent constants (up to 21) and the dependence of material properties on the orientation of the **crystallographic axes**, evaluation of material constants, in these cases, is a complex task and the results are very sensitive to all experimental parameters. In this report, a general procedure for the evaluation of material constants for anisotropic materials is presented. The objective here is two-fold:

- To provide a means of interpreting the results of static tests on anisotropic materials (with arbitrary stress state, orientation of material axes, and orientation of measured strains)
- To formulate a theoretical background, methodology, and software design for a priori (i.e., before the experiments) optimizing the orientation of the strain measurements (gauges), so as to minimize the sensitivity of results to measured angles, orientation, etc.

Toward this end, a general formulation and methodology (valid for arbitrary **crystal** classes) was developed. A special "locator" matrix was introduced to represent the compliance matrices of various **crystal** classes in a very general way. It was assumed that:

PRECEDING PAGE BLANK NOT FILMED

- The type of **crystal** is known.
- The orientation of the **crystallographic** axis in all the specimens is known (but is arbitrary).
- The specimen is subject to a tensile test or any other tests with a prescribed stress state.
- The strains in the specimen are measured by strain gauges or other techniques with arbitrary orientation.
- The test may be repeated several times for different specimens of the same materials. The number of tests (measurements) is at least equal to the number of independent material constants.

Under these assumptions, the methodology can calculate the values of the material constants for arbitrary classes of anisotropic materials. Moreover, a major benefit of the devised approach is that it is capable of estimating the optimal orientation of the strain gauges for a given **crystal** class, material axes, and stress state. The criterion for this optimization is to minimize the sensitivity of the results (material constants) to the orientation of material axes and strain gauges. Thus, the best possible results for a given specimen and testing are guaranteed.

L. Kiefling/ED22
(205) 544–1498
Sponsor: Office of Aeronautics and Exploration Technology

Microgravity Activities

The weightlessness of space reduces buoyancy forces, hydrostatic pressure, sedimentation, and thermally-induced convection flow. It also eliminates the need for containers during certain processes. Flight results indicate novel effects on a wide spectrum of important materials, including inorganic crystals and biological fluids. Space experiments help provide critical insights into terrestrial materials processes and may possibly produce unique and valuable products from space technology.

Work sponsored by the Office of Space Science and Applications (OSSA) has resulted in several hardware systems and experiments qualified for ground-based and flight microgravity activities. Conducted by selected investigators, these experiments form the technical basis for microgravity experiments in space. The Office of Commercial Programs, supported by MSFC, has established policies and procedures for making business and legal arrangements with commercial firms. This office provides technical assistance to research and development work aimed at the commercial applications of materials processing in space.

MSFC ground-based microgravity facilities offer accessibility to short-term, **low-gravity** periods. Experiments in these facilities stimulate ideas for research and serve as test beds for microgravity experiments and equipment development. Ground-based facilities available through MSFC can provide microgravity conditions for up to 20 s. These facilities include a 105-meter drop tube (≈4.6 s) and a KC-135 aircraft (≈20 s of **low gravity** via parabolic trajectory). This year, MSFC drop-tube research has investigated the nucleation and resulting rapid solidification of highly undercooled metals and metal alloys. A new technique, using a single-color **pyrometer**, will measure the nucleation temperature of an undercooled drop-tube sample for studies aboard the International Microgravity Laboratory-2 (IML-2) mission. The KC-135 continues to have extensive utilization, with over 1,000 parabolas

flown this year for ground-based, low-gravity studies. Almost 50 distinct areas of microgravity experimentation have been covered using this particular facility.

MSFC also develops microgravity apparatus for space flight. Modular design is emphasized to allow a variety of experiments, and to foster hardware evolution/maintenance and in-orbit flexibility. Advances have been made in heater technology, temperature control, insulating materials, and sample containers. Some of this flight hardware will fly in the upcoming United States Microgravity Laboratory (USML) and IML.

On USML, the **Crystal Growth Furnace** (**CGF**, fig. 29) will grow electronic crystals and photonic materials. The **CGF** will process large samples and allow sample change-out in orbit. Figure 30 shows the **CGF** in its experimental apparatus container.

The Advanced Automated Directional Solidification Furnace (AADSF, fig. 30) is being developed for various U.S. microgravity payload missions. This furnace will provide precise control of the melt growth of electronic materials and research data on the material effects of thermal- and density-driven convection.

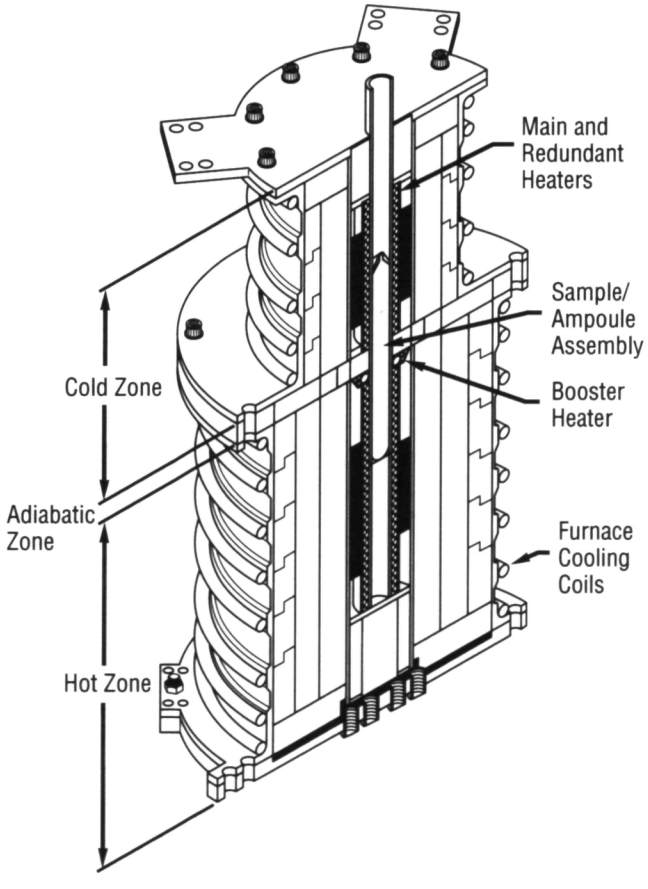

Figure 29. Crystal Growth Furnace

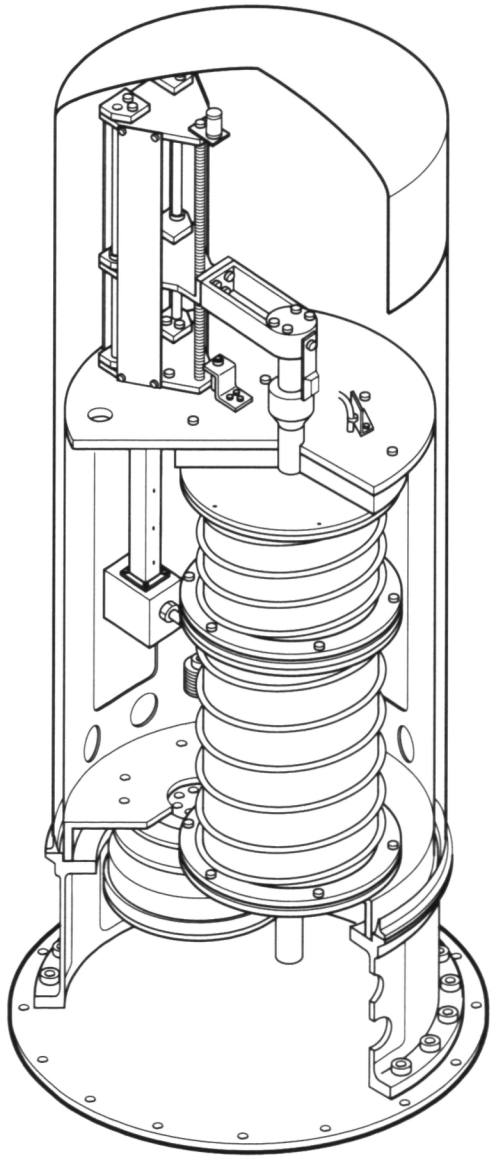

Figure 30. CGF in Experiment Apparatus Container

In FY90, the Protein Crystal Growth (PCG) apparatus and experiment were flown on STS-32 and STS-31. Protein crystals were selected for their importance in the treatment of diseases such as emphysema and high blood pressure, as well as their roles in other biochemical applications. For the first time on STS-31, protein crystals were grown at temperatures other than standard room temperature. The isocitrate lyase crystals produced from this study were the largest ever obtained and may offer breakthrough data in the prevention of crop disease. Likewise, crystals of canavalin and a tobacco mosaic virus were the largest and most perfect grown to date. Crystals grown of the human protein, serum albumin, were of exceptional size and appearance. These crystals could provide data leading to the cure of cancer and viral diseases.

Two experiment facilities, the Fluid Experiments System (FES) and Vapor Crystal Growth System (VCGS), are being prepared for the IML-1 mission. The three investigations selected for these facilities on this mission will study solution crystal growth of triglycine sulfate (a room temperature infrared radiation detector), vapor growth of crystals of mercuric iodide (a room temperature high-energy radiation detector), and casting-and-solidification technology.

For FY90, NASA/MSFC has negotiated the modification and use of the European Space Agency's (ESA's) Glovebox facility to accommodate many NASA experiments in **low gravity**. The Glovebox is scheduled for flight on USML-1 in March 1992. There are 17 microgravity experiments baselined for use of the Glovebox from the following three disciplines: fluid phenomena, crystal growth and ordering phenomena, and combustion processes. Experiments were chosen according to their potential to contribute to critical science issues and future space technology. Four of these experiments are being developed at MSFC involving Marangoni convection, microgravity fiber dulling, double-float zone processing, and solution crystal growth.

Conceptual designs have begun for two systems to be used on Space Station *Freedom*: the Space Station Furnace Facility (SSFF) and the Advanced Protein Crystal Growth (APCG) Facility. The SSFF will consist of a core and several advanced furnace modules like the transparent furnace, the crystal growth furnace, and the programmable multizone furnace. The APCG will allow growth of larger, more perfect protein crystals utilizing advanced hardware and processing techniques. These crystals will then be analyzed to determine how proteins control and affect key biological processes.

The Centers for the Commercial Development of Space (CCDS) Program was instituted by the Office of Commercial Programs to provide a focus for industrial, academic, and governmental elements to advance from pure research through commercial applications. Participants from 175 industrial businesses and 53 universities have combined to form 16 CCDS's. Seven of these CCDS's are associated with MSFC; five of these specialize in materials processing in space activities.

The CCDS at The University of Alabama in Huntsville has now flown three suborbital missions aboard the Consort rocket. Each flight provides 7 minutes of microgravity. A new rocket program, Joust, will provide 14 minutes of microgravity. Its first flight is currently scheduled for early 1991. This program will be followed by the Commercial Experiment Transporter (COMET), a program placing payloads in orbit for periods up to 30 days. This system has the capability to deorbit the payloads and to recover them after reentry. The University of Tennessee Space Institute CCDS will manage the COMET project, and the first launch is scheduled for late 1992.

The Vanderbilt University CCDS has discovered a new alloy of platinum-cobalt-boron that exhibits very large magnetic coercivity after rapid solidification and heat treatment, while retaining the ductility and corrosion-resistance of standard platinum-cobalt

alloys. This new alloy is expected to have specialty magnet applications where fracture toughness and corrosion-resistance are of paramount importance. The patent is pending, with notice of allowance received. A patent application has also been made for a "Method and Apparatus for Making Rapidly Solidified Particulate" in which the particulate exhibits exceptional grain structure and properties. This novel method promises manufacturing productivity advantage over standard rapid-solidification technologies and has application in producing high-value aerospace components.

The CCDS at The University of Alabama at Birmingham flew two sets of PCG experiments (on STS-32 and STS-31) during FY90. Protein crystals were selected for their importance in the treatment of diseases such as emphysema and high blood pressure, as well as their roles in other biochemical applications.

MSFC, under the Office of Commercial Programs, is working on seven joint agreements with commercial users for potential applications of materials processing in space. As a result of these efforts, the 3M Company experiment, Polymer Morphology, flew in October 1989 aboard STS-34. Several patents have been filed by 3M, and they are preparing the experiment for another shuttle flight.

The Rockwell International Corporation Fluids Experiment Apparatus flew on STS-32 to investigate orbiter- and crew-induced gravity disturbances on the stability of molten zones in float-zone crystal growth. The Indium Corporation of America provided the indium samples that were processed.

MSFC is supporting the planning for Space Station *Freedom* by providing materials processing technical data and analyses and by developing the requirements for potential users. Specifically, a payload traffic model has been submitted for review. It covers the years 1996, 1997, and 1998, and will consist of 21.2 racks of internal payloads and 2,982 kilograms (6,575 pounds) of external payloads.

J.F. Stone/JA81
(205) 544–0196
Sponsor: Office of Space Science and Applications, and Office of Commercial Programs

Model Immiscible Systems

Directional solidification experiments on slightly hypomonotectic succinonitrile-ethanol alloys in thin-gap (100-μm) glass cells with and without silicon oil coatings give evidence that the relative wetting characteristics of the solution components on the cell walls affect the bulk phase morphology over the thickness of these cell gaps. Figure 31 shows micrographs of two **directional solidifications** of succinonitrile-**ethanol** solutions carried out in narrow path-length cells where one cell was uncoated (fig. 31a), and the other (fig. 31b) was siliconized. The wetting characteristics are such that **ethanol** preferentially wets both surfaces, however, succinonitrile is significantly less wetting against the coated surface than the uncoated surface. The translation rate in each case is 0.97 mm/h; the thermal gradient is about 16 °C/cm; and solution compositions are about 21 percent wt **ethanol**, slightly hypomonotectic.

In the uncoated cell, the **ethanol**-rich phase spreads unevenly on the top and bottom glass ahead of the solidification front, and the bulk phase morphology is likewise nonuniform. Dendrites were observed to grow from the spaces between islands of **ethanol**-rich **films**, and then to redissolve at the base of the dendrite at the solidification interface. In the coated cell, the **ethanol**-rich phase spreads much more evenly on the cell walls, and the bulk phase morphology is also more uniform. Dendrites were not observed to grow in this system. The appearance of the **film** near the monotectic composition ahead of the solid-liquid interface suggests that this **film** is appearing in a region (about 1° above monotectic temperature) which should be single phase. There are several possibilities to explain the presence of an **ethanol**-rich **film** in a region which should be homogenous. It is likely, however, that **film** formation conditions are established prior to

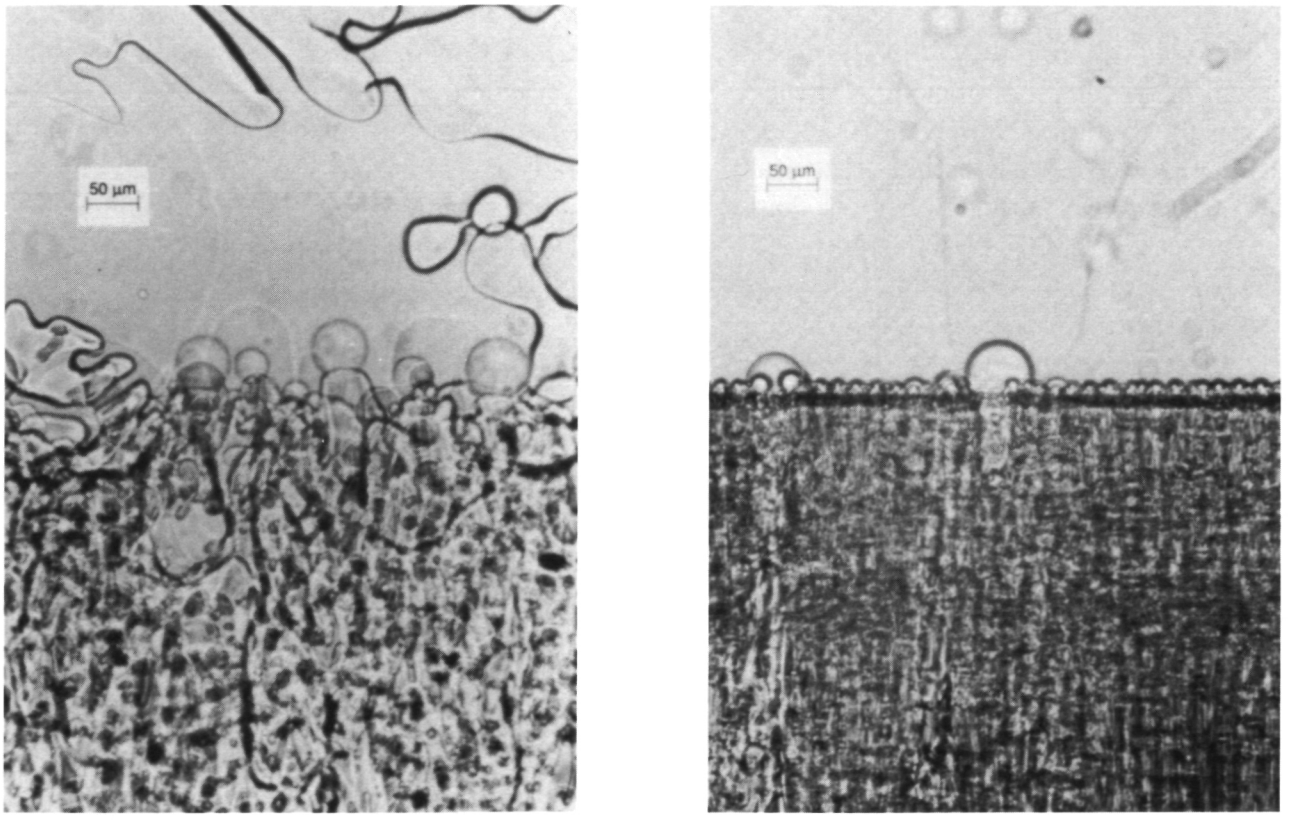

Figure 31. (a) Directional Solidification of Succinonitrile-Ethanol in 100-μm Gap Uncoated Pyrex Cell. Translation Rate = 0.97 mm h^{-1}; Thermal Gradient = 16 °C cm^{-1}; Initial Composition = 21 percent wt Ethanol. (b) Same Conditions as in (a) Except That the Cell is Now Siliconized.

ORIGINAL PAGE
BLACK AND WHITE PHOTOGRAPH

solidification, as evidenced by the uniform morphology in the coated cell, which is not likely the result of capillary spreading from the interface and diffusion throughout the cell over the relatively short time scale. Cahn has indicated, relative to critical wetting theory, that **film** formation is possible in undersaturated, single-phase regions near the critical points of miscibility-gap-type systems. These films are the result of regions of fluctuating compositions in solution driven by the Helmholtz free energy and, for bulk-phase compositions near the coexistence curve, may result in formation of the conjugate phase at the surface. Cahn indicates that above a first-order transition temperature, adsorption is high, and below this temperature, adsorption is low. When the film is nonuniform, as it is in the uncoated cell, one might expect that the resulting composition profiles in the bulk would also be nonuniform, producing the observed nonuniform morphology. Similar films, in front of bulk-phase advancing solid-liquid interfaces, have been observed during **directional solidification** of succinonitrile-water solutions.

The "fungoid" morphology itself has had some attention in the literature, but little attention has been given to the films themselves. It is not expected that the observed **film** is entirely the result of a Gibbs surface excess, but that the composition profile at the surface is a result of the Gibbs adsorbed layer, and may be consistent with Cahn's critical wetting theory.

Frazier, D.O., Facemire, B.R., Loo, B.H., Burns, D., and Thiessen, D.B., "Solidification Behavior of Impurity-Doped Succinonitrile Solutions in High-Surface Area, Low-Bulk Volume Containers," *J. Crystal Growth*, in press, 1990.

D.O. Frazier/ES74
(205) 544–7825
Sponsor: Office of Space Science and Applications

Advanced Technology Materials

The work reported here is part of a continuing effort to develop materials and associated processes for use in advanced technological applications satisfying NASA-unique needs and requirements.

This effort involves two areas of extreme importance in our technology and the use of new materials in device and process applications. These two areas are: (1) organic materials that possess **nonlinear optical (NLO)** properties, and (2) **high-temperature superconducting materials (HTSC)**.

The study of **NLO** materials, in particular **L-arginine phosphate (LAP)**, is continuing with the fabrication of relatively large **LAP crystals** of good optical quality. These crystals were produced by isothermal evaporation, a process which does not allow for absolute control of all the growth parameters. Therefore, an apparatus has been constructed which will permit growth by controlled cooling and so have a better control on the degree of supersaturation. Furthermore, this equipment will allow a change of configuration with respect to the gravity vector in order to study the effect of reduced convection. This work is now in progress. A ground-based proposal has been submitted to NASA Headquarters for the study of solution growth on **NLO** materials in a simulated space environment.

In the field of **HTSC** materials, we are actively pursuing the preparation and characterization of bulk samples. Our purpose has been and will be, the optimization of the critical current (Jc) density of the bulk materials and the improvement of flux pinning in order to obtain bulk material with high levitation forces.

The main **HTSC** effort this past year took several directions: single crystals, new materials, and optimized bulk samples. A new method was initiated for growing single crystals of 123-type materials from high temperature flux, and the growth parameters such as flux composition, temperature, and duration for obtaining large single crystals of good quality

have been optimized. Such crystals can be used both for fundamental studies and device applications. This method has, so far, produced large, plate-like crystals of approximately 5-mm cross-section and good surface quality. The effort to characterize these crystals and optimize their quality and size will continue.

New materials are being studied, notably the system $YBa_{2-x}Sr_xCuO_7$ by substituting Ba by Sr in the 123-type phase. This work was performed in the hope of improving the Jc and the chemical and mechanical behavior of the ceramic superconductor. We have been successful in obtaining 100-percent substitution of Ba by Sr, and in so doing, synthesized a new phase $YSr_2Cu_3O_7$ which had eluded many in the field. The study of the properties of the solid solutions is now in progress.

The enhancement of the Jc in bulk ceramics has also been studied in both the 123-type and Bi-based materials. Two methods of processing have been adopted, melt texturing of pressed pellets and arc-melting with subsequent annealing of the ceramic sample. Both methods will help in the alignment of grains in the direction of maximum current flow (a-b plane) of these anisotropic superconductors. X-ray diffraction measurements show that the samples are highly aligned and have Jc close to those of thin films. Detailed studies of electrical and magnetic properties of these samples is now in progress.

In support of these activities we have several phase I and II Small Business Innovation Research (SBIR) contracts. Two of these contracts deal with the commercial applications of **HTSC** materials, and the third with the measurement of surface and interfacial tensions of liquids.

The phase I project, entitled "Increasing Critical Current Densities in High-Tc Superconductors" from Castel Technology Corporation, deals with the production of a new grain morphology to improve the "weak link" intergrain contacts in ceramic superconductors. The first reports show that they were able to produce silver-coated powders which, when consolidated, will give high critical currents.

A phase II project, titled "Fabrication of Multifilament Conductors by a CVD [chemical vapor deposition] Process" from Advanced Technology Materials, Inc., has just been awarded and deals with the production of superconducting composite fibers to provide high-strength and high-Jc wire for applications in magnetic suspension systems, shielding, and electric power transmission. The first progress report is expected to be made this year.

A second phase II project, entitled "A New Method for the Measurement of Surface Tension" from H&N Instruments, Inc., was awarded for the study of a method to measure surface tension in liquids at low and high temperature. Progress indicates that the hardware is now in place and preliminary measurements show that the obtained surface tension values for a number of liquids agree with those determined by other methods. The uniqueness of this method is that it can be used in situ and at high temperatures.

M. Vlasse/ES74
(205) 544–7781
Sponsor: Center Director's Discretionary Fund,
Office of Space Science and Application,
Office of Aeronautics and Exploration
Technology, and Office of Commercial Programs

Solution Crystal Growth

Research is continuing on the growth of **crystals** from solution. This effort includes both ground-based laboratory studies and flight experiments. It is directed towards increasing our understanding of the basic **crystal** growth process, growth techniques, and their applications and relations to a **microgravity** environment.

A new activity, initiated during the past year, is the design and fabrication of experiments to be carried out in Spacelab missions using the European Space Agency (ESA) Glovebox facility. We have designed and proposed a number of experiments for this facility. At present, one of these experiments has been approved for flight on United States Microgravity Laboratory-1 (USML-1). It will study **crystal nucleation** from solution using a new technique designed specifically for application in the microgravity environment. This technique, which involves localized injection of a heated, highly supersaturated solution into a host growth solution, is designed to control the onset, location, and character of **nucleation** when applied in a microgravity environment. A **nucleation** cell, injection mechanism, solution reservoir, and optical system (fig. 32) are being designed and will be tested and interfaced with the Glovebox facility. Supporting ground-based research has been initiated to evaluate several candidate **crystal growth solutions** and their **nucleating** properties for suitability in this experiment.

In the laboratory, there is continued emphasis on supporting research to measure and study the physical properties of solutions from which **crystals** are grown. Basic properties such as viscosity, density,

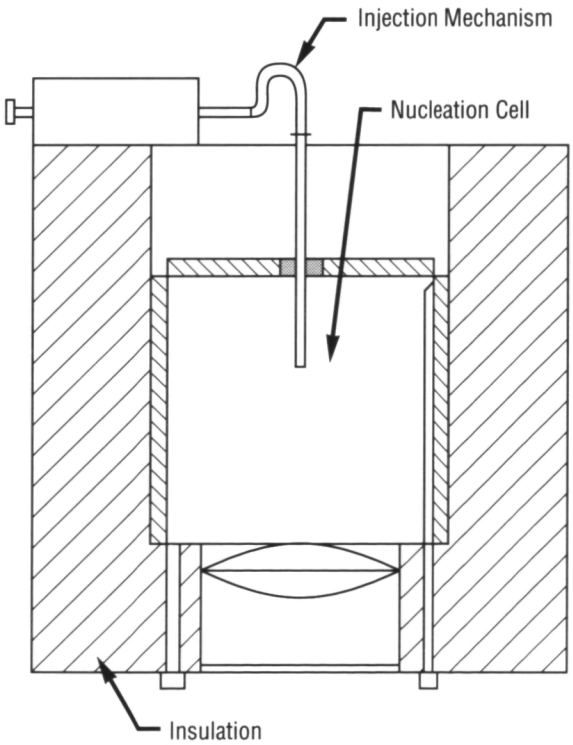

Figure 32. USML-1 Crystal Nucleation Cell

thermal conductivity, and mass diffusivity are measured. Techniques have been developed for studying synthesis, purification, solubility, and **nucleation** of new materials for crystallization. The internal structure of solutions at or above supersaturation concentration is not well understood. An internal reflectance cell is being used to investigate the structure of solutions using infrared spectroscopy.

Wide use is made of optical techniques both for enhanced visualization and for specific measurements. Schlieren and shadowgraph images are made of growing **crystals** to image their growth or dissolution plumes. Holograms and interferometric images are used for detailed measurements of growth rates, concentration depletion regions surrounding growing **crystals**, and density gradients due to temperature or concentration variations in a growth solution. A laser-scattering microscope is used to map microscopic defects in **crystals**. Index of refraction measurements are made on solutions for direct concentration determination and for use in analysis of interferograms.

Ground-based research is also focusing on new candidate growth materials which have high technology applications. Particular emphasis is being placed on nonlinear optical and infrared (IR) detector materials.

Reiss, D.A., Kroes, R.L., and Anderson, E.E., "Growth Kinetics of the (001) Face of TGS Below the Ferroelectric Transition Temperature." *J. Crystal Growth* 84 (1), pp. 7–10, 1987.

Kroes, R.L., and Reiss, D.A., "Development of New Techniques for the Characterization of Crystals and Their Growth Solutions," NASA TM-100371, June 1989.

Kroes, R.L., Reiss, D.A., and Facemire, B. "Concepts For Microgravity Experiments Utilizing Gloveboxes," NASA TM-100378, September 1989.

R.L. Kroes/ES74
(205) 544–7770
Sponsor: Office of Space Science and Applications

Protein Crystal Growth

As part of the ongoing investigation by our laboratory into the effects of microgravity on protein crystal growth, several advances in protein structure have been made. Recently, crystals suitable for the structure determination of an antibody to the **human immunodeficiency virus type I (HIV-I)** were grown (fig. 33). This antibody is directed against the viral transmembrane protein gp 41 and corresponds to the subclass IgG1. The three-dimensional structure determination of the antibody is proceeding rapidly. The present study, taken together with other known antibody structures, should provide for a more complete understanding of antibody-antigen interaction. A basic understanding of antibody chemistry, combined with advances in genetically engineered antibodies, promises avenues for new therapeutic treatments to a variety of immunologically recognizable illnesses, including those of the **acquired immune deficiency syndrome (AIDS)**.

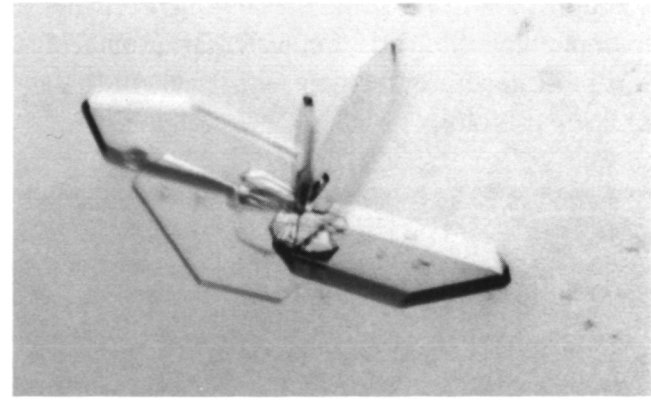

Figure 33. Crystals of an IgG Antibody (FAB) to the Human Immunodeficiency Virus (HIV-1) (AIDS) (Grown at MSFC) (Ground-Based Crystal Growth)

ORIGINAL PAGE
BLACK AND WHITE PHOTOGRAPH

The structure of human serum albumin (HSA) has been extended to a resolution of 4.0 Å through ground-based research activities (fig. 34). The 4.0-Å electron density has revealed an alternate quaternary arrangement of the six subdomains reported at lower resolution. A diverse variety of evidence supports this quaternary configuration. The subdomains assume a heart shape which agrees with the dark-field electron micrograph images of human and bovine alphafetoprotein (AFP) (the fetal counterpart of serum albumin). Domains I, II, and III may be superimposed (fig. 35), which is consistent with the homology within the amino acid sequence. The major binding regions are located within subdomains IIA (previously labeled IA) and IIIA, which is consistent with the competitive drug displacement experiments and the reported acetylation of Lys 199 by aspirin. Distances measured between various amino acids and bound ligands to HSA and bovine serum albumin obtained from a variety of fluorescence and resonance energy-transfer studies also support the AFP-type configuration. Furthermore, proteolytic cleavage of HSA would produce two halves of the molecule which could reassociate in solution, thereby restoring the binding properties of the intact albumin. Thus, this quaternary arrangement is in more general agreement with the chemistry and molecular biology of HSA.

Crystals of HSA grown on flights STS-31 and STS-32 have been successfully analyzed. Trends in the diffraction statistics which are suggestive of more highly ordered crystals are similar to those previously reported by other **crystallography** groups. We have recently collected higher resolution x-ray diffraction data on HSA at the Institute for High Energy Physics in Tsukuba-shi, Japan. The higher resolution structure and the binding positions of a variety of biological and pharmaceutical compounds will be determined.

Carter, D.C., and He, X.M., "Structure of Human Serum Albumin," *Science*, Vol. 249, pp. 302–303, 1990.

Carter, D.C., He, X.M., Munson, S.H., Twigg, P.D., Gernert, K.M., Broom, M.B., and Miller, T.Y., "Three-Dimensional Structure of Human Serum Albumin," *Science*, Vol. 244, pp. 1195–1198, 1989.

Delucas, L.J., Smith, C.D., Smith, H.W., Senadhi, V.K., Ealick, S.E., Carter, D.C., Snyder, R.S., Weber, P.C., Salemme, R., Ohlendorf, D.H., Navia, M.A., McKeever, B.M., Nagabhushan, T.L., Nelson, G., and Bugg, C.E., "Protein Crystal Growth in Microgravity," *Science*, Vol. 246, pp. 651–654, 1989.

D.C. Carter/ES76
(205) 544–5492
Sponsor: Office of Space Science and Applications

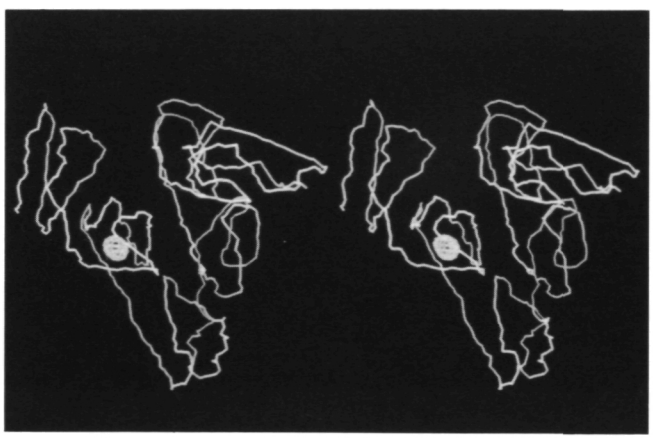

Figure 34. Stereoview of a Simplified Tracing (Not Alpha-Carbons) Representing Type Convolution of Electron Density Within a Molecule of HSA Based on the Interpretation of the 4.0 Electron Density. The Subdomains From Left to Right Are IIIB, IIIA, IIB, IIA, IB, and IA. The Difference Density Illustrating the Major Binding Locations for Ibuprofen (Advil) Within IIIA is Shown

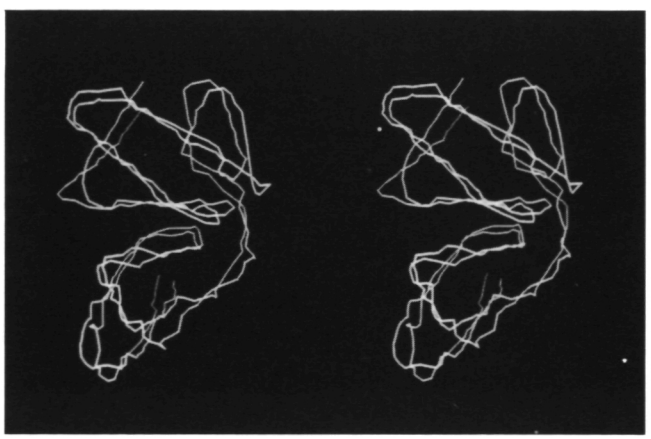

Figure 35. A Stereoview of Independent Tracings of the Electron Density Within Domain II (Yellow) and III (Blue) Superimposed to Illustrate the Structural Homology

Astronomy and Astrophysics

Astronomy and Astrophysics have been a major part of the scientific space program since its beginning. Observations from above the Earth's atmosphere have brought exciting scientific discoveries and have opened new disciplines of research such as x-ray astronomy and gamma-ray astronomy. Historically, MSFC has been actively involved in various areas of astronomy and astrophysics with flight experiments, scientific payloads, and missions. The Center has had an increasing role in developing scientific instruments and managing major science projects starting with Skylab, including the Apollo Telescope mount, followed by the three High Energy Astronomy Observatories, the Hubble Space Telescope, and Spacelab experiments. Responsibilities for future missions include the Astro Mission and the Advanced X-Ray Astronomy Facility (AXAF).

The Astrophysics Division of the Space Science Laboratory has a strong research program in astronomy and astrophysics including x-ray astronomy, gamma-ray astronomy, cosmic-ray research, and infrared astronomy. Research activities include theoretical and experimental research, development of new detector systems and scientific instruments, and flight experiments. Advanced technology development in support of scientific instrument development is being carried out in several areas, for example, in cryogenic systems and high-temperature superconductivity. An active balloon flight experiment program in high-energy astrophysics and cosmic-ray research is being conducted for scientific measurements and to test new detector systems and instruments. One of the major science operations in the near future will involve the Burst and Transient Source Experiment (BATSE) on the Gamma-Ray Observatory (GRO) to be launched in 1991.

Gamma-Ray Burst Studies

Gamma-ray bursts are perhaps the least understood phenomena in high-energy astrophysics today. About a hundred times per year, intense **bursts** of **gamma rays** are seen to occur at random. It has become clear that there are several classes of **bursts** which, perhaps, are due to different types of objects and/or emission mechanisms. The "classical" **gamma-ray bursts** were the first type discovered about 20 years ago. They last from about 0.1 s to 200 s and have not been identified with any known object. These **bursts** have a very hard spectrum, in some cases extending up to 100 MeV. The repeating class of **gamma-ray bursts** have softer spectra, and at least one has been associated with a supernova remnant in the Large Magellanic Cloud.

Although many theories of **gamma-ray bursts** have been proposed, the explanation of **gamma-ray bursts** is still quite speculative. Most recent theories propose that **gamma-ray bursts** are associated with old neutron stars within the galaxy. However, some models place the **gamma-ray burst** sources at cosmological distances, requiring exotic and extremely energetic emission processes.

For the past 12 years, the experimental study of **gamma-ray bursts** has been the primary focus of the **gamma-ray** astronomy research at MSFC. Early balloon-borne observations using large-area scintillation detectors showed a sparsity of weak **gamma-ray bursts**. These observations remain the most sensitive observations of **gamma-ray bursts** that have been made to date. Although the interpretation of these observations is somewhat controversial, we conclude that they indicate that the **burst** sources are not uniformly distributed throughout space and that a galactic confinement is the most reasonable explanation.

In addition to the balloon-borne measurements, there have been other opportunities to observe **gamma-ray bursts**. The fortuitous observation of a strong **gamma-ray burst** during the Spacelab 2 Mission in August 1985 provided unique spectral

data on short timescales. The observation was made by the nuclear radiation monitor which was placed aboard Spacelab to determine the radiation environment of the space shuttle/Spacelab system. This particular **gamma-ray burst** was seen to have a very hard spectral component which peaked about 3 seconds before the primary part of the **burst**. A softer component persisted at least 20 seconds after the peak of the main pulse expired. This type of **burst**, which is also characterized by the lack of any large amplitude and short-timescale variations, is thought to comprise a separate class of **bursts**, accounting for perhaps 25 percent of all classical **gamma-ray bursts**.

The principal effort of the **gamma-ray** astronomy team at MSFC has been in the development of the **Burst and Transient Source Experiment (BATSE)** on the **Gamma-Ray Observatory (GRO)** (fig. 36). **BATSE** (fig. 37) is one of the four instruments on the **GRO**, which is the second of the Great Observatories in space astronomy that NASA intends to place in Earth orbit by the year 2000. During the past year, final assembly, testing, and calibration of **BATSE** was performed on the **GRO** at the facility of the mission contractor, TRW. The integrated spacecraft was delivered to KSC in January 1990 for launch by the space shuttle on STS-37.

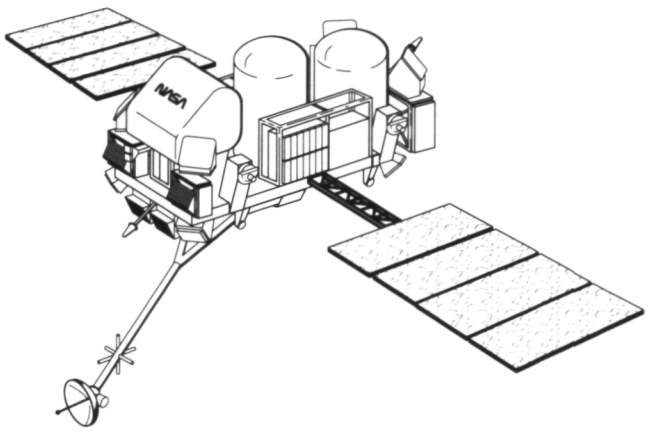

Figure 36. Gamma-Ray Observatory

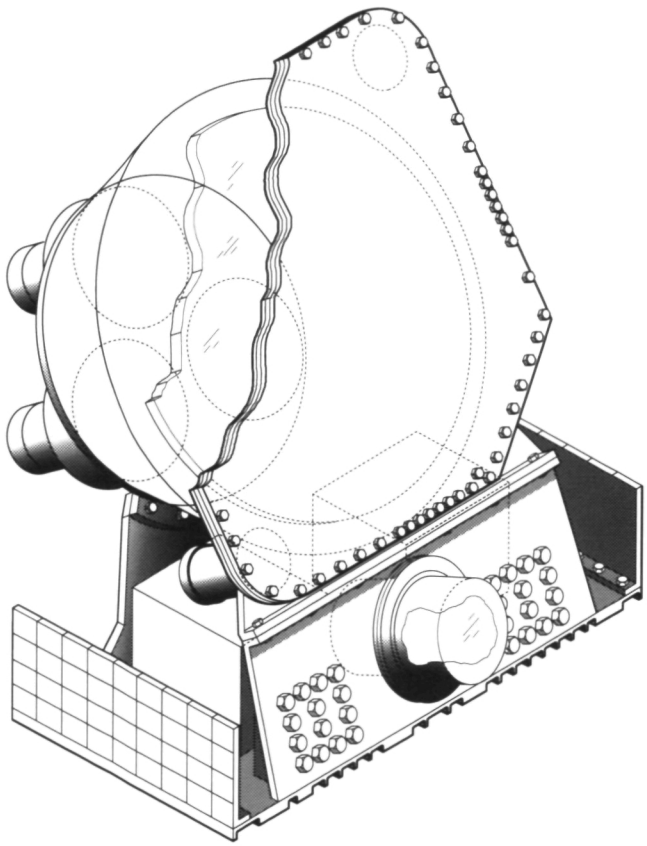

Figure 37. BATSE Detector Module

BATSE consists of eight detector modules arranged on the corners of the **GRO** to provide the maximum unobstructed view of the celestial sphere. Each detector module contains a large-area detector, optimized for sensitivity and directional response, and a spectroscopy detector optimized for broad energy coverage and energy resolution.

The **BATSE** instrument will allow the observation and location of hundreds of **gamma-ray bursts** with unprecedented sensitivity for performing spectral observations and rapid temporal variability studies. In addition, the locations of some stronger **bursts** will be determined more quickly than previously possible, so that longer-lived emission at other wavelengths can be searched. **BATSE** also provides a **gamma-ray burst** signal and a solar-flare trigger signal to the other experiments on the **Gamma-Ray Observatory**.

One of the primary objectives of **BATSE** is the determination of the spatial distribution of the different classes of **gamma-ray bursts**. This can be met through the detection and localization of many hundreds of **gamma-ray bursts**. The spatial distribution of **bursts** in galactic coordinates or the association of certain types of **bursts** with extragalactic objects, such as the LMC, M31, or Virgo cluster, would immediately provide the much sought-after distance scale needed to provide luminosities. Sensitive observations by the **BATSE** large-area detectors will provide the required large population sample along with the single-spacecraft determination of these **burst** locations.

G.J. Fishman/ES62
(205) 544–7691
Sponsor: Office of Space Science and Applications

Induced Radioactivity Analysis of the Long Duration Exposure Facility

The retrieval of the **Long Duration Exposure Facility (LDEF)** in January 1990 presented a unique opportunity for investigating long-term radiation exposure of spacecraft materials in low Earth orbit. Throughout its mission life of nearly 6 years, the **LDEF** spacecraft maintained a stable configuration with respect to the Earth and flight vector directions with less than 1° of wobble. This stability allowed a sampling of the characteristics of the environmental radiation in low Earth orbit from measured residual radioactivity in spacecraft materials.

Extremely small amounts of radioactivity (≈picocuries/kg) are produced in most materials due to bombardment by high-energy cosmic rays and geomagnetically trapped particles (mainly protons). Even though many nuclides are produced from the reactions with these particles, only a few isotopes are radioactive and emit gamma rays at a significant level that can be detected weeks or months after retrieval. Measurements of the gamma radiation in returned samples can be made with special low-background germanium detectors.

Laboratories with shielded, low-background spectrometers at MSFC, Johnson Space Center, Lawrence Livermore National Laboratory, Lawrence Berkeley Laboratory, Batelle Northwest Laboratory, Savannah River-Westinghouse, Los Alamos National Laboratory, and the Tennessee Valley Authority are currently being utilized to measure residual radioactivity in a wide range of material from various locations on the **LDEF** spacecraft. Some materials that are being analyzed were directly exposed to the space environment, and others were in shielded locations at various depths which can sample higher energy fluxes. Examples of spectra showing peaks from gamma-decaying radionuclides produced in two samples of steel are shown in figures 38 and 39. The samples were exposed primarily to proton fluxes, respectively, from the west (onto the trailing side of the spacecraft, fig. 38), and the east (onto the

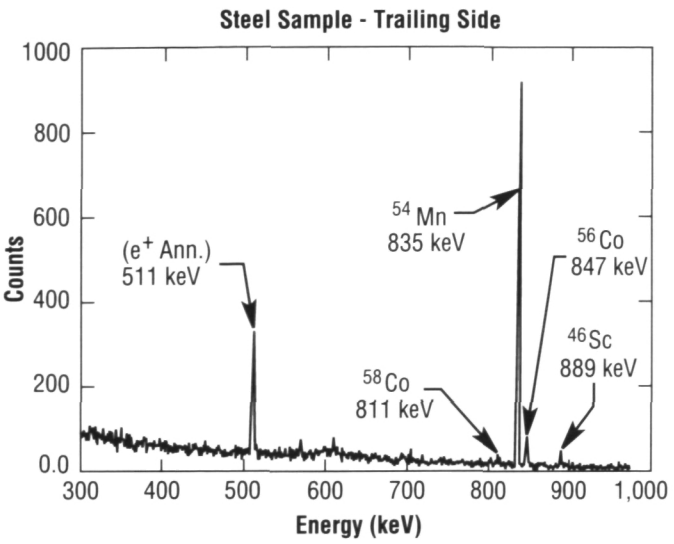

Figure 38. Steel Sample (Trailing Side)

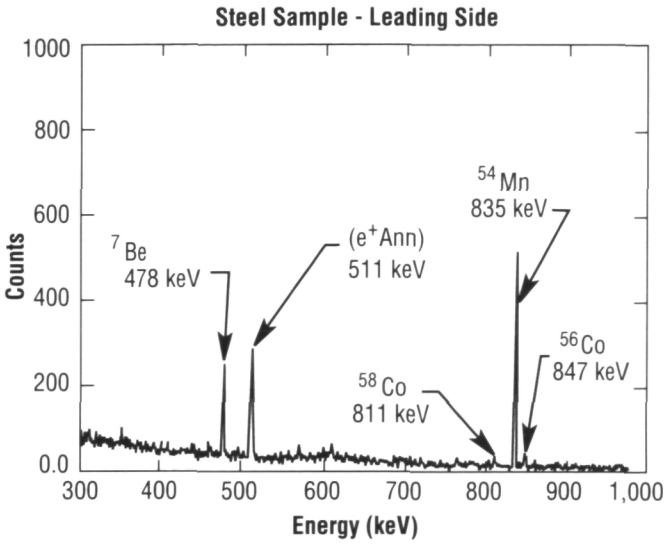

Figure 39. Steel Sample (Leading Side)

leading side of the spacecraft, fig. 39). These spectra show production of ^{56}Co, ^{58}Co, ^{54}Mn, and ^{46}Sc, with half-lives ranging from 71 to 312 days. An enhancement of the strength of the lines in the west-facing sample relative to the east-facing sample can be seen clearly, which is a combined effect of the geomagnetic field geometry and interactions of the trapped flux with the upper atmosphere.

An unexpected observation from early measurements of surface materials was the presence of relatively large amounts of ^{7}Be (half-life = 53 days) found only on the leading surfaces of the spacecraft. The gamma peak at 478 keV for ^{7}Be decay. This can be seen in the spectrum for the leading side (fig. 39) steel sample, while it is not present in the spectrum on the trailing side (fig. 38). This observation was also confirmed from measurements conducted by the Naval Research Laboratory at Kennedy Space Center prior to deintegration of the **LDEF** experiments. The absence of the beryllium isotope on trailing surfaces, coupled with a study of its properties on the leading surfaces, lead to the proposition that the ^{7}Be is a trace atmospheric constituent being implanted in the ram direction of the spacecraft. A gradual buildup to a saturation surface concentration of ~10^{6} atoms per square centimeter was deduced from measurements on LDEF exterior materials at MSFC. The ^{7}Be is known to be formed by cosmic-ray spallation reactions with atmospheric oxygen and nitrogen at lower altitudes; however, the presence of ^{7}Be at orbital altitudes was not previously known.

The information gained from the **LDEF induced-radioactivity** studies on the directional aspects, energetics, and magnitudes of the particle radiation in low Earth orbit, along with a knowledge of which radionuclides are produced, should provide an excellent method of predicting activities in extremely long-duration missions, such as Space Station *Freedom*, which will have similar orbital characteristics. Also, in the case of long-duration orbital gamma-ray or high-energy x-ray astronomical observations, the LDEF measurements will help to characterize detector backgrounds, especially where long-term increases of background fluxes are a concern.

Fishman, G.J., Parnell, T.A., and Harmon, B.A., *Long Duration Exposure Facility (LDEF) Induced Radioactivity Analysis Plan.*

Fishman, G.J., Harmon, B.A., Gregory, J.C., Parnell, T.A., Peters, P., Phillips, G.W., King, S.E., August, R.A., Ritter, J.C., Cutchin, J.H., Haskins, P.S., McKisson, J.E., Ely, D.W., Weisenberger, A.G., Piercey, R.B., and Dybler, T., "Observation of ^{7}Be on the Surface of the LDEF Spacecraft," submitted to *Nature*.

G. J. Fishman/ES62
(205) 544–7691
Sponsors: Office of Aeronautics and Space Technology
and Office of Space Science and Applications

Superconducting Magnetic Suspension Systems and Bearings

Discovery of magnetic suspension based on combined attractive and repulsive forces between a magnet and a high-temperature **superconductor** was reported more than 2 years ago. The mechanism for the suspension involves attractive forces on the magnet from strongly pinned magnetic **flux** in type II **superconductors** which offset the weight and repulsion from diamagnetic currents. Thus, equilibrium positions are obtained for given weights and levels of **flux** trapping.

To investigate the properties of this type of suspension technique for applications to vibration-damped pointing systems and **magnetic bearings**, an apparatus with **flux** trapped in pieces of niobium in a low-temperature cryostat was designed and set up to allow rapid experimentation on masses and rotors suspended outside the cold environment of the cryostat. This hardware allows modifications and measurements on the suspended items to be carried out in air at room temperature. Since niobium's properties are reasonably well understood and are good for suspension applications, niobium has been the material of choice, but other materials can be easily substituted.

So far, total masses (rare-Earth magnet plus attached optics or rotors) as large as 0.15 kg have been suspended quite stably without the necessity of sensing the position of the mass for providing any outside feedback; (i.e., the system is self-stable). This is shown in figure 40 where a 0.1-kg rotor is suspended beneath the cryostat's external surface. By altering the magnitudes of the trapped **flux**, its field gradient, geometrical dimensions, and values of external nontrapped vector fields, it is possible to accomplish numerous desirable functions. These include variable levels of suspension stiffness and decoupling of mechanical vibration of the suspended mass from the cryostat, damping using eddy currents in normal metals; pointing along controllable field vectors, or rotation if the field vectors are rotated; and a relatively large unobstructed solid angle over which the unrestricted pointing can occur. While gimballed systems may accomplish similar dampening and pointing, vibration-dampening and bearings are a necessary part of such a system. Pneumatic bellows and air bearings have constraints for use in vacuum and low-g environments, and magnetic bearings have a number of desirable features compared to mechanical bearings. Absence of lubricants, cryogenic operation, and high tolerance to rotor-mass imbalance are but a few.

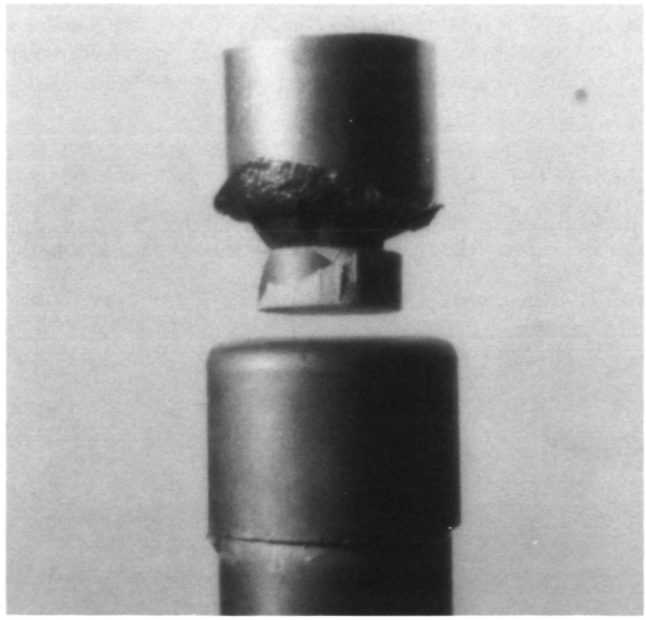

Figure 40. Superconducting Magnetic Superior Systems and Bearings

Additional details of specific axial and transverse loads, stiffness, etc., on a suspended rotor are to be reported and published in an upcoming conference proceeding.

In a related effort, a study was performed by MTI Corporation to determine basic feasibility and general requirements for application of high-temperature **superconductor magnetic bearings** in hydrogen turbopumps for rocket

ORIGINAL PAGE
BLACK AND WHITE PHOTOGRAPH

engines. Present-day, high-Tc superconductor materials are more likely to exhibit the properties necessary for such an application because the operating temperature would be near 30 K.

A model of a Meissner-type **superconductor magnetic bearing** was built by Cornell University. The rotor consists of permanent magnets suspended in superconducting blocks. The model has been operated at speeds of up to 15,000 r/min. It is being used to study low-load **superconductor magnetic bearings**. Cooling is provided by liquid nitrogen.

Peters, P.N., Sisk, R.C., Urban, E.W., Huang, C.Y., and Wu, M.K., "Observation of Enhanced Properties on Samples of Silver Oxide Doped $YBa_2 Cu_3 O_x$," *Appl. Phys. Letter*, 52, pp. 2066–2067, 1988.

Peters, P.N., Sisk, R.C., and Decher, R., "Self-Stable Suspended Rotors Utilizing Superconducting Niobium," accepted for 25th IECEC presentation and publication, August 1990.

P. Peters/ES63
(205) 544–7728
Sponsor: Office of Aeronautics and Exploration Technology, and Center Director's Discretionary Fund

X-Ray Astronomy Research

The main emphasis on the experimental work in **x-ray astronomy** has been the development of advanced x-ray detectors for the energy range 5–100 keV. This work has led to a balloon-flight program involving two collaborations, one with the Harvard College Observatory/Smithsonian Astrophysical Observatory (HCO/SAO), and another involving Berkeley, Lawrence Livermore Laboratories, and the University of California, Santa Barbara. The MSFC instrument for these collaborations is the imaging multistep proportional counter which was developed in-house and uses new techniques to greatly improve the sensitivity over more conventional instruments.[1,2] Briefly, the first of these techniques, multistep operation, divides the detector into two regions, one devoted to measuring the energy of the absorbed x ray and the other region devoted to position sensing. In this way, the detector can be simultaneously optimized for both parameters, a condition impossible to achieve in a standard proportional counter. The second technique is that of fluorescent gating, which makes use of the fact that above the K-shell in xenon (35 keV), true x-ray interactions predominantly induce fluorescence in the detector gas. By detecting this fluorescence, and accepting only those events that produce it, the pervasive cosmic-ray background, against which all sources must be measured, is effectively discriminated.

The first flight in the development of the MSFC instrument was in May 1989, from Alice Springs, Australia, as part of NASA's SN1987A balloon campaign. This flight, a collaboration with HCO/SAO, produced 14 hours of useful data which are currently being processed. The initial analysis has concentrated on understanding the instrument background in the fluorescence-gated mode, and these results are currently being utilized to redesign the instrument for its next flight, scheduled for spring 1991. It is anticipated that, as a result of this redesign, the residual background will be reduced by nearly two orders of magnitude.

In addition to building flight instruments, work continues on developing new instruments and techniques for **x-ray astronomy**. This includes both hardware development and software support, in the form of Monte Carlo simulations, for future missions. Typical of the former is an investigation of the light produced in the avalanches of proportional counters. The goal is to develop an optical-imaging system that would replace the current charge-based one. The benefits of such a system are reduced complexity and immunity to electronic damage from high-voltage breakdown, as well as greatly enhanced spatial resolution and charged-particle rejection capabilities. A second project is concerned with developing new techniques for building focusing x-ray telescopes to operate at energies above those accessible to current-generation telescopes. Such an instrument could improve sensitivities above 10 keV by several orders of magnitude and bring astronomy in this energy regime to a level of maturity comparable to that at lower energies.

In addition to imaging, a further area of major interest is that of x-ray **polarimetry**, a powerful diagnostic tool for probing important properties of cosmic x-ray sources. **Polarimetry** has not yet realized its full potential due to the limitations of available instrumentation and the lack of flight opportunities. The advent of grazing incidence telescopes, together with new techniques of measuring x-ray polarization, now promise an increase in the number of objects with measurable x-ray polarization from one supernova remnant (the Crab Nebula) to hundreds, including rotation powered and accretion-powered x-ray pulsars, black hole candidates, and active galactic nuclei. The MSFC **x-ray astronomy** group is participating in an international collaboration, with Columbia University as the lead institution, to build and fly a sensitive x-ray polarimeter (the **Stellar X-Ray Polarimeter** or **SXRP**) at the focus of one of the Soviet Danish X-Ray Telescope (SODART) telescopes on the SPECTRUM-X-Gamma mission.[3] At MSFC, a Monte Carlo code has been written which provides a detailed simulation of the operation of the Bragg crystal and x-ray scattering components of the **SXRP** experiment (fig. 41). These simulations provide important information on the expected operation and sensitivity of these polarimeter components. The insights provided by these simulations of various instrumental systematic effects, for example the increased understanding of off-axis effects, have impacted the design of the **SXRP**. With a planned launch in 1993, the **SXRP** will soon provide important constraints on the emission mechanisms and geometries of cosmic x-ray sources.

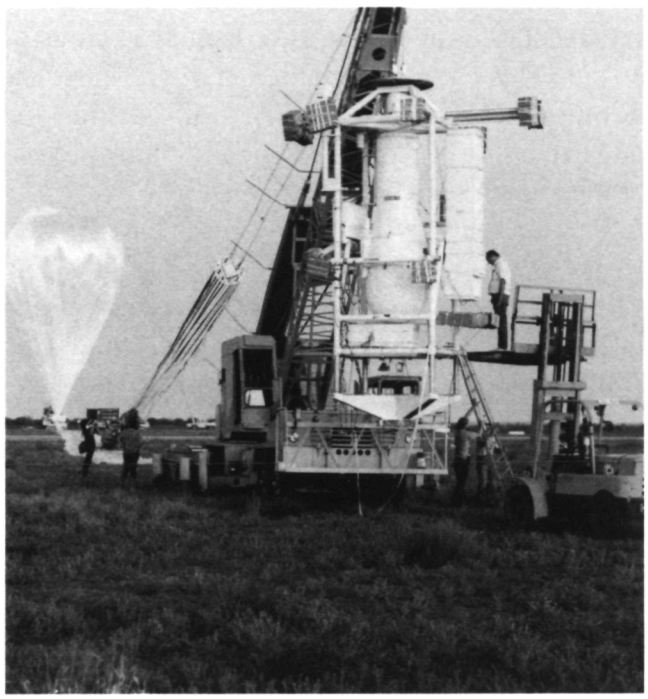

Figure 41. SXRP Experiment

[1]Ramsey, B.D., Weisskopf, M.C., and Joy, M.K., "The MSFC Large-Area Imaging Multistep Proportional Counter," EVUV, X-Ray, and Gamma-Ray Instrumentation for Astronomy and Atomic Physics, SPIE Vol. 1159, p. 246, 1989.

[2]Weisskopf, M.C., and Joy, M.K., "High Energy, High-Resolution X-Ray Optics," Proceedings of the TAOS meeting on Astrophysics in the 21st Century, Taos, New Mexico, December 1989.

[3]Elsner, R.F., Weisskopf, M.C., Novick, R., Kaaret, P., and Silver, E., "On the Performance of the Scattering and Crystal Polarimeters for the SPECTRUM-X-Gamma Mission," Proc. SPIE Conference on Polarimetry, Huntsville, Alabama, May 15–16, 1990, in press.

M.C. Weisskopf/ES65
(205) 544–7740
Sponsor: Office of Space Science and Applications,
Center Director's Discretionary Fund

ORIGINAL PAGE
BLACK AND WHITE PHOTOGRAPH

Expert System Reasoning

Abstract Time Slice (ATS) charts and Visualization of Reasoning (VISOR) are two software systems implementing methodologies for the visualization of the reasoning processes of expert systems written in the **CLIPS (C-language production system) expert system** language (**CLIPS** was developed for NASA and is available through the COSMIC program). These methodologies provide a flexible visual component that has been lacking in previous efforts. This previous deficiency has prevented the debugger/developer user from gaining an understanding of the underlying reasoning process of the **expert system** application.

Both systems, currently running on Sun Microsystems workstations, process trace information from an executing **expert system** application and convert that information into a visual form for easy assimilation. **ATS** charts process standard **CLIPS** trace information and produce static monochrome visualizations of the primitive inferencing processes. VISOR processes user-specified information from a modified version of **CLIPS** and creates animated visualizations of the more abstract application reasoning processes.

Generation of **ATS** charts is straightforward. The user performs a "Watch All" command in **CLIPS** and captures the output to a trace file. This file is read by the **ATS** processor which generates the charts on a laser printer.

Animated reasoning visualization is performed using a dual-process system consisting of a modified version of **CLIPS**, called V-CLIPS, and an animation component, VISOR. Users instrument their **expert system** application by adding parameterized messaging calls at various rule locations corresponding to the **CLIPS** operations of rule activation, deactivation, and firing. There are also facilities to monitor the assertion and retraction of facts. The modifications in V-CLIPS are such that all message calls can be specified in a manner transparent to the unmodified **CLIPS**, allowing the same application file to be used for both development and production.

As the application executes, these messages are sent to VISOR which executes visualization scenes written by the user in a C-based animation language. This language allows the user to construct complicated graphical entities and animate them by modification of their various attributes, including position, color, and visibility.

Planned future work includes: (1) converting the **ATS** program to run interactively instead of as a printer-based post-processor; (2) extending the capabilities of VISOR for more flexible animation scripting; and (3) applying the VISOR paradigm more directly to various scientific data analysis efforts for the visualization of both the analysis process and the results themselves.

W.J. Selig/ES53
(205) 544–7608
Sponsor: Office of Space Science and Applications

Infrared Astronomy and Cometary Research

This year, **infrared (IR) astronomy** at MSFC has focused on three research areas: the extensive observation of comets, star-forming regions, and brown dwarfs with the previously developed MSFC mid-IR camera; the laboratory development of a new near-IR camera; and the scientific and technical participation in the European Space Agency's (ESA's) Infrared Space Observatory program.

The mid-IR camera, with 20 extremely sensitive bolometer detectors, has been operational for 5 years, and continues to provide unique astronomical observations at major observatories. The mid-IR camera has permitted the only sustained program of comet imaging in the thermal IR. During the last year, the comets Brorsen-Metcalf and Austin were imaged at the NASA **IR Telescope Facility (IRTF)** on Mauna Kea, Hawaii. The IR radiation from comets is emitted by dust grains which have been expelled from the comet nucleus and heated by sunlight. Detailed analysis of the IR images has provided insight into the rate at which particulates leave the nucleus, the types of particles leaving, and their temporal behavior. Because nearby comets rapidly change appearance, the MSFC IR camera is uniquely suited to obtain an image in a short enough time period for the results to be meaningful.

Because of its outstanding sensitivity, in late 1989 the MSFC mid-IR camera made the first detection at 10 μm, and also at the **IRTF**, of the principal brown dwarf candidate Giclas 29-38. Brown dwarfs are substellar objects that are not massive enough to sustain nuclear reactions in their cores. They do not emit visible radiation, being detectable only at IR wavelengths. Brown dwarfs may make up the "missing mass" of the universe. Our observations showed, however, that Giclas 29-38 is too bright in the IR to be a brown dwarf, but instead is probably warm dust near an old star.

This year marked the first laboratory operation of the new indium antimonide IR array camera to be used for astronomical observations at 1–5 μm. That 3,596-pixel array will operate in conjunction with the mid-IR camera so that the full wavelength range from 1 μm to 30 μm will be efficiently observed.

In parallel with the IR observational and instrumental programs, the MSFC **IR astronomy** program has continued to contribute to the development of **Infrared Space Observatory Spectro Photometer (ISOPHOT)**, an IR spectrophotometer that will be one of four IR instruments to be flown aboard ESA's Infrared Space Observatory (ISO) scheduled for launch in 1993. Specifically, during the last year, the role of the MSFC Co-investigator on that program has been to contribute to, and help coordinate, the broad scientific program of observations to be carried out with ISO by the **ISOPHOT** team during their guaranteed observing time. Furthermore, the MSFC Co-I has also played a lead role in defining how **ISOPHOT** will be astronomically calibrated during the mission. ISO will be the next major IR space experiment, and will be available to all American astronomers for guest observation.

Telesco, C.M., Joy, M., and Sisk, C., "Observations of G29-38 at 10 Microns," *Astrophys. J.*, Vol. 358, in press, 1990.

Campins, H., Lien, D.J., Decher, R., Telesco, C.M., and Clifton, S.K., "Infrared Imaging of the Coma of Comet Wilson," *Icarus*, Vol. 80, p. 289, 1989.

C.M. Telesco/ES63
(205) 544–7723
Sponsor: Office of Space Science and Applications

Solar Physics

The President's challenge to undertake the manned exploration of the inner solar system has given new importance to the understanding of the influence of the Sun's radiative and particulate emissions upon the environments of interplanetary space, the Moon, and the outer atmospheres of Earth and Mars.

The Sun has a well known activity cycle with an 11-year period generated by a dynamo action arising from the interaction between convective and rotational motions deep within the Sun at the base of the convection zone. As the amplitude of the dynamo builds, the magnetic field rising through the solar atmosphere increases, concentrating and heating atmospheric material into a wide range of structures. The increased heating raises the Sun's extreme ultraviolet emission, which warms and expands the Earth's outer atmosphere, increasing the drag on orbiting satellites such as Space Station Freedom. *The continual convective motions and the emergence of new fields create instabilities in the pre-existing structures which frequently collapse, releasing energy in the form of high-energy radiation and particles. The latter propagate outward, reaching the orbit of Earth in times of tens of minutes to 1 hour. The particles are prevented from penetrating to the Earth's surface, except at the poles, by Earth's magnetic field. But outside this protection, for instance between the Earth and the Moon or Mars, or on the lunar surface, the flux of these particles can present a serious threat to the health and safety of astronauts. Although solar activity has been studied for many years, many problems are unanswered. We remain unable to estimate reliably the amplitude of future activity on either short- or long-time scales or to predict which magnetic configurations will give rise to solar flares. Answers to these questions are inexorably linked to the physics of the solar magnetic field which forms the basis of the research at MSFC.*

Through direct observation of the vector field, a capability developed at MSFC which is still quite unique, we have had considerable success in understanding how the energy stored in the magnetic field by the convective motions of the Sun's atmosphere is released. We are now testing a data-based algorithm to locate in real time those magnetic regions which will give rise to large flares. We have under development an experimental vector magnetograph which will be used as a test bed for advanced technologies including improved polarimeters and large focal plane arrays with high-speed readouts. Our plans include development of a balloon-borne instrument based on these ideas as a precursor to a satellite mission.

We are continuing to develop instruments for directly imaging the multi-million-degree plasma that forms the solar corona. The technologies involved include normal incidence, multilayer optics for the x-ray ultraviolet and soft-x-ray regimes, ultra-smooth grazing incidence mirrors for extending the short-wavelength limit of these telescopes into the hard-x-ray regime, and a variety of concepts based on Fourier transform techniques for imaging the very highest energy emissions. We have also begun to create conceptual designs for a series of advanced solar instruments for location on the lunar surface. These instruments will take advantage of the stable surface, the lack of atmosphere sensitivities, and angular resolutions which will be needed to advance solar physics in the 21st century.

Electron Irradiation of GaAs Solar Cells

The Space Environmental Effects Facility (SEEF) is currently exploring **gallium arsenide (GaAs)** solar cell behavior after exposure to high-energy electrons (e^-). Previous experiments with **electron irradiation** of Si, GaAs, and GaA1As **solar cells** indicate that the efficiency decreases with increased electron fluence. This investigation shows a noticeable efficiency reduction, beginning at an electron fluence of $1x10^{14}$ e^-/cm^2 ($6.5x10^{14}$ e^-/in^2). After the final electron exposure, $1x10^{15}$ e^-/cm^2 ($6.5x10^{15}$ e^-/in^2), the **solar cells** were annealed to investigate thermally induced recovery of **solar cell** efficiency. The results indicate a partial recovery of cell efficiency after 2 hours at 250 °C (482 °F).

The **solar cells** used in this investigation were composed of **GaAs** on a gallium wafer. These cells were equipped with a borosilicate cover slide and a magnesium fluoride antireflective coating. This cell type had been proposed for use on the Orbital Maneuvering Vehicle.

The **solar cells** were exposed to a 1.0-million electron volt (MeV) electron flux which was generated by a Van de Graaff accelerator. This investigation utilized an iterative procedure, with one iteration being an electron exposure followed by flash testing to generate the characteristic **solar cell** current-voltage (I-V) curves. A total of six iterations were completed and the results are shown in table 1.

Table 1. Results of Solar Cell Exposures in the Van de Graaff Accelerator

Electron Fluence e^-/cm^2 (e^-/in^2)	Average Efficiency	Average Pmax (mW)	Average Efficiency Change
0.0	18.8% ± .77	204.1 ± 8.3	0.0
$1x10^{13}$ ($6.5x10^{13}$)	18.4% ± .75	199.6 ± 8.2	2.1% ± 5.6
$5x10^{13}$ ($3.2x10^{14}$)	17.5% ± .71	189.1 ± 7.7	6.9% ± 5.4
$1x10^{14}$ ($6.5x10^{14}$)	17.0% ± .7	183.8 ± 7.5	9.6% ± 5.2
$2.5x10^{14}$ ($1.6x10^{15}$)	15.9% ± .65	172.7 ± 7.1	15.4% ± 4.9
$5.3x10^{14}$ ($3.4x10^{15}$)	14.9% ± .6	161.3 ± 6.6	20.7% ± 4.0
$1x10^{15}$ ($6.5x10^{15}$)	13.3% ± .54	144.0 ± 5.9	29.3% ± 4.0

After the final electron exposure of $1x10^{15}$ e^-/cm^2 ($6.5x10^{15}$ e^-/in^2), the **solar cells** were annealed, in air, at various temperatures. Table 2 shows the annealing schedule and the **solar cell** efficiency recovery obtained relative to the beginning of life (BOL) characteristics.

Phase I of the solar cell investigation has been completed and plans are being formed for phase II, in situ testing of cells under a standard load. These cells will be exposed to a combined environment of ionizing radiation, ultraviolet radiation, and high-vacuum and thermal cycling while under load. Phase II also includes further investigation of the thermally induced recovery phenomenon demonstrated in phase I.

Tada, H.Y., TRW Systems Group; Anspaugh, B.E.; Downing, R.G.; and Carter, J.R., Jr.; "Jet Propulsion Laboratory Solar Cell Radiation Handbook," JPL Publication 82-69, Pasadena, California, 1982.

D.L. Edwards/EH15
(205) 544–4081
Sponsor: Space Station Project Office

Table 2. The Annealing Schedule and the Solar Cell Efficiency Recovery Relative to BOL Characteristics

Annealing Temperature °C (°F)	Time (Hours)	Before Annealing % BOL Efficiency	After Annealing % BOL Efficiency
200 (392)	2	70.8% ± 7.1	72.9% ± 7.3
200 (392)	4	70.8% ± 7.1	75.1% ± 7.5
250 (482)	2	70.9% ± 7.1	87.8% ± 8.9
250 (482)	4	70.9% ± 7.1	87.0% ± 8.8
300 (572)	2	69.6% ± 6.9	22.4% ± 2.4
300 (572)	4	69.6% ± 6.9	22.0% ± 2.5

Coronal and Interplanetary Physics

The **solar atmosphere**, or corona, expands supersonically and becomes the solar wind while the Sun's highly structured magnetic field superimposes a complex temporal and spatial pattern on the expansion. Eventually, the solar wind runs into the **local interstellar medium (LISM)**, is slowed and deflected to flow to the **heliotail**. All this is shown by the model calculation illustrated in figure 42.

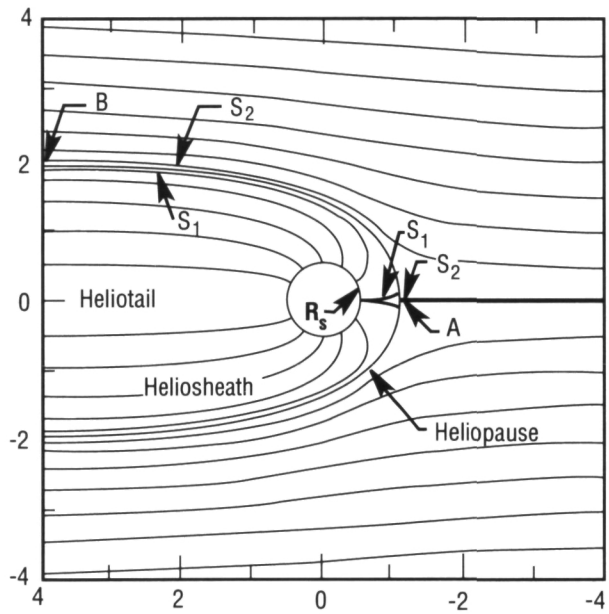

Figure 42. Effect of Sun's Magnetic Field on the Solar Atmosphere

In this figure, the Sun is at the center of the circle of radius R_s, and the scale is such that the orbit of Pluto lies inside R_s. The solid lines are streamlines of the solar wind inside the **heliopause** and the **LISM** outside the **heliopause**. The solar wind goes through a standing-shock transition at R_s from supersonic to subsonic flow, after which it turns to flow down the **heliotail**. The **LISM** simply flows around the outside of the heliosphere. The model is a new development designed specifically to examine solar wind flow between the terminal shock at R_s and the **heliopause** and **LISM** flow beyond the **heliopause**.

This model has revealed an important new result for planning exploration of the outer heliosphere.

The model has been used to show that the distance from R_s to the stagnation point between the solar wind and **LISM**, at A, is much smaller than R_s. The significance of this is that a spacecraft traveling in the upstream direction toward A has a relatively small additional distance to go to reach the **heliopause** once it passes through the terminal shock. Presently, there are three spacecraft in the outer solar system—Pioneer 10 and Voyagers 1 and 2. Pioneer 10 is heading downwind (to the left on the diagram) while both Voyagers 1 and 2 are heading upwind in the general direction of the stagnation point. All three spacecraft have returned data indicating they may be nearing and may soon penetrate the terminal shock.

Until recently, it was believed that the distance between R_s and A would be at least as large as that to R_s and hence there would be no hope the Voyagers would survive long enough to reach the **heliopause**. Now, however, just the opposite seems to be true. If either of the Voyagers encounters the shock within the next decade, it will have an excellent chance of encountering the **heliopause** within another 5 years. This has also given impetus to planning for the Heliospheric Probe which would move outward from the Sun at a speed several times that of Pioneer 10 and the Voyagers, and therefore would reach the terminal shock and the **heliopause** in just a few years instead of in decades.

The reason the **heliopause** is such a sought-after goal is that when reached, it will permit in situ sampling of interstellar plasma. The composition, temperature, and density of interstellar plasma can be used to assess global properties of the Milky Way and to learn how the solar system differs from them.

C-2

The heliospheric flow model is now being extended to include magnetic field effects and asymmetries that have already been discussed qualitatively. This research is a part of the ongoing Coordinated Heliosphere Observations (CoHO) program involving all of the above-mentioned spacecraft, and of the Ulysses mission.

Suess, S.T., and Nerney, S.F., "Flow Downstream of the Heliospheric Terminal Shock 1: Irrotational Flow," *J. Geophys. Res.*, Vol. 95, No. A5, pp. 6403–6412, 1990.

S.T. Suess/ES52
(205) 544–7611
Sponsor: Office of Space Science and Applications

Solar Magnetic Fields

The interaction of **magnetic fields** and plasmas is the root cause of the dynamic, high-energy phenomena of **flares**, mass ejections, and eruptive filaments observed on the **Sun**. Thus, in current solar research, extensive observational studies are carried out to develop an understanding of just how the solar **magnetic field** plays this key role in solar activity. MSFC has a unique instrument for observing the **Sun's magnetic field**, the MSFC Solar **Vector Magnetograph**. The information derived from observations with it has made significant contributions to an understanding of solar activity. Because of this research, MSFC is now recognized worldwide as a leader in the study of solar **magnetic fields**. Over the past year, research efforts in this MSFC program have been concentrated in three major areas, with the significant accomplishments in these areas summarized below.

The observational program to upgrade the vector magnetograph system has been completed and an H-α telescope was mounted alongside the **vector magnetograph**. We now obtain simultaneous, coaligned images of the vector **magnetic field** in the photosphere and the chromospheric "field" as outlined by H-α structures. The data analysis facilities have been upgraded by a micro-Vax 3500 computer, array processor, and optical disk. A video processor has been installed to combine **vector magnetograms** and H-α images in a movie format, thereby enhancing studies of solar activity.

Observations with the coaligned magnetograph and H-α telescope have been undertaken since September 1989; in the first 2 months of operation, several major **flares** were observed, including an x-ray **flare** on October 15. This **flare** started 6 minutes after a **vector magnetogram** was obtained at 1424 u.t. Analysis of the data showed characteristics of highly stressed **magnetic fields** where energy is known to be stored. This analysis showed that there was only one area of strongly stressed fields in this active region, near its center. An H-α image, recorded during the **flare** with the coaligned telescope, was

compared with the magnetic field data. This comparison of the two images clearly showed that the **flare** occurred in the area where the field was stressed the most.

The importance of having coaligned, cotemporal magnetograms and H-α images was borne out by an analysis of observations obtained during the period October 28–30, 1989. Initial analysis showed reconfigurations of the **magnetic field** going hand-in-hand with changes in filament structures in an active region. On October 28, a long filament was observed to run parallel to the measured transverse **magnetic field**. On the 2 succeeding days, realignments were seen in the **magnetic field**, the transverse field in the area of the filament disappeared, and the filament was no longer visible in the H-α image.

We have developed an analysis program to derive the vector **magnetic field** in a sunspot from MSFC **vector magnetograph** data using a method of nonlinear least square optimization whereby the observed filtered Stokes profiles are compared with those generated from theoretical solutions of the polarized radiative transfer equations. In addition to the **magnetic field** components, this method gives values for the ratio of the line-center to continuum opacities (h_0), Doppler width, damping constant, and slope of the source function.

A detailed mathematical analysis of the foundations and limitations of the techniques used in calculating force-free magnetic fields from magnetograph observations was carried out. The study has led to an understanding of the limitations inherent in the two basic extrapolation methods, and thus has provided guidance as to the directions to be taken in developing extrapolation procedures that have credible mathematical foundations. In collaboration with G. Poletto, modeling of extended magnetic structures between active regions is taking place. The topology of large interconnecting loop systems seen by Solar Maximum Mission x-ray observations is being studied with the model to determine processes that form these loops.

The Experimental Vector Magnetograph (EXVM) facility modifications for the EXVM were completed with the installation of a new telescope dome at the Solar Observatory. Facilities were also constructed to house a 0.91-m (3-ft) diameter heliostat that will be used for bench tests of the EXVM. Modifications to the 30-cm (12-in) Cassegrain EXVM telescope were made, and the mirrors of the telescope were recoated. The EXVM detector and data system were delivered; both systems were developed under a Small Business Innovation Research Program. The detector is a large-area, high-speed charge-coupled device (CCD) camera that is designed for a 2,048×2,048 pixel array with multi-port readout. A unique polarimeter was designed by MSFC scientists to be used in the EXVM which will give much higher sensitivity than other designs.

Hagyard, M.J., "The Significance of Vector Magnetic Field Measurements," in *Memorie della Societa Astronomica Italiana*, in press (1990).

Balasubramaniam, K.S., and West, E.A., "Polarization Studies of Zeeman Affected Spectral Lines Using the MSFC Magnetograph," to appear in SPIE Polarimetry Conference Proceedings, May, 1990.

Gary, G.A., "Mathematical Basis for the Extrapolation of Solar Nonlinear Force-Free Magnetic Fields," in *Memorie della Societa Astronomica Italiana*, in press (1990).

M.J. Hagyard/ES52
(205) 544–7612
Sponsor: Office of Space Science and Applications

Magnetospheric Physics

Magnetospheric physics is the application of continuum mechanics and plasma physics to obtain an understanding of the flow of matter, momentum, and energy near and within the volume occupied by the Earth's magnetic field. The otherwise dipolar magnetic field is compressed on the sunward side and stretched into a long tail on the antisunward side, by the supersonic flow of plasma emanating from the Sun, the solar wind. The currents which affect this distortion of the geomagnetic field are carried through geospace by the ionized gas of charged particles (plasma) which is present. As our understanding of this system improves, we are better able to comprehend and anticipate the interactions between solar events, interplanetary conditions, and terrestrial responses. Moreover, our solar-terrestrial environment also serves as the laboratory of opportunity for in situ observations of processes which are of astrophysical importance in such situations as planetary and cometary magnetospheres and stellar atmospheres. Having studied such processes both remotely and locally, we gain an improved ability to interpret the electromagnetic radiations received from distant astrophysical plasmas.

The research emphasis of the Magnetospheric Physics Branch at MSFC continues to be the observation of low-energy or core plasma which originates in the ionosphere and has been found to supply plasma to the entire magnetosphere. Highlights of our activities during the previous year include:

- *Development of a double-focusing electrostatic mirror design has provided dramatically improved sensitivity for the Superthermal Ion Composition Spectrometer (STICS), which was successfully flown aboard a University of New Hampshire sounding rocket flight in February 1990,*
- *Development of a new ultraminiaturized thermal electron spectrometer for space flight in planetary ionospheres and magnetospheres,*
- *Successful completion of the design phase for the Thermal Ion Dynamics Experiment/Plasma Source Investigation (TIDE/PSI) for the International Solar Terrestrial Physics Program (ISTP) POLAR spacecraft,*
- *Continued definition of the Cometary Retarding Ion Mass Spectrometer (CRIMS) for the Comet Rendezvous Asteroid Flyby mission,*
- *Integration and test of the flight unit of the Research on Orbital Plasma Electrodynamics (ROPE) investigation for the Tethered Satellite System (TSS),*
- *Modeling of the acceleration effects of magnetospheric dynamics on low-energy convecting plasma entering the magnetotail,*
- *Discovery that the orientation of the interplanetary magnetic field has a strong effect on the polar wind of plasma from the Earth's ionosphere, presumably due to varying penetration of solar plasma into the polar cap region,*
- *Further development of the MSFC empirical plasma specification model, including the development of a capability for ray tracing of plasma waves within the observed distribution of plasma in the magnetosphere,*
- *Identification of source and propagation effects in the funnel-shaped wave-emission spectrograms seen in equatorial magnetosphere,*
- *Discovery of evidence that the heating of plasma in the equatorial plasmapause region is much more localized to the Equator than is the heated plasma itself, indicating a very localized heating mechanism.*

Neutral Environment With Plasma Interactions Monitoring System

Space Station *Freedom* will provide a large, stable platform with high electrical power capabilities needed to support several large attached payloads. This capability will offer opportunities for a variety of investigations in the fields of space physics, astrophysics, communications, and Earth observations. Unfortunately, the very size of the **space station**, the large solar arrays, the frequent transportation traffic, the operations of reboost thrusters, periodic vacuum venting, and other sources will create perturbations in the external **environment** which are currently beyond our capabilities to predict.

Over the past 2 1/2 years, a study has been in progress to define a system of instruments to be placed on Space Station *Freedom* to measure, understand, and model these environmental perturbation effects. This system, called the Neutral Environment with Plasma Interactions Monitoring System (NEWPIMS), will include three baseline units to be located along the **space station** truss (fig. 43) to provide measurements of the neutral gas; **plasma**, electric, and magnetic fields; particulates; and stimulated emissions from the ultraviolet to the near-infrared. These instruments will provide information on the gas species, surface deposition, field variations, electrical charging, and other processes as a function of the various operations of the station.

This study has also been coordinated with the space station international partners in Canada, Europe, and Japan, and the results have been widely disseminated throughout NASA and the science community. There is widespread recognition that a monitoring system with the NEWPIMS capabilities is needed during early Space Station *Freedom* construction. Once the NEWPIMS program is approved, we propose to initiate the selection of instruments and the design of the NEWPIMS units.

W.T. Roberts/PS02
(205) 544–0621
Sponsor: Space Physics Division and Office of Space Science and Applications

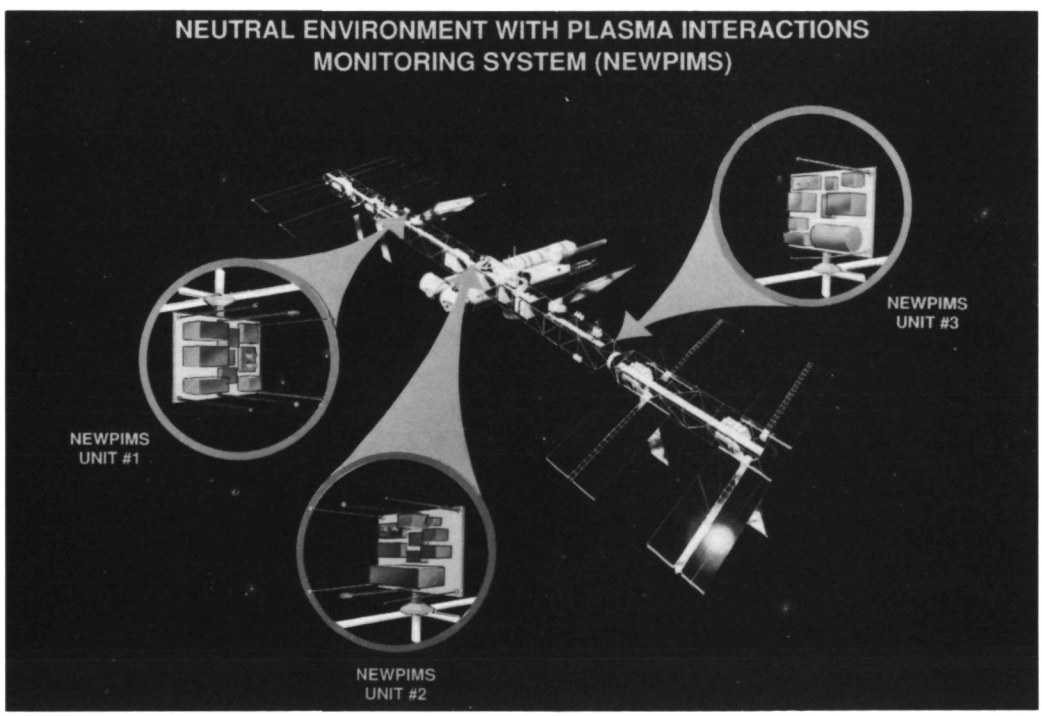

Figure 43. Neutral Environment With Plasma Interactions Monitoring System (NEWPIMS)

Plasma Waves and Ion Heating at the Earth's Magnetic Equator

Electromagnetic **plasma** waves occurring between the proton gyrofrequency and the lower hybrid reasonant frequency are found to be closely correlated with heated **plasma** at the Earth's **magnetic equator**. Both occur in a region within 5° to 10° in latitude of the **magnetic equator** and in the vicinity of the plasmapause. Frequency-versus-time spectrograms of the emission electric field strength are often found to display a funnel-shaped structure, as shown in figure 44. The funnels are characterized by a relatively narrow frequency spectrum just below the lower hybrid frequency at latitudes above and below the **magnetic equator**. The bandwidth of the emission broadens to a maximum at the Equator, with a lower frequency limit that minimizes near the proton gyrofrequency at the **magnetic equator**. The upper frequency limit for the emission remains near the lower hybrid frequency.

Figure 44 also shows the simultaneous occurrence of heated hydrogen at the **magnetic equator**. The lower panel in the figure shows hydrogen count rates as variations in gray-scale intensity, in a spin-phase-versus-time format. The solid and dashed lines in the panel correspond to the field-aligned and antifield-aligned directions. Two elongated intensifications in counting rate appear in the panel corresponding to heated and trapped hydrogen **ions**. The **ions** are found with temperatures that range from 10 eV to 50 eV and are heated relative to the usual 1-eV plasmaspheric **plasma**. The **ions** are trapped by the mirror force, owing to the magnetic minimum at the Earth's **magnetic equator**. Also evident in the spin-phase **ion** spectrogram are field-aligned and antialigned, counter-streaming **ion** populations. These **ions** also have a low temperature of about 1 eV.

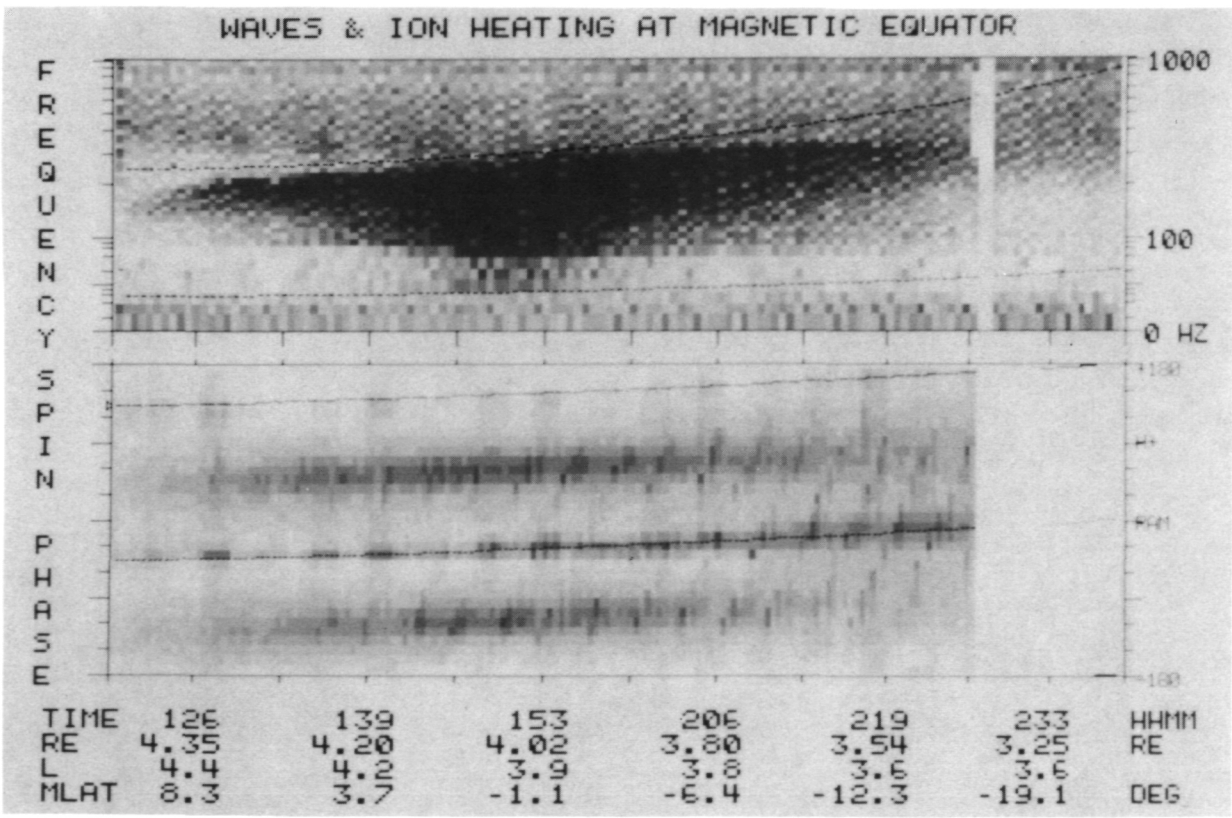

Figure 44. Simultaneous Occurrence of Heated Hydrogen at the Magnetic Equator

The origin of the waves, the cause of the often-observed funnel-shaped frequency-time structure, and the mechanism and source of the heated **ions** are under study. The waves are currently thought to result from an energetic ring distribution that is found in observations of the ring-current **plasmas**. These waves are then expected to reduce the free energy of the phase space ring distribution and to heat, in the perpendicular direction, the low-energy, field-aligned streaming **plasma**. This perpendicular heating is thought to eventually lower the mirror latitude of these heated **ions** to those observed.

The funnel-shaped spectral structure appears to be the result of wave propagation effects coupled with the initial-wave-normal near-90° angle for largest growth of the waves. Wave group velocities, at frequencies well below the lower hybrid frequency, are nearly along the initial wave vector angle to the magnetic field. These waves are tightly confined to the **magnetic equator**, as they propagate outwards. Wave group velocities, at large wave-normal angles, become nearly field-aligned for emission just below the lower hybrid frequency as a result of resonance distortion of the index of refraction surface. These waves propagate up or down the field lines to larger latitudes until reflected by propagation into regions of larger magnetic field strength and a corresponding relaxation of distortion in the index of refraction surface for the **plasma** waves. The result is that the higher frequency waves are able to propagate to higher latitudes and are seen before the lower frequency waves when observed from an orbiting spacecraft, roughly following magnetic field lines, during orbital passes across the **magnetic equator**.

Overall, a picture of energy transport associated, possibly, with plasmaspheric refilling and trapping is emerging from the study. A mechanism may have been found for energetic ring-current **ions** to heat and trap outflowing ionospheric **plasma** at the **magnetic equator** through a particle-wave-particle process. This possible role for the observed fast-mode Alfven or whistler mode waves continues to be studied.

Olsen, R.C., Shawhan, S.D., Gallagher, D.L., Green, J.L., Chappell, C.R., and Anderson, R.R., "Plasma Observations at the Earth's Magnetic Equator," *J. Geophys. Res.*, 92, pp. 2385-2407, 1987.

Boardsen, S.A., Gallagher, D.L., Gurnett, D.A., and Peterson, W.K., Funnel Shaped Low Frequency Equatorial Waves, EOS Abstract, Spring AGU Conference, 1990.

D.L. Gallagher/ES53
(205) 544–7587
Sponsor: Office of Space Science and Applications

Superthermal Ion Composition Spectrometer Double-Focusing Electrostatic Analyzer

Study of the new transport features of the ionosphere/magnetosphere requires a new class of instruments with greater sensitivity and resolution and the desired trade-off between the two. The Superthermal Ion Composition Spectrometer (STICS) provides such a capability. STICS first measures the particles' arrival angle by means of an **electrostatic angle analyzer**. Particles then pass into the cylindrical **energy analyzer** where the ions' energy/charge is then measured. They are then accelerated into a scanning magnetic mass spectrometer which is monitoring two species simultaneously.

The STICS analyzer is a combination of two **electrostatic deflection analyzers** as shown in figure 45. The **electrostatic angle analyzer** consists of two electrodes at two oppositely swept potentials which effectively deflect the "look" direction of the device. Slits in the exit plate of the angle analyzer admit particles to the **energy analyzer**. This **energy analyzer** has a back plate and cylindrical sides at the selecting potential, and the front plate at the potential of the instrument chassis. Due to this cylindrically symmetric shape, the electric potential contours are concave so that it focuses in two dimensions.

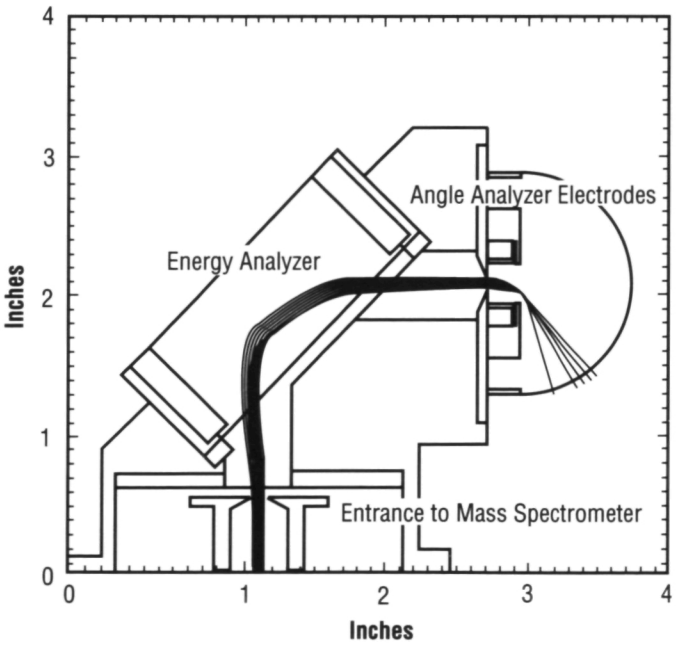

Figure 45. Numerical Ray Tracing of Particles Through the STICS Instrument

In 1989 and 1990, this design was optimized by means of numerical potential solutions and particle ray tracing, the result of which is illustrated in the figure. Ray tracing studies showed that the **electrostatic analyzer** can be designed to provide greatly expanded solid angle and energy response bandwidth, thereby increasing the sensitivity. Increasing the depth of the cylinder showed that the effective focal length of the mirror decreased. In an iterative fashion, this focal length was optimized so as to bring the entrance slit to a focus at the exit to the mass spectrometer. This enabled the **energy analyzer** to accept a much wider range of energies and angles.

Preflight lab tests in late 1989 showed the STICS geometric factor to be greatly increased. Data obtained from STICS during its February 1990 launch in Alaska has shown this flight to be successful, and shows some interesting results which are now being analyzed.

V.N. Coffey/ES53
(205) 544–7635
Sponsor: Magnetospheric Physics

The Statistical Behavior of Hydrogen Ion Temperatures From Dynamics Explorer 1/Retarding Ion Mass Spectrometer

This investigation examines the statistical behavior of the temperature of magnetospheric hydrogen ions as a function of L-shell, local time, and solar and geomagnetic activity. The purpose of this study is to detail the behavior of the temperature with physical parameters as a precursor to developing an empirical model of H^+ temperature in the **plasmasphere**.

A study of the statistical behavior of plasmaspheric **ion temperatures** is a necessary step in preparation for generating an empirical model of temperature. The average effects of different heating mechanisms can be studied by using an empirical model of **ion temperature** to delineate the average distribution of energy throughout the **magnetosphere**. Such a model can be used as a check on heating studies or as a base with which to compare the results from computer models. It is also useful for prescribing appropriate conditions in theoretical studies. **Ion temperature** is a reflection of the efficiency of heat sources and sinks (e.g., photoelectrons, ring current, solar flux, particle precipitation, density of neutrals, etc.) that are active in the **magnetosphere** and ionosphere so that, in effect, a study of the statistical behavior of **ion temperature** is also a study of the sources, sinks, and transport of heat.

The data base used in this study is composed of about 20,000 **ion temperatures** derived for hydrogen from measurements made during 1981, 1982, and 1983 by the Retarding Ion Mass Spectrometer (RIMS) on the Dynamics Explorer 1 satellite. Each of these temperatures is derived from a 1-minute average of retarding potential analyzer (RPA) data from RIMS. Each derived temperature value is characterized by the local time, L-shell, solar activity (F10.7), and geomagnetic activity (Kp). Local times are divided into two 12-hour bins, one for dayside (from 0600 through 1200 to 1800 hours) and one for nightside (from 1800 through 2400 to 0600 hours).

Solar activity is divided into three ranges: low, medium and high, using a 30-day average of the solar F10.7 flux. Low activity included F10.7 ranges to 150 (10**-22 W/m^2/Hz), medium from 150 to 210, and high included ranges above 210. Geomagnetic activity is measured using the maximum 3-hour Kp level in the 24 hours preceeding the time of the temperature measurement. The L-shells are grouped into bins of one unit (i.e., L-shell of 2 includes all L-shells from 2.0 up to, but not including, 3.0).

The study has shown that a wide range of temperatures (about three orders of magnitude) is encountered at almost all levels of either solar or geomagnetic activity on L-shells greater than two. For each of the local time groups, the lowest and highest temperatures appear to show systematic behavior with L-shell, solar, and geomagnetic activity. Since these temperatures are indicative of the extremes in conditions encountered by the ions, a statistical study of their behavior is useful in understanding the influences on **ion temperatures**.

Scatter plots of the lowest temperatures on each L-shell suggest that these temperatures have little dependence on the geomagnetic activity and can be represented by a single weighted average. The average is found by weighting each minimum according to the number of temperature values in the particular group from which the minimum is drawn. Such a weighting recognizes the fact that the larger the population from which a temperature is taken, the greater the likelihood that the actual limiting temperatures are contained in that population.

While the minimum **ion temperature** can be represented by a single value, the maximum temperature appears to have a bimodal distribution, having one temperature for maximum Kp levels

below some critical value and another, higher value above that Kp level. The first order, the maximum temperatures above and below the critical Kp value, show no clear Kp dependence. For this reason, the two temperatures on each L-shell, one above and one below the critical Kp value, are represented by a weighted average in the same way as the minimum temperatures. The critical Kp value for each L-shell is found by examining plots, such as figure 46, of the maximum temperature as a function of the maximum Kp. Figure 46 is an example of the behavior of the maximum temperatures for L=2. In this example, the critical Kp value is 4.5.

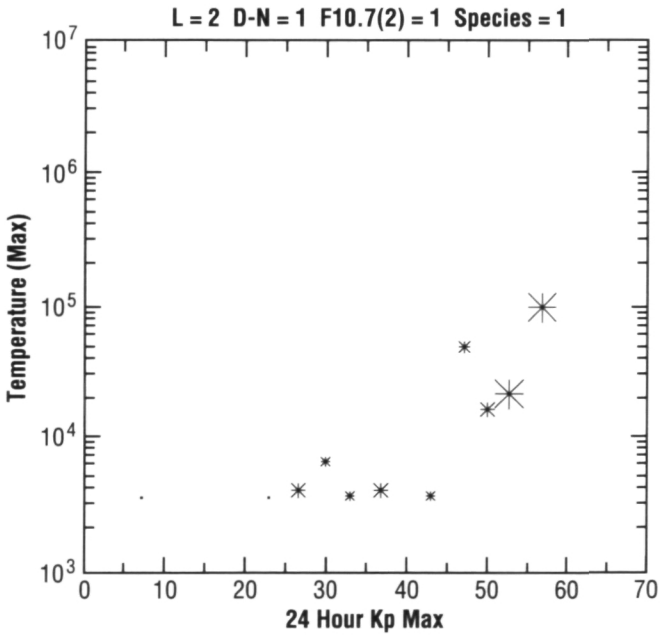

Figure 46. Temperature as a Function of the Highest Level of Kp in the Preceding 24 Hours. The Bimodal Behavior of the Temperature is Seen as the Change in Level at a Kp of About 4.5

Two trends are seen in the data. One of the trends is that the temperature tends to increase with increasing solar activity. This trend is evident in the nightside as well as the dayside local time sectors. The other trend is that for the lower L-shells, the nightside temperatures are lower than the corresponding dayside temperature. In addition to these two trends, it appears that the critical Kp value for the maximum temperatures decreases with increasing L-shell, and vice versa, as though the effects of the higher levels of geomagnetic activity are able to penetrate further into the **plasmasphere**. This behavior is thought to be related to the heating of ions by particles in the ring current and, through this, to the level of geomagnetic activity.

The increase in temperature with solar activity is consistent with a photoelectron heat source. Heat is transferred to the ions from the photoelectrons through collisions. More photoelectrons are generated during times of high solar activity so that the ion temperature is higher during these times. The increase in heat should occur over all L-shells and this is, in fact, what appears to happen. The lower temperatures on the nightside for the lower L-shells probably indicate the loss of the photoelectron heat source at or near the foot of each of the L-shells. The higher nightside temperatures during times of high solar activity must result, in part, from the higher dayside temperatures.

In summary, this study has shown that the temperature of the H^+ ions in the **plasmasphere** behave as one might expect on physical grounds if two heat sources are acting. One is the photoelectron heat source which is controlled by the solar flux. The other source seems to be related to ions in the ring current which is related to geomagnetic activity.

P.D. Craven/ES53
(205) 544–7639
Sponsor: Office of Space Science and Applications

Imaging of Magnetospheric Energy in the Vacuum Ultraviolet

Energetic particles from the solar wind that are swept up by the Earth's magnetic field are accelerated by the various electromagnetic processes operative within the **magnetosphere**, and large fluxes of these particles (equivalent to 100-million kilowatts during the almost-daily events known as magnetic substorms) are channeled down into the atmosphere at high latitudes. The resulting collisions between the energetic particles and the atmospheric gases produce the aurorae. The aurorae occur around a magnetic field-line footprint that roughly corresponds to a geomagnetic latitude of 70°, but are displaced to lower latitudes at local midnight, forming a band of emissions known as the **auroral oval**. Imaging of this oval from space provides spatial/temporal information that maps back to different regions of the **magnetosphere**, and provides information on the total energy influx, acceleration processes, and (with careful selection and interpretation of emission features) can provide characteristic energy of the incoming particles. The energetic particle collisions produce emissions throughout the spectrum from the vacuum ultraviolet to the infrared. However, to date, almost all of the work has been in the visible, and restricted to nightside aurorae because of the severe limitations imposed by the bright scattered sunlight on the dayside of the Earth. A carefully designed instrument, operating in the vacuum ultraviolet can provide information on both the sunlit and dark auroras, vastly increasing the scope and value of the data for the global studies now needed. The **Ultraviolet Imager (UVI)** is presently under development for the POLAR spacecraft of the Global Geospace Science (GGS) program and is intended to perform these global studies (fig. 47).

The **UVI** will provide information on:

- The spatial and temporal morphology of the aurorae
- The total energy deposited into the atmosphere in the form of energetic charged particles
- The characteristic energy of the particles.

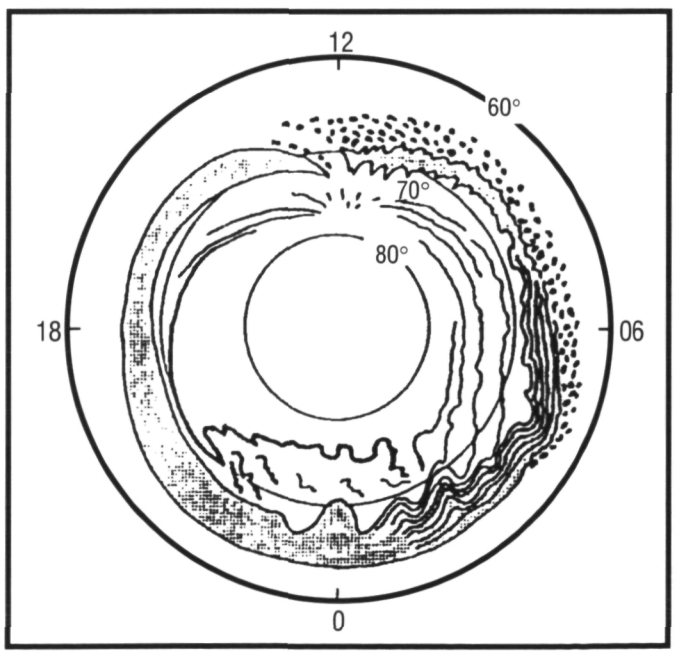

Figure 47. Typical Auroral Oval With 8×8 Degree of View from 9Re Apogee

It will provide a frame of reference that allows the auroral features to be related to events monitored in remote regions of the Earth's vast **magnetosphere**.

The interpretation of these images requires comprehensive models of the Earth's atmosphere and its interaction with charged particles.

This instrument will be located on a despun platform on one end of the satellite (fig. 48) and will be able to view the **auroral oval** steadily while the spacecraft spins about its orbit. This orbit is to be highly eccentric (9×2 Earth radii) allowing excellent viewing of the entire **auroral oval** for approximately 9 hours per orbit, and higher spatial resolution studies of smaller regions for the remaining 9 hours. In order to meet its objectives, the instrument design has had to push the technology in several areas: optics, vacuum ultraviolet filters, and detectors. The instrument is a fast optical system (f/2.8) that achieves good imaging over its full eight-degree field of view. The focal plane detector is an intensified-charge-coupled device (-CCD) system that represents an evolution of systems developed by our group for other programs. In order to make quantitative measurements in the 1,200 to 2,200 Å wavelength region, new filters have been developed that achieve passbands of down to 50 Å (fig. 49), a major advance on the previously attainable passbands in this region. The instrument has a low threshold of detection and a large signal dynamic range.

The instrument is scheduled for launch in June 1993 and, over the multiyear mission, should produce several hundred images a day yielding information on the energetics and physics of the solar-terrestrial system that we do not have today.

Germany, G.A., Torr, M.R., Richards, P.G., and Torr, D.G., "The Dependence of Modeled O1 1356 and N_2 Lyman Birge Hopfield Auroral Emissions on the Neutral Atmosphere," *J. Geophys. Res.*, p. 7725, 95, 1990.

Zukic, M., Torr, D.G., Spann, J.F., and Torr, M.R., "VUV Thin Films Part I: Optical Constants of BaF_2, CaF_2, LaF_3, MgF_2, Al_2O_3, HfO_2, and SiO_2 Thin Films in the VUV," in press, *Applied Optics*, 1990.

Zukic, M., Torr, D.G., Spann, J.F., and Torr, M.R., "VUV Thin Films Part II: Vacuum Ultraviolet All-Dielectric Narrowband Filters," in press, *Applied Optics*, 1990.

M.R. Torr/ES51
(205) 544–7591
Sponsor: Office of Space Science and Applications

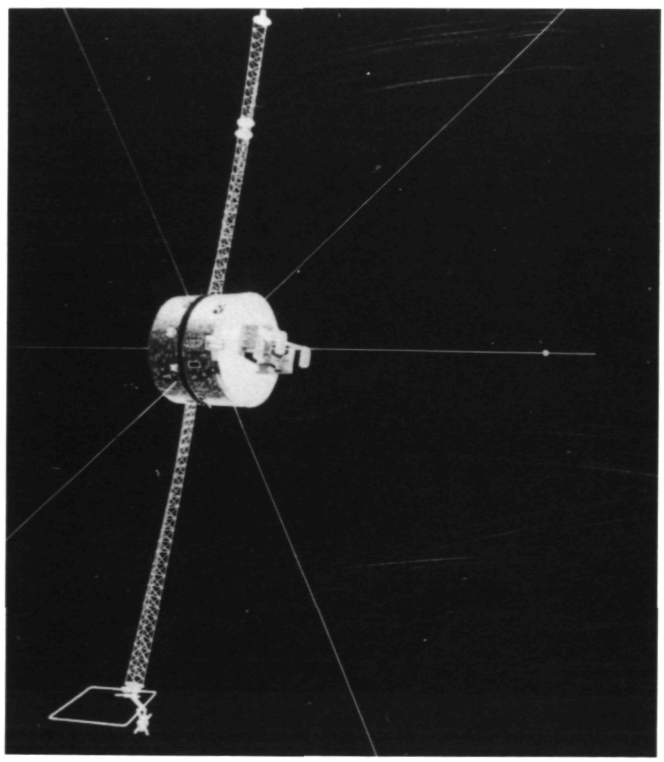

Figure 48. Polar Spacecraft With UVI on Despun Platform

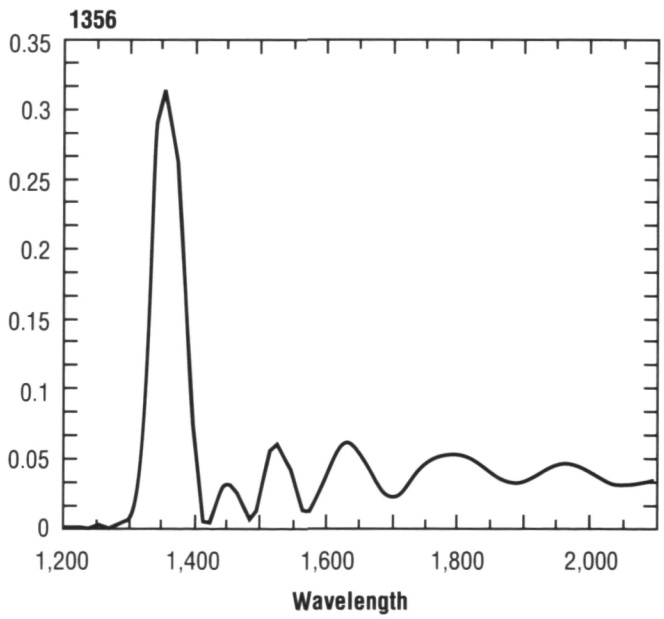

Figure 49. Example of Narrow VUV Filters Developed for the UVI

Interplanetary Magnetic Field Influences on the Polar Wind

The outflow of plasma from the polar cap has long been a subject of interest in **magnetospheric** physics. One reason is that the polar cap is a location where the ionosphere is believed to be influenced not only by Earth's magnetic field and **plasma** but also by the magnetic field and **plasma** within **interplanetary space**. This latter combination of **plasma** and fields emanates from the Sun and is a prime means by which the Sun influences Earth. The interaction between the magnetic field from the Sun and Earth produces interesting paths for charged particles which move easiest along the magnetic field lines. Under certain configurations these two fields are believed to merge, thus making it possible for solar particles to reach the Earth and for Earth-borne particles to reach **interplanetary space**. How these separate sets of particles, one streaming away from Earth and the other towards, coexist along these magnetic field lines has been a subject of much speculation.

Observations of this interaction have been limited by the unavailability of properly instrumented and located satellites. Recently Chandler, et al., (1990) used data from the Dynamics Explorer 1 satellite to study the ions which are produced in Earth's polar ionosphere. Using observations of the lowest energy ions in the polar ionosphere, made by the MSFC/ Retarding Ion Mass Spectrometer, Chandler, et al., were able to investigate the variation of the velocity, flux, and density of these ions as a function of altitude and varying geophysical conditions, including magnetic field orientations. Ions in this region of Earth's **magnetosphere** are generally observed to be flowing upward with velocities of several kilometers per second and are referred to as the polar wind. Altitude profiles of the hydrogen ion (H^+) velocities from this study reveal a dependence on the north-south, or "z," component of the interplanetary magnetic field (IMF B_z). Most noticeable were the differences in the maximum outflow speeds for H^+ which showed a marked dependence on both the magnitude and direction of B_z (fig. 50).

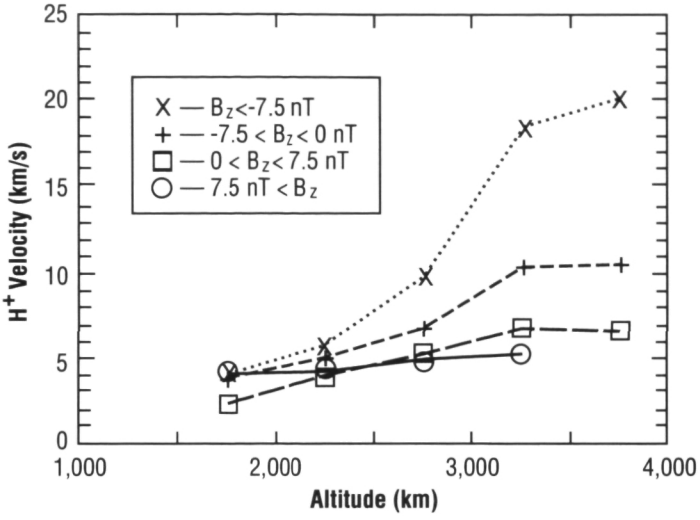

Figure 50. Variation in the Average H^+ Velocity With the Direction and Magnitude of IMF B_z

Recent theoretical work (Barakat and Schunk, 1984; Ho, et al., 1990) suggests that the presence of hot **magnetospheric** electrons on polar cap field lines will significantly affect the nature of the polar wind. Barakat and Schunk (1984) showed that in their model the presence of hot electrons over the polar cap could lead to contact surfaces between the hot and cold electron populations which would produce an upward-directed electric field. Such an electric field would reflect ionospheric electrons while accelerating the ions. This prompted Barakat and Schunk to conclude that the polar wind outflow would be enhanced under such conditions. In contrast, Ho, et al., (1990), using a different approach, concluded that if hot electrons raised the electron temperature significantly at high altitudes above the polar ionosphere, the resulting thermal gradients would reflect upgoing ions.

Not only is the effect of hot, precipitating **magnetospheric** electrons on the polar wind under debate, but the conditions under which such electrons are present in the cap are not fully known either. A naive view of the polar cap might suggest that under conditions of southward B_z the field lines are more likely to be connected to the solar wind field lines,

and thus have less pressure at their distant ends. On the other hand, a more open **magnetosphere** may make the entry of hot electrons more likely.

How can the observations of higher outflow speeds for polar wind H^+ under conditions of large and positive values of B_z be reconciled with an open/closed **magnetosphere** and hot particle precipitation? Continued study of the existing polar wind data through detailed comparisons with theoretical model results is necessary to determine the mechanisms which control the polar wind as the magnetic configurations change.

Barakat, A.R., and Schunk, R.W., "Effect of Hot Electrons on the Polar Wind," *J. Geophys. Res.*, 89, p. 9771, 1984.

Chandler, M.O., Waite, J.H., and Moore, T.E., "Observations of Polar Ion Outflows," (submitted to *J.Geophys.Res.*, in review).

Ho, C.W., Horwitz, J.L., Wilson, G.R., Singh, N., and Moore, T.E., "Magnetospheric Electron Effects on Polar Plasma Outflow," *Trans. AGU*, 71, p. 599, 1990.

M.O. Chandler/ES53
(205) 544–7645
Sponsor: Office of Space Science and Applications

Atomic Physics and Aeronomy

The mixture of gases comprising the upper atmosphere interacts with the incoming solar energetic particles and the electromagnetic radiation (photons) in the x-ray, ultraviolet, visible, and infrared part of the spectrum. Aeronomy is the study of the variety of physical and chemical processes in the upper atmosphere arising from this interaction. The photons at low energies are absorbed, emitted, and scattered by the atmospheric gases at various levels, involving electronic, vibrational, and rotational transitions, exhibiting a characteristic spectrum. The photons with sufficiently high energies ionize and dissociate atmospheric molecules producing reactive species or free radicals which interact with other molecules in a complex set of reactions. The characteristic thermal structure and the composition of Earth's atmosphere is a consequence of this complex interaction with the atmospheric gases.

A great deal of knowledge about the physical state of the atmosphere and the complex photochemical and dynamical processes can be obtained from the observations and analysis of atmospheric spectra in the ultraviolet and the infrared spectral regions. This information about the rich array of photochemical and dynamical processes that arise from the interaction of the solar radiation with the upper atmosphere is crucial to an understanding of the nature of this part of Earth's environment. The ongoing studies involve ground-based and space-borne atmospheric observations, laboratory experiments for measurements of molecular parameters, and development of theoretical models and analytical techniques for interpretation of the observations.

Development of a Microchannel Plate-Based Low-Energy Electron Spectrometer

For many years, space scientists have measured the spectrum of **electrons** in the near-Earth space using single-particle spectrometers. These measurements have been limited to energies above several electron volts (eV's), however, due to the difficulty of carrying out single-particle **electron** measurements at low energies. It is nevertheless true that the vast majority of **electrons** in the Earth's **ionosphere** are at energies of less than 1 eV. The technique most commonly used to diagnose this population of low-energy **electrons** is the Langmuir probe, which involves immersing an electrically biasable probe into the **ionospheric** plasma and measuring the electric current to the probe as a function of applied electrical bias. The collected current includes contributions from both the **electrons** and ions in the plasma. The resulting current voltage curve may be analyzed to yield the temperature and density of **electrons** and ions in the sample's plasma. Several disadvantages associated with this measurement technique include:

- The requirement that a specific form (i.e., Maxwellian) be assumed for the ion and **electron** distribution functions
- The inability to identify spectral features in the distribution function
- The inability to identify anisotropies in the distribution function.

On the other hand, the specific spectral shape and any anisotropies in the ambient **electron** population are very important parameters to the diagnosis of **plasma heating** and instability.

One of the major difficulties associated with measurement of the **electron** distribution at very low energies is that these **electrons** are gyrating about the Earth's magnetic field in circles whose sizes are as small or smaller than the **instruments** deployed to make the measurements. These **instruments** generally operate under the assumption that, in the **instruments'** absence, the charged particles under study would move in straight lines. We have begun to address the dearth of low-energy **electron** measurements in near-Earth space through the development of a thermal **electron** capped hemisphere spectrometer (TECHS). This **instrument** will be a highly miniaturized version of the capped hemisphere electrostatic analyzer (Carlson, et al. 1983), and it will utilize microchannel plate detectors, with eight discrete anodes feeding Amptek A-111 charge-sensitive preamplifiers.

Figure 51 contains a schematic illustration of the TECHS **instrument**, along with the orbit of a typical detected ionospheric **electron**. Note from the scale of the diagram that the actual sensor size is 2.5 cm (1.0 in) (diameter) by 5 cm (2.0 in) (length). This high degree of miniaturization represents significant technical difficulty and is the major advance required to dip into the important range of low-energy **electrons**. **Electrons** entering the entrance aperture will be selected by energy per charge and directed onto the MCP/multiple anode detector system, where imaging with respect to arrival azimuth will be carried out. The sensor will be deployed from the spacecraft to prevent shadowing of the low-energy **electrons** by the spacecraft.

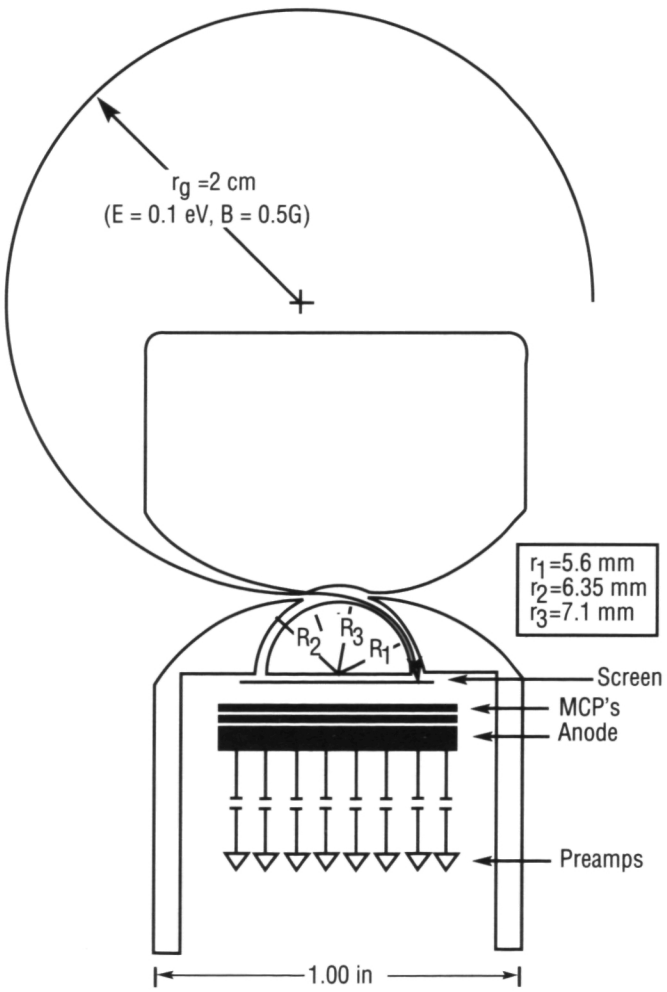

Figure 51. TECHS Analyzer

TECHS will be flown for the first time on one of the **Chemical Release and Radiation Effects Satellite-(CRRES-)** associated NASA sounding rockets (AA-4) in the summer of 1991 in the **ionosphere** above Puerto Rico. It will be used to measure the response of the ionospheric **electron** population to pumping by high-power electromagnetic waves injected by the Arecibo **ionospheric** heating facility. Such pumping has been inferred by ground-based optical measurements to energize ambient **electrons** to several eV (Carlson, et al., 1982). Bulk **electron** heating by nearly a factor of two, to more than 1,000 K, has also been inferred to result from the pumping, based on ground-based incoherent scatter radar (Duncan and Gordon, 1982). However, no direct spectral measurements will have been made prior to the maiden flight of TECHS over Arecibo.

Carlson, H.C., Wickwar, V.B., and Mantas, G.P., "Observations of Fluxes of Suprathermal Electrons Accelerated by HF Excited Instabilities," *J. Atm. and Terr. Phys.*, 44, p. 1089, 1982.

Carlson, C.W., Curtis, D.W., Paschmann, G., and Michael, W., "An Instrument for Rapidly Measuring Plasma Distribution Functions With High Resolution," *Adv. Space Res.*, 2, p. 67, 1983.

Duncan, L.M., and Gordon, W.E, "Ionospheric Modifications by High Power Radio Waves," *J. Atm. and Terr. Phys.*, 44, p. 1009, 1982.

C.J. Pollock/ES53
(205) 544–7638
Sponsor: Office of Space Science and Applications

Infrared Spectroscopy of the Stratosphere

A research program for continuing development of radiative transfer models and spectral inversion techniques for **infrared spectroscopy** of Earth's atmosphere has been in progress. The developing analytical techniques are being employed for analysis of balloon-borne **stratospheric** thermal emission observations in the middle- and far-infrared spectral regions. The middle-infrared investigation is being carried out in collaboration with the research group at Goddard (Kunde et al.), and the far-infrared work with the group at the Harvard-Smithsonian Center for Astrophysics (Traub, et al.).

An analysis of the observed infrared thermal emission spectra provides simultaneously determined profiles of a number of trace gases controlling the stratospheric **ozone** chemistry. It is now well-recognized that the numerous oxides of nitrogen, hydrogen, chlorine, and, to a lesser extent, bromine, control the destruction of **stratospheric ozone** through potent catalytic cycles such as:

$$\begin{aligned} & X+O_3 \rightarrow XO+O_2 \\ & XO+O \rightarrow X+O_2 \\ \text{Net:} \quad & O+O_3 \rightarrow 2O_2 \end{aligned}$$

where X represents any free radical species of the $NO_x(NO, NO_2)$, $HO_x(HO, HO_2, H_2O_2)$, $Cl_x(Cl, ClO)$, and the $Br_x(Br, BrO)$ families (Cicerone, 1987). The main catalytic cycles involving chemically active species of the above families are coupled through inactive reservoir species, notably HNO_3, N_2O_5, and $ClONNO_2$.

The reservoir species tend to buffer **ozone** destruction by sequestering the active species from two coupled families. The efficiency of the **ozone** loss process depends on the lifetimes of the chemically active species relative to the reservoir species. The current models of **stratospheric** chemistry are generally based on more than 200 reactions involving various species of the above families.

Of all the main families involved in the catalytic destruction of **ozone**, the NO_x family is believed to play the dominant role. The reactive nitrogen compounds of this family are formed in the stratosphere through photolysis of nitrous oxide (N_2O) transported upward from the troposphere. The maximum production rate of NO occurs at about 30 km (19 mi). Through a series of coupled photochemical reactions, **stratospheric** NO forms a number of reactive nitrogen-bearing species including N, NO, NO_2, NO_3, N_2O_5, HNO_3, HNO_4, and $ClONO_2$. The sum of all reactive nitrogen species (not including N_2) is referred to as the total odd nitrogen, and its concentration is defined here as $[NO_y] = [N] + [NO] + [NO_2] + [NO_3] + [2N_2O_5] + [HNO_3] + [HNO_4] + [ClONO_2]$. A knowledge of the vertical distribution of all reactive nitrogen species is important for a quantitative understanding of stratospheric photochemistry and **ozone** loss processes. In addition to partitioning of the NO_x family into various reactive and reservior species, it is also useful to have information about the total odd nitrogen concentrations in the **stratosphere**. It has been shown that the reduction of **ozone** due to processes involving the Cl_x species is strongly influenced by NO_y concentrations. It is thus important to have simultaneous measurements of the elements of NO_y and their diurnal variations. However, because of the difficulty involved in such measurements requiring both high spectral resolution and high sensitivity, the available data generally consist of simultaneous measurements of only a portion of the odd nitrogen family, and the total budget has to be inferred from several different data sets.

The only simultaneous measurements of all important elements of the odd nitrogen family that have been reported so far are the daytime absorption measurements of the **Atmosphere Trace Molecules Observed by Spectroscopy (ATMOS)** experiment on Spacelab 3 by Russell, et al. [1988], involving solar observations in the 2- to 15-μm region. They reported simultaneous measurements of the stratospheric distributions of NO, NO_2, HNO_3, N_2O_5, HNO_4, and $ClONO_2$, and the inferred distribution of NO_y for the Northern Hemisphere (29° N) at sunrise, and for the Southern Hemisphere (48° S) at sunrise.

Infrared thermal emission spectra of Earth's atmosphere in the 700–2,000 cm^{-1} region were obtained by the Goddard group with a cryogenically cooled high-resolution interferometer spectrometer (SIRIS) launched on a balloon flight from Palestine, Texas, on September 15–16, 1986. The observations exhibit spectral features of a number of stratospheric constituents, including important elements of the odd nitrogen family. A portion of the observed data has been analyzed for simultaneously measured vertical distributions of O_3, H_2O, N_2O, NO_2 (fig. 52), N_2O_5, HNO_3, and $ClONO_2$ (fig. 53). The measurements permit the first direct nighttime determination of the nighttime total odd nitrogen concentrations and partitioning of the important elements of the NO_x family. Comparisons of the total odd nitrogen budget made with the measurements by the **ATMOS** experiment and with the predictions of one-dimensional and two-dimensional photochemical models indicate significant discrepancies.

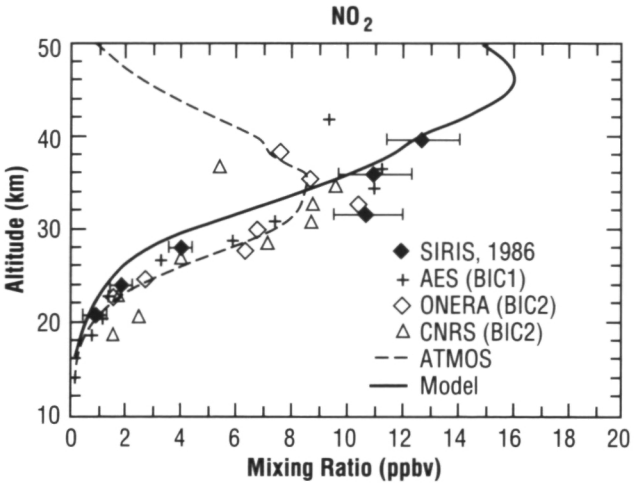

Figure 52. The NO_2 Profile Retrieved From the 1986 SIRIS Data With the Measurements by Other Groups Shown for Comparison

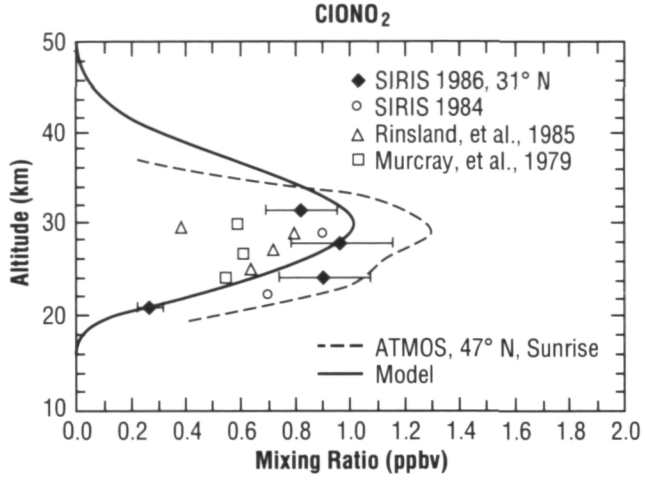

Figure 53. The $ClONO_2$ Profile Retrieved From the 1986 SIRIS Data With the Measurements by Other Groups Shown for Comparison

The far infrared thermal emission observations made by the Harvard-Smithsonian group during the Balloon Intercomparison Campaign (BIC II) in 1983 are presently being analyzed with a focus on the **stratospheric** distribution of $H_2{}^{16}O$ and $H_2{}^{18}O$.

Abbas, M.M., Glenn, M.J., Kunde, V.G., Brasunas, J., Conrath, B.J., Maguire, W.C., and Herman, J.R., "Simultaneous Measurement of Stratospheric O_3, H_2O, CH_4, and N_2O From Limb Thermal Emissions," *J. Geophys. Res.*, 92, pp. 8343–8353, 1987.

Cicerone, R. J., "Changes in Stratospheric Ozone," *Science*, 237, pp. 35–42, 1987.

Russell, J.M., III, Farmer, C.B., Rinsland, C.P., Zander, R., Friodevaux, L., Toon, G.C., Gau, B., Shaw, J., and Gunson, M., "Measurements of Odd Nitrogen Compounds in the Stratosphere by the ATMOS Experiment on Spacelab 3," *J. Geophys. Res.*, 93, pp. 1718–1736, 1988.

M.M. Abbas/ES55
(205) 544–7680
Sponsors: Office of Space Science and Applications,
Center Director's Discretionary Fund

Earth Science and Applications

The two goals of the MSFC Earth Science and Applications program are:

- *To develop and utilize space technology to observe the Earth and gain a more comprehensive understanding of the geophysical processes and their role in defining the interactions between the components of the Earth system*
- *To use the understanding of the Earth's atmosphere to define the launch environment of the space shuttle and advanced launch vehicles.*

Research and development activities are conducted in support of NASA's Mission to Planet Earth and Global Change Research Programs. The activities involve theoretical and analytical model development, remote sensor development, flight payload analyses, laboratory and field experiments, and information system development. A major area of focus is support to the Earth Observing System (EOS) and implementation of the Hydrologic Cycle Distributed Active Archive Center at MSFC as one node of the EOS Data and Information System. Hydrologic cycle research includes ground- and space-based measurements of Earth parameters and uses these to develop and verify analytical and theoretical models of global and mesoscale processes. Field experiments provide data required to verify the operation of air- and space-borne sensors. Data derived from observations are used as input to model computer codes. Extensive use is also made of interactive data display and access systems to study time-dependent development of Earth system processes on all scales.

Intelligent Protection System for Space Power Applications

An intelligent **protection** system based on microcomputer technology can implement advanced functions for the accurate and secure detection of all types of faults on a space-borne electrical distribution system. A key component of such a **protection** system is an intelligent remote **power** controller (RPC). The intelligent RPC will implement conventional **protection** functions such as overcurrent, under voltage, and ground fault **protection**. Additionally, advanced functions for the detection of soft faults, which cannot presently be detected, can also be implemented. These techniques will enhance the overall safety and reliability of the distribution system.

Any electrical **power** system which distributes **power** to loads is occasionally subject to abnormalities in operation. The function of a **protection** system is to **automatically** identify when such an abnormality occurs, and to take corrective action to separate the damaged section from the rest of the system.

The distribution of power on Space Station *Freedom* has evolved as an integrated **automated** system. However, the first-line power system **protection** functions have, to date, not been **automated**. Distribution system protection is a function which is critical to mission success, and it is beneficial to **automate** this function in an intelligent manner. Of particular interest for this discussion is the **automation** of fault-detection functions in the RPC.

Conventional design of the RPC circuitry which performs the **protection** function consists of solid state devices which implement fixed functions with fixed settings. Significant advantages can be achieved by implementing the RPC functions with microcomputer technology. The recommended functions of an intelligent RPC include those summarized in table 3.

Table 3. Protection Functions of Intelligent RPC

Instantaneous overcurrent trip	Overtemperature trip
I^2t overload (time overcurrent) trip	Load anomaly detection
Enhance time overcurrent trip	Undervoltage trip
Adaptive overcurrent detection	Ground fault trip
Soft fault detection	Arcing fault detection
Incipient fault detection	Excessive inrush trip

The benefits of an intelligent RPC are summarized as follows:

- Flexibility–The intelligent RPC has settings and operating characteristics which adapt to particular load conditions.
- Sensitivity–An intelligent RPC will provide substantial improvements in the sensitive detection of low-current faults.
- Safety–Because more faults will be detected, crew safety will be enhanced, and there will be less chance of fire.
- Reliability–The addition of incipient fault detection and circuit reconfiguration will enhance the reliability of service to critical loads.

An intelligent RPC would augment the **autonomous** operation of the distribution system, a benefit which is of particular importance on long-duration space missions.

Weeks, D.J., and Starks, S.A., "Advanced Automation Approaches for Space Power Systems," *IEEE Computer Applications in Power*, October 1989, pp. 13–17.

Lollar, L.F., and Weeks, D.J., "The Autonomously Managed Power Systems Laboratory," 1988 IECEC, Denver, July/August 1988.

Aucoin, B.M., Russell, B.D., and Watson, K.L., "Detection of Incipient and Low Current Faults in Electric Distribution Systems," 1989 IECEC, Washington, August 1989.

N.R. Dugal-Whitehead/EB12
(205) 544–3304
Sponsor: Information and Electronic Systems Laboratory

Trace Atmospheric Carbon Monoxide Sensor

Carbon monoxide is difficult to detect at trace levels with usual multigas analysis techniques. Therefore, it was decided that a nondispersive **infrared** sensor dedicated to carbon monoxide monitoring would provide the needed instrument. The Trace Atmospheric Carbon Monoxide (CO) Sensor (TACOS) is such a sensor with a cospecific light source. This specific light source greatly increases sensitivity as compared to conventional black body source absorption technology. The source was developed to emit in the 4.6-μm wavelength region. The lamp emission consists of high-intensity CO lines superimposed on a low-intensity continuum. A breadboard was constructed using this source, a filter wheel with CO-absorbing and nonabsorbing cells, a sample cell, and a detector with signal processing. A detection sensitivity of 1-ppm CO in air was obtained.

A preliminary design for a brassboard has been developed and this will be constructed and tested in the upcoming months. As a result of these investigations, a small, low power-requirement, real-time **CO sensor** with sensitivity better than 10 ppm for use on long-duration manned space missions can be expected.

A. Hafner/EB22
(205) 544–3443
Sponsor: Small Business Innovation Research

Habitable Atmosphere Contaminant Monitoring

It is necessary to know the composition of habitable atmospheres in closed-cycle situations such as long-duration manned space flight missions in order to warn of the buildup of toxic or hazardous constituents. The approach that has been used to date is a modification of commercial analysis equipment. This effort extends that technology. The instrument under development uses a combination of two advanced technologies: **gas chromatograph with mass spectrometer detector (GC/MS)** and **tandem mass spectrometry (MS/MS)**. **The gas chromatograph mass spectrometer/mass spectrometer (GC/MS/MS)** will use a dual-column gas chromatograph in conjunction with the two mass spectrometers to eliminate ambiguity in qualitative analysis, and also to provide speed of analysis. This instrument will be greatly miniaturized in comparison to existing instrumentation.

This technique was investigated in a phase I Small Business Innovation Research contract and a breadboard **MS/MS** was tested. The present 2-year effort is about half completed. This is expected to result in a "brassboard" instrument, the design of which can be readily converted to flight configuration. Innovations expected in the **MS/MS** system include the interstage ionization method. This will be a surface-induced dissociation using a microchannel plate. Another innovation will be the second-stage detector, an electro-optical ion detector.

Effort to date has concentrated on design on the sample inlet system and the GC, the first-stage mass spectrometer, and the interstage ionizer.

A. Hafner/EB22
(205) 544–3443
Sponsor: Small Business Innovation Research

The Geophysical Fluid Flow Cell

The **Geophysical Fluid Flow Cell (GFFC)** provides a means of examining thermal **convection** on a rotating sphere. The **GFFC** experiment simulates a wide variety of thermal **convection** phenomena on a spherical surface with a radially directed body force. By applying an electric field across a spherical capacitor filled with a dielectric liquid (low-viscosity silicon oil), a body force analogous to **gravity** is generated around the fluid. The force acts as buoyancy in that its magnitude is proportional to the local temperature of the fluid and is in the radial direction perpendicular to the spherical surface. In this manner, cooler fluid sinks toward the surface of the inner sphere while warmer fluid rises toward the outer sphere. The value of this artificial **gravity** is proportional to the square of the voltage applied across the sphere and can thus be imposed electronically as desired. With practical voltages, its magnitude is only a fraction of Earth's **gravity** and so requires a microgravity environment to be significant. A unique feature of these experiments is the latitudinal dependence of the Coriolis effect resulting in flows more relevant to geophysical applications. The experiment was flown on Spacelab 3 (SL-3) and is scheduled for reflight on a future Spacelab mission.

During this year, much research was completed at MSFC, the University of Colorado, and Los Alamos National Laboratory. The plane parallel model of nonlinear platform selection was extended to spherical geometry. In planar geometry, the **GFFC**-observed tendency (SL-3) for down-center hexagons at low Taylor numbers was generated by the fact that the inner **GFFC** spherical surface has stronger **gravity**. In spherical geometry, a similar effect is present. However, numerical simulations have indicated a preference for down-center hexagons even with inverse r-fifth **gravity**, with a small enhancement for inverse r-fifth **gravity**. The weakly nonlinear model does not have this property, suggesting that the **GFFC** experiments may have been influenced by more than one desymmetrizing force. Future **GFFC** experiments, looking again at a range of low Taylor numbers with better thermal boundary control than on SL-3, shall readdress this platform selection issue.

The rather astounding superposition of spiral waves alongside strong north-south columnar convective at moderate Taylor numbers was addressed by studying the linear stability properties of local Hadley circulations. The locally planar, exact solution of the governing equations in the form of a Hadley circulation changes with latitude. At the poles, the zonal flow is strong, whereas, at the Equator, it is very weak (with the bulk of the basic-state flow being tied up in a simple meridianal circulation). Linear eigen functions tended to line up with the ambient shear (for the moderate Prandtl number of the **GFFC** experiment). As one approaches the pole, the linear modes are locally at any angle of up to 45° with respect to stable modes and within 10° of a meridian. This tendency may explain the different characteristics of the polar and equatorial modes observed in the SL-3 **GFFC** data. Recent numerical simulations show that the columnar "spine-modes" observed in both previous simulations and in the SL-3 **GFFC** data disappear after a long evolution time. Future **GFFC** experiments shall address this evolution time issue by conducting longer runs at fixed external parameters.

Linear instability calculations indicate that the **GFFC** should exhibit classic baroclinic instability at accessible parameter settings. Such experiments will be run on a future Spacelab mission to look at nonlinear baroclinic instability in spherical shells. Of interest are mechanisms of transition to temporal chaos, and the evolution into spatiotemporal chaos. To understand more about such transitions, it is necessary to conduct high-resolution numerical experiments, especially when the transition is dominated by defects (as in spatiochaotic chaos). Such calculations have been carried out for two-layer models in quasi-geostrophic channel flows with interesting results.

The **GFFC** flight data has been studied in detail in order to understand the competition between columnar cells (banana cells) at lower latitudes and strong non-columnar disturbances at higher latitudes. We find that there remains distinct signatures of banana cells at low latitudes even when the mid- and high-latitude flows are strongly asymmetric and turbulent. This suggests that similar giant **convection** cells may indeed be present deep within the solar **convection** zone. The **GFFC** data provides the only experimental means to directly study such rotationally-constrained **convection**, and thus our data is of great interest to the observational and theoretical efforts in helioseismology which will use the oscillations of the Sun to probe the interior dynamics of this start. The **GFFC** imaging data on the banana cells, along with velocity and thermal fields from our three-dimensional simulations of these **GFFC** experiments, will be provided to the helioseismology working groups dealing with both the ground-based Global Oscillations Network Group (GONG) project and the now-approved NASA/ESA Solar and Heliospheric Observatory (SOHO) spacecraft solar oscillations imager experiment. The simulation data will permit frequency splittings to be calculated for potential oscillation modes that will be used to search for the flows of the giant cells.

Cattaneo, F., and Hart, J.E., "Multiple States for Quasiogeostrophic Baroclinic Channel Flows," in Geophys, and Astrophys. Fluid Dyn., in press (1990).

Toomre, J., Hart, J.E., and Glatzmaier, G., "Spacelab Experiments on Convection in a Rotating Spherical Shell With Radial Gravity," in The Internal Solar Angular Velocity, Durney, B.R., and Sofia, S., editors, pp. 27–44, D. Reidel (1987).

F.W. Leslie/ES42
(205) 544–1633
Sponsor: Office of Space Science and Applications

Thermosphere Model Verification Studies With the Long Duration Exposure Facility

Thermospheric neutral density models are currently being evaluated by coupling models with an orbit decay-prediction algorithm and comparing the output of the models with actual satellite track data. The difference in the predicted decay and the actual decay of a satellite is an indication of how accurately the thermospheric density models predict the total density at orbital altitudes. At this time, two models, the **Marshall Engineering Thermosphere (MET) model** and the **Mass Spectrometer and Incoherent Scatter (MSIS)** model, are being evaluated. Both are empirical models, with the **MET model** derived from satellite-decay data and the **MSIS model** derived from mass spectrometer data. The two models require similar solar-parameter inputs, and both models are used to predict orbital lifetimes of satellites.

Over the past several years, many comparisons have been made between the two models, and each has been compared with various data sets. The results of these studies indicate that the two models are in agreement with each other to within about 15 percent. However, many of these studies were performed with data acquired during solar conditions not as extreme as are being experienced during the peak of the present solar cycle (cycle 22). For this reason, the **Long Duration Exposure Facility (LDEF)** satellite provided an opportunity to compare orbit decay data with model predictions during a time of high solar activity. Moreover, **LDEF** was well-suited for this task because of its fixed orientation with respect to the velocity vector, its

fairly simple shape, and its large cross-sectional area. The results of the study should be able to validate the models' performances for use in orbital lifetime predictions during periods of high solar activity.

In addition to validating the above models, the differences between the model outputs and **LDEF**-derived total densities are being investigated. One area of investigation will be to determine if these differences are due to inadequately modeled relationships between the solar inputs (F10.7 cm radio flux) and density fluctuations at high solar activity, or are due to the inadequacy of using the F10.7 radio flux as a proxy for the solar extreme ultraviolet (EUV) radiation that actually drives the thermosphere fluctuations. An attempt will also be made to correlate other solar radiation measurements that lie close to the EUV spectrum, while observing the differences in density.

R.J. Suggs/ES44
(205) 544–7797
Sponsor: Space Station Freedom Office

Revised Gust Model for Space Vehicle Performance Assessments

Structural loads induced on the National Space Transportation System orbiter by small-scale wind **gusts** have been modeled by simulations of vehicle ascent flight through an artificial quasi-square wave **gust** with an amplitude of 9 m/s and a length of 300 m. The orbiter was designed to fly through such a **gust** with a 99-percent probability of not exceeding any load limits. Flight simulations have shown that the **gust** is a large contributor to the loading on the orbiter's vertical tail. Many years of detailed wind observations have been acquired since this **gust** model was developed and evidence for a 9-m/s amplitude **gust** has not been found. These facts motivated a review of the **gust** model.

The revised **gust** model was developed from a spectral representation of wind perturbations versus vertical wavenumber (inverse wavelength). Spectra of 2-km segments of measured wind profiles were computed, centered on every kilometer in height. Then at each height, a power-law shape, envelope spectrum was found that would be exceeded by only 1 out of 100 spectra at some wavenumber between 0.001 cycles/m (1,000 m) and 0.005 cycles/m (200 m). To cover wavelengths smaller than 200 m, a clear-air **turbulence** (CAT) model spectrum for moderate CAT was added to the envelope spectrum. Moderate CAT was chosen because one of the launch criteria is that no observations of moderate or greater **turbulence** are reported by support aircraft in the launch pad area.

A revised discrete **gust** was designed by matching the spectrum of a discrete **gust** to the 99-percent envelope spectrum. Various discrete **gust** shapes, amplitudes, and lengths were considered. The spectra of these **gust** shapes were computed and compared to the model spectrum. An excellent fit was found with a **gust** consisting of a wind velocity linearly increasing to a value of 6.5 m/s over a 500-m height interval, then with an abrupt transition to −6.5 m/s followed by a linear increase over the

next 500 m of altitude back to 0.0. This **gust** is clearly an artifice that is extremely unlikely to be found in nature, but it does have the desirable property of yielding a fairly close match to the model spectrum.

Load simulations using the revised discrete and spectral **gust** models have been performed by Rockwell-Downey. These simulations were complicated by the fact that the **gust** models possessed lengths of 1,000 m, compared to the 300 m of the previous model. Such a length of wind profile required a trajectory simulation and derivation of guidance and control effects throughout the **gust** profile. The 300-m **gust** was sufficiently short that a reference trajectory was used, and the **gust** did not exert an effect on the guidance and control commands. The revised **gust** models lead to smaller flexible body loads on the vertical tail. Part of the reduction is due to the vehicle steering through the **gust** profile and part due to the smaller **gust** amplitude. However, a Monte Carlo simulation using an inversion of the spectral model back to the height domain revealed the mean loads to be smaller than the previous model, but the dispersion about that mean indicated potentially large loads. It appears that control throughout the **gust** profile produces a nonlinear load response to the assumed Guassian **gust** spectrum.

S. Smith/ES44
(205) 544–4481
Sponsor: Office of Space Science and Applications

Mars-Global Reference Atmosphere Model

The advent of such NASA projects as the **Mars** Observer, **Mars** Rover, **Mars** Aeronomy Orbiter, and proposed manned **Mars** missions, along with the ongoing research of aerobraking techniques for aerocapture by **Mars**, have necessitated the construction of a more detailed global climatological model for **Mars**—the **Mars Global Reference Atmosphere Model (Mars-GRAM)**. Figure 54 compares **Mars-GRAM's** instrument data with that of **Viking 1**. Figure 55 compares **Mars-GRAM's** instrument data with that of **Viking 2**.

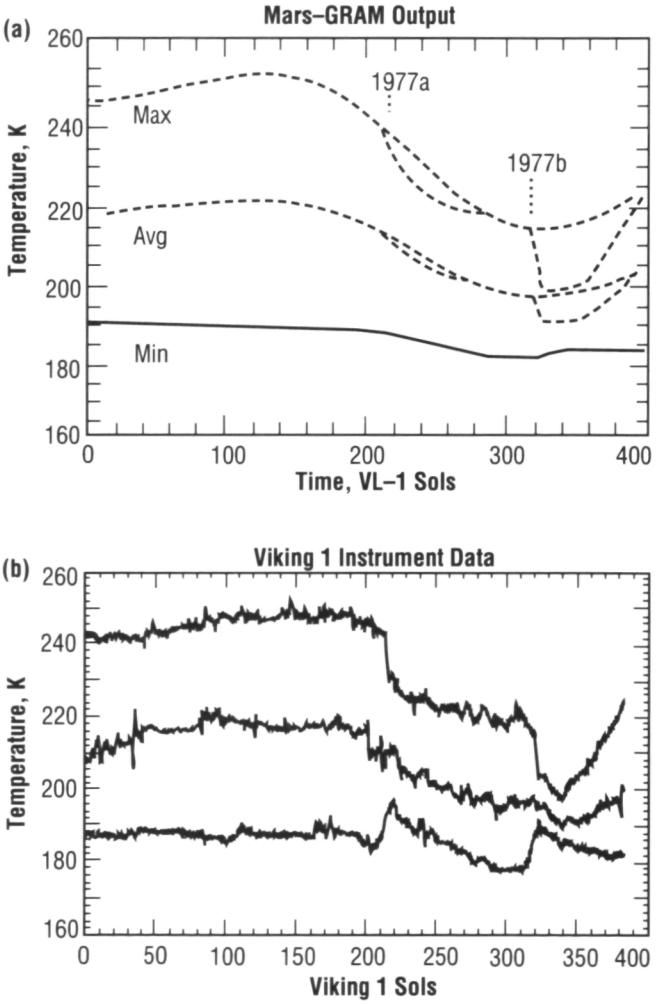

Figure 54. Mars-GRAMS Output vs. Viking 1 Instrument Data for Same Period

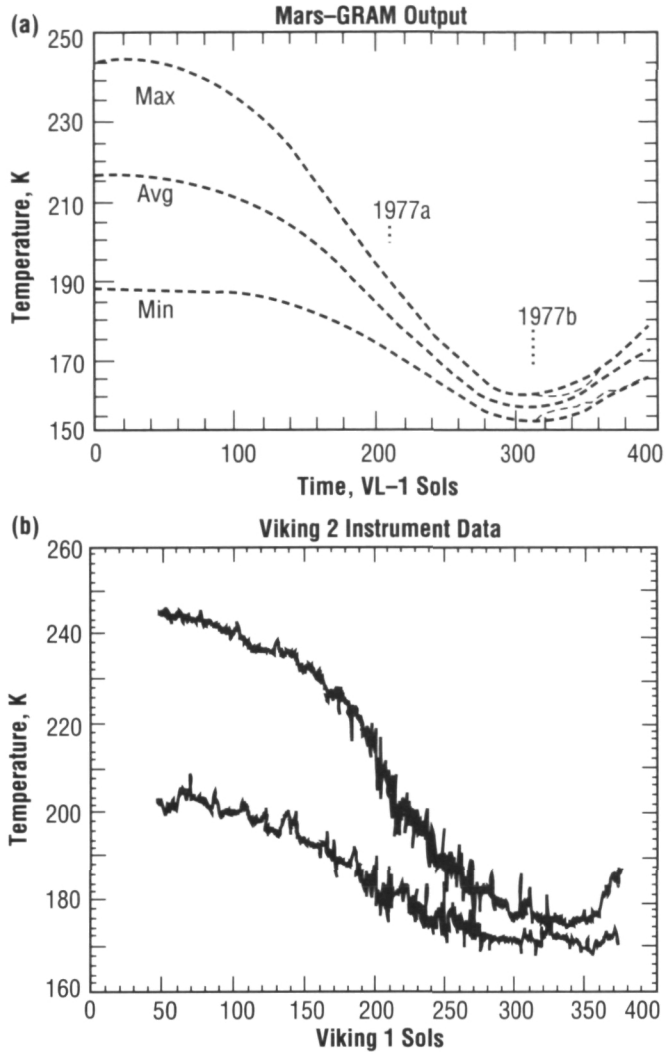

Figure 55. Mars-GRAM Output vs. Viking 2 Instrument Data for the Same Period

This PC/VAX-based model operates with similar run characteristics to MSFC's successful Earth-GRAM, and also gives similar results. The **Mars-GRAM** provides total density, temperature, pressure, and wind conditions for any location, any date, any time of day, from the surface to 600 km (373 mi). Small-scale density perturbations and long-term average values are also calculated. Realistic modeling of a Martian dust storm and its effect on the thermodynamic and wind structure can also be obtained. Figure 56 shows the variation of daily mean temperature due to a dust storm.

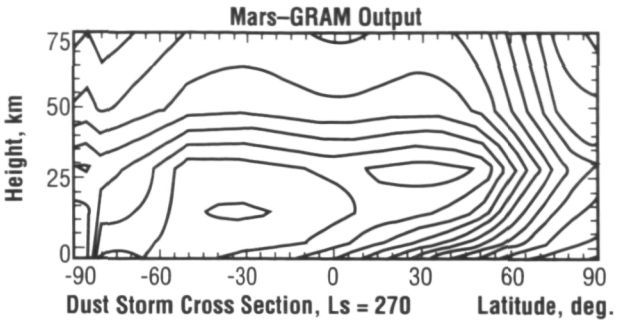

Figure 56. Variation of Daily Mean Temperature Due to Dust Storm

The **Mars-GRAM** couples the Culp-Stewart upper atmosphere model with a lower atmosphere parameterization scheme based on data received from previous **Mars** missions. To enhance areas where data were sparse, theoretical calculations were added. More than 40 different data sets were utilized throughout the empirical modeling process.

The first official release version was distributed in October 1989, and already the **Mars-GRAM** is being used in a wide variety of mission studies. Recently, **Mars-GRAM** was baselined for the **Mars** Rover program and is also being used for the joint U.S.–Soviet **Mars** '94 balloon mission. The **Mars-GRAM** is being extensively used for ongoing aerobraking research with special use of the model's density perturbation modeling, random density profile capabilities, and mountain wave simulation features.

Currently, various upgrades to the **Mars-GRAM** are underway. Ongoing research will provide even more realistic dust modeling with improved wave structure influences. Presently, new data sets are being incorporated into the empirical modeling structure such as unpublished data sets from various Mariner and **Viking** instruments. These modeling efforts will provide improved modeling of the atmospheric characteristics of **Mars**.

B.F. James/ES44
(205) 544–6985
Sponsor: Earth Science and Applications Division

Aerosol Physicochemistry and Backscatter Modeling

During FY90, two survey missions were conducted in the Pacific Ocean basin as part of the **Global Backscatter Experiment (GLOBE)** program. **GLOBE** supports engineering design and performance studies of the Laser Atmospheric Wind Sounder (LAWS). Results of the **GLOBE** program, as a whole, are used to successively refine a global-scale model of clean background **aerosol backscatter** over remote oceans. LAWS, a satellite-borne Doppler lidar system, will provide global tropospheric wind measurements as part of NASA's Earth science initiative, the Earth Observing System. Knowledge of physicochemical and **backscatter** properties of **aerosols**, which act as passive wind tracers, is essential for the LAWS development effort. Wind measurement accuracy depends critically on **backscattered** signal strength, which in turn is a function of the **aerosol** properties.

The **GLOBE** instrument complement was carefully selected to provide a comprehensive, synergistic, internally consistent set of aerosol measurements. Zenith and nadir profile measurements of **backscatter** were obtained using a CO_2 gas lidar operating at 9.25 μm, and an Nd:YAG solid state laser operating at 0.53, 1.06, and 1.54 μm. In situ instrument packages consisted of two continuous-wave CO_2 lidars to measure **backscatter** at 9.11 and 10.6 μm; two optical particle counters to measure **aerosol** concentrations and size distributions between 0.1 and 43 μm; a filter/impactor system to determine sulfate and soil **aerosol** components; a preconditioned laser optical particle counter system to obtain size-segregated information on **aerosol** physicochemistry in near-real time; and two integrating nephelometers for measuring visible scattering coefficients at 0.63 μm and at 0.45, 0.55, and 0.7 μm (**GLOBE I** only). Supporting data include visible and infrared wavelength satellite imagery of meteorological conditions, multi-wavelength extinction profiles from the Stratospheric Aerosol and Gas Experiment (SAGE II), networks of ground-based **aerosol** samplers, and ground-based and airborne CO_2 solid state lidars.

The principal investigators responsible for the development and operation of the **GLOBE** instruments will continue analysis of the measurement sets. The Remote Sensing Branch, Earth Science and Applications Division, is responsible for synthesizing the processed measurements of physical, chemical, and optical parameters, obtained over *ten* wavelengths, into a refined model of the background **aerosol backscatter** over remote ocean areas. An important tool for relating the measured **aerosol** properties to **backscatter** values at CO_2 wavelengths is Mie scattering theory. Existing measurement climatologies of different **aerosol** properties, many of which were obtained at near- and middle-infrared wavelengths, indicate the existence of a ubiquitous, global clean background **aerosol** mode in the troposphere. Observations by airborne and ground-based CO_2 lidars have been combined into a preliminary airmass-based model of **aerosol backscatter** at CO_2 wavelengths. To assess the impact of LAWS, emphasis is placed on expressing model results in terms of microphysical and meteorological parameters (e.g., water vapor) accessible to atmospheric general circulation models. The **GLOBE** survey mission results will be incorporated into a refined model that will provide a comprehensive description of the optical and microphysical properties of the background tropospheric **aerosol**. The model will allow for extension to any wavelength, from the ultraviolet to the middle infrared, to accommodate technological development of Doppler lidar at wavelengths competitive with CO_2 technology.

J. Rothermel/ES43
(205) 544–1685
Sponsor: Office of Space Science and Applications

Global Backscatter Experiment

In 1986, the **Global Backscatter Experiment (GLOBE)** program was initiated to provide inputs to engineering design and performance studies of the **Laser Atmospheric Wind Sounder (LAWS). LAWS**, selected as a facility instrument for NASA's Earth Observing System (EOS) Earth science initiative, will measure global tropospheric winds using Doppler-shifted laser radiation **backscattered** from micron-size **aerosol** particles. Since the accuracy of the wind estimates is a function of the **backscattered** signal strength, **LAWS** performance will depend in part on the spatial distribution, and physical, chemical, and optical properties of **aerosols**. The **GLOBE** program includes a global-scale lidar network, laboratory measurements, satellite-based measurements, a centralized data base, **backscatter** data analysis, and **backscatter** modeling. The centerpieces of the **GLOBE** program are two survey missions over the Pacific Ocean basin, where **backscatter** levels are considered to be lowest and where LAWS will have the greatest impact on knowledge of the Earth system, due to severe undersampling by the current Earth-based wind measurement system. The objectives of the survey missions are: (1) obtain direct measurements of **aerosol backscatter** coefficients at infrared lidar wavelengths (9–11 μm) in remote Pacific Ocean, particularly the Southern Hemisphere; (2) obtain concurrent measurements of **aerosol** optical and physicochemical properties in background marine free troposphere; and (3) extend application of existing background **aerosol backscatter** models to remote oceans.

During FY90, survey missions were flown with the NASA DC-8 research aircraft in November 1989 (GLOBE I) and May-June 1990 (GLOBE II), providing information on seasonal contrast in both hemispheres. Zenith and nadir profile measurements of **aerosol backscatter** were obtained between 0.53–9.25 μm using a carbon dioxide gas and Nd:YAG solid-state lidars. Additionally, four instrument packages obtained in situ measurements of **aerosol backscatter** at 9.11 and 10.6 μm, aerosol concentrations and size distributions, sulfate and soil **aerosol** components, size-segregated information on aerosol physiochemistry in near-real time, and visible scattering coefficients.

Approximately 170 flight hours were used for engineering check out, comparisons with airborne and ground-based lidars and **aerosol** samplers, and transit flights in the middle and upper troposphere. Portions of transit flight were made over ground-based **aerosol** samplers (physiochemical properties), and below satellite-based solar occulting instruments (**aerosol** extinction), all of which have developed substantial measurement climatologies relevant to **LAWS** studies. Preliminary comparisons among **GLOBE** instruments show agreement generally to within a factor of three. Within the troposphere, a boundary layer, a cloud-pumped layer, and a clean background layer were typically observed. **Backscatter** between 9 and 11 μm was significantly affected by compositional variations at different altitudes and locations. Lidar returns were frequently obtained from within deep cirrus layers, suggesting that **LAWS** may yield wind information in dynamically active regions. In situ measurements of high **aerosol** mass concentrations often correlated positively with high water-vapor concentrations, suggesting that **LAWS** may contribute significantly to water vapor transport studies. Future work will concentrate on data analysis and synthesis of multiparameter measurements over ten wavelengths into a refined model of background **aerosol backscatter** over remote oceans.

J. Rothermel/ES43
(205) 544–1685
Sponsor: Office of Space Science and Applications

Aerosol Optical Properties Laboratory

The extensive use of the two MSFC continuous wave CO_2 Doppler lidars for the **Global Backscatter Experiment (GLOBE)** I and II survey missions, described elsewhere in this report, motivated the development of the **Aerosol Optical Properties Laboratory (AOPL)** in 1989. The **AOPL** initially is providing space for calibration, alignment, and hardware modifications of the two **lidars**. After the **GLOBE I** mission ended in December 1989, the 10.6- and 9.1-μm **lidars**, along with the supporting data system hardware, were installed in the **AOPL**. In January and February 1990, the post-**GLOBE I** calibration of the two **lidars** was performed. The calibration experiments provide estimates of the **lidar** efficiency and the calibration factor that is used to convert the signal-to-noise ratio (SNR), measured during the **GLOBE** missions, to the **aerosol** backscatter coefficient. During March 1990, in the **AOPL** the 10.6-μm **lidar** was modified to incorporate a new and higher-powered CO_2 laser, and the 9.1-μm **lidar** was realigned, thus improving the sensitivity of both **lidars** for **GLOBE II**. In March and April 1990, another calibration of the 9.1-μm **lidar** was performed in the **AOPL**. The calibration was done at close-focus and far-focus settings. In March, the lidars were shipped to Ames Research Center for deployment in the **GLOBE II** survey mission in May 1990. After the mission, the two **lidars** will be returned to the **AOPL**, where a detailed post-**GLOBE II** calibration experiment will be performed. The beam shape, size, and quality of the modified 10.6-μm **lidar** will be carefully analyzed, and performance of the **lidar** for several operating parameters will be investigated experimentally. The 9.1-μm **lidar** will be modified by replacing the present laser tube to obtain higher output power, more sensitivity, and wavelength tuning capability between 9 and 11 μm.

The long-term research plan for the **AOPL**, apart from **lidar** calibration and modification, will focus on the study of **aerosol**-scattering properties using the CO_2 **lidars**. Different **aerosol** species will be generated in the laboratory, using a Berglund-Liu Vibrating Orifice Aerosol Generator to simulate atmospheric **aerosols** encountered in the **GLOBE** missions. Simulated **aerosols** will include sea salt, ammonium sulfates and bisulfates, sulfuric acid, and dust. Backscatter, extinction, and other scattering parameters will be measured as a function of size, composition, refractive index, and shape. This effort will begin in early FY91. **Aerosols** generated in the laboratory will also be used to calibrate the **lidars**. Thus, calibration conditions will be more representative of expected atmospheric operating conditions during field measurements. This method, rather than the standard method of using a hard target of known reflectance, permits operation of the **lidars** with system parameter settings more commonly used under atmospheric conditions. Consequently, the necessity for employing electrical or optical attenuation when using hard targets, usually accompanied by uncertainties in **lidar** receiver performance over large dynamic range, is avoided.

Research conducted in the Aerosol Optical Properties Laboratory using the MSFC CO_2 **lidars** will support design and performance studies of the Laser Atmospheric Wind Sounder (LAWS), an Earth Observing System (EOS) facility instrument. The MSFC's 9.1-μm **lidar** matches the prospective design wavelength for LAWS. Future studies of **aerosol** optical properties will prepare the **lidars** for future field experiments. This will be useful to the fundamental interpretation of LAWS findings and relate to the observations by other EOS instruments influenced by the presence of atmospheric **aerosols**.

J. Rothermel/ES43
(205) 544–1685
Sponsor: Office of Space Science and Applications

Atmospheric Electricity Research

Electrical processes in thunderstorms are closely coupled to the dynamical and microphysical development in the **storms**. For example, research conducted at MSFC has shown that there appears to be an almost direct proportionality between total rain volume and the number of **lightning** flashes. Similarly, a linear relationship has been found in the total **lightning** flash rate and the total electric (i.e., Maxwell) current generated by a thunderstorm. Recent observations also indicate that peak lightning rates coincide with the maximum vertical development, and that abrupt decreases in the total flash rate signify the **storm** collapse and provide a precursor to microburst formation at the surface.

The primary focus of the atmospheric electricity research program at MSFC is to study relationships between **lightning** and **storm** electrification and a number of underlying and interrelated phenomena including the structure, dynamics, and evolution of thunderstorms and thunderstorm systems, precipitation distribution and amounts, atmospheric chemistry processes (e.g., NO_x production), and the global electric circuit. In this research, an emphasis is placed on establishing quantitative relationships that could employ **lightning** data derived from satellite observations of optical **lightning** emissions as the independent parameter.

This research requires the obtaining of correlated ground-based, airborne, and satellite data sets. Measurements of the optical and electrical emissions of **lightning** and the electrical environment above thunderstorms have been obtained from a high-altitude NASA U-2 aircraft. In the future, these measurements will be obtained using a NASA ER-2 aircraft. The data sets acquired in conjunction with the ER's **lightning** measurements will include Doppler and conventional radar, ground-based and in situ electricity and microphysical observations, detailed precipitation measurements, ground-strike **lightning** mapping, and visible and infrared **Geosynchronous Operational Environmental Satellite (GOES)** images. In addition, the ER-2 **lightning** instruments will generally be flown with other sensor systems (e.g., infrared, passive microwave, etc.) that will support detailed satellite simulations of **storm** measurements through the acquisition and analysis of multiparameter data sets.

As previously noted, atmospheric electricity research at MSFC is particularly motivated by the desire to develop the understanding needed for the effective utilization and interpretation of data from the satellite-based **lightning** detection systems expected to be in Earth orbit in the mid-1990's. These satellite **lightning** detection systems will be characterized by high detection efficiencies (i.e., 80–90 percent) and the capability to detect both intracloud and cloud-to-ground discharges during day and night. One such instrument, the Lightning Mapper Sensor, is presently under development by NASA and will be placed in geostationary Earth orbit on a **GOES** satellite. Another instrument called the Lightning Imaging Sensor is being developed for the Earth Observing System polar platform and Space Station *Freedom*. A **lightning** detector system with significantly improved detection capabilities can be expected for the geostationary platform. These satellite **lightning** detection systems will support Earth system science studies in the next decade and beyond.

Christian, H.J., Blakeslee, R.J., and Goodman, S.J., "The Detection of Lightning From Geostationary Orbit," *J. Geophys. Res.*, 94, pp. 13329–13337, 1989.

R.J. Blakeslee/ES43
(205) 544–1652
Sponsor: Office of Space Science and Applications

Lightning Simulator and Sensor Calibration

The Earth Science and Application Division Remote Sensing Laboratory is continuing to develop the capability to design and test sensors in support of **Earth Observing System (EOS)** objectives. Also, the laboratory will be utilizing this technology in support of operational sensors like the **lightning mapper sensor (LMS)** slated for launch on the Geosynchronous Operational Environmental Satellite (GOES) satellite series. The need for testing these sensors with field-filling, real-time lightning simulations has been difficult to obtain with current technology. The **lightning imaging sensor (LIS)** is one of the **EOS** instruments that will be calibrated and checked by the simulator during its development and predeployment.

The calibration facility will provide the capability to quantitatively calibrate detectors and detector arrays in systems such as the **LMS** and **LIS** over the ultraviolet to the midinfrared spectrum. At present, the facility is addressing the requirements to calibrate the **LIS** and the **LMS** with two calibration test stations defined as follows.

The first calibration station is for the static characterization of the detector which will provide the responsiveness, quantum efficiency, dynamic range, and dark current noise versus temperature, readout speed, and background for single detectors or multiple detector elements. In the case of an image array detector system, this station will also provide pixel uniformity information and the fixed-pattern noise of the array. The combined information will give the required calibration coefficients to determine the amount of radiation energy incident on the array. Most of this calibration will be done with a monochromator tied to a personal computer for control and data acquisition. For array real-time control and data acquisition, a separate transient data recorder will be utilized for imaging of the array data.

The second station will provide an end-to-end calibration of the detector system which includes the optics and signal processing electronics. For the **LIS** and **LMS**, this station will simulate lightning as seen from space and provide the same worst-case and ideal-background conditions in which these systems will have to be able to detect lightning. Figure 57 shows the lightning scene generator. This configuration will provide the real-time stimulus to calibrate the instrument in the laboratory while simulating the characteristics of lightning. The major component of the simulator will be the acoustic optical scanner which will scan an amplitude-modulated laser beam around the array. Due to limitations of acoustic optical scan speed, the entire array cannot be covered in one frame period even with a mechanical x–y translator. With current specification for the **LIS** of 128×128 array size, the simulator will be able to illuminate 100×100 pixels. The problem is the acoustic optical scanner has a scan angle of 3° at the 200-kHz scan rate. This 3°-scan angle must be expanded through a diffuser to 80°, which is the field of view for the **LIS**. Figure 57 is a prototype optical layout for the lightning simulator. Between these two calibration test stations, the remote sensing laboratory will be able to calibrate detectors and detector systems in the 0.25 to 1.0 μm wavelength region.

M.W. James/ES43
(205) 544–5020
Sponsor: Office of Space Science and Applications

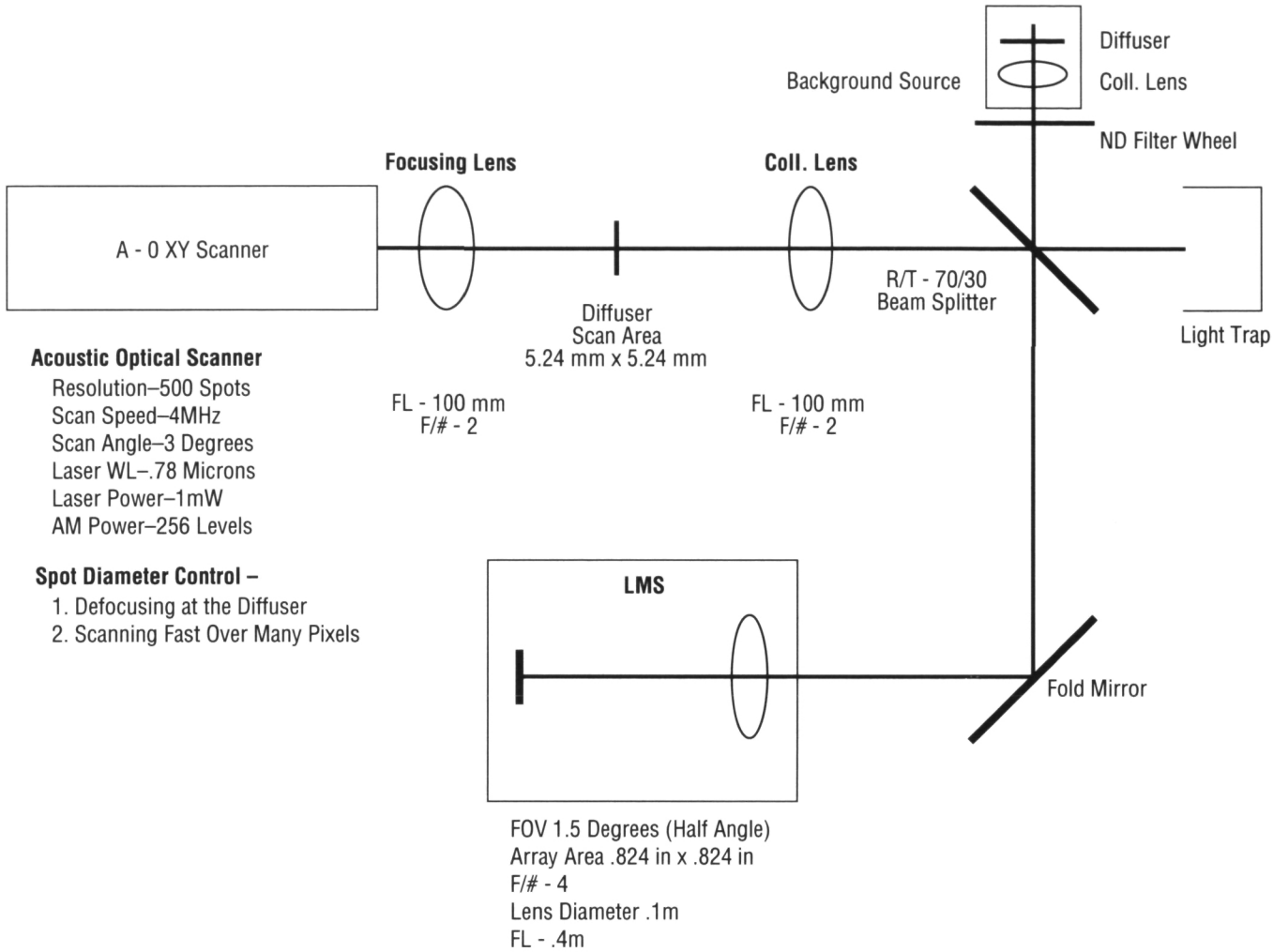

Figure 57. Lightning Scene Generator

Quick View System for Aircraft Data

Last year demonstrated the need for a prototype **data analysis** capability for engineering and scientific evaluation of aircraft data in the field. The aircraft instrument for which this capability was developed was NASA's **Multispectral Atmospheric Mapping Sensor (MAMS)**. The **MAMS** is a line-scanner with eight visible and three infrared (IR) channels. The eight visible channels range from 0.42 to 1.05 μm with three IR channels ranging from 3.73 to 12.56 μm.

Data from the **MAMS** spectrometer is stored on a high-density digital tape (HDDT) which has 14 tracks, of which only 12 are used for scanner data. Serial biphase-low data is contained on each track with synchronization, housekeeping, and data making up the scan-line recorded. Data from the tape is read and stored in a file compatible with the data analysis software so that the scientist/engineer can quickly evaluate the data and determine any instrument problems that may have developed. This ground station also required the ability to quickly look at the data in a work station environment to allow more accurate planning of missions for the remainder of the deployment.

The Quick View System (QVS) was developed to address this deficiency by reading data directly from the instrumentation tape after a science flight and to present to the scientist a quick and powerful data analysis station. The prototype system was tested on data in the field last fall with excellent results. The interface between the two software packages, Man-Computer Interactive Data Access System (McIDAS) and the data gathering software, will require improved **computing** power to fully realize the QVS's capabilities. Much of the calibration, presentation, and navigation software runs under the OS-2 operating system in McIDAS, while the engineering/data collecting software package was developed under DOS and runs on the Industry Standard Architecture (ISA) bus. In order to combine the two systems under one operation system, with minimal effort and uncertainty, it was decided to stay with the ISA/Extended ISA (EISA) bus combination for future multichannel frame-synchronization boards with the OS-2 operating system on an improved computing platform.

The QVS consists of a single PC-AT form-factor card which performs the bit- and frame-synchronization of the incoming serial biphase-L-encoded data. This dual-channel card can collect independent channel data so tape-head skew will not become a problem for adjacent channels. Data are recovered from the QVS card by interrupts to the processor when a channel has five scan lines stored in local memory. With the speed available from the improved computer platform, current data rates available are 15 in/s with work progressing to 30 in/s for display and post-flight review. Data are also presented in a side-by-side scrolling image on a separate monitor, using a frame grabber card. This card is only needed to visually preview the data before it is stored in a file for later calibration and navigation. It displays scan-line number and time code over the image to allow the most efficient transfer of selected data to the **data analysis** software package.

M.W. James/ES43
(205) 544–5020
Sponsor: Office of Space Science and Applications

MSFC Shuttle Lightning Research

In recent years, NASA/MSFC has used both space **shuttle** missions and high-altitude U-2 aircraft to observe **lightning** from above convective storms. The main objective of these observations has been to determine some of the baseline design requirements for a satellite-borne optical **lightning** mapper sensor. Other objectives have been to study the overall optical and electrical characteristics of **lightning** as viewed from above the cloud top and to investigate the relationship between storm electrical development and the structure, dynamics, and evolution of thunderstorms and thunderstorm systems.

Scientists have largely satisfied the need to acquire a qualitative and quantitative data base for design of a **lightning** mapper sensor. The **lightning** research goals now focus on understanding the behavior of **lightning** and the global distribution of **lightning** rather than characterizing the types of optical and electrical signals it produces. The **shuttle** effort, in particular, is directed toward using a low Earth orbit to observe the global distribution of **lightning** and the behavior of **lightning** with respect to other storm characteristics.

The **shuttle Mesoscale Lightning Experiment (MLE)**, recently flown on STS-26, -30, -32, and -34, focuses on quantitative measurements of **lightning** characteristics and observational techniques for simulations of a future space-borne **lightning** mapping system and a future experiment using a hand-held sensor and camera located on the aft mid-deck to observe nighttime **lightning**. The **shuttle** payload bay camera, for the MLE, was pointed directly below the **shuttle**, or, under certain conditions, the payload bay camera was operated from the ground to obtain video when the crew was not available to operate the camera. Moonlight illumination of the Earth is preferred because cloud details and cities can be used to aid in navigation of the storm data sets. Figure 58 shows a typical **lightning** storm over the Southeastern U.S.A. during a moonlight-illuminated pass while STS-32 was on its 140th orbit. Figure 59 shows a typical **lightning** storm over Brazil, taken on the 56th orbit. The imagery is analyzed for the frequency of flashes while active storm clouds are within the camera's field of view, the length of **lightning** discharge within the cloud, and global estimates of **lightning** activity in storm systems that are oblique to the **shuttle's** orbital track on a time-available basis. These observations provide information for the development of observation simulations for an upcoming Earth Observing Satellite polar satellite and space station instrument, the Lightning Imaging Sensor, and for the Lightning Mapper Sensor which is planned for a future National Oceanic and Atmospheric Administration geostationary satellite.

O.H. Vaughan/ES43
(205) 544–1648
Sponsor: Office of Space Science and Applications

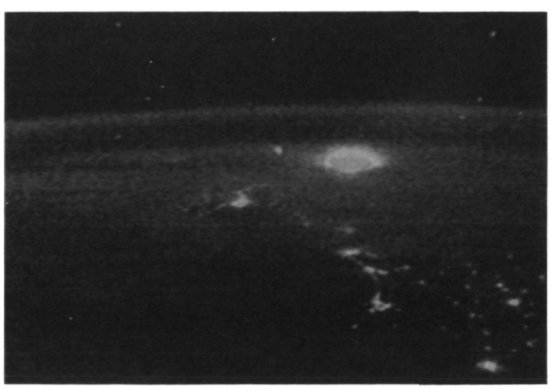

Figure 58. Typical Lightning Storm Over Southeastern United States (Largest Bright Area is Lightning; Other Areas are Cities).

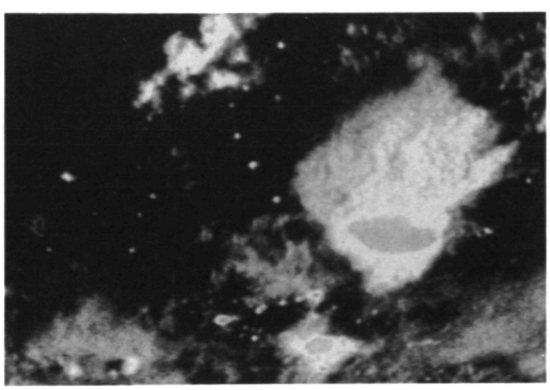

Figure 59. Typical Lightning Storm Over Brazil (Largest Bright Area is Lightning; Other Areas are Cities).

ORIGINAL PAGE
BLACK AND WHITE PHOTOGRAPH

Lightning/Rainfall Relationships

Radar and **lightning** data from the Cooperative Huntsville Meteorological Experiment (COHMEX) are being analyzed in an attempt to define a relationship between **lightning** and **rainfall** in **convective storms.** COHMEX was a multiagency field program conducted in the northern Alabama/central Tennessee region of the southeastern United States during June and July 1986. Establishment of a successful relationship would allow large-region **rainfall** estimations from a space-based **lightning** detection system.

A large mesoscale convective system was observed for nearly 7 hours of its life cycle on July 13, 1986. At maturity, this system consisted of a convective leading edge and an adjacent region of stratiform precipitation. Positive cloud-to-ground discharges were common within the trailing stratiform region. These aspects show that this is a typical system. The evolution of cloud-to-ground **lightning** rates and radar-derived convective rain flux for 10-minute intervals is shown in figure 60 for this system. There is an excellent agreement (r = 0.96) between the **lightning** and convective rain flux.

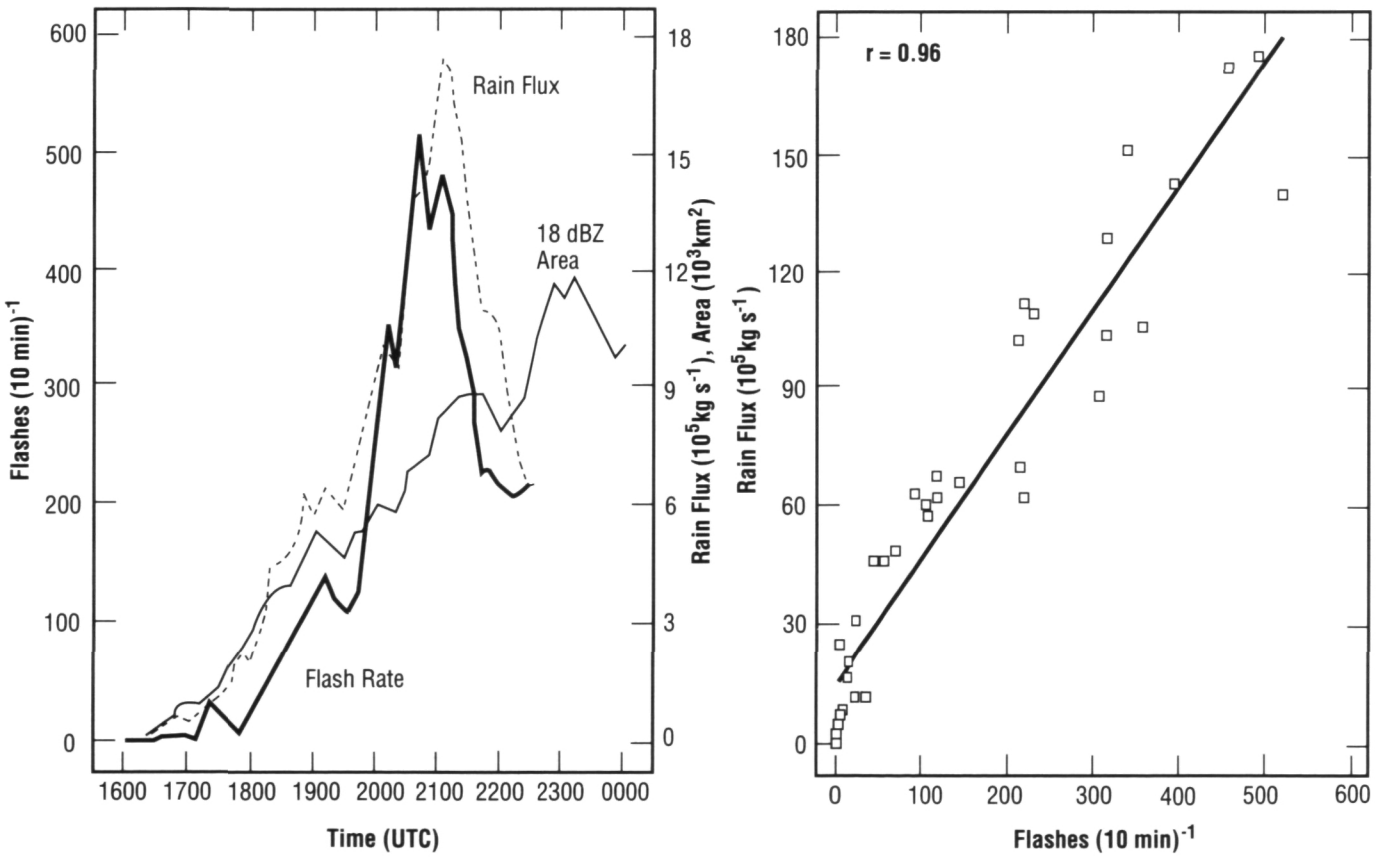

Figure 60. Lightning-Rainfall Relationships for a Mesoscale Convective System on July 13, 1986

Work has begun to determine how different environmental conditions will affect a **lightning/rainfall** relationship. To do this, the vertical velocity due to buoyancy was computed from environmental soundings taken at 1800 u.t. on each day. These were then compared to the average rain volume per flash on the days studied. Although only 5 days have been examined thus far, the data suggest that the days with the highest buoyancy produce less rain per ground flash. Data from other regions are being examined to extend the data sets.

Goodman, S.J., and Buechler, D.E., "Lightning-Rainfall Relationships," *Preprints, AMS Conference on Operation Precipitation Estimation and Prediction*, Anaheim, CA, Feb. 7–8, 1990.

R.J. Blakeslee/ES43
(205) 544–1652
Sponsor: Office of Space Science and Applications

Global Atmospheric Temperature Monitoring from Satellites

With the current public concern over potential global warming from increased man-made emissions of greenhouse gases, there is an increasing need for precise methods of monitoring global atmospheric **temperatures**. Reliable temperature records have been gathered only during the last 100 years or so, and the thermometers are restricted to the more populated land areas. The oceans, accounting for about three-quarters of the surface of the Earth, go largely unmeasured. Microwave radiometers designed to measure deep-layer average **temperatures** have been routinely flying since late 1978 on the Topographical Infrared Operations Satellite (TIROS)-N series of National Oceanographic and Atmospheric Administration (NOAA) **satellites**. These **microwave sounding units (MSU's)** measure the thermal emission of radiation by oxygen in the atmosphere at four frequencies near 60 GHz, a region of strong interaction between radiation and the oxygen molecules. These instruments were originally designed to provide deep-layer measurements over four layers extending from the surface of the Earth to the lower stratosphere. These measurements are then used to try to retrieve the detailed vertical **temperature** structure of the atmosphere, as a weather balloon (radiosonde) does, for daily weather forecasting purposes. They have been only marginally useful for this purpose.

Analysis of the entire **MSU** archive (since 1978) for climate-monitoring purposes has never been attempted. The data processing and storage requirements are formidable, and remote sensing data have not yet been proven to be of sufficient precision to allow monitoring to, say, 0.1°. Out of a total of seven **MSU's** flying on seven separate spacecraft to date, typically two are operating at any one time. We were able to compare those **satellites** with overlapping coverage to determine the level of agreement between them. Of most interest was **MSU** channel 2, which provides an unevenly weighted average **temperature** from the surface of the Earth to the base of the stratosphere, with a peak response from the middle

troposphere (about 20,000 feet in altitude). It was determined that the **MSU's** can measure **globally averaged temperature** variations to a precision of one one-hundredth of a degree per month. Figure 61 shows the variability of **globally averaged temperature** anomalies during the 10-year period 1979–88. The record is surprisingly erratic, with relatively frequent swings between warm and cold conditions. Most of these events can be traced to the tropical oceans.

This data set is now being distributed to climate researchers for comparison to climate models and other global data sets. Future work will include extraction of information from the other three **MSU** channels.

R.W. Spencer/ES43
(205) 544–1686
Sponsor: Office of Space Science and Applications

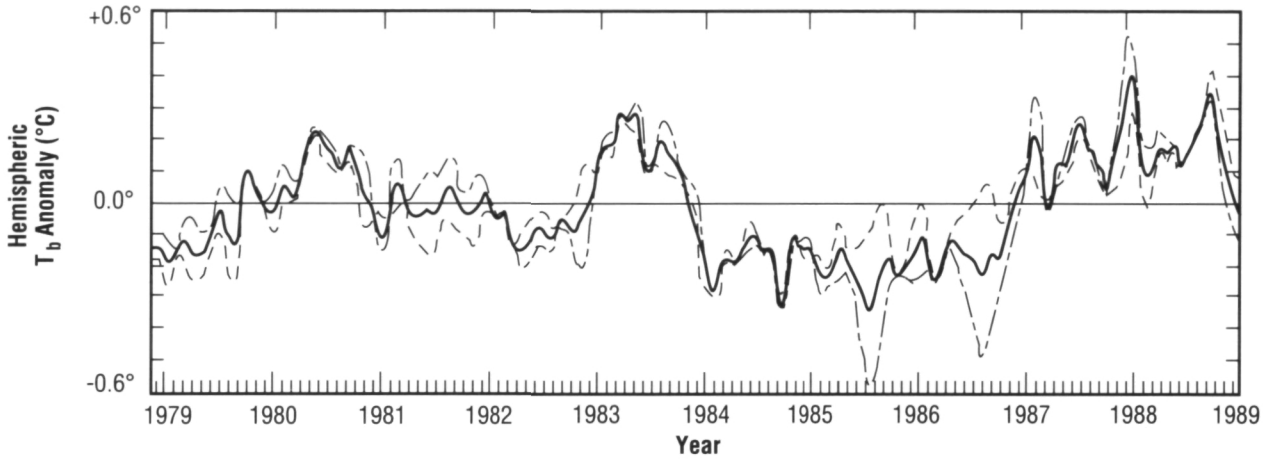

Figure 61. Satellite Global Tropospheric and Hemispheric Temperature Trends

The Advanced Microwave Precipitation Radiometer

Satellite passive **microwave** remote sensing of the Earth has proven valuable for monitoring various weather and climate variables such as precipitation, temperature, oceanic water vapor, surface wind speed, cloud water, sea ice, and snow cover parameters. Typically, spatial resolution of these instruments from satellite altitudes (around 800 km or 497 mi) has been less than optimum since at **microwave** wavelengths, any reasonable-size antenna (0.5 to 2.0 m (2 to 6.5 ft)) will not be able to resolve features smaller than about 15 to 70 km (9 to 43 mi) in diameter, depending upon the channel frequency.

Precipitation is especially difficult to quantify due to its fine spatial structure combined with the often nonlinear response of the **radiometer** to rain rate. The advanced **microwave** precipitation **radiometer** (AMPR) was designed for aircraft over-flight of rain systems to examine the multifrequency signature of **rain** systems over land and ocean at high (0.8 to 4 km (0.5 to 2.5 mi)) spatial resolution. It is a crosstrack scanning **radiometer** with frequencies at 10.7, 19.35, 37, and 85.5 GHz. Utilizing a copy of a multifrequency feedhorn currently flying on a Department of Defense weather satellite, the AMPR was designed to allow more precise interpretations of data from current spaceborne **microwave** sensors. It also includes new frequencies which are anticipated to be very valuable when they are utilized as part of Mission to Planet Earth in the late 1990's.

AMPR fabrication was recently completed, and it is now undergoing testing at MSFC. The AMPR will make periodic upward-viewing measurements over the next year, through rainclouds, to test current radiative transfer theories of how **microwave** radiation interacts with **rain** and cloud drops, as well as ice particles above the **rain**. It will make its first engineering test and science flights over the next year, in the NASA ER-2 high-altitude aircraft to collect oceanic **rain** system data of the Florida coast.

R.W. Spencer/ES43
(205) 544–1686
Sponsors: Office of Space Science and Applications
and Center Director's Discretionary Fund

The High-Resolution Microwave Spectrometer Sounder

The history of satellite passive microwave remote sensing of the atmosphere and Earth can be traced back to 1972, with the launch of Nimbus-5. This NASA research satellite carried two microwave **radiometers** built to test the ability to measure air temperature, humidity, and rain and cloud processes. Since then, about a dozen separate types of civilian **radiometers** have flown, each with additional capabilities, on a number of separate satellites. After analysis of data from these different sensors, most of the important lessons have now been learned concerning calibration strategy, lowest noise necessary to make measurements, antenna performance, frequency selections, etc. Combined with the rapid improvements in microwave receiver technology, it is now possible to design an extremely useful **radiometer** to make a wide variety of measurements of the atmosphere, lithosphere, hydrosphere, and cryosphere.

The **High-Resolution Microwave Spectrometer Sounder (HIMSS)** was proposed to be the first of the next generation of Earth-viewing microwave **radiometers**. As part of the **Earth Observing System (EOS)** Polar Platform series of three identical satellites, three **HIMSS's** would make measurements over at least 15 years to provide data for monitoring global change of various climate processes. The **HIMSS** was selected through competition by NASA for phase B studies, which are now completed. The **HIMSS** design employs an offset-fed parabolic reflector 2 m (6.6 ft) in diameter (the largest yet to fly on a civilian spacecraft), and it will feature dual polarization channels at 6.6, 10.7, 18, 21, 37, and 90 GHz. The antenna design emphasizes high main-beam efficiency (low sidelobes), exceeding 95 percent for most of the channels. This ensures that most of the microwave energy collected is from the feature in the instrument's line of sight. Low-noise amplifiers are used at most of the frequencies to achieve low radiometric noise (0.2° to 0.5°). The instrument continuously rotates at 40 r/min, conically scanning to allow V- and H-polarization measurements to be made at a constant Earth incidence angle of 53°. The resulting swath width from the EOS altitude of 700 km (435 mi) would be 1,470 km (913 mi). Final selection of most instruments for **EOS** will be made in fall 1990.

R.W. Spencer/ES43
(205) 544–1686
Sponsor: Office of Space Science and Applications

Doppler Radar Wind Profiler

The 50-MHz **Doppler radar** wind profiler, installed at the Kennedy Space Center (KSC) along the shuttle runway in November 1988, has been upgraded to operate at high power (250 kW). For comparison, the high-power system is two orders of magnitude more powerful than the original **limited capability system (LCS)**. The high-power wind profiler measures the upper-level winds from 2 to 18 km (1 to 11 mi) at 150-m (492-ft) intervals, whereas the **LCS** had measured the winds in two modes: 2 to 9 km (1 to 6 mi) at 150-m (492-ft) intervals and 4 to 14 km (2.5 to 9 mi) at 600-m (1,969-ft) intervals.

Unfortunately, technical problems created delays in the delivery of the high-power system. In the meantime, the **LCS** was used by the **Launch Systems Evaluation Advisory Team (LSEAT)** in an experimental mode to test the usefulness of the doppler wind profiler in the launch countdown process. The **LCS** was used to monitor the upper level winds during space shuttle launches which occurred between November 1988 and February 1990. The doppler wind profiler technology was found to be useful to the **LSEAT** for monitoring upper-level wind changes; however, the **LCS** data were not always reliable because of antenna and transmitter problems.

Upon completion of factory acceptance testing this summer, the high-power wind profiler began an 18-month validation assessment in preparation for the incorporation of the profiler into the operational launch support environment. During the validation process, the high-power wind profiler data will be compared to the jimsphere and windsonde measurement systems existing at KSC. Statistical assessments will be performed to ascertain the differences in the wind measurement systems and the differences that the measurement systems have on the space shuttle load simulation results. In the future, the **LSEAT** would like to use the high-power wind profiler to accurately assess day-of-launch wind variability in time periods less than 2 hours.

C. Carlson-Lapenta/ES44
(205) 544–2755
Sponsor: Office of Space Flight

Space Applications of Sensor Development

Sensor development at both the detector level and system level has continued in three major areas for the Remote Sensing Laboratory. On-focal-plane signal processing is being addressed with the **hybrid mosaic on stacked silicon (HYMOSS)** technology developed by Irvine Sensors Corporation through the Small Business Innovation Research (SBIR) program sponsored by MSFC. Two SBIR's are addressing this technology: a phase II titled, "On-Focal Plane Signal Processing for Atmospheric Measurements," and a phase I titled, "Space Sensor Common Module Electronics."

The phase II is currently addressing the packaging processes for **HYMOSS** technology. In this technology, a layer is made up of 128 channels, where 1 channel consists of a transimpedance amplifier, adaptive bandpass filter, thresholding, comparing, and 1 random-access multiplexer signal path. To complete the module, 128 layers are stacked to form a cube on which a detector array is bump-bonded to the face of the module using the same technology as planar hybrids. Processing the module front face for receiving the mosaic detector array is critical for full 128×128-channel operation. There is difficulty in obtaining good passivation and metal pad deposition, and indium bumps to the edge from the center are affected by the discontinuity of the edge itself. Edge build-up has reduced the usefulness of the outer pixels. Phase II will concentrate on the correction of this edge buildup so full, 128×128, buttable modules will be obtained. Phase I will address the uniqueness of each application for on-focal-plane signal processing with a common module approach. This module will address three instrument classes consisting of an infrared sounding Fourier transform infrared (FTIR) **spectrometer**, an advanced lightning mapper sensor, and the high-resolution imaging **spectrometer**. These remote sensing instruments have various requirements that necessitate operation of the common module over the spectral range between 0.4 and 14 μm with detectors varying in size between 50 and 100 μm using integration periods between 0.1 ms and 1,000 s. With the development of the **HYMOSS** technology, the circuitry can be designed to allow programmability per channel for both the analog and digital sections. This study will design the baseline elements to allow this capability by investigating varying requirements of bandwidth, sample rates, noise performance, and power dissipation. With this programmability and the buttability between modules of the previous phase II, tunability within the array of a number of channels for low noise, wide dynamic range information is possible without affecting the remainder of the array.

For a number of space shuttle missions, an experiment, the **Mesoscale Lightning Experiment (MLE)**, has been flown to record lightning flashes from low Earth orbit. An improved instrument is being developed that will not only record the flashes on video tape but will record the spectrum and pulse duration of the lightning flashes. A shuttle optical lightning imaging system is being developed as a portable hand-held **spectrometer** for use during future shuttle flights. It will consist of a video camcorder with an 8-mm tape format, a **spectrometer**, and an optical pulse detector. The video will be used to navigate the image and for storage of the **spectrometer** data and optical pulse data. The time code will be placed on an additional video track with another recorder. Two approaches are being considered at this time for the hand-held **spectrometer**. The first approach would use two camcorders for regular video on one and the other will be modified to perform the **spectrometer** function. The optical pulse data would be multiplexed with the **spectrometer** data on the video track. The second approach would use one camcorder and a portable video recorder to collect the **spectrometer** data. Simplicity in operation is one of the key forces driving this development, so that ease of use in a space environment is maintained while utilizing the video bandwidth for quality data recording.

M.W. James/ES43
(205) 544–5020
Sponsor: Office of Space Science and Applications

Organization of Cloud and Precipitation Patterns Within Extratropical Baroclinic Waves

Investigations of rainbands embedded within extratropical cyclones have documented a spectrum of linear features with varied characteristic dimensions, preferred development locations with respect to **hyperbaroclinic zones**, and differing physical growth mechanisms. The largest structures are those which have length scales comparable to the supporting baroclinic wave, and which define the macroscale ascent of air in a system-relative sense. Included in this class of structures would be the warm and cold "conveyor belts" that constitute the main influxes of moisture and heat into baroclinic waves. At the other end of the spectrum are mesoscale bands which vary widely in width from a few kilometers to several tens of kilometers. These features evolve with characteristics thought to be constrained by the environmental shear and the thermodynamic stabilities of the larger airstreams.

Recent increases in computational power and advances in physical parameterizations have made numerical simulations attractive as a complementary means of investigating the dynamics of these moist atmospheric systems. We are currently using a version of the Drexel University **LAMPS (Limited Area Mesoscale Prediction System)** as a source for internally consistent data sets to diagnose processes in synoptic and mesoscale flows. The objective of this work is to understand the processes determining the morphology and bulk microphysical composition of condensation in baroclinic waves. The **LAMPS** model is notable in that it carries grid-scale predictive equations not only for water vapor, but also for cloud and precipitation. Recently, the model has been improved to account for ice condensate which enables a more physically correct treatment of precipitation initiation.

Our investigations this year have focused essentially on the macroscale organization of cloud and precipitation which occurred during the 4th Intensive Observing Period (IOP-4) of the **Experiment for Rapidly Intensifying Cyclones over the Atlantic (ERICA)**. This experiment, held off the East Coast of the United States during the winter of 1989, documented several episodes of rapid cyclonic storm development. Also playing a major role as validation and ground truth in these studies are **Special Sensor Microwave/Imager (SSM/I)** retrievals of precipitable water, total liquid water, and ice, which are generated by other MSFC-supported investigations. Model simulations produced, to date, suggest that, while the large-scale

atmospheric dynamics was an essential driving mechanism, the role of condensation was crucial in facilitating the exceptionally rapid spinup of the cyclone and the low surface pressure. The majority of precipitation involved the production of ice with model condensate distributions matching well with **SSM/I** observations. A model simulation of the precipitation rate at the time of most rapid storm intensification is shown in figure 62.

The next phase of this work will be to compare the model simulations and **SSM/I** observations to aircraft radar returns and in situ measurements of atmospheric temperature, moisture, wind, and microphysics data. We also anticipate studying the role of ocean surface fluxes of moisture and heat in preconditioning the overlying lower atmosphere prior to storm development. The approach of combining remote observations from space, ground truth, and model simulations should enable a more thorough study of the rapid cyclogenesis process.

Robertson, F.R., Doty, K., and Perkey, D.J., "Numerical Simulation of Cloud and Precipitation Structure During GALE IOP-2," Submitted to *Mon. Wea. Rev.*, 1989.

F.R. Robertson/ES42
(205) 544–1655
Sponsor: Office of Space Science and Applications

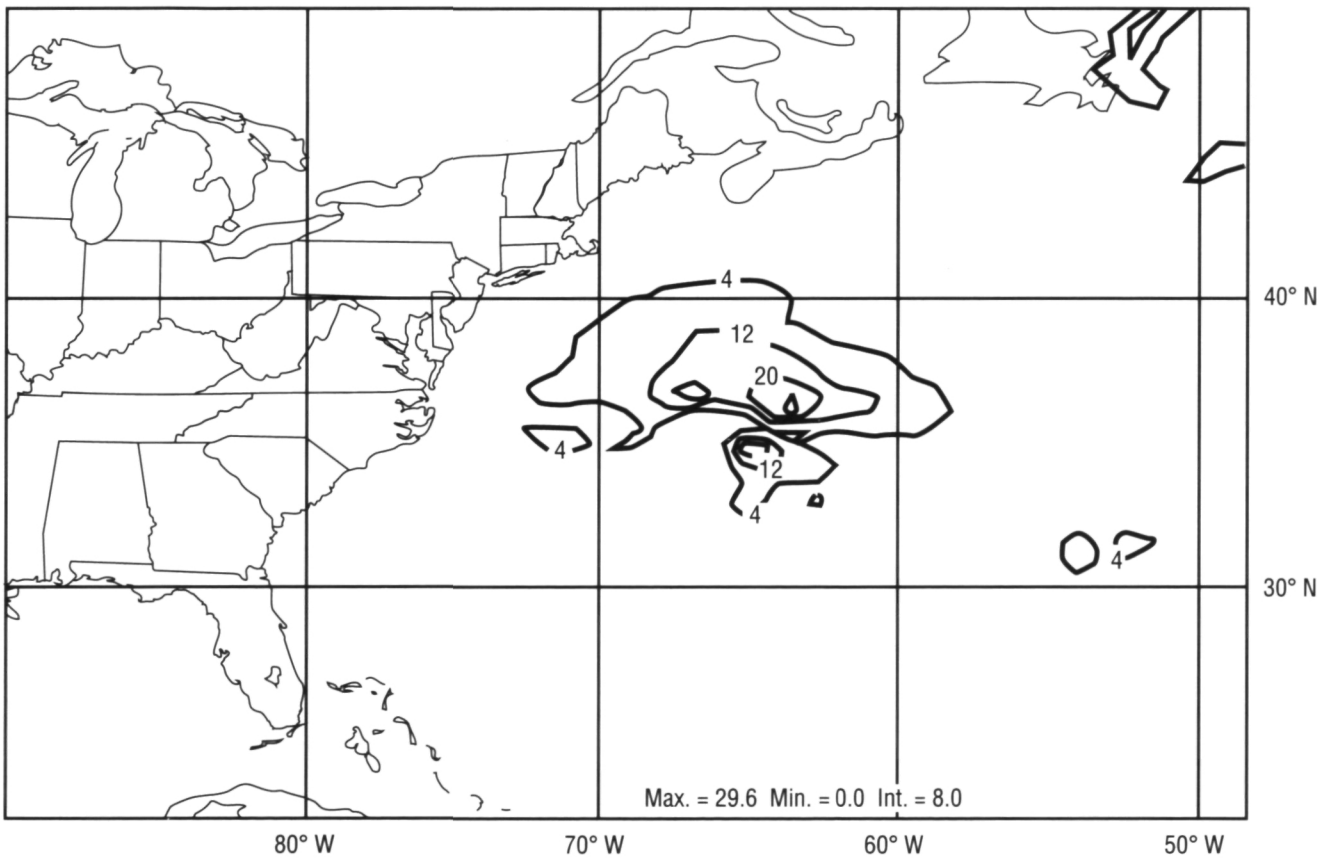

Figure 62. Model Simulation of Precipitation Rate During Intense Storm

Atmospheric Laboratory for Applications and Science

NASA's Upper Atmosphere Research Program is charged with the responsibility to study the processes which determine the distribution of ozone in the Earth's stratosphere. As is well known, the presence of ozone is necessary to shield humans and other life forms from deadly ultraviolet radiation from the Sun. The discovery in recent years of ozone depletion in the Antarctic spring, and the determination that human-produced chemicals play a role in this depletion, has raised an alarm throughout the world that our planet is an intricate system which can be upset by human activities. The **Atmospheric Laboratory for Applications and Science (ATLAS)** program is part of an effort to collect data on this system to facilitate a better understanding of these processes and provide a long-term data set for the purpose of monitoring any changes which may occur. The **ATLAS** program consists of a series of space shuttle missions which will be conducted approximately annually throughout the 1990's utilizing Spacelab pallets. **ATLAS-1** consists of a broad range of experiments including Earth science, solar physics, space physics, and astronomy; launch is planned for the spring of 1991. From **ATLAS-2** and beyond, there will be a smaller set of experiments with goals focusing on the Earth's atmosphere. The core instruments, which are listed in tables 4 and 5, measure energy output from the Sun—including detailed spectral information—and trace constituents and other properties of the Earth's middle and upper atmosphere. The instruments involve scientific investigators from Europe as well as the U.S. The orbits for the first three **ATLAS** missions are planned to be at 57° inclination and at 160 nmi in altitude (about 300 km).

The two, core **ATLAS** instruments which use remote sensing techniques to measure properties of the Earth's atmosphere are Atmosphere Trace Molecules Observed by Spectroscopy (ATMOS) and **Millimeter-Wave Atmospheric Sounder (MAS)**. ATMOS measures the absorption of solar radiation by the Earth's atmosphere during each solar occultation event (two per orbit). The technique used is a fast Fourier transform (FFT) interferometer which operates in the near- and middle-infrared region of the spectrum. By comparing the spectrum of solar radiation which is transmitted through the atmosphere at a given height with that transmitted above, including that received well above the atmosphere, concentrations of trace atmospheric species can be inferred. The vertical resolution is about 2 km (1.2 mi), which is the distance the Sun rises through the atmosphere during a single scan of the instrument,

Table 4. ATLAS Atmospheric Instruments

Name	Acronym	Method
Atmosphere Trace Molecules Observed by Spectroscopy	ATMOS	Measures atmospheric absorption of solar radiation during solar occultations
Millimeter-Wave Atmospheric Sounder	MAS	Measures atmospheric emission of millimeter wave radiation
Co-Manifested with ATLAS:		
Shuttle Solar Backscatter UV	SSBUV	Stratospheric ozone by backscatter of solar UV radiation
Cryogenic Infrared Spectrometers and Telescopes for the Atmosphere	CRISTA	Measures atmospheric emissions in the infrared

Table 5. ATLAS Solar Instruments

Name	Acronym	Objective
Solar Spectrum	SOLSPEC	Solar spectrum from 170 to 4,000 nm
Solar Constant	SOLCON	Total solar irradiance
Active Cavity Radiometer	ACR	Total solar irradiance
Solar UV Spectral Irradiance Monitor	SUSIM	High-resolution solar spectrum from 120 to 400 nm

which takes 1 second. The spectral region of 2.1–18 mm (0.1 to 0.7 in) is covered at a resolution of 0.01 cm^{-1} through the use of four filters. Because of the high spectral resolution of the instrument, a large data volume is created, at a rate of 16 megabits per second. The ATMOS instrument is a project of the Jet Propulsion Laboratory (JPL) in Pasadena, California.

The **MAS** instrument also measures the concentration of certain trace species in the atmosphere, but it does so using a very different technique, and the number of species measured is considerably less. (On the other hand, **MAS** operates continuously, rather than only during solar occultations as does ATMOS.) **MAS** senses the emission by the Earth's atmosphere of radiation in the microwave region of the spectrum. The atmosphere is scanned vertically as **MAS** points to the side of the shuttle and scans the limb of the Earth. The major data acquired are temperature, pressure, water vapor, ozone, and chlorine monoxide. The **MAS** instrument, which is the most massive of the **ATLAS** instruments, is a joint venture of the University of Bern (Switzerland), the Max Planck Institute (Germany), and the Naval Research Laboratory (U.S.).

The solar instruments make up an ensemble which measures both the total energy output of the Sun (the solar constant) as well as spectral information of particular interest to atmospheric scientists. The two solar constant instruments, **Solar Constant (SOLCON) and Active Cavity Radiometer (ACR)**, use two different techniques to measure very small changes in this quantity and therefore provide powerful validation and comparative information. The JPL-developed **ACR** uses three active cavity radiometers and **SOLCON** (from Belgium) uses a high-resolution absolute pyrheliometer. **Solar UV Spectral Irradiance Monitor (SUSIM)** and **Solar Spectrum (SOLSPEC)** measure the solar spectrum. **SUSIM** concentrates upon the ultraviolet region (important in the Earth atmosphere photochemistry), and **SOLSPEC** measures the spectrum through a broader range, from infrared to ultraviolet. **SUSIM** is an experiment of the Naval Research Laboratory, and **SOLSPEC** is a French experiment.

The Goddard Space Flight Center instrument, **SSBUV (Shuttle Solar Backscatter Ultraviolet)**, will be a companion to the **ATLAS**, perhaps on all flights, beginning with **ATLAS-2**. This instrument is a near copy of the National Oceanic and Atmospheric Administration (NOAA) **SSBUV** instruments which monitor stratospheric ozone from NOAA operational satellites. The degradation of these instruments as they perform their duties from Earth orbit has been one of the major problems in determining the extent and rate of global ozone depletion. The major goal of **SSBUV** is to provide a calibration check on the NOAA instruments.

Cryogenic Infrared Spectrometers and Telescopes for the Atmosphere (CRISTA) will be a partner of the **ATLAS-3** mission. This German instrument senses properties of the Earth's atmosphere by scanning the limb and recording emitted infrared spectral information. **CRISTA** resides in its own carrier, and it will be deployed to fly free of the shuttle during the mission. The spectral information is acquired through the use of

Ebert-Fastie spectrometers which cover the spectral range of 4–80 mm (0.2–3 in). There are actually three telescopes, which view at 162°, 180°, and 198° from the craft's velocity vector. This results in data points about 700 km (435 mi) apart, cross-track, while the speed of the instrument gives an along-track horizontal resolution of about 400 km (249 mi). The vertical resolution will be about 1 km (0.6 mi).

One of the major goals of **ATLAS** is to acquire a series of well-calibrated data sets which will provide a reference against which to calibrate instruments on free-flying space platforms which would be flying in space for extended times and hence cannot be physically checked for calibration and other performance characteristics. In 1992 and 1993, **ATLAS-2** and possibly **ATLAS-3** will underfly the Upper Atmosphere Research Satellite (UARS), which will have several instruments very similar to some of the **ATLAS** instruments. In the middle 1990's, **ATLAS** will provide a set of measurements for NASA's Global Change program, and in the late 1990's, **ATLAS** will provide calibration data for the Earth Observing System (EOS), a set of polar-orbiting platforms and attached payloads on Space Station *Freedom,* which will be the first phase of NASA's "Mission to Planet Earth."

T.L. Miller/ES42
(205) 544–1641
Sponsor: Office of Space Science and Applications

Numerical Modeling of Nonlinear Baroclinic Fluid Systems

In developing an understanding of the processes which affect global change of the planet Earth, a component which offers one of the greatest challenges is the fluid system comprised of the atmosphere and oceans. Clearly, the objective of understanding this system is an important one, since the atmosphere is the fluid system in which we live, which supplies the land with fresh water and which shields life from harmful solar radiation. Due to the complex nature of this system and the difficulty in obtaining sufficient observational data on it, accurately predicting or even understanding its behavior for all but very short time periods remains an elusive goal. The goal of the research efforts described here is to develop a better understanding of the Earth system through the use of computer models which allow the study of the complicated behavior of a rather simple fluid system which is driven by horizontal temperature gradients and influenced by rotation of the planet.

One of the means for studying the behavior of the Earth's atmosphere and oceans is to conduct laboratory experiments in cylindrical and spherical containers where a fluid, such as water, is differentially heated and rotated. Depending upon the strength of the differential heating and the rate of rotation, the flow may be very simple; steady in time and axisymmetric in structure. For other values of the heating and rotation, the flow may be made of steady, regular waves, or it may be quite irregular and chaotic. Such experiments have been conducted in the laboratory, both at MSFC and elsewhere, and a numerical model developed at MSFC is being used to test our ability to predict the type of flow and to assist us in the development of an understanding of such processes as heat and momentum transport. Studies are being performed additionally to help design future spaceflight experiments using the Geophysical Fluid Flow Cell (GFFC) apparatus, described elsewhere in this document.

The model which we have developed for the study of these flows, **GEOSIM (geophysical fluid flow simulation)**, is able to study either spherical or cylindrical flows. Analysis of the flows proceeds in several steps: calculation of the axisymmetric flow (that which would be seen if no variations in longitude were allowed), calculation of the linear stability of that flow to three-dimensional wave perturbations, calculation of the wave amplitude where interaction between the wave and the longitudinal mean flow is allowed, and, finally, the calculation of the fully nonlinear flow with full interaction between all components of the flow. The extent to which each of these steps can be directly applied to the actual flows depends upon the nonlinearity of the flow, which in turn depends upon the experimental parameters. Figure 63 shows a color image of the temperature field which has been created by a highly nonlinear flow in the GFFC experiment. This image is from a computer animation of the evolution of the flow over time, which is quite complex and very sensitive to the initial conditions and numerical parameters used in the model.

In addition to using models of a simple fluid system which can be constructed in the laboratory, we are using a complex atmospheric model which considers a domain approximately equal to a 2,500×2,500 km square (1,554×1,554 mi). This model **(LAMPS—Limited Area Mesoscale Prediction System)** was developed at the National Center for Atmospheric Research and Drexel University and is used for some of the other research efforts described in this document, as well. It includes the effects of water substance in the atmosphere, of which latent heat release by condensation is particularly important. In our case, we are interested in the nonlinear development of a single baroclinic wave (a midlatitude low-pressure center) and in the ensuing mesoscale (about 100 km (62 mi)) phenomena. While the large-scale storm is a result of strong horizontal temperature gradients and acts to reduce those gradients on the large scale, in smaller regions, the storm actually increases the gradients, resulting in such important weather-making features as cold fronts and rainbands.

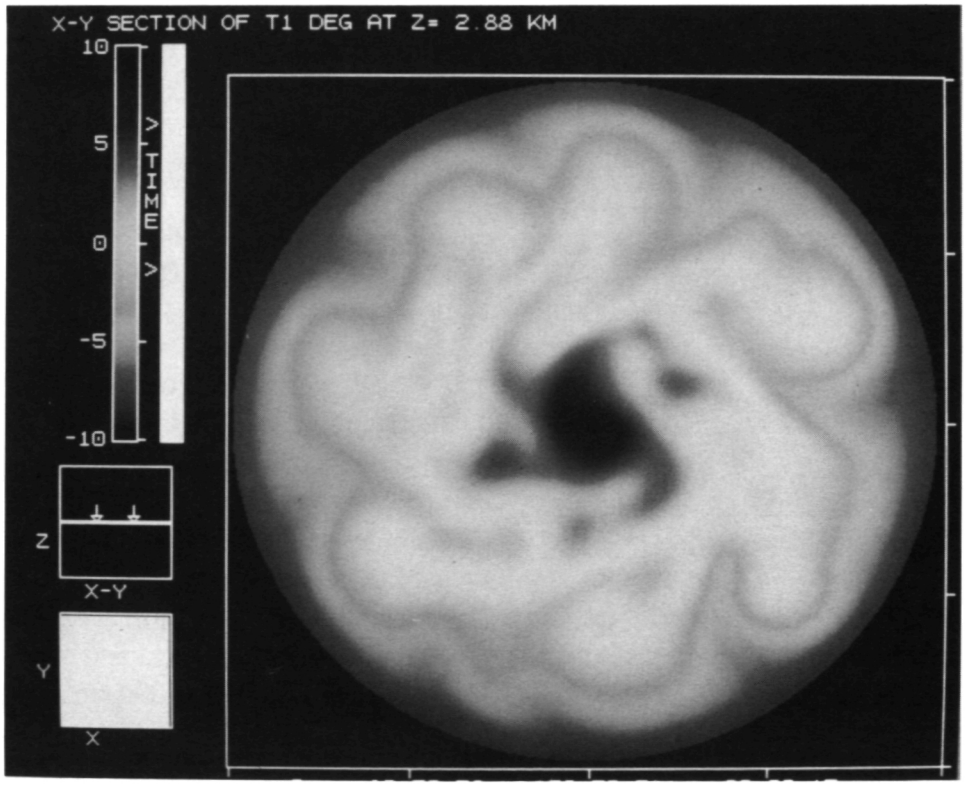

Figure 63. Temperature Field Produced by Motions in the Geosphysical Fluid Flow Cell, as Predicted by the Computer Model GEOSIM

The research with the **LAMPS** has led us to utilize the **GEOSIM** model to study the small-scale (horizontal length about 10 km (6 mi)) convection that occurs when the air is unstable in the presence of horizontal temperature gradients. The results have indicated that strong slantwise convection can occur even when the air is stable to vertical convection, and that the resulting motions give rise to strong transport of heat and momentum. It is expected that this modeling effort will result in a method to more accurately include the effects of the small-scale, slantwise convection in larger scale models such as **LAMPS**.

Miller, T.L., and Fehirback, J.D., "A Numerical Study of the Onset of Baroclinic Instabilities in Spherical Geometry," *Geophys. Astrophys. Fluid Dynamics, 52,* 25–43, 1990.

Miller, T.L., and Butler, K.A., "Hysteresis and the Transition Between Axisymmetric Flow and Wave Flow in the Baroclinic Annulus," to appear in *J. Atmos. Sci.*

Butler, K.A., Miller, T.L., and Lu, H.-I., "GEOSIM–A Numerical Model for Geophysical Fluid Flow Simulation," NASA Tech Memo., in preparation.

T.L. Miller/ES42
(205) 544–1641
Sponsor: Office of Space Science and Applications

Remote Sensing Perspectives on the Global Hydrologic Cycle

The cycling of water through the geophysical environment has long been recognized as crucial to understanding the Earth's physical climate system and various biogeochemical processes. Space-based remote sensing is rapidly becoming a tool of critical importance for inventorying and understanding the global water cycle. The requirement for a perspective from space results in part from the paradox that while the distribution of water is globally extensive, the processes of phase change between vapor, liquid, and ice; associated Earth radiation budget influences; and interaction with other chemical constituents all occur on scales ranging from global to molecular. While no single observing system or research tool can address the whole problem, space observations make a unique and critical contribution.

For several years, the Space Science Laboratory has focused on studies involving the atmospheric component of the **hydrologic cycle**. These studies have sought to understand how heat sources and sinks induced by phase condensation and evaporation modify atmospheric thermal structure and wind fields. For example, it has been shown that persistent atmospheric condensation and heating in tropical cloud bands over the South Pacific is important in maintaining the thermal gradient and associated Southern Hemisphere subtropical jet stream.

Recently, passive microwave measurements of atmospheric water vapor, liquid water, and ice have become available from the **Special Sensor Microwave/Imager (SSM/I)** flying on a polar orbiting DOD satellite. During the past year, we have been analyzing these measurements in a number of ways. Global monthly distributions of column-integrated water vapor (precipitable water) have been generated and compared against similar measurements taken from conventional observing networks. This comparative analysis has demonstrated the variability of water in the atmosphere and shown that our conventional observing system, while describing a significant fraction of this variability,

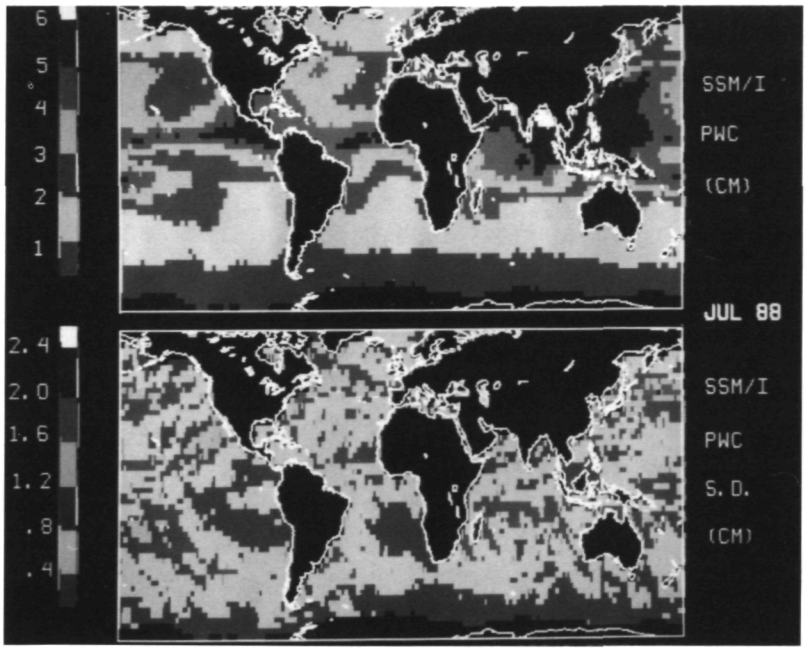

Figure 64. Global Monthly Mean Precipitable Water and Its Standard Deviation for September 1987

undersamples many transient features. Figure 64 shows the September 1987 monthly variability of water vapor, detailing especially well the high variability of moisture in middle-latitude storm tracks.

The rich structure seen in global moisture distributions attests to the complex dynamical processes which both transport water and determine sources and sinks. A program of numerical modeling and simulation has been developed to allow controlled experiments which assist in sorting out these processes. The **LAMPS (Limited Area Mesoscale Prediction System)** numerical code is serving as a tool to investigate mesoscale moist processes. During the past year, this model has been used to simulate winter storms off the east coast which owed their rapid development in part to condensation in widespread cloudiness. The evolution of these numerically simulated clouds and precipitation has been compared to **SSM/I** measurements. To address processes on a global scale, we have recently acquired a version of the Community Climate Model (CCM1) developed at the National Center for Atmospheric Research (NCAR). This tool will enable a series of experiments that explore how global land and sea surface characteristics and radiative processes operate on time scales from weeks to months and years in determining the global hydrologic balance. During the past year, we began an activity to verify the CCM1 moisture balance with **SSM/I** measurements

During the next year, this research will become more focused toward science issues within the framework of the Earth Observing System (EOS) initiative. The research effort proposed by MSFC and selected under the EOS program will build on the remote sensing observations and modeling outlined here and point toward solving issues of the global water cycle that require space-based observations planned for the 1990's.

Robertson, F.R., and Huang, H.J., "Atmospheric Moisture and Cloud Structure Determined from SSM/I and Global Gridpoint Analyses," Preprints, Symposium on the Role of Clouds in Atmospheric Chemistry and Global Climate, *Amer. Meterol. Soc.*, January 1989.

F.R. Robertson/ES42
(205) 544–1655
Sponsor: Office of Space Science and Applications

Global Atmospheric Modeling

Numerical models of the atmospheric general circulation are powerful tools for probing the nature of physical processes which control the dynamics of climate. The complex aspects of surface energy fluxes, cloud radiative forcing, and orographic influence are just a few of the important physical processes which can be studied. Over 2 years ago, we initiated a cooperative effort with the National Center for Atmospheric Research (NCAR) through which the NCAR **Community Climate Model (CCM1)** would be implemented on the EADS for use in MSFC science studies. The **CCM1** is currently formulated as a global spectral model which predicts atmospheric temperature, winds, and moisture subject to physical laws governing hydrodynamic flow; also treated are radiative processes, cloud cover, subgrid-scale deep **convection**, and exchanges of energy with the underlying land or ocean.

Currently, we are investigating the sensitivity of the model climate to lower boundary conditions. Exchanges of heat, moisture, and momentum between the surface and overlying atmosphere exert a fundamental control on climate. The **CCM1** formulation of land hydrology involves a simple water balance model accounting for rainfall, evaporation, runoff, and storage. Experiments to date have shown that the **CCM1** climate is sensitive to the amount of stored water since this strongly modulates surface evaporation rate. Surface temperature, a critical climate variable is strongly regulated by the fraction of the surface energy flux occurring through the evaporation process. Figure 65 shows the difference in surface temperature in two experimental **CCM1** integrations, one having the standard **interactive hydrology** and one having a fixed amount of soil moisture. Temperatures in the

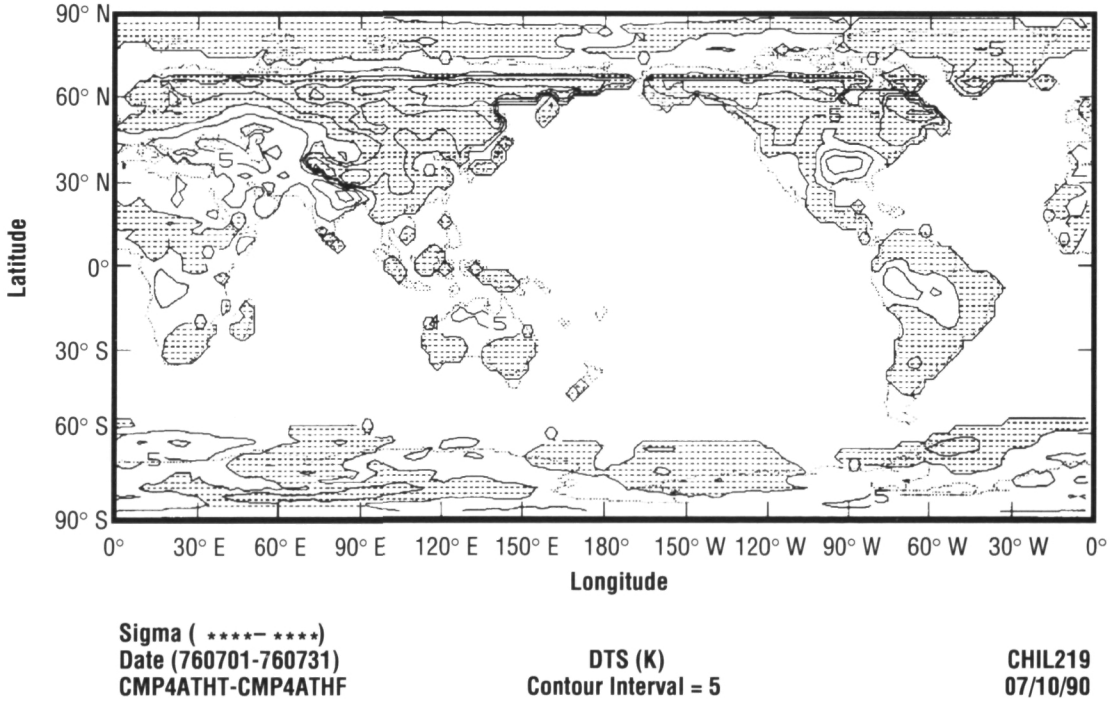

Figure 65. Surface Temperature Difference in Two Experimental CCM1 Integrations

Southeast United States are over 10 °C (18 °F) warmer with the **interactive hydrology** because the soil has been realistically dried by evaporation.

Sea-surface temperature (SST) anomalies are also a crucial mechanism by which subseasonal and longer atmospheric temperature and precipitation anomalies are generated. One of our scientific objectives is to understand how land-surface hydrology acts to modulate climate perturbations initially triggered by SST anomalies. For example, if the atmosphere responds to a warm pool in the Pacific Ocean by decreasing rainfall over the U.S. Central Plains, the ensuing reduction in soil moisture may further exacerbate such an incipient drought through the surface energy balance (i.e., more of the solar energy received by the soil/vegetation complex is used to heat the overlying atmosphere since there is less soil moisture to enable evaporation). This scenario is being examined in the **CCM** by conducting numerical experiments in which SST anomalies are imposed and the soil moisture is either fixed (a control experiment) or is allowed to evolve as predicted in the model.

A key aspect of these studies is comparison to remote observations from space. A recent compilation of global temperature structure from the Microwave Sounding Unit will provide a source for comparison to vertical mean temperature in the **CCM1** experiment. Comparison of **CCM1** computed outgoing longwave radiation and rainfall estimates from several sources is also anticipated. Both infrared and microwave measurements have been used in constructing global data sets.

F.R. Robertson/ES42
(205) 544–1655
Sponsor: Office of Space Science and Applications

Aircraft Data Evaluation Workstation Development

The **Multispectral Atmospheric Mapping Sensor (MAMS) Quick View System (QVS)** is a PC-based **image analysis** and display system designed to provide an enhanced capability to evaluate **MAMS** data in the field immediately after a data collection flight. It was developed in the latter part of FY89, and demonstrated in FY90 in support of aircraft flights from Ames Research Center. The **QVS** offers the portability of a personal computer with the advanced analysis and display features of a mainframe **image analysis** system. It also provides the capability to access real-time weather data via a Dial Access Facility (DAF) from supporting mainframe Man-computer Interactive Data Access System (McIDAS).

The original **QVS** developed in 1989, was based on an IBM AT PC with 4 megabytes of RAM and 30 megabytes of disk space. An IBM OS-2 operating system (version 1.0) was used along with a special version of the McIDAS software designed to run on the PC. An interface card (developed in the MSFC Earth and Atmospheric Sciences Division's Remote Sensing Lab) occupied a PC slot and served as the communication link between the **MAMS** flight recorder and the PC. The QVS provided stand-alone **MAMS** processing capabilities which, at the time, were only available on larger mainframe computer systems.

Computer speed, disk space, available memory, and OS-2-compatible supporting hardware and software are limiting factors in the performance of the original QVS. In order to provide more effective support for the analysis of **MAMS** data in the field, an advanced system was proposed to replace the current **QVS**. In FY90, an AST 486/33MHz OS-2/McIDAS PC was acquired to serve as the central processor for the advanced **QVS** system (QVS2). This system allows for use of the existing **MAMS** interface card design without modification. Preliminary tests conducted in the winter of 1989 indicated that the **QVS** interface card is 100-percent compatible with the 486/25MHz machine. This machine was also

shown to support the latest version of PC McIDAS under OS-2. This approach eliminated the redesign of the interface card for the microchannel architecture of the IBM PS-2 (current PC McIDAS standard machine).

In addition to the basic computer system, four other hardware components were required. First, an upgrade to the AT interface card is being developed to provide dual channel "decom" capabilities. This card will be a standard PC card (not wire-wrapped) and will serve as the interface between the **MAMS** flight recorder and the AST. It will display two channels simultaneously and will occupy only one ISA slot. An upgraded frame-grabber card which is supported under OS-2 is required. This card and its supporting software should allow for windowing and scrolling, features which were unavailable with the previous card. This feature, along with the two-channel capability, will allow for more advanced displays of **MAMS** data in the preview mode. The **MAMS** interface card will be refined in-house at minimal cost to produce dual-channel capabilities.

Two other hardware components are being considered which will greatly enhance the capabilities of the **QVS**. Communications with a host McIDAS system are possible from off-site with an external modem. This capability has been demonstrated for both the UW/SSEC and MSFC/EADS/WetNet systems and will allow access to the entire real-time weather data bank available on these systems. This capability will prove invaluable during deployment in support of aircraft flights and for flight planning.

Finally, the **QVS** can be used for a **MAMS** data archive. In its current configuration, **MAMS** collects over 232 Mbytes of data per hour. During the course of a typical 4–5 hour flight, over a gigabyte of data is collected from the instrument. This data could be made available to the scientist without interaction with Ames Research Center if such a storage device were available. Currently, magneto-optical systems are under evaluation for their application to the data archive problem for PC's, as well as additional hard disk space accessed through the scuzzy (SCSI) interface.

The **QVS** hardware and supporting software will allow for greater capabilities and flexibility in the evaluation of **MAMS** data after each aircraft flight. The first step in this evaluation is to get a preview of the **MAMS** data throughout the flight. This will be accomplished using the new frame-grabber card under OS-2 (non-McIDAS mode). The new system allows for the preview and side-by-side display of any two channels in a moving window mode as the data is read from the flight recorder. The **QVS2** will support a preview-to-collection speed of 8:1 (30 in/s). Thus, a 4-hour flight can be completely previewed in two channels in 30 minutes (factor of 8 increase over the original **QVS**). The preview mode will be used to verify the general performance of the scanner and to select specific scenes for more detailed evaluation. For detailed analysis of **MAMS** data, the data are ingested from the flight recorder through the **MAMS** interface card via a menu driven set of panels. The user inputs the desired time or scanline for the data, the number of scanlines to collect, and the destination file name. Two channels can once again be collected and saved to disk. This specification allows for the capture of data starting at the same scanline for additional channels.

The use of an OS-2-supported frame-grabber card for data preview allows for the immediate collection of digital data on the PC. It also allows for instantaneous switch to McIDAS to calibrate and display the image data. Processing can continue with PC McIDAS for the analysis of **MAMS** data in the usual way. The increased hard disk space will allow for the storage of selected data sets from a series of flights for comparison.

The **QVS** can be used to support other instrument flights on the ER-2 aircraft, if desired. Other Daedalus scanners (TMS and AOCI) have identical tape structure so the interface card functions remain unchanged. Some **MAMS**-specific routines for calibration, navigation, and data display would need to be modified to reflect the channel structure of the other spectrometers which use the scanner. Application of the **QVS** to other flight data structures (such as AMPR) is certainly possible. The McIDAS is general enough so that once the data file

has been established, the display and processing software is available for use. For AMPR, a new interface card would be required, as well as some additional supporting software for calibration and navigation. Once the data is in the PC McIDAS data structure, the general-purpose programs will be able to manipulate the image data as requested. Current efforts are underway to develop an interface card and supporting software as part of the AMPR data system.

Jedlovec, G.J., Atkinson, R.J., James, M.W., and Smith, M.R., "The MAMS Quick View System (QVS): A PC-Based Filled Evaluation Workstation." Presentation and Summary Paper to the McIDAS Users Group Meeting, November 1989, Madison, Wisconsin, 9 pp., 1989.

G.J. Jedlovec/ES43
(205) 544–4481
Sponsor: Office of Space Science and Applications

Geophysical Parameter Retrieval From Multispectral Aircraft Measurements for Geostationary Earth Observatory Science Applications

MSFC and its contracting organizations are conducting preliminary studies on a **Geostationary Earth Observatory (GEO)** to be launched as part of NASA's Mission to Planet Earth program around the year 2000. This **GEO** platform will have a large number of interdisciplinary Earth science instruments to study major elements of the hydrological, biogeochemical, and physical climate cycles (see discussion elsewhere in this report). The **GEO** will complement the low Earth orbiting platforms being developed under the EOS program. Together, these instruments will address small-scale, regional, and global-scale processes, interactions between scales and between the surface of the Earth and its atmosphere, in order to study global climate change.

Important to the **GEO** development is the collection of unique data sets which: (1) demonstrate the utility of the **GEO** measurements; (2) provide data sets which can be used to specify the proper spatial and spectral resolutions required from geostationary orbit; and (3) ascertain information on new geophysical parameters which can be derived from appropriate **GEO** measurements. **The Multispectral Atmospheric Mapping Sensor (MAMS)*** is currently being used to collect unique data sets which address these issues. The multispectral character of **MAMS** (8 visible/4 infrared channels), its high spatial resolution, and its ability to fly on the NASA ER-2 aircraft, allow for the collection of multitemporal data sets over many regional areas. **MAMS** data sets have been collected, calibrated, and specific **geophysical parameters** have been derived which address coastal ocean circulations, surface fluxes of heat and moisture, and soil moisture variability, all of which are used to detect environmental changes due to human and nature influences.

Several data sets have been collected along the coasts of California and Louisiana which capture time variability of visible and thermal signatures in the **MAMS** data. This time variability has been physically related to ocean circulations by identifying and tracking natural "targets" present in the imagery. The displacement of these targets as a function of time is transformed into ocean current estimates. Future efforts will focus on refinements to tracking algorithms to determine the most appropriate displacements in the visible and infrared imagery, subsampling of the measurements to address time and space resolution requirements from geostationary orbit, and the determination of the spatial scales and geographic distribution of "targets" which are used as passive tracers. This work is being performed jointly with coinvestigators at the University of Colorado.

In a continuing investigation with high-resolution **MAMS** thermal imagery over the Konza prairie in Kansas, **MAMS** infrared channels have been used to calculate land surface temperature (LST) and fluxes of energy and moisture from the surface. The variability of these parameters preceding the peak heating period during the day is quite large and is related to the land cover and its use, as well as the soil moisture content. These findings help provide a better understanding of the potential impact of future geostationary measurements on the energy and hydrologic processes of the surface and lower atmosphere. Other data sets collected over different geographical regions in late FY90 will be used to contrast the microclimates of the regions.

*See Previous R&T Reports for Description

G.J. Jedlovec/ES43
(205)544–5695
Sponsor: Office of Space Science and Applications

Satellite Sensor Simulations

Progress over the past year has been made in three areas pertaining to the simulation of data from current and future **satellite sensors**: (1) simulating existing channels from current **satellite sensors** with simple empirical relations between transmittance and atmospheric constituent concentrations; (2) verifying empirical results with very accurate line-by-line methods; and (3) studying channel selection for future geostationary **satellite sensors**. This work focuses mainly on the infrared portion of the spectrum between 3.5 and 17 μm, with some specification in the 50–60-GHz oxygen-absorption band in the microwave region. These simulations allow for a better understanding of the atmospheric constituents affecting measurements currently being made from space and for the specification of new channels for **satellite sensors** planned for future NASA missions.

Fast and accurate methods have been utilized which relate atmospheric transmittance to atmospheric constituents using empirical functions of constituent concentration, pressure, and temperature. These methods have been applied with numerical model data as input to produce simulated radiance imagery for current geostationary and polar orbiting **satellite sensors**. The simulated imagery is used to study numerical model performance and identify the cause of specific features detected in observed satellite data. Simulations based on profiles of atmospheric temperature, moisture, and ozone from in situ balloon measurements are used to develop and verify infrared retrieval techniques for atmospheric moisture and ozone. These trace gases, while their concentrations may be small, play an important role in the physical climate and hydrological cycles of the Earth system.

A recent version of the **Fast Atmospheric Signature Code (FASCOD)** has been installed on the MSFC Earth Science and Applications Division and **Engineering Analysis and Data System** computers. This code is used to verify the faster empirical code for accuracy in its transmittance calculations, to study absorption bands not currently represented in empirical radiative transfer models, and to simulate future satellite channels with narrow bandwidths.

G.J. Jedlovec/ES43
(205) 544–5695
Sponsor: Office of Space Science and Applications

Investigations of Atmospheric Moisture Variability

Research continues in the development of algorithms to retrieve atmospheric **moisture** variability from aircraft and satellite remote sensing instruments. The **Split Window Variance Ratio (SWVR)** technique, originally developed with aircraft **Multispectral Atmospheric Mapping Sensor (MAMS)** measurements, has been applied to **Advanced Very High Resolution Radiometer (AVHRR)** data on the current series of polar orbiting meteorological satellites to further study the role of low-level atmospheric **moisture** in the hydrologic cycle. The application has been successful, particularly in regions of large amounts of **moisture**. The split window channels on **AVHRR** are positioned in a spectral region of the atmospheric window where **moisture** absorption is at a minimum, thereby providing little or no signature for low values of total column precipitable water. For values of precipitable water greater than 20 mm (0.8 in), the **SWVR**-derived **moisture** values provide detailed information on the spatial variability of **moisture** in the atmosphere. While the spatial resolution of the thermal channels of **AVHRR** is not as fine as **MAMS**, the greater availability of the operational **AVHRR** data allows for many other investigations of atmospheric **moisture**, in order to study its sources and sinks and its role in cloud development over large regional study areas.

While the availability of **AVHRR** data is limited by the polar-orbiting satellite coverage (typically, a given region is covered twice a day), split window channel radiance measurements are available with the **Visible-Infrared Spin Scan Radiometer (VISSR) Atmospheric Sounder (VAS)** from geostationary orbit at 8-km (5-mi) resolution. Even though this resolution is much coarser than the 1-km (0.6-mi) **AVHRR** and 0.1-km (0.06-mi) **MAMS** data, the **VAS** provides hourly measurements useful for atmospheric **moisture** studies. While the course resolution does not lend itself to the application of the **SWVR** technique, a physically based retrieval technique is being developed for **VAS** applications.

Unlike other techniques to retrieve precipitable water with **VAS** (which require many channels and significant a priori information), this physical technique uses only the split window measurements with a minimum of supplementary information. Mesoscale **moisture** variability can be monitored over a large region at 50-km (31-mi) resolution as a function of time to monitor diurnal fluctuations in low-level precipitable water. This technique performs well and is much simpler in application than other techniques, thus making it more applicable to current problems. Unlike the **SWVR**, the physical technique can be applied over both land and water so studies of global **moisture** variability can be made.

Jedlovec, G.J., "Precipitable Water Estimation From High-Resolution Split Window Radiance Measurements," *J. Applied Meteorology*, to appear in August 1990 edition.

Jedlovec, G.J., "Retrieval of Precipitable Water from AVHRR Imagery," *Preprints Fifth Conference on Satellite Meteorology and Oceanography*, London, England, September 1990 (in press).

G.J. Jedlovec/ES43
(205) 544–5695
Sponsor: Office of Space Science and Applications

Imaging of the Atomization Process

In liquid rocket engines, propellant **atomization** is the first step in the process to prepare the fluids for the chemical reaction. The breakup of the liquid jets into **droplets** is currently initiated with coaxial and impinging injection elements where either a high-speed gas flow strips **droplets** from a liquid core or two liquid jets impinge to mechanically disintegrate each other. There exists a variety of element design patterns for either type such as straight coaxial or hollow cone flow, with and without swirl, and showerhead, doublet, triplet, etc., with like and unlike propellant impingement schemes. Unfortunately, little is known about the **atomization** mechanism, and steps are being taken to obtain visual information of the breakup process which will form a basis to tackle the analytical simulation of the complex process. Test information as to the liquid surface behavior, the location of **droplet** ejection, rate of **droplet** formation, and **droplet** size with respect to different flow-speed conditions will also serve in the verification process of the developed new simulation techniques.

During a Small Business Innovation Research (SBIR) contract, NAS8-38043, with MetroLaser at Irvine, California, holography was used to record a three-dimensional image of the spray regime with nanoseconds exposure time. Figure 66a shows the very detailed flow structure after a two-dimensional water jet leaves the injection element port and interacts with coflowing air. An enlargement (fig. 66b) exhibits the presence of a cellular arrangement which grows downstream and forms bubbles (fig. 66c) prior to the sheet disintegration. At present, no explanation can be given as to the origin and the appearance of the **cellular structure**, however, its detection will promote future investigation.

ORIGINAL PAGE
BLACK AND WHITE PHOTOGRAPH

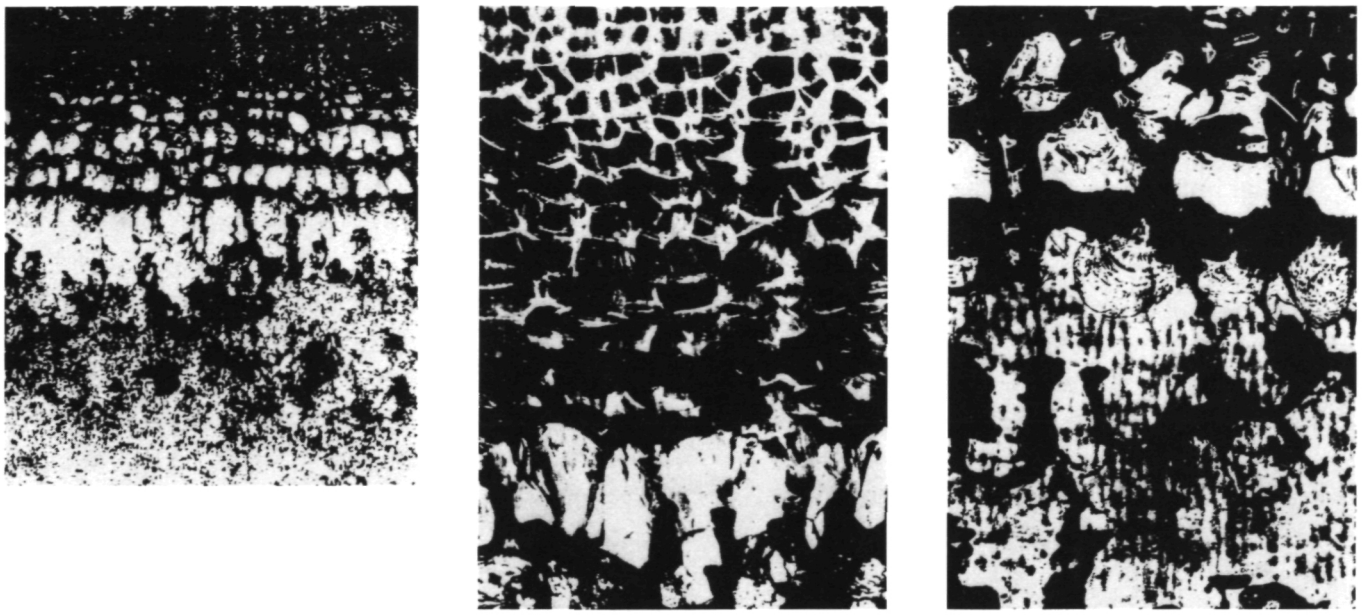

Figure 66. (a) Photographs of Holograms of Shearing Liquid Water Sheet With Co-Flowing Air Along Each Face (Exit Liquid Velocity is 6 m/s; Exit Air Velocity is 46 m/s). (b) Detail of Cellular Structure of Sheet as it Emerges From the Nozzle (Exit Water Velocity is 4 m/s; Exit Air Velocity is 25 m/s). (c) Detail of Liquid Bubbles Just Prior to the Breakup of the Sheet (Exit Water Velocity is 4 m/s; Exit Air Velocity is 25 m/s).

Another ongoing effort under grant NAG8-126 with the Carnegie Mellon University in Pittsburgh, Pennsylvania, also investigates the breakup of liquid jets of coaxial and impinging elements. Here, high-speed, high-magnification, high-contrast photography, shadowgraph, schlieren, interferogram, and measurements of the spray, as well as Malvern laser diffraction and aerometrics phase doppler particle analyzer are employed. Some of the most important measurements will provide information related to waves and disturbances at the liquid/gas interface, shear and turbulence on either side, jet intact length, drop size/velocity correlations, and number density values. In figure 67, liquid sheet issues from a two-dimensional slit and exhibits a pattern of surface waves which disappear when the jet contracts to a thicker three-dimensional shape downstream as a consequence of surface tension. At the moment, the surface waves are assumed to result from an instability in the flow field. Whether a perturbation is carried within the liquid from upstream, produced by minute material roughness effects at the discharge opening, or caused by flow recirculation is currently unknown and needs further investigation.

After testing with water jets, a repetition of many conditions with flow simulants and cryogenic propellants will be attempted.

K.W. Gross/EP55
(205) 544–2262
Sponsor: Office of Aeronautics and Space Technology

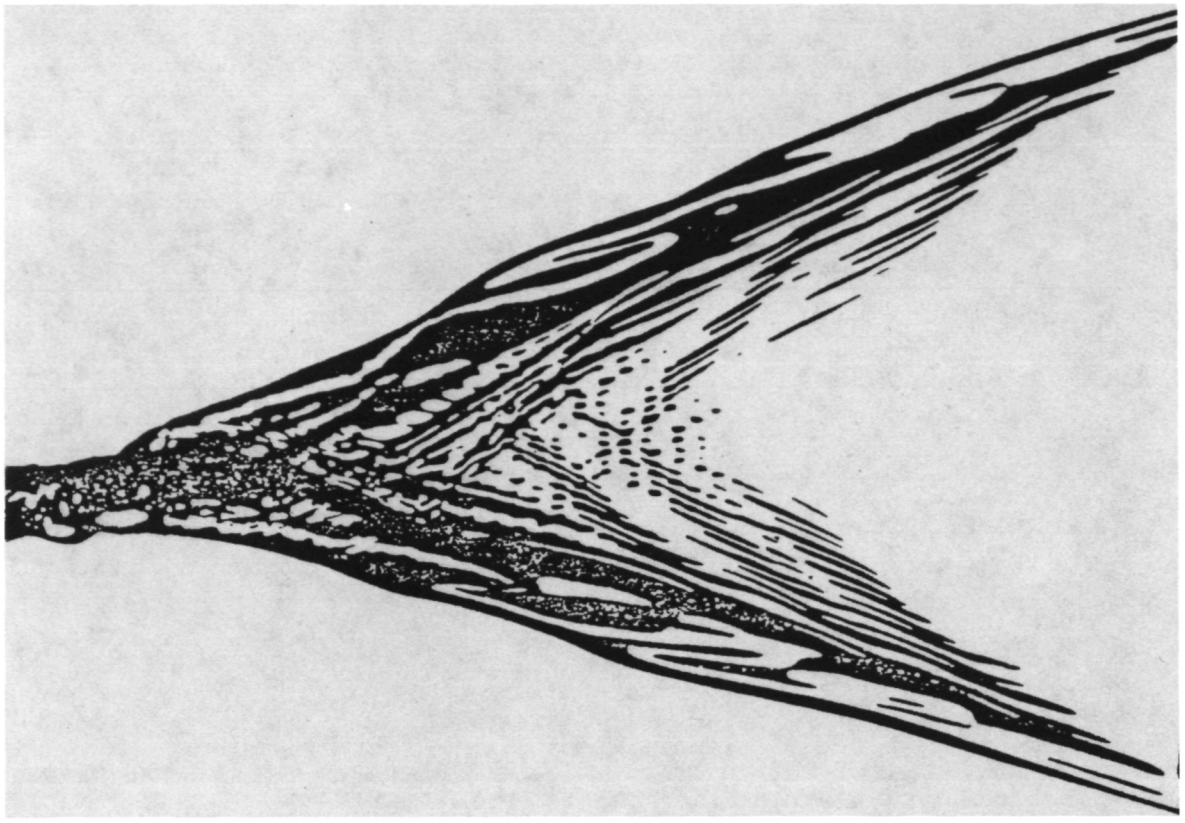

Figure 67. Characteristic Development of a Liquid Sheet

Page intentionally left blank

Technology Programs

Thirty years ago, we were already in the midst of progressive programs which were rapidly developing technologies that would soon carry us to the Moon, and beyond. We could sense the excitement being generated in the process of stretching the limits of technology—in a real sense, the very limits of what man could then achieve. We also correctly sensed then, in spite of the glamour of the successes achieved and anticipated, that technology breakthroughs and engineering accomplishments would not plateau; that the continued pushing of the limits of men and technology would yield the wonders of tomorrow.

We at the Marshall Space Flight Center are resolved to continue to help America remain strong, and to lead the future technology development which will allow our country to remain preeminent in space. This section depicts representative selections describing exciting technology development in the areas of Propulsion, Materials and Processes, Structures and Dynamics, Automated Systems, Space Systems, and Avionics. We believe that, with such technology development work, the boundaries of today and tomorrow will dissolve in the coming months and years, just as they did during the past 30 years.

G.R. Wallace
Director, Research and Technology Office

Propulsion

Computational Fluid Dynamics Flow Analysis of the Bearings, Seals, and Material Tester

The Bearings, Seals, and Material Tester (BSMT) is a test vehicle being used at MSFC to evaluate the performance of conventional rolling contact bearings. Computational fluid dynamics (CFD) analysis of the flowfields inside the BSMT cavities and manifolds has begun with the following objectives:

- To estimate the hydrodynamic loads on the bearings
- To provide inlet and exit **flow** conditions for the calibration and evaluation of bearing models
- To recommend feasible design modifications for BSMT to simulate conditions of advanced turbopumps of various Earth-to-orbit (ETO) transfer vehicles.

The flowfields inside BSMT cavities are very complex due to the presence of both stationary and rotating walls. REFLEQS, an advanced finite-volume Navier-Stokes code,[1, 2, 3] has been selected to perform CFD analysis. As part of task I, the code has been validated for a number of **flows** in **rotating cavities** and stator-rotor systems. Preliminary axisymmetric analyses of cavities No. 1 (drive-side) and No. 2 (load-side) have been accomplished using the standard k-e model and wall functions. Figure 68 shows a sectional view of the

PRECEDING PAGE BLANK NOT FILMED

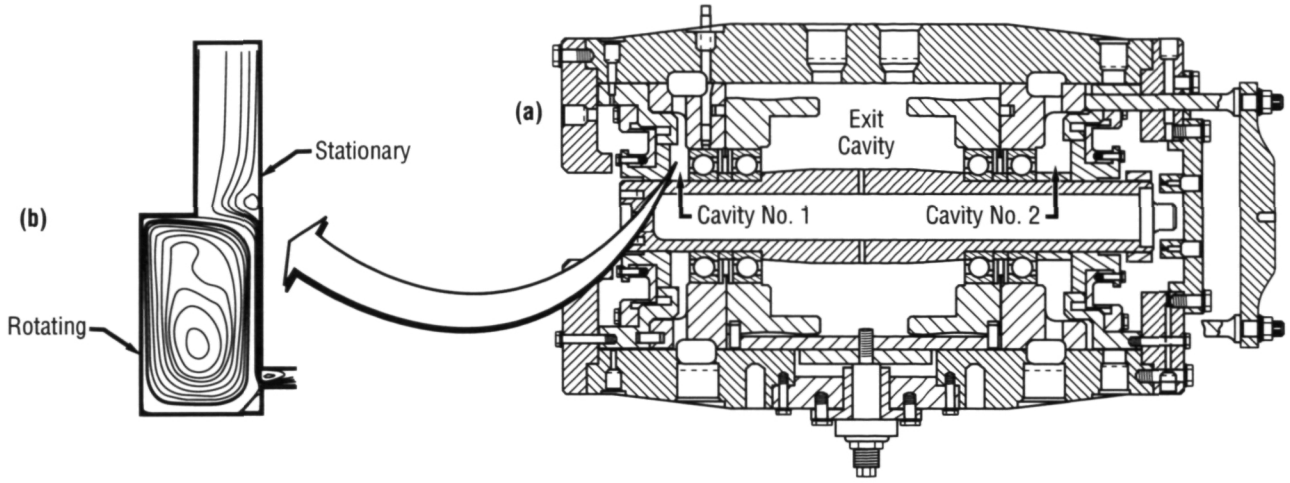

Figure 68. MSFC Bearings, Seals, and Material Tester and Predicted Streamlines in Cavity No. 1

BSMT and the predicted streamlines for cavity No.1. The analysis suggests that the predicted swirl at the BSMT bearing inlets is much higher than expected at the space shuttle main engines high-pressure oxygen turbopump bearing inlets. The predicted axial (parasitic) loads are in the range of earlier estimates obtained with 1-D models.

The future plan includes axisymmetric analysis of the exit cavity followed by 3-D analyses of both the inlet and exit cavities to get a more accurate representation of the flowfields inside BSMT.

[1]Smith, C.E., Ratcliff, M.L., Przekwas, A.J., and Habchi, S.D., "Validation of an Advanced Turbulent Combustion Code: REFLEQS," Presented at the Seventh SSME CFD Workshop, NASA, MSFC, Huntsville, Alabama, 1989.

[2]Avva, R.K., Smith, C.E., and Singhal, A.K., "Comparative Study of High and Low Reynolds Number Versions of k-e Models," AIAA-90-0246, 1990.

[3]Talpallikar, M.V., Yang, H-Q., and Przekwas, A.J., "Numerical Analysis of Turbulent Flow in I.C. Engine Port/Valve Assembly," ASME Paper No. 90-ICE-10, Presented at the Energy-Sources Technology Conference and Exhibition, New Orleans, LA, January 14–18, 1990.

G. Wilhold/ED31
(205) 544–2651
Sponsor: Office of Aeronautics and Space Technology

Computational Fluid Dynamics Methodology for Fast Transients

Successful analysis of the nonlinear, combustion instability problems in liquid rocket engines greatly depends on the accuracy of the numerical method used to solve governing transient transport equations. Comprehensive assessment study of advanced **computational fluid dynamics (CFD)** methods for fast transient, resonant flows was undertaken in a phase I Small Business Innovation Research study in 1989[1]. The objective was to identify the requirements for **CFD** techniques, select advanced numerical schemes, and validate them on benchmark flow problems. Several shock-capturing schemes have been evaluated including flux-corrected transport (FCT), total variation diminishing (TVD), essentially nonoscillatory (ENO), flux-splitting, and Godunov-type schemes. Results of the assessment studies for flows in resonant pipes and resonators for axial radial acoustic modes were presented at the 1990 Computational Fluid Dynamics Working Group Meeting[2].

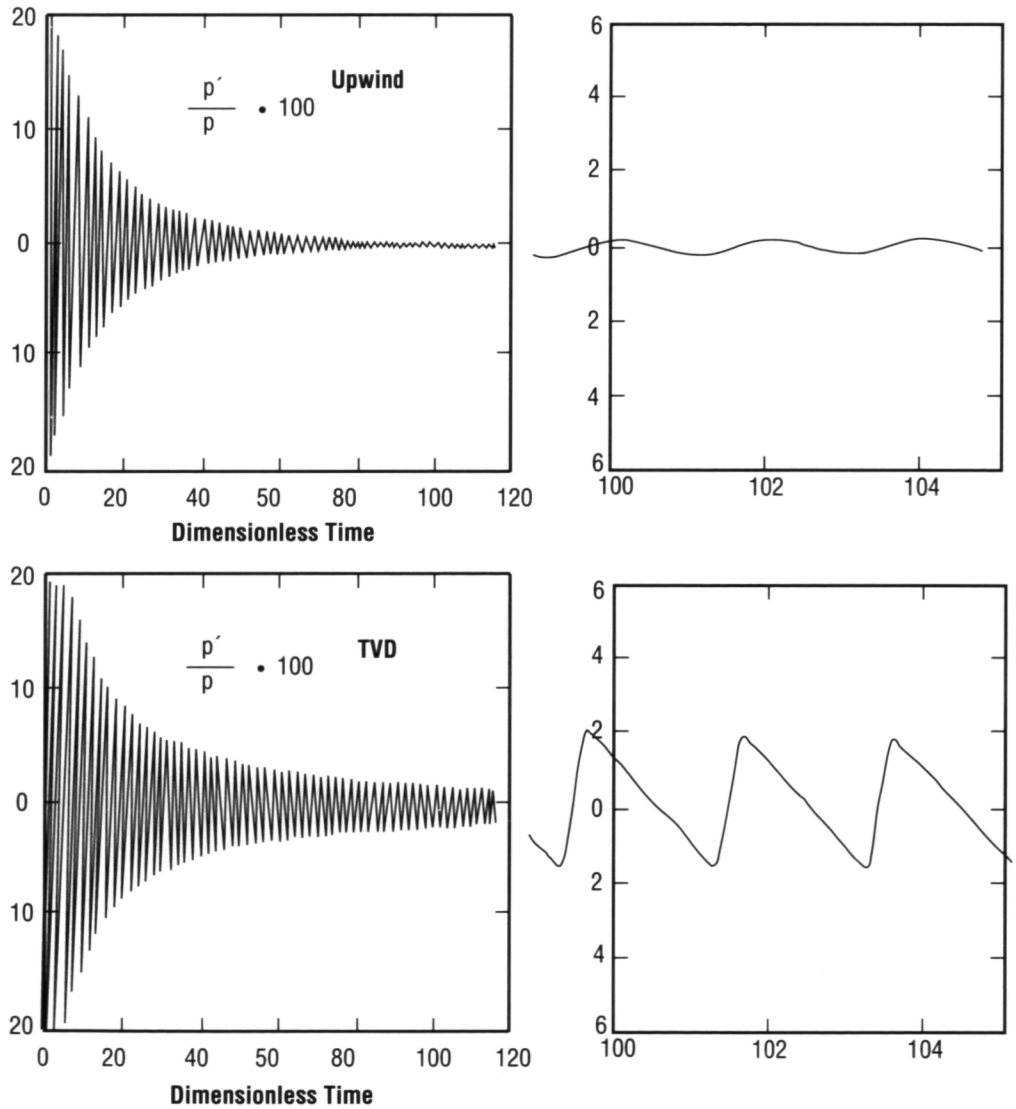

Figure 69. Time Evolution of Normalized Pressure Oscillations at the End of Resonant Pipe for Upwind and TVD-Type Schemes (Note: Lines Intentionally Cross Graph Boundaries)

Figure 69 presents selected results from the assessment study for flow in a closed-end reasonant tube. The results, shown in terms of pressure responses at the tube end, indicate that high-order TVD-type schemes are capable of capturing the wave growth, wall reflection, and transmission problem with greater accuracy than classical upwind schemes. Computational studies of nonlinear acoustic properties of resonant tubes with acoustic cavities indicated that in addition to the viscous energy dissipation, acoustic wave-damping occurs due to the energy frequency shift between natural modes of pipe and cavity. Comparison of acoustic wave patterns between axial and radial instability modes showed that in the first case a classical N-wave develops whereas in the radial modes a spike-type wave is generated. The acoustic damping rate of smooth-base sharp-spike radial mode was much smaller than the damping rates for N-waves. Further work is being performed under the follow-up phase II SBIR study for the development of a multidimensional, fast-**transient analysis** code.

[1]Przekwas, A.J., and Yang, H.Q., "Advanced CFD Methodology for Fast Transients Encountered in Nonlinear Combustion Instability Problems," 26th JANNAF Combustion Meeting, 1989.

[2]Przekwas, A.J., and Yang H.Q., McCannaughey, P., and Tucker, K., "Assessment of Shock Capturing Schemes for Resonant Flows in Nonlinear Instability Analysis," AIAA-90-2358, 1990.

G.A. Wilhold/ED31
(205) 544–2651
Sponsor: Office of Aeronautics and Space Technology

Velocimetry With Refractive Index Matching

The study of internal **flows** involving complex geometries presents a challenge to both analytical Methodology and experimental investigation. Some examples are aircraft engine ducts, heat exchangers, pumps, rocket engine fuel and oxider systems, and multiple injector systems. The **Laser Doppler Velocimeter (LDV)** is the tool of choice for experimentally studying such **flows**, being nonintrusive and insensitive to the fluid properties. However, it requires optical access to the **flow** and use of relatively transparent fluids.

Even if **flow** models were fabricated of transparent acrylic, their surface curvature acts as a lens which repositions the **LDV** laser beams and prohibits beam intersection at the point of interest to form the required measurement volume. If, however, the working fluid and the acrylic model components have the same index of refraction, deflections and defocusing due to refraction at the surfaces vanish, then the **LDV** beams can be positioned anywhere within the model.

A Small Business Innovation Research (SBIR) proposal was accepted to bring this matched-index technology from laboratory research apparatus to widely applicable general purpose engineering test equipment. The program was quite successful and led to a phase II SBIR award for further development and proof of the technology for commercial applications.

The phase II program had four objectives. It was to demonstrate, by measurements, the applicability of the technology to **flows** in:

- A complex model similar to the space shuttle main engine (SSME) injector bowl
- Two-phase **flow**
- A rotating model **flow** typified by a bearing cavity **flow** and a pump impeller or inducer **flow**
- A duct with a backward-facing step with recirculation.

All work has been completed, with the first two items documented in references 1 and 2 showing good agreement with published data. Results of the last two items are in reference 3.

[1]Thompson, B.E., "Flow in a Model of The SSME Main Injector Bowl," SRA Contractor Report R98-900072-T2, June 1989, also presented at the 1st Canadian Symposium on Aerodynamics December 4–5, 1989, Ottawa, Canada.

[2]Lui, C.H., Nouri, J.M., Thompson, B.E., Tse, D.G.N., and Whitelaw, J.H. "Two-Phase Flow Measurements With Refractive-Index-Matching Techniques," SRA Contractor Report R89-900072-T4, June 1989.

[3]Thompson, B.E., Tse, D.G.N., Hogan, M.B., Whitelaw, J.H., Nouri, J.M., and Liu, C.H., "SRA Contractor Final Report R90-900072-F," NASA Contract NAS8-37410, June 1990.

J.P. Heaman/ED35
(205) 544–1604
Sponsor: Small Business Innovation Research

Combustion Chamber Analysis Code

In most liquid-fueled rocket engines, the propellants are injected into the **combustion** chamber in the form of finely atomized **sprays**. The **combustion**, in this case, is critically governed by the dynamics of liquid **spray** and the vaporization process. The **spray** dynamics, in turn, largely depend on the droplet-size distribution and the velocity and temperature of the droplets as a function of time and space. The gas phase and the liquid droplets form a tight feedback loop, and it is crucial to understand this mutual interaction in order to study the performance and stability of **spray combustion** systems.

In this study, the gas-phase equations are being solved in an Eulerian frame of reference using finite volume methods, and Lagrangian particle methods were used to track the liquid droplets. The mass conservation equation for the droplets accounts for the vaporization of fuel into the gaseous phase; the momentum equation accounts for the acceleration or deceleration of the droplets due to the drag imposed by the gas flow; and the energy equation accounts for the heating and subsequent evaporation of the droplets. The Lagrangian calculations give rise to source/sink terms (for mass, momentum, and energy) that need to be included in the gas conservation equations to close the feedback loop. In the gas phase, the **combustion** process is governed by finite rate Arrhenius chemistry.

Figure 70a shows the temperature distribution in the Advanced Launch System (ALS) thrust chamber. Liquid oxygen is injected into the chamber in the form of a spray through the **injectors**, and gaseous hydrogen enters through the slots around the **injectors**. Figure 70b shows the gaseous oxygen distribution in the chamber. These preliminary calculations[1] demonstrate the capability of the scheme in resolving the complex physical interactions between various processes in this problem.

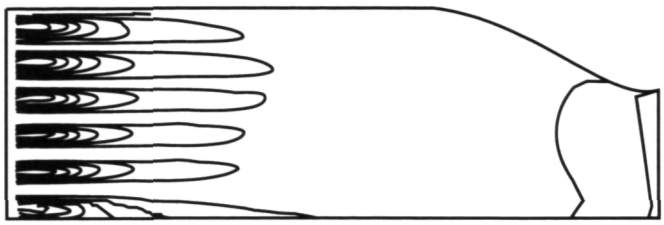

a. Temperature Contours

b. Oxygen Mass Fraction Contours

Figure 70. Temperature Contours and Oxygen Mass Fraction Contours

Future work will be oriented toward implementing advanced physical models for dense **sprays**, atomization phenomena, and **combustion**; and systematically validating the code. The base code, REFLEQS[2,3], has already been validated for a large number of nonreacting flows.

[1]Krishnan, A., and Przekwas, A.J., "Analysis of Spray Combustion in Multi-Injector Liquid Rocket Engine Thrust Chambers," Eighth SSME CFD Workshop, NASA MSFC, April 1990.

[2]Avva, R.K., Smith, C.E., and Singhal, A.K., "Comparative Study of High and Low Reynolds Number Versions of K- Models," AIAA-90-0246, 1990.

[3]Talpallikar, M.V., Yang, H.Q., and Przekwas, A.J., "Numerical Analysis of Turbulent Flow in I.C. Engine Port/Valve Assembly," ASME Meeting, New Orleans, LA, January 14–18, 1990.

G.A. Wilhold/ED31
(205) 544–2651
Sponsor: Office of Aeronautics and Space Technology

Cold Flow Aerodynamic Turbine Testing

In an effort to improve existing liquid rocket engine turbopump **turbine performance**/environment predictions and validate **turbine** computational fluid dynamic (CFD) codes, an in-house experimental cold air flow **turbine** test program was initiated. The MSFC Turbine Test Equipment (fig. 71) is a blowdown tunnel which operates by expanding high pressure air from 2.76-mPa (400-psig) storage to atmospheric conditions. Power absorption is provided by a 447-kW (600-hp) drive train consisting of a torquemeter, gear box, and dynamometer. The facility allows the testing of full-scale **turbines** at scaled shaft speeds, mass flows, pressures, and temperatures. The ability to test full-scale turbopump **turbines** and accurately control the pressure, temperature, shaft speed, and pressure ratio make the facility unique among government and industry facilities.

Testing of the space shuttle main engine (SSME) high-pressure fuel turbopump (HPFTP) **turbine** is currently underway. The HPFTP **turbine** test article (fig. 72) is a highly instrumented model utilizing actual HPFTP first- and second-stage stators and rotors. Detailed pressure, temperature, and flow angle measurements allow accurate **performance** and environment determinations to be made. With as many as 400 pressure and 100 temperature measurements, a comprehensive data base for CFD code validation will be generated.

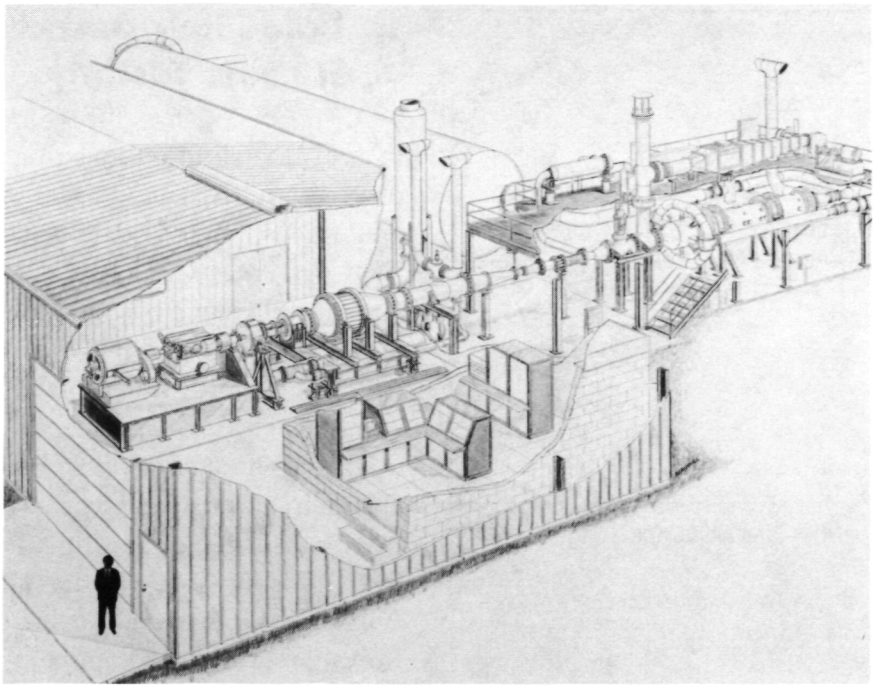

Figure 71. MSFC Air Flow Turbine Test Equipment

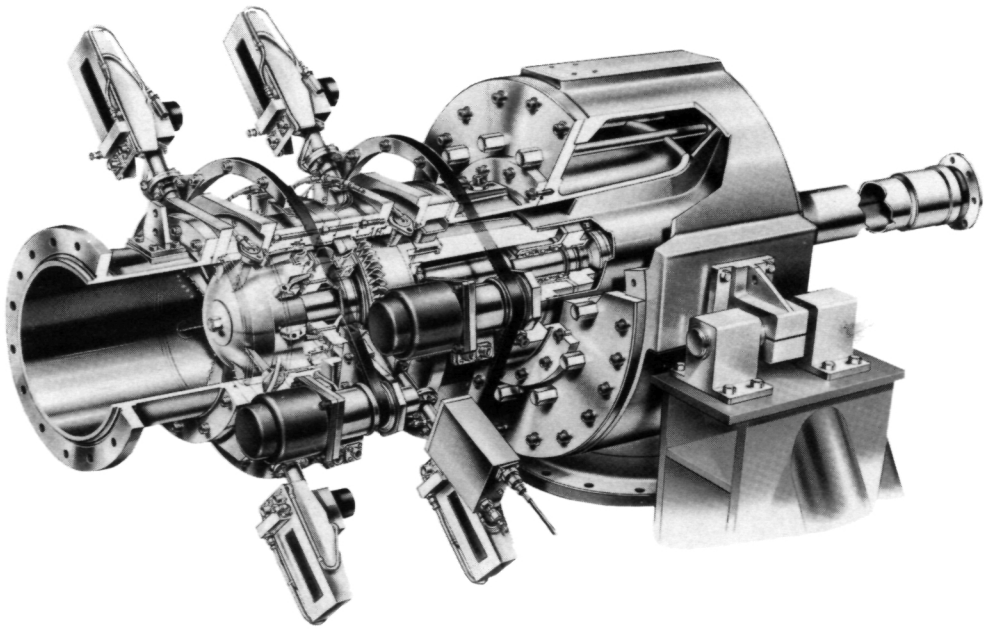

Figure 72. Space Shuttle Main Engine High-Pressure Fuel Turbopump Turbine Test Article

Future test plans include testing of different model configurations of the SSME baseline HPFTP **turbine**, the SSME alternate turbopump development (ATD) HPFTP **turbine**, and a generic technology **turbine**. Testing of the baseline HPFTP **turbine** will provide detailed **turbine** flow loss breakdown measurements by testing in a series of buildups from a single stator to the complete two-stage **turbine**. Additional configurations will be tested to investigate tip clearance, disk coolant flow, and blade-roughness effects.

W.J. Bordelon, Jr./ED33
(205) 544–1579
Sponsor: Space Shuttle Main Engine Project Office and
Office of Aeronautics and Space Technology

Adaptive High Order *h-p* Finite Element Method for Complex 3-D Flows

The complex nature of flows in liquid rocket engines such as the space shuttle main engine (SSME) demands a thorough understanding of their flow paths for safe and reliable hardware designs. Experience with the current SSME has shown that the internal hot gas flow path in a staged-rocket has a significant influence on overall engine performance, operability, and durability. Consequently, methods for identifying potential flow-path problems are vital to the success of the SMME.

In an effort to provide a highly accurate, computationally efficient design tool, research has begun on the development of new two- and three-dimensional incompressible finite element computational fluid dynamics codes for complex geometries. The codes employ a fully automated adaptive procedure using *h*- and/or *p*-mesh refinements. Solution refinements by *h*- and *p*-methods utilize a posteriori estimates of local errors from solutions obtained on an initially coarse, low-order solution. Additionally, the adaptive algorithm developed will attempt to automatically determine which combination of these adaptive steps will provide the most accurate and economical results.

In terms of the flow physics, the flow environment in the SSME fuel and oxidizer turbopumps is turbulent (Reynolds number > 1×10^6). Additionally, for flow domains with curved boundaries, as in the SSME turnaround ducts (TAD), regions of counter-rotating vortices are present. Consequently, the FEM code must be capable of accurately predicting flow separation, subsequent shear reattachment, and redevelopment of the wall boundary layers.

To reduce the total number of degrees of freedom associated with a computational mesh and provide increased accuracy in the final solution, higher order **spectral elements** are employed. This is demonstrated in figure 73, where preliminary calculations of flow in an SSME fuel TAD-like geometry (see Sandborn, et al.)[1] are presented. A recirculation region occuring at the exit of the bend is clearly apparent even though only 216 (6×36) quadratic elements were used.

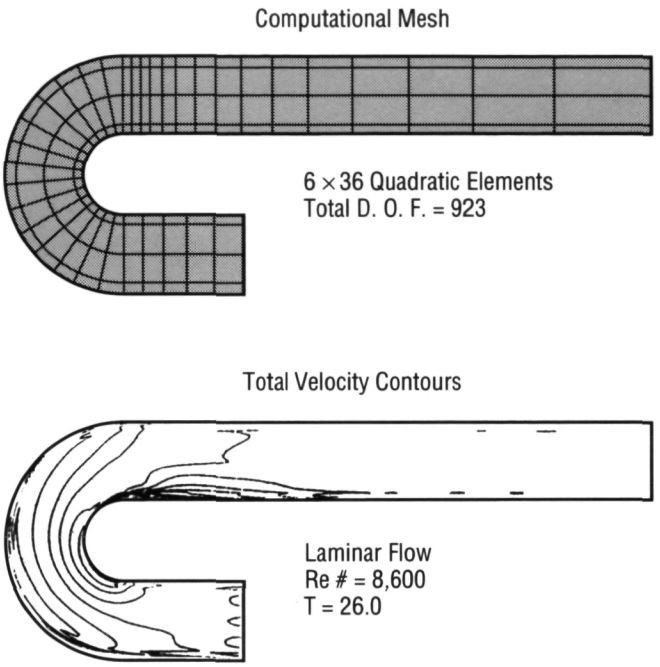

Figure 73. Computational Mesh and Preliminary Velocity Contours for Sandborn Planar TAD Experiment

In another case, unsteady flow around a cylinder with Reynolds number 1,000 was calculated using the ***h-p* adaptive** code. In this calculation, the total number of degrees of freedom was 1,531, with a uniform spectral order of 3. As observed in figure 74, vortex-shedding behind the cylinder is predicted extremely well. Comparable results using a conventional finite difference mesh or even a **finite element code** with linear elements would require significantly more elements. For example, **incompressible flow** over a backward-facing step was predicted by Ghia, et al.,[2] using approximately 12,000 degrees of freedom, while comparable results were obtained using the *h-p*-FEM code with only 60 cubic (p = 3) elements or 1,400 degrees of freedom. The predicted reattachment lengths for both calculations are nearly identical.

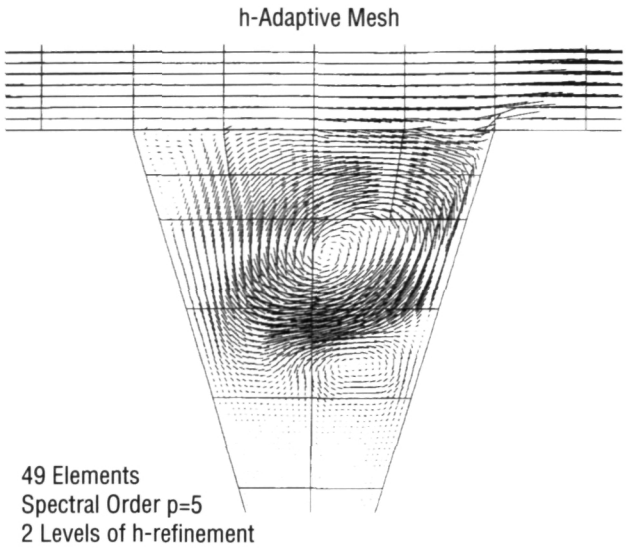

Figure 74. Velocity Vectors for a Flow-Driven Cavity Problem, Re #=1,000, Total D.O.F. = 1,852, Uniform p=5

Illustrated in figure 74 are preliminary results of a flow-driven cavity problem. High-order **spectral elements** of p = 5 were used in the entire flow domain giving approximately 1,852 total degrees of freedom. Multiple recirculation regions occuring in the cavity region are being captured with only 12 elements utilized. Similar results were obtained by Ghia, et al.,[3] using 16,000 grid points. It is believed that for even higher Reynolds number problems and complex flows, the use of adaptive high order *h-p* schemes will produce results that are unobtainable by other low-order methods.

[1]Sandborn, V.A., and Shin J.C., "Evaluation of Turbulent Flow in A 180° Bend for Bulk Reynolds Numbers From 70,000 to 160,000," NASA CR NAS8-36354, June 1987.

[2]Ghia, K.N., Osswald, G.A., and Ghia, U., "Analysis of Incompressible Massively Separated Viscous Flows Using Unsteady Navier-Stokes Equations," *Internal Journal for Numerical Methods in Fluids*, 1981.

[3]Ghia, U., Ghia, K.N., and Shin, C.T., "High-Re Solutions for Incompressible Flow Using the Navier-Stokes Equations and Multigrid Method," *Journal Computational Physics*, Vol. 48, pp. 387–411, 1982.

P. McConnaughey/ED32
(205) 544–1599
Sponsor: SBIR Phase II Effort

Verification of Internal Flow Analysis in 3-D Geometries

Analysis of **internal flow** in advanced rocket propulsion systems is complicated by hardware geometry, high Reynolds numbers, rotation, high-frequency phenomena, and near incompressibility. Typical of such problems is the space shuttle main engine (SSME) hot-gas manifold (HGM).

Previous analysis of flow in the SSME HGM has been compared to air-flow data and found to be inaccurate with respect to system losses, outer-wall static pressures, and transfer-duct environments. Such discrepancies could arise from flow measurement methodology, low-order algorithms, turbulence modeling, and/or poor grid resolution.

The objective of this work is to compare **internal flow** computational analyses to laser Doppler velocimeter (LDV) flow measurements for the HGM pilot model configuration. A single continuous grid with about 2×10^6 nodes is being generated using EAGLE grid-generation code. Part of the grid near the transfer duct is shown in figure 75. Upon completion of grid generation, the GMINT computer code, which solves the ensemble-averaged Navier-Stokes equations using a linearized-block implicit-solution algorithm, will be used to predict the benchmark HGM experimental data obtained in the MSFC water flow facility.

G.A. Wilhold/ED31
(205) 544–2651
Sponsor: Office of Aeronautics and Space Technology

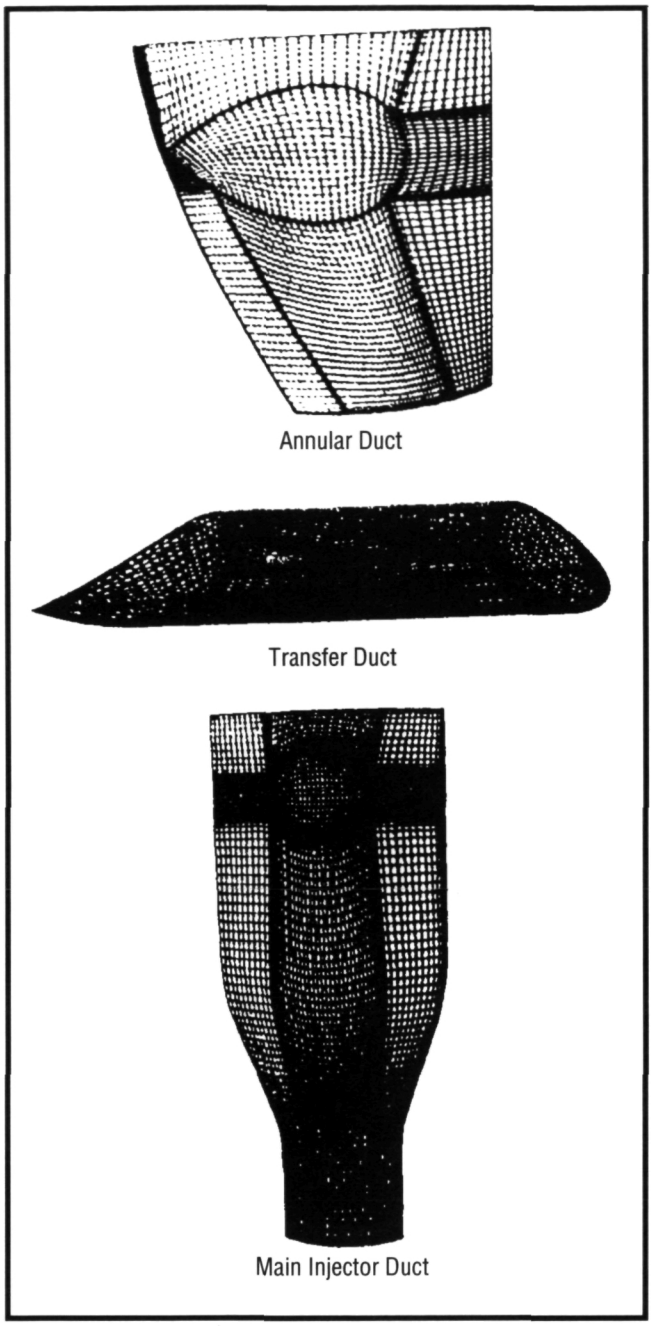

Figure 75. Grid Near the Transfer Duct

Development of Unsteady Aero/Heat Transfer Experimental Data Base for Axial Turbines

Radial and circumferential gradients in temperature, at the inlet to the **turbine** used in the rocket propulsion systems, cause **unsteady** flows in rotors. The hotter gases tend to migrate toward the pressure side of the rotor whereas the colder gases migrate towards the suction sides. These preferential migrations of gases in the rotor passages cause both performance deficits and durability problems. The **computational fluid dynamics (CFD)** codes used in the current **turbine** design procedures do not account for these real flow effects resulting in less than optimum designs. New **CFD** codes[1] have, however, recently

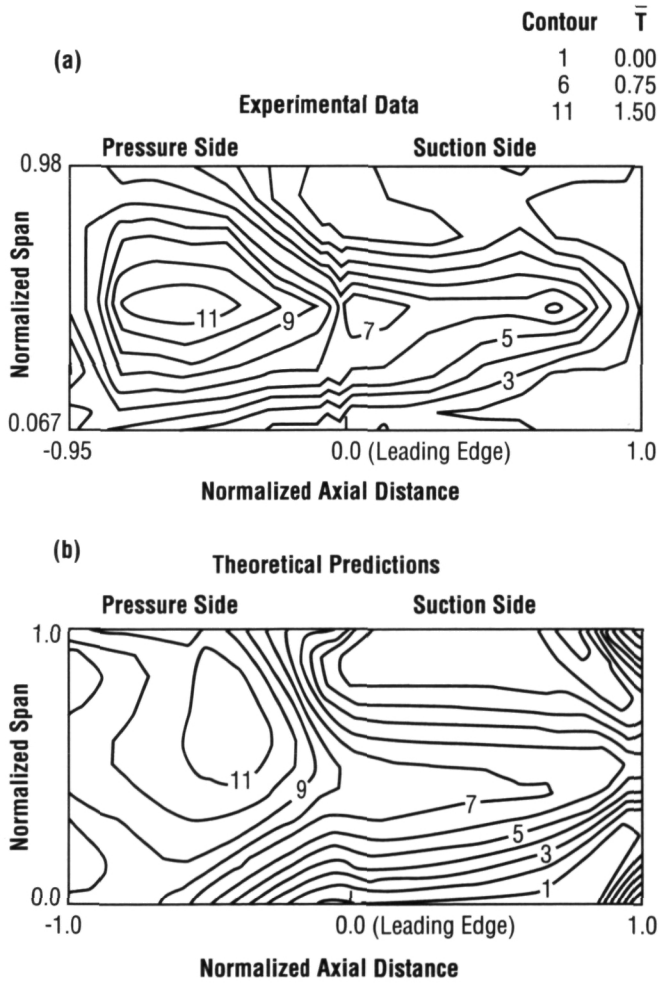

Figure 76. Theoretical Predictions Conducted by an Unsteady 3-D Euler Code Yields Good Estimates of Time-Averaged Temperature Patterns on Rotor Airfoil Surfaces

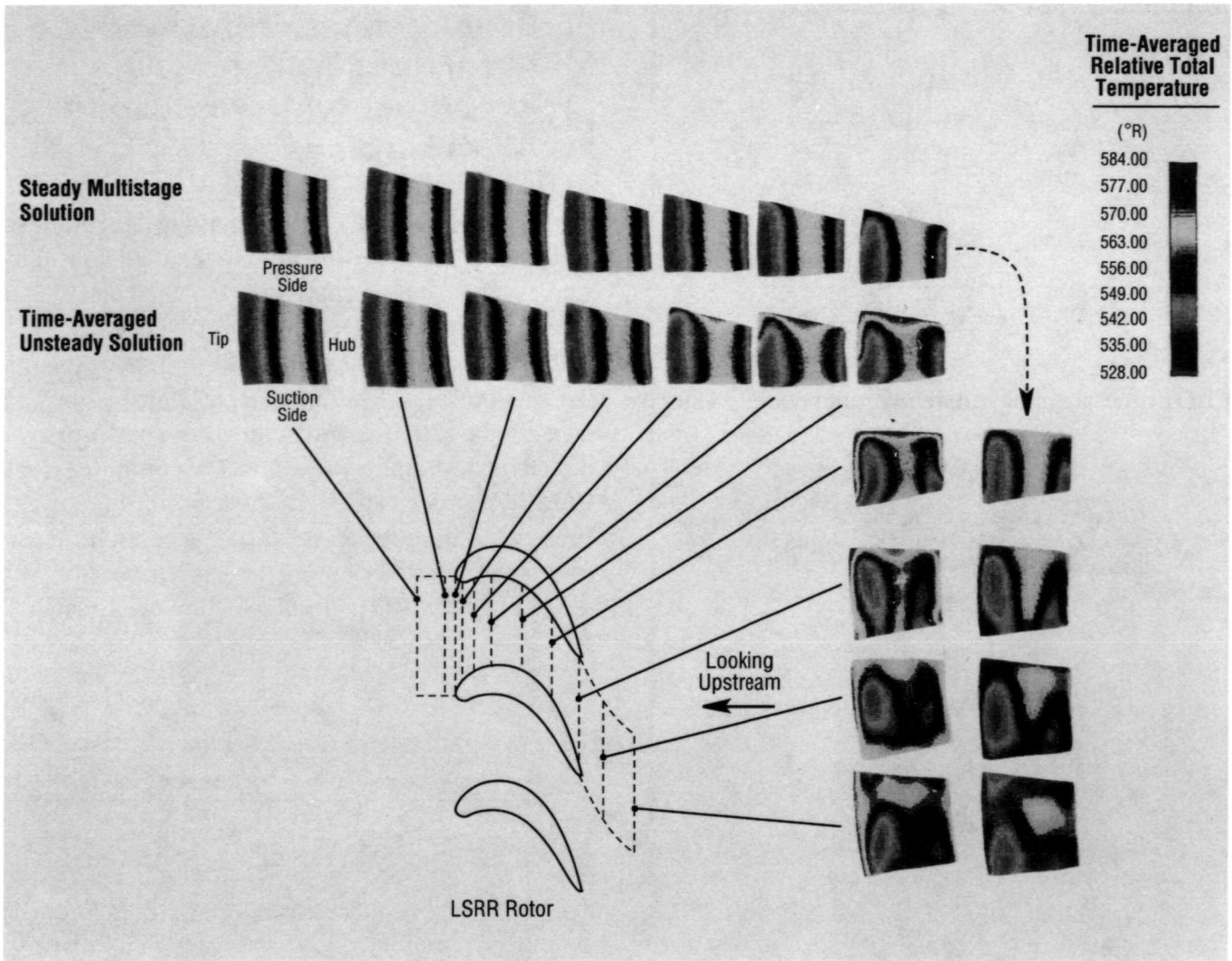

Figure 77. Current Prediction Method, Used in the Turbine Design Process (Steady Multi-Stage Euler Code), Predicts Lower Temperatures Than Those Predicted by Utilizing an Unsteady 3-D Multistage Euler Code. Predicted Time-Averaged Temperature Patterns by the Unsteady Code Show Similarity With the Data

recently emerged that show the potential to predict these real flow effects. The primary objective of this program is to provide a **data base** that will permit validation of these new **CFD** Codes.

Time-averaged temperature data were previously acquired[2] at the United Technologies Research Center in a one and one-half stage, low-speed, large-scale rotating rig (LSRR) **turbine**. Numerical simulations were also conducted for this experimental configuration by using a three-dimensional (3-D), time-accurate, **unsteady** Euler code.[1] Results from this numerical simulation show good agreement with the experimental data on the two sides of the rotor airfoil, as indicated in figures 76a and b. Additional results from this simulation are compared to those obtained from a steady **CFD** code that is used in the current **turbine** design system (fig. 77). These results, given as contour plots at various axial locations in the rotor passage, clearly show that for the same inlet temperature profile, time-averaged temperatures from the **unsteady** code yield much higher temperatures on the airfoil pressure side and the two endwalls. Experimental data between the airfoils, however, is unavailable to verify these predictions.

The purpose of this program is to provide temperature distributions in the flow field at two exit planes for the rotor. These experimental data will provide validation of the **unsteady CFD** code and will encourage **turbine** designers to apply these new codes to optimize future **turbines**. Hardware and instrumentation to acquire this data have been fabricated and the experimental program is expected to be completed by fall 1990.

[1]Sharma, O.P., Pickett, G.F., and Ni, R., "Assessment of Unsteady Flows in Turbines," ASME Paper #90-GT-150, 1990.

[2]Ni, R., and Takahashi, R., "Hot-Streak Migration in a Turbine - An Unsteady Flow Simulation", NASA MSFC **CFD** Workshop, April 1989.

G.A. Wilhold/ED31
(205) 544–2651
Sponsor: Office of Aeronautics and Space Technology

Three-Dimensional Turbopump Flowfield Analysis

The overall objective of this program is to develop, implement, and verify a **computational fluid dynamics (CFD)** code which will predict the transient, three-dimensional, viscous flow in the space shuttle main engine (SSME) turbopump. An unsteady, three-dimensional, thin-layer, Reynolds-averaged Navier-Stokes code, developed at NASA/Ames by M.M. Rai (1987) to simulate unsteady flow in a **turbine** stage, is being used as the core code for this application. The unsteady flow prediction capabilities of this code have been demonstrated by Rai through comparisons against the unsteady and the time-averaged loadings on airfoil surfaces in a **turbine** stage. Heat load, loss, and **secondary flow**-prediction capabilities of this code are being verified and enhanced as a part of this program. A steady cascade version of this code (RAI3DC) has been developed to permit this verification effort to be done in a cost-effective manner.

The **secondary flow**-prediction capabilities of this code are demonstrated in figure 78. This figure shows a comparison of experimental and theoretical total pressure-loss contours downstream of Langston's cascade (1977). Experimental data in this figure were obtained for both a thin and a nominal boundary layer at the cascade inlet. The code is shown to predict qualitative features of the flow field accurately in both cases, including the location of the **secondary flow** vortices. Predicted midspan loss levels, however, are higher than the measured data, as indicated in the figure where predicted midspan wakes are wider than the measured data. Application of an improved turbulence model, being developed as a part of this program, is expected to yield improved predictions of losses.

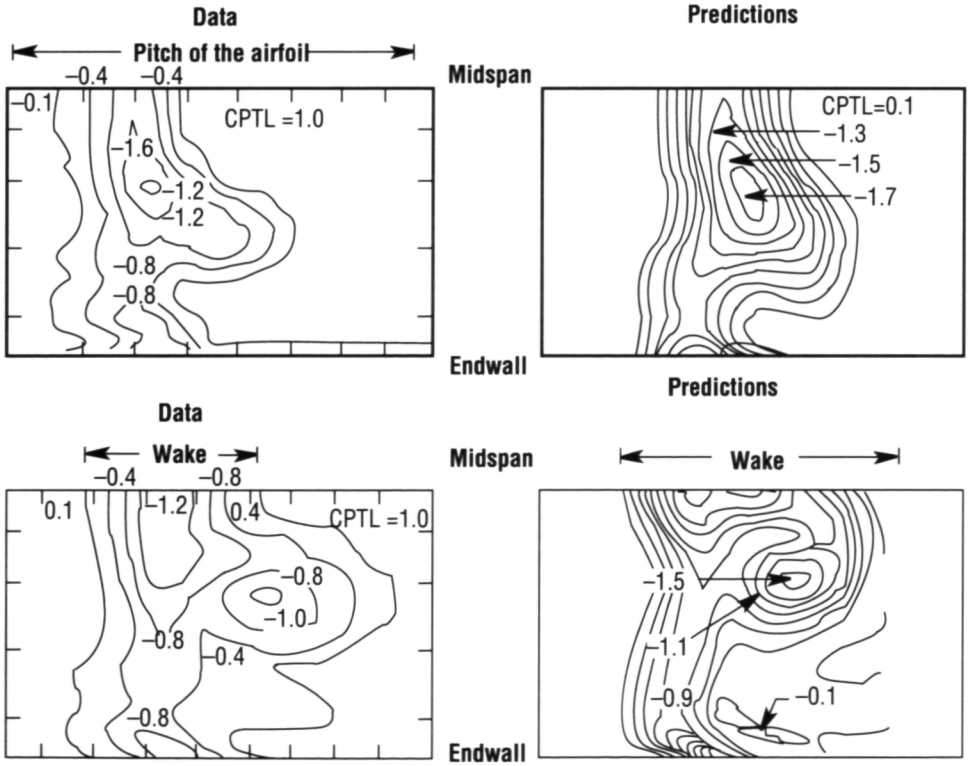

Figure 78. Steady Cascade Version of the RAI Code (RAI3DC) is Shown to Yield Good Predicitons for Total Pressure Loss Contours Downstream of the Cascade for Two Different Incoming End Wall Boundary Layers. The Width of the Wake at Midspan, However, is Overestimated.

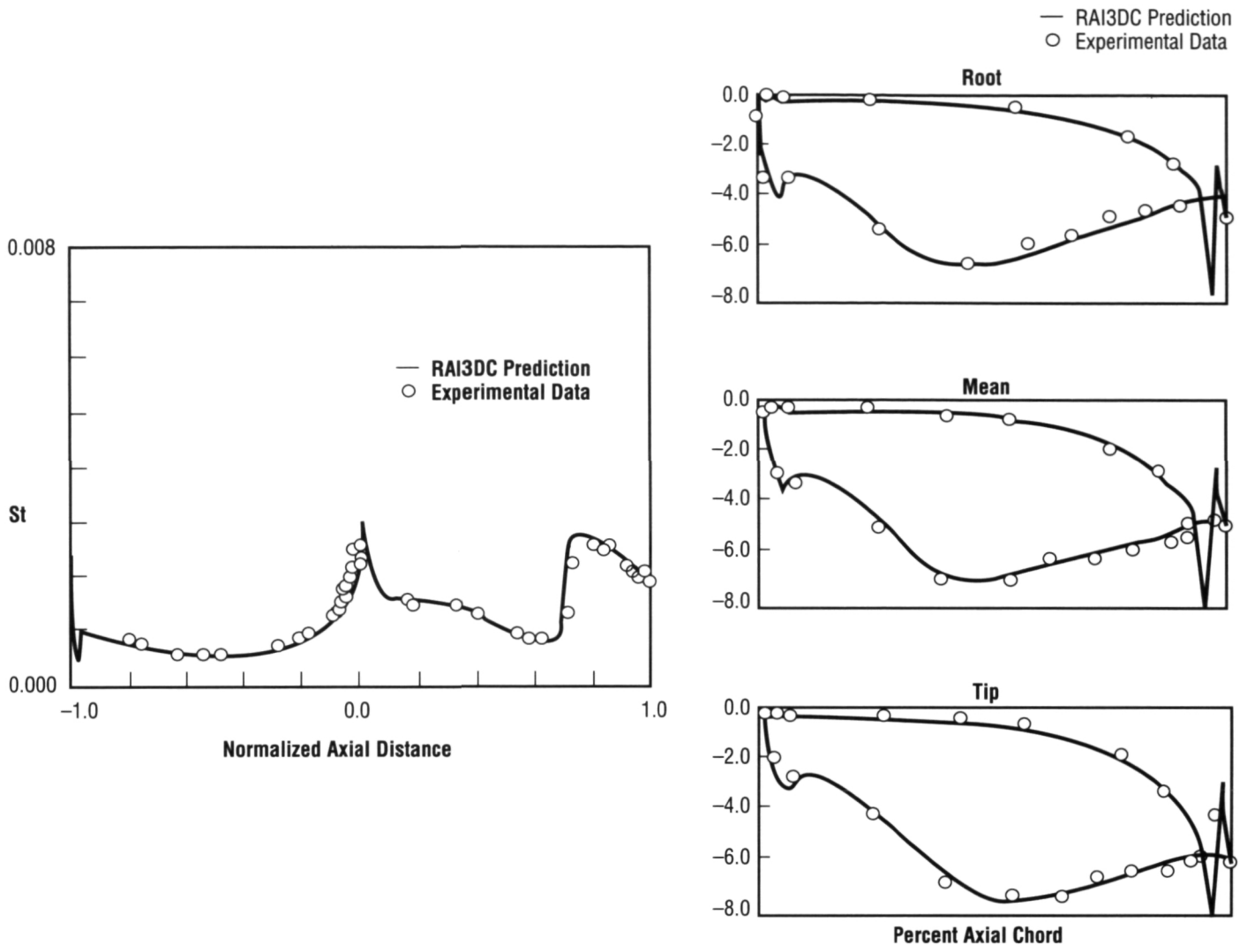

Figure 79. Steady Cascade Version of the RAI Code (RAI3DC) Yields Excellent Predictions of Heat Transfer Co-Efficient (Stanton Number = St) at the Midspan and Static Pressures (cp) at the Midspan, Root, and Tip for the United Technologies Research Center Large-Scale Rotating Rig First Stator.

The capability of RAI3DC to predict heat transfer is demonstrated in figure 79. A comparison is shown between measured and computed Stanton numbers at the midspan of a three-dimensional annular cascade. The calculation was performed with specified transition location and specified surface temperature, and the computational grid was refined to ensure that the Reynolds number (based on distance from the wall, friction velocity, and kinematic viscosity) at the first grid point away from the wall was no greater than one. Agreement between the prediction and the experimental data is excellent. Predicted airfoil loadings for this case at 2–50 percent, and 98-percent span, are shown in figure 79, and also exhibit excellent agreement.

Rai, M.M., "Unsteady Three-Dimensional Simulations of Turbine Rotor Interaction," AIAA Paper #2058, 1987.

Langston, L.S., Nice, M.L., and Hooper, R.M., "Three-Dimensional Flow Within a Turbine Cascade Passage," *ASME Journal of Engineering for Power*, January 1977, pp. 21–28.

Griffin, L.W., and Belford, K.A., "Prediction of the Aerodynamic and Thermal Environment in Turbines," ASME Paper #90-GT-227, 1990.

G.A. Wilhold/ED31
(205) 544–2651
Sponsor: Office of Aeronautics and Space Technology

Turbine Stage Computational Fluid Dynamics Analysis and Data Base for Unsteady Aero/Heat Transfer

Flows in low aspect **turbines**, such as the space shuttle main engine (SSME) fuel **turbine**, are three-dimensional and highly **unsteady** due to the relative motion of adjacent airfoil rows and the circumferential and spanwise gradients in total pressure and temperature. The systems to design these **turbines** are, however, based on ***computational fluid dynamics (CFD)*** *codes which primarily* solve steady-flow equations. The unsteadiness effects in **turbines** are accounted for through the use of empirical correlations and experience factors which invariably result in less than optimum and durable designs.

CFD codes have recently been developed that explicitly account for the effects of **unsteadiness** through numerical solutions of either the Euler[1] or the Reynolds-averaged Navier-Stokes[2] equations. The resources required to execute and to analyze information from these codes, however, prohibit their near-term use in a routine **turbine** design process. In addition, the predictive capabilities of these codes have yet to be validated through comparisons with a reliable data base. The primary objective of this program is to analyze and document a benchmark-quality data base that can be used to validate the available and emerging **unsteady CFD** codes. These data[3] were obtained in a large-scale low-speed 1–1/2 **turbine** rig at the United Technologies Research Center.

The data, acquired at four axial stations in the **turbines** over a window covering two first-stage stator gaps, include total and static pressure, three components of velocity, and six components of turbulence stress. These data provide a complete description of the flowfield to allow validation of a Reynolds-averaged Navier-Stokes equation code that simulates periodic unsteady flow through a multistage **turbine**. The documentation of these data has been 60-percent completed and will have been delivered to MSFC by August 1990.

Until the execution time of the unsteady **CFD** codes[1,2] is reduced by two to three orders of magnitude, **turbine** designers will have to rely on codes that simulate steady flows through multistage **turbines**. Currently available steady **CFD** codes, however, yield inaccurate estimates of flowfield for airfoil rows embedded in a multistage **turbine**, as indicated in figure 80. This figure shows spanwise distribution of measured and predicted gas-angle distribution downstream of the second stator in the large-scale rotating rig (LSRR). This prediction, conducted by using a state-of-the-art steady **CFD** code, clearly yields inaccurate estimates of spanwise distribution of angles. The inadequacy of currently used steady **CFD** codes in the turbomachinery design was highlighted by scientists at NASA in a publication.[4] This publication showed that additional mathematical terms appear in steady-flow equations of motion when Reynolds-averaged Navier-Stokes equations are ensemble-averaged to account for the relative movement of adjacent airfoil rows.

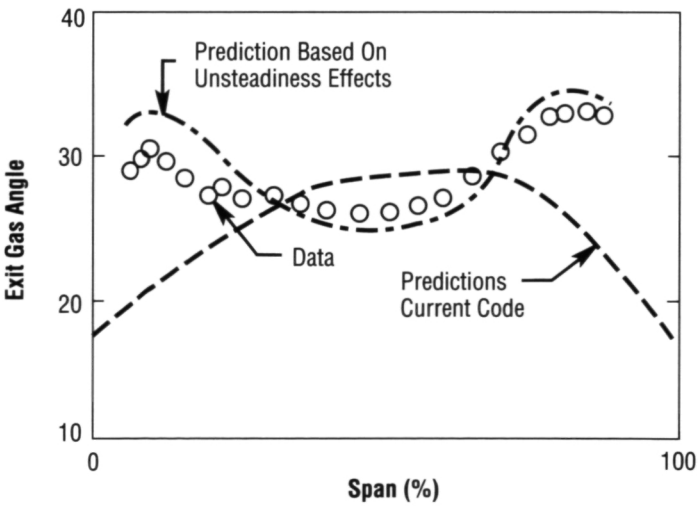

Figure 80. Example of Significant Improvement in Predictions Using New Method Based on Unsteadiness Effects.

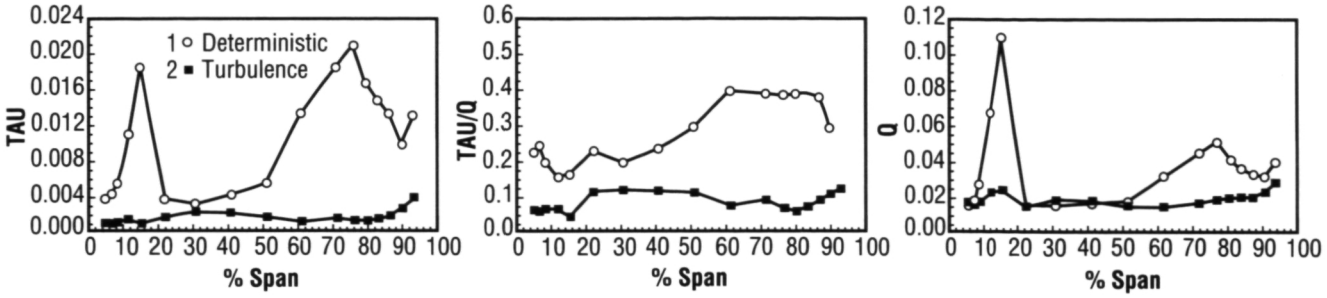

Figure 81. Comparison of Spanwide Distribution of Total Intensities (Q), Stresses (t), and Ratio of Stresses to Intensities at the LSRR Rotor Inlet. Larger Values of all of These Three Quantities Are Shown for the Deterministic Aspect of the Flow Indicating That the Terms Induced Due to Periodic Unsteadiness Are More Important Than Those Due to the Turbulence.

The second objective of the present program is to analyze the above-noted **unsteady** data and to deduce the magnitudes of these additional mathematical terms, called "deterministic stresses." Magnitudes of these deterministic stress terms have been calculated from the data, and spanwise distribution of these terms are compared to the equivalent turbulence terms at inlet to the rotor in figure 81. This figure demonstrates that the magnitudes, spanwise gradients, and intensity of the deterministic stress are larger than for the turbulence. Since considerable effort is spent in accounting for turbulence, there is also a need to account for the deterministic stresses in the **turbine** design procedures.

The third objective of the present program is to develop simple closure models for these deterministic stresses by using the experimental data. This modeling activity is currently underway and is expected to have been completed by fall 1990.

[1]Ni, R., Sharma, O., Takahashi, R., and Bogoin, J., "3D Unsteady Flow Simulation Through a Turbine Stage," Paper Presented at the 1989 Australian Aeronautical Conference - *Research and Technology—The Next Decade*, Melbourne, Australia, October 9–11, 1989.

[2]Rai, M.M., "Unsteady Three-Dimensional Simulations of Turbine Rotor-Stator Interaction," AIAA Paper #87-2058, 1987.

[3]Sharma, O.P., Renaud, E., Butler, T.L., Milsaps, K., Dring, R.P., and Joslyn, H.D., "Rotor-Stator Interaction in Multistage Axial Turbines," AIAA Paper #88-3013, 1988.

[4]Adamczyk, J.J., "Model Equation for Simulating Flows in Multistage Turbomachinery," ASME Paper #85-GT-226, 1985.

G.A. Wilhold/ED31
(205) 544–2651
Sponsor: Office of Aeronautics and Space Technology

Plume Temperature Measurements

Research is being conducted to measure the exit-plane properties of the space shuttle main engine (SSME) and other engine systems for determination of performance code accuracy and to provide data to guide development of future computational fluid dynamics codes. Nonintrusive techniques are being developed which are based on the emission and absorption of infrared (IR), ultraviolet (UV), and visible radiation from species in the plume gases. The species currently under consideration are H_2O, hydroxal radicals (OH), and trace sodium. These measurements are being developed on the MSFC Technology Test Bed (TTB).

The IR emission/absorption technique is to be used to determine the temperature profile and species concentration for H_2O using the available infrared transitions of the H_2O molecule from 2.7 to 3.3 μm. A band model for radiative transport in the plume[1] is utilized to compute the distribution and temperature of emitting molecules in each assumed axially symmetric zone of the plume gases (fig. 82). The solution is obtained from a best fit of the emission/absorption data and from experimentally determined band model parameters for H_2O molecules. Work to date has included initial checkout of the **IR detector system** and IR lamp system on the MSFC TTB. The test control and data acquisition system is currently being fabricated for the final phases of testing.

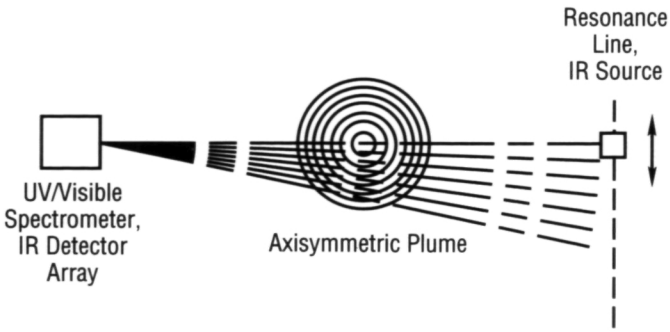

Figure 82. Geometry of the IR Emission/Absorption Experiment for Temperature Measurement

The OH radical resonance-line absorption technique is based on the use of a microwave-pumped discharge tube to produce characteristic OH radical radiation which is transmitted through the plume to determine rotational temperature and species concentration of OH.[2] The OH concentration is of particular interest due to its impact on the kinetics of the rocket engine expansion and combustion process and due to its dependence on oxidizer/fuel ratio. Current work on the OH technique has been limited to theoretical computation of absorption spectra and the development of a model for the line-pressure shift which is critical for its application to the SSME.

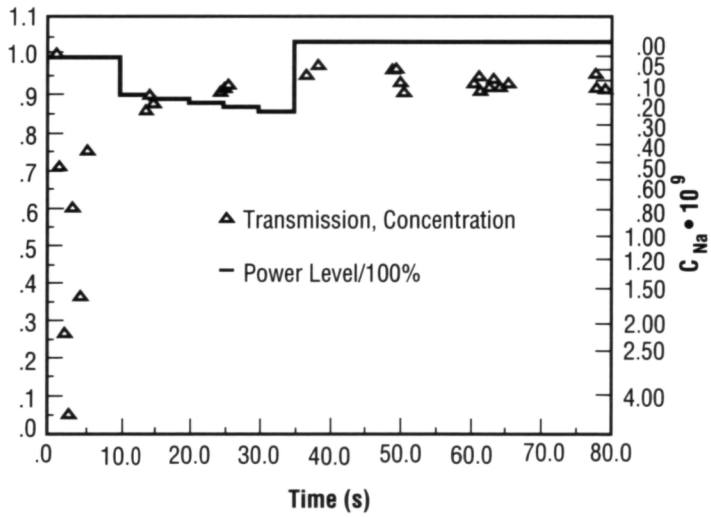

Figure 83. Transmission and Concentration of Na Atoms for TTB19

Additional work has focused on the presence of trace species in the plume gases which include sodium. Sodium is often used as a seed element in combustion studies for determination of temperature. A model for pressure-shifted sodium absorption in the plume has been developed. Sodium absorption measurements have been conducted on tests TTB12-TTB19.[3] These measurements were made possible by the construction of a differential-absorption 3-line polychromator and the introduction of a second instrument to measure the transmitter lamp spectral characteristics during the test. Results

from TTB19 indicate a transmission of 94 percent across the plume centerline which corresponds to an approximate sodium concentration of 0.09 parts per billion, based on theoretical exit-plane conditions computed using the TDK computer code. The absorption data from TTB19 are shown in figure 83. The measured sodium emission is considerably in excess of that predicted from thermal equilibrium. It is expected that this super-equilibrium emission is due to chemiluminescent excitation of the sodium by interaction with excited hydroxal radicals. Unfortunately, the indications of Na nonequilibrium may rule out this species as a candidate for determination of **plume temperature** by the emission/absorption technique. The presence of Na is of continued interest, however, as a diagnostic for exit-plane velocity and pressure using a laser-pumped fluorescence technique.

[1]Brewer, L.E., "A Noninterference Method for Determining Temperature and Water Vapor Concentration Profiles in Cylindrically Symmetric Combustion Systems," AEDC TR-71-80, 1971.

[2]Neer, M.E., and Burde, D.H., "The Advanced Development of a High Frequency Response Spectroscopic Probe for Analysis of Supersonic Combustor Flowfields," NASA CR-145363, 1978.

[3]Dobson, C.C., and Eskridge, R.H., "Resonant Absorption and Emission Measurements of Atomic Sodium in the SSME Exit Plane," Proceedings of the 1990 Conference on Advanced Earth or Orbit Propulsion Technology, May 1990.

R.H. Eskridge/EP55
(205) 544–7119
Sponsor: Office of Aeronautics and Space Technology

Injector Diagnostics Development

Research is being conducted to characterize the injector properties (i.e., droplet size distribution) droplet breakup, and combustion phenomena for single-element injector configurations. A pressurized, hot/cold flow test facility is being constructed for this purpose at MSFC.

This research is composed of measurement efforts for cold-flow characterization and hot-fire testing of injector assemblies for **Advanced Launch System** (**ALS**) engine development. A two-dimensional stability research combustor will also be tested as part of the **ALS** effort to determine stability margins for LOX/H_2 hardware development. The data acquired will be used to anchor CFD codes currently under development.

Cold flow data will be acquired for simulated injector sprays at 1,000 psig using liquid nitrogen and gaseous nitrogen as simulant fluids. The cold-flow pressure chamber is shown in figure 84. The initial test article will consist of an SSME preburner injector element. Droplets will be sized for this spray configuration using a phase-Doppler particle sizer/velocimeter.

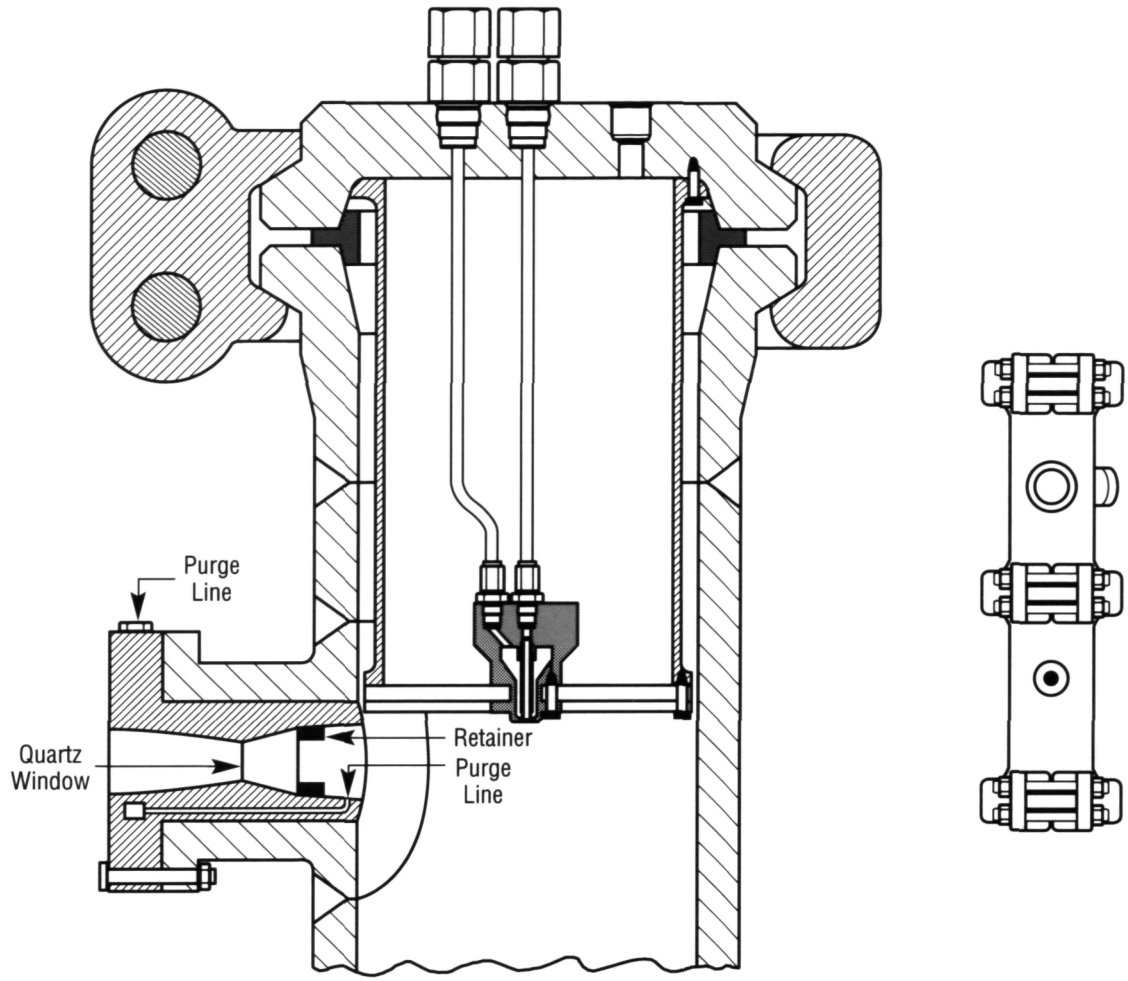

Figure 84. Cold-Flow Pressure Chamber for Injector Spray Testing

The hot-fire system will consist of a single-element hot-fire chamber with windows for combustion diagnostics and phase-Doppler particle-sizing measurements. A test stand laser-based diagnostic assembly is currently being designed for nonintrusive temperature measurements using an excimer-pumped dye laser for **Raman spectroscopy**. A dedicated laser Raman polychromator is under construction to allow high-speed determination of temperature and chemistry in the probe volume using the Raman spectra of hydrogen, water, and oxygen. Cooled photomultipliers and gated amplifiers are being procured to allow fast spectral data acquisition with minimum noise. Initial efforts have included laboratory studies of the Raman system for data-reduction algorithm validation. A heated and pressurized cell is used for these studies to provide gases at known temperatures and pressures for calibration of the system.

A scanning optical head is also being developed for radial profiling of the single-element injector configuration. The system will utilize a single optic for focusing the laser beam and collecting the backscattered laser radiation. The collected laser signal will be coupled to the remote Raman polychromator via fiber optic.

R.H. Eskridge/EP55
(205) 544–7119
Sponsor: Office of Aeronautics and Space Technology

Completion of Forbidden Orbit Transfer Study

A study entitled "Forbidden Tangential Orbit Transfers Between Intersecting Keplerian Orbits" was published in *Acta Astronautica,* Vol. 19, No. 8, pp. 649–656, 1989. The journal article was a scaled-down summary of a larger effort; the full study is in the final stages of publication as NASA TP 3031.

The study can best be summarized by quoting the abstract as follows:

> "The classical problem of **tangential impulse** transfer between coplanar **Keplerian orbits** is addressed. A completely analytic solution which does not rely on sequential calculations is obtained and this solution is used to demonstrate that certain choices of initial true anomaly can produce singularities in the parameters of the **transfer orbit**. A necessary and sufficient condition for the existence of such singularities is that the initial and final orbits intersect."

The journal publication addressed only the most general case. Other cases of importance occur when either the target orbit or initial orbit are circular. Those cases, which cannot be readily obtained from the general solution, are treated in detail in the forthcoming NASA technical paper.

The results of this study were initially surprising in that the field of tangential **impulsive transfer** is quite old and well studied. To turn up a result of such generality and sweeping application is most unusual. This report vitiates a large number of past papers from various authors.

R. Burns/EL58
(205) 544–2284
Sponsor: Space Science Laboratory

Space Shuttle Main Engine Preburner Temperature Profiler

Laser-based diagnostic instrumentation is being developed to measure temperature profiles in the **preburner** combustion chambers. The staged combustion cycle used on the Space Shuttle Main Engine (SSME) burns liquid hydrogen fuel, rich with liquid oxygen, to generate gas to drive the propellant turbopumps. The pressures in the **preburners** are nominally 5,500 psia (34.5 MPa) and the temperatures are 800–1,700 K. The post-combustion gases are 89-percent molecular hydrogen and the balance is water vapor. This paper describes progress on the development of instrumentation for temperature measurements in two applications: (1) the Technology Test Bed fuel **preburner**, and (2) **preburners** to be used for the alternate turbopump development (ATD) program being conducted by Pratt & Whitney-GEB.

The main advantage of optical diagnostics for temperature measurements is that they are nonintrusive and, with judicious use, do not perturb the flow being measured. A physical probe inserted in the flow must be robust and therefore of heavy construction to survive. For this reason, flow perturbation is unavoidable and instrument response time becomes long (i.e., seconds). The temporal response of **laser** techniques, however, is determined by the time required to acquire a sufficient number of signal photons for an accurate measurement. With powerful **lasers**, the response time can be a small fraction of a second for the SSME **preburner** application.

A nonintrusive means of measuring temperature profiles in the SSME **preburner** is desired to support future combustor development and refinement. Raman scattering was selected for fuel **preburner** diagnostics in a feasibility study. The combination of limited access existing in the **preburner**, the lack of particles in the flow, and the low-visible-neutral luminosity of the hydrogen-oxygen flame favor Raman diagnostics in the backscattering configuration, as schematically shown in figure 85. The

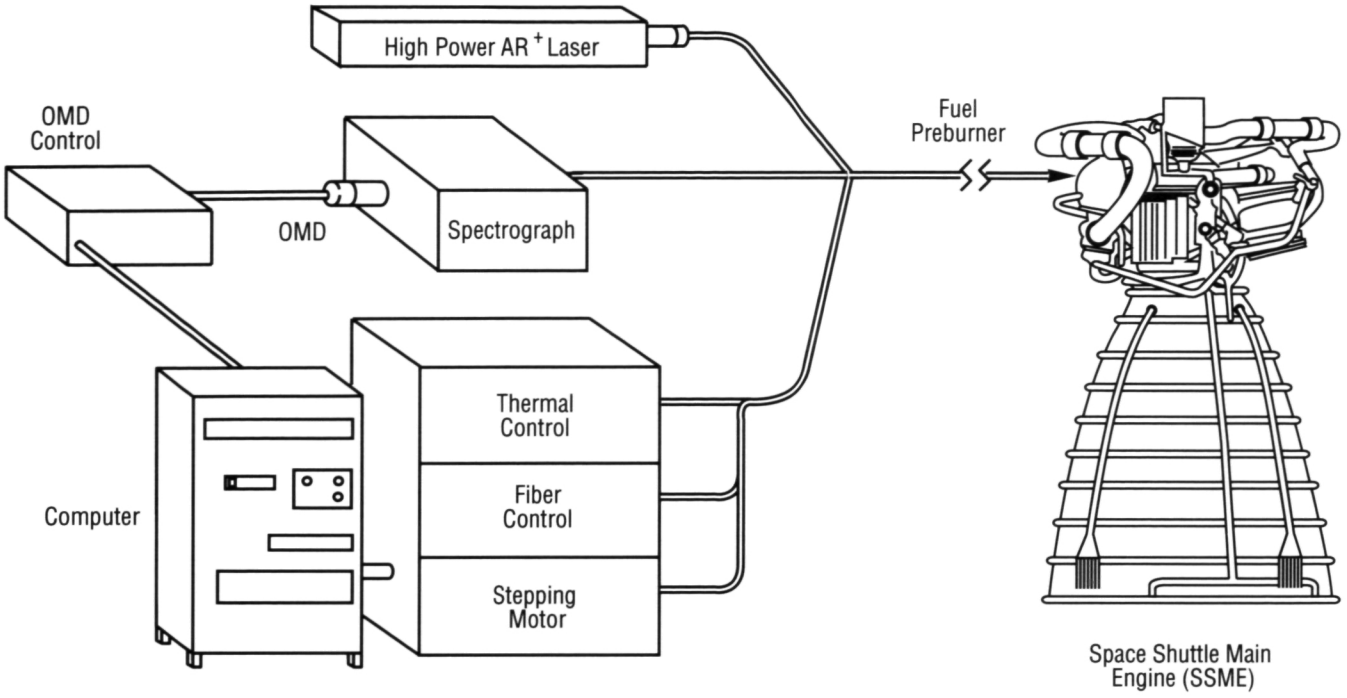

Figure 85. FORT Diagnostics System

fiber-optic Raman thermometer (FORT) laser diagnostic system, described in previous reports is designed to use optical fibers both to carry **laser** light for excitation to the combustor and to carry scattered light to remotely located equipment used for acquisition and analysis. This system permits measurement of the **preburner** temperature distribution across a diameter from an existing transducer port on the SSME **preburner**.

The **FORT** system depicted in figure 86 consists of a high-power argon ion **laser** for excitation; an optical head attached to the **preburner** which focuses light into the combustor and collects backscattered light; a spectrograph and optical multichannel detector to disperse and rapidly detect the Raman-shifted radiation; a computer system to acquire and analyze data; and control instrumentation to position optics and thermally stabilize the head. The most unique aspect of the instrument design is the use of multimode optical figures to transmit backscattered radiation from the head to the spectrograph.

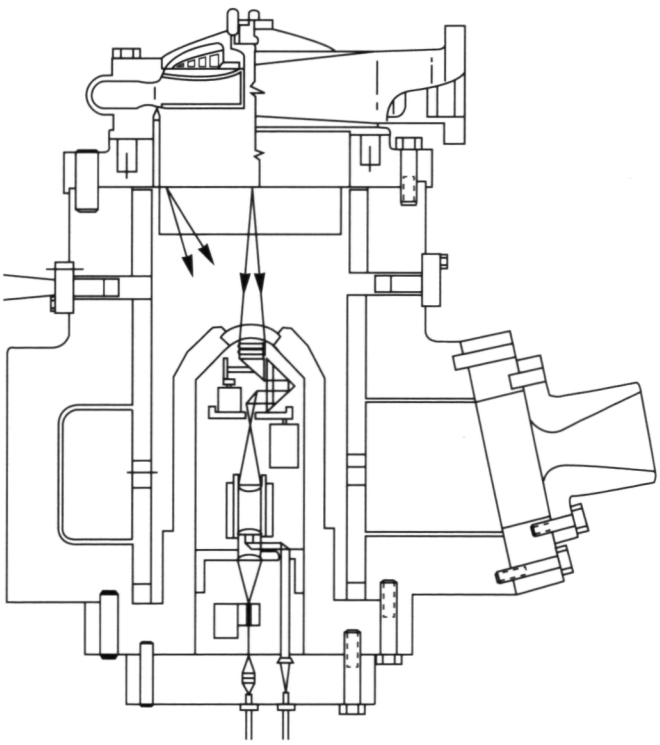

Figure 86. FORT in ATD Combustor

A **FORT** diagnostic system was developed for measurements under the SSME Alternate Turbopump Development (ATD) program. This **FORT** system was used for **preburner** testing without the turbomachinery. Optical access to the **preburner** was gained by placing the Raman optics behind a hemispherical, quartz dome at the position of one of the turbine inlets. In this location, a greater area in the combustor may be probed as opposed to the side window-mounted approach. An optical design was chosen to enable temperature measurements to be made in a planar region downstream of the injector face.

The optical system utilizes a part of rotating prisms to point the optical axis in virtually any direction. A diagram showing the configuration of the optical system for scanning the **laser** probe volume is shown in figure 87. The figure shows the position of the probe as mounted in the Pratt & Whitney checkout chamber.

Shirley, J.A., United Technologies Research Center: "Development of Fiber Optic Raman Diagnostics for SSME Preburner Temperature Measurements," Presented at 1990 Conference on Advanced Earth-to-Orbit Propulsion Technology, MSFC, May 17, 1990.

Shirley, J.A., United Technologies Research Center: "Investigation of Breadboard Temperature Profiling Systems for SSME Fuel Preburner Diagnostics," 24th Joint Propulsion Conference, Boston, MA, July 12, 1989.

W.T. Powers/EB22
(205) 544–3452
Sponsor: Office of Aeronautics, Exploration, and Technology

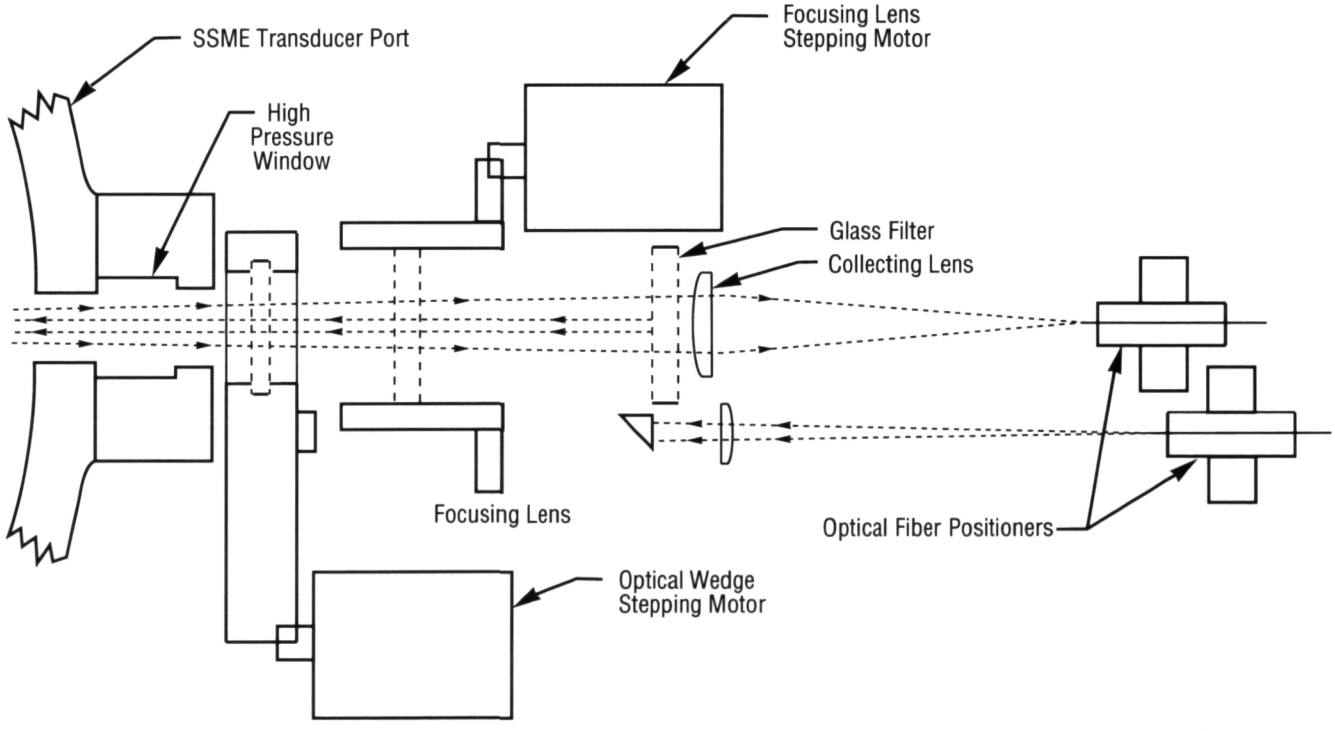

Figure 87. Interior Design of Fiber Optical Raman Thermometer (FORT) Optical Instrument Head.

Space Shuttle Main Engine Exit Diagnostics

Maps of temperature, species concentration, and velocity, measured in a plane at the exit of the engine, would be valuable for anchoring engine performance codes and evaluating the performance of individual engines. Even if the perturbations that physical probes cause were tolerable, it is not likely that probes could survive in the hot, high-velocity exhaust streams. Nonintrusive, optical **diagnostics** are being developed to measure gas-flow parameters at the exit of the space shuttle main engine (SSME).

Spontaneous **Raman scattering** was selected for measurement of temperature and major species concentrations with an ultraviolet laser used to increase the efficiency of signal generation. The same laser would be used for velocity measurements, providing a source of excitation, that marks a spatially defined region of the flow. Convection transports excited molecules from the marked region. A second pulsed laser, triggered a short time after the first, indicates the position of the marked molecules through fluorescence. The convection of the marker can be recorded with an imaging detector.

A conceptual design study has led to identification of ultraviolet UV laser approaches for temperature, species concentration, and velocity measurements in the exit plane of the SSME (fig. 88). Spatially resolved temperature and species concentration are obtained by UV **Raman scattering** from hydrogen and water, using a KrF (248-nm) injection-locked excimer measurement by enhanced OH flow tagging. The KrF (248-nm) excimer laser photo disassociates a small amount of the water to produce a zone of enhanced OH. This zone is convected by the dye laser. Fluorescence induced in the enhanced OH is detected with an optical multichannel analyzer. The enhanced OH technique has been applied to measure velocity in a small supersonic steam jet.

Preliminary results have been obtained with a narrowband, injection-locked excimer laser, using laboratory hydrogen-air flames to simulate SSME exit plane conditions. Resolved hydrogen Raman spectra have been obtained, which demonstrate that the narrowband operation has been successful, and accurate determinations of flame temperature are

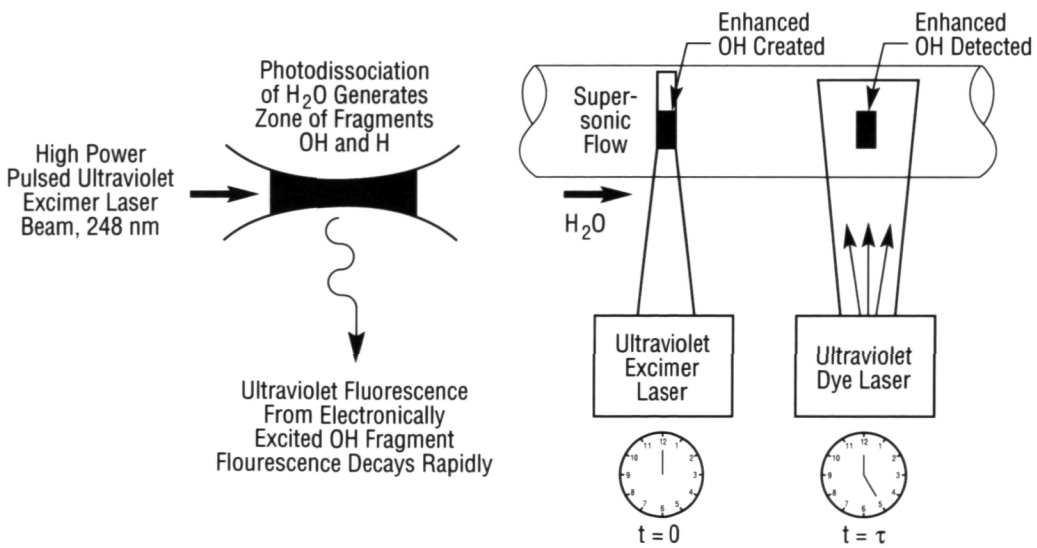

Figure 88. Flow Testing for Velocity Determination

possible. A bandpass filter strategy for faster acquisition of temperature and species data, based on water vapor and hydrogen Q-branch filters and hydrogen S (5) isolation with a monochromator, has been identified and explored. A more efficient approach has been identified for future study—spectral separation of all three band signals with prisms. Spatial imaging of enhanced OH has been studied in a premixed hydrogen-air-nitrogen flame at about 1,200 K. Significant enhancement of OH has been observed with a vidicon detector. The enhancement exists in a narrow spatial zone at significant time delays. Accurate velocity measurements have been demonstrated with a small free-jet-flow containing water.

With regard to velocity measurements, a new technique which is eminently applicable to the SSME exit has been demonstrated. Uncertainty on the order of 10 percent has been shown. Improved timing circuits are available which should reduce the delay jitter, and curve-fitting techniques to define peak locations should enable velocity measurements to be made with accuracy as high as ±1 percent.

Boedecker, L.R., and Shirley, J.A., United Technologies Research Center: "Laboratory Measurements for the Feasibility of Exit Plane Laser Diagnostics." Presented at 1990 Conference on Advanced Earth-to-Orbit Propulsion Technology, MSFC, May 17, 1990.

Shirley, J.A., United Technologies Research Center: "UV Raman Spectroscopy of H_2/Air Flames Excited With a Narrowband KrF Laser," *Optical Letters*.

W.T. Powers/EB22
(205) 544–3452
Sponsor: Office of Aeronautics, Exploration, and Technology

Vortex-Shedding Flowmeter for Space Shuttle Main Engine

In order to measure the actual propellant **flow** in the space shuttle main engine (SSME), a meter of sufficient ruggedness to withstand the extremely high velocities encountered is required. Meters with moving parts are generally unacceptable and low pressure loss and meter weight are desired. **Vortex-shedding flowmeters** were examined as candidates. They offer no moving parts, an output which is linear with **flow** (making them potentially more accurate at low **flows** than venturis), and are physically short. Their geometry is such that fewer modifications are required for installation. Figure 89 depicts the 1989 vane 88-6-1.

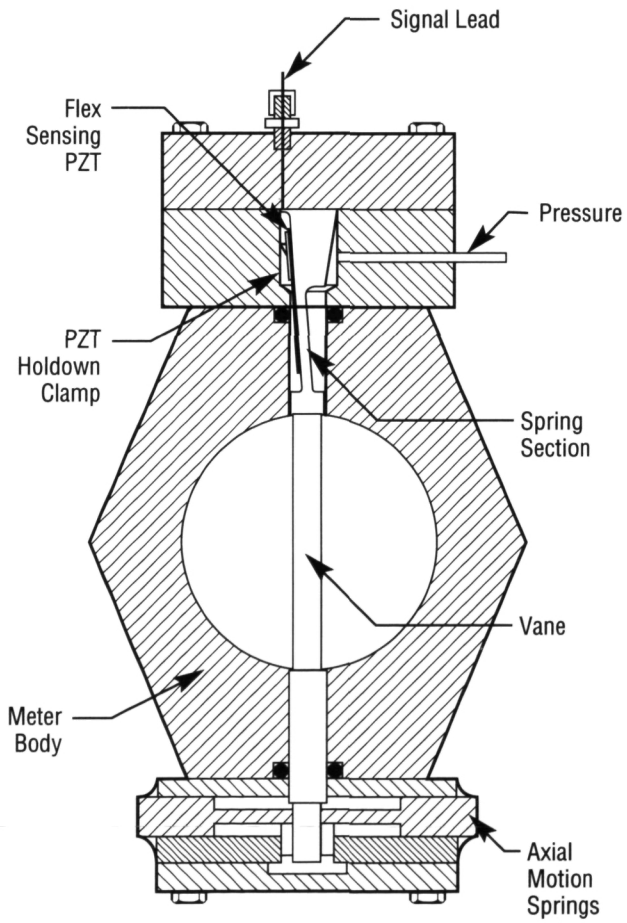

Figure 89. Scale Drawing of Vane 88-6-1

Several designs have been built and **flow**-tested with water and air at velocities encountered within the SSME ducts. Most testing was done in ducts of 4.06- and 5.84 cm (1.6- and 2.3-in) internal diameter; testing is done in actual SSME ducts. Meters to be used with liquid oxygen (LOX) are tested with water drawn from a high-head system owned by the City of Boulder, Colorado. Large heads are necessary to achieve the required velocities. Meters to be used with GH_2 are tested in high-pressure air systems provided by a testing laboratory. Correlations of gaseous hydrogen (GH_2) from the data obtained with air are computed for these tests.

The **vortex-shedding flowmeter** and its application to the measurement of **flow** in the ducts of the SSME has been introduced in previous reports and has shown that it is possible to measure the **flow** in ducts with a **vortex-shedding** meter that installs through an opposed pair of the standard 11.2-mm (0.44-in) diameter instrument ports used for the SSME ducts. A narrow signal spectrum line at constant **flow** can be obtained with no upstream **flow** conditioning in the duct. This has been demonstrated for liquids to average velocities of more than 30 m/s (98 ft/s). Successful airflow tests have indicated that air **flows** to at least 150-m/s (492-ft/s) average velocity can be measured in engine ducts with no upstream **flow** conditioning. The maximum gas **flow** is limited to this maximum by the properties of air. The limit for hydrogen (H_2) should be much higher. One set of fuel and oxidizer **flowmeter** locations to diagnose SSME performance required meters in 58.5-mm (2.3-in), 51-mm (2-in), and 28-mm (1.1-in) bore ducts. Fuel **flowmeters** are desired in 38.9-mm (1.53-in), 51-mm (2-in), and 91.4-mm (3.6-in) bore ducts.

Siegwarth, J.D., NIST/Boulder, "Vortex Shedding Flowmeter for Measurement of Liquids at High Flow Velocities," *International Journal of Heat and Fluid Flow*, 1988.

Siegwarth, J.D., "Vortex Shedding Flowmeter Performance at High Flow Velocities," NBS Tech Note 1302, October 1986.

Siegwarth, J.D., "Vortex Shedding Flowmeters for Space Shuttle Main Engines," Presented at 1990 Conference on Advanced Earth-to-Orbit Propulsion Technology, MSFC, May 17, 1990.

W.T. Powers/EB22
(205) 544–3452
Sponsor: Office of Aeronautics, Exploration, and Technology

Space Shuttle Main Engine Propellant Path Leak Detection, Real Time

The development, qualification, and reliability improvement testing of space shuttle main engines (SSME's) has resulted in the loss of a significant number of engines and associated resources, including project time. Each qualification or component improvement engine represents a critical program resource which includes the accumulated costs of all test time on the hardware. Loss of high-time fleet-leader engines during ground testing has become more important as the SSME inventory matures.

A proposal is underway which addresses one mode of engine failure which may be detected and analyzed with sufficient speed to save critical engine test hardware from destruction. The complicated high-pressure cycle of the SSME provides many opportunities for **propellant** path **leaks**, both internal and external, while the engine is running. The **leaks** indicate failure modes which will damage or destroy an engine if undetected. Failure of high-pressure line fittings, welds, and internal component parts caused by thermal shock, thermal cyclic stress, stress corrosion, erosion, and high-cycle fatigue can result in failure modes with sufficiently long time constants to allow detection and safe shut-down. Millisecond detection rates (sampling rates) and 10-ms data processing can result in failure detection to shutdown signal of less than 100 ms. Although the required time constants for detection and action have not been established from analysis of expected leaks, it appears that significant improvement in the engine protection system can be obtained with an advanced **propellant** path **leak** detection system. Optical sensors combined with computer image analysis and expert systems is one approach to address this problem.

The primary objective of this investigation is the experimental validation of techniques for detecting and analyzing **propellant** path external **leaks** which have a high probability of occurring on the SSME. In order to select candidate detection methods, one requires a good model for the **leak** plumes which will develop from external **leaks** and a sound understanding of the mission environment around the SSME. Gas species, temperature, and plume shape will be used to characterize a **leak** plume. Due to the compact and complex **propellant** path configuration of the SSME, plume shape and resulting temperature distributions will be difficult to predict. Significant plume impingement on other components will result in solid surface radiation as well as gas plume radiation. This investigation will consider both cryogenic fuel and oxidizer **leaks**, as well as hot gas **leaks** that may occur anywhere between the **propellant** inlet lines, turbomachinery, valves, preburner, etc., and the main thrust chamber.

It is recognized that detection of internal gas path anomalies will be more difficult and will most likely require a different approach, such as the plume spectral analysis for metals. The combination of internal **flow**-path performance measurements with external component-temperature distributions may allow rapid diagnosis of internal-**flow** problems. Observations will be restricted to the region above the nozzle throat to avoid the intense radiation field from the nozzle exit. Thus, only those internal **leaks** which change the external temperature distribution on fluid lines or components upstream of the main thrust chamber would be detectable.

Selected **leak**-detection sensors, primarily optical (operating in the IR range), will be evaluated on subscale laboratory plumes to determine sensitivity, signal-to-noise, and general suitability for the application. The actual detection system will require sensor integration into high data-acquisition-rate video-to-digital image conversion for processing.

M.L. Johnson/EB22
(205) 544–5519
Sponsor: Office of Space Exploration and Technology

Optical Leak Detection for Ground-Based Operations

During factory and test stand operations involving space shuttle main engines (SSME's), a **leak testing** at the many joints is necessary to ensure tightly fitted assembly. Currently used methods involve pressurizing the assembly, or subassembly, and using a bubbling-type **leak-test** fluid, or, when small leaks are sought, using a totally enclosing bag and a mass spectrometer. A method which is faster, easier to use, and possibly more sensitive is being developed for use in the factory and on test stands under purged, nonoperating conditions. This technology, originally developed under a U.S. Air Force contract, involves pressurizing the configuration under test with a gas containing a selected "seed" gas, illuminating the configuration with light which can be absorbed by the pressurant, and imaging the result with a video camera. Any leaking gas in the vicinity will then be visible in the image and can be quantified and located with automated digital image processing.

The SSME which has been used as a baseline for this program has over 150 separable joints. In addition to minimizing human intervention, the process will simplify leak location, quantify leak rates from individual joints, and reduce the time needed to complete testing without sacrificing reliability.

Figure 90 shows a diagram of an infrared absorption-based optical leak-imaging method that was developed. It employs an infrared camera and an infrared **laser**. An expanding lens in front of the **laser** spreads the beam to illuminate the entire test object. The component under test is pressurized with a gas which absorbs strongly at that **laser** wavelength. The **laser** bathes the area to be inspected, as it is being viewed with the infrared camera. Any leaking gas absorbs the infrared energy and appears as a black cloud to the camera.

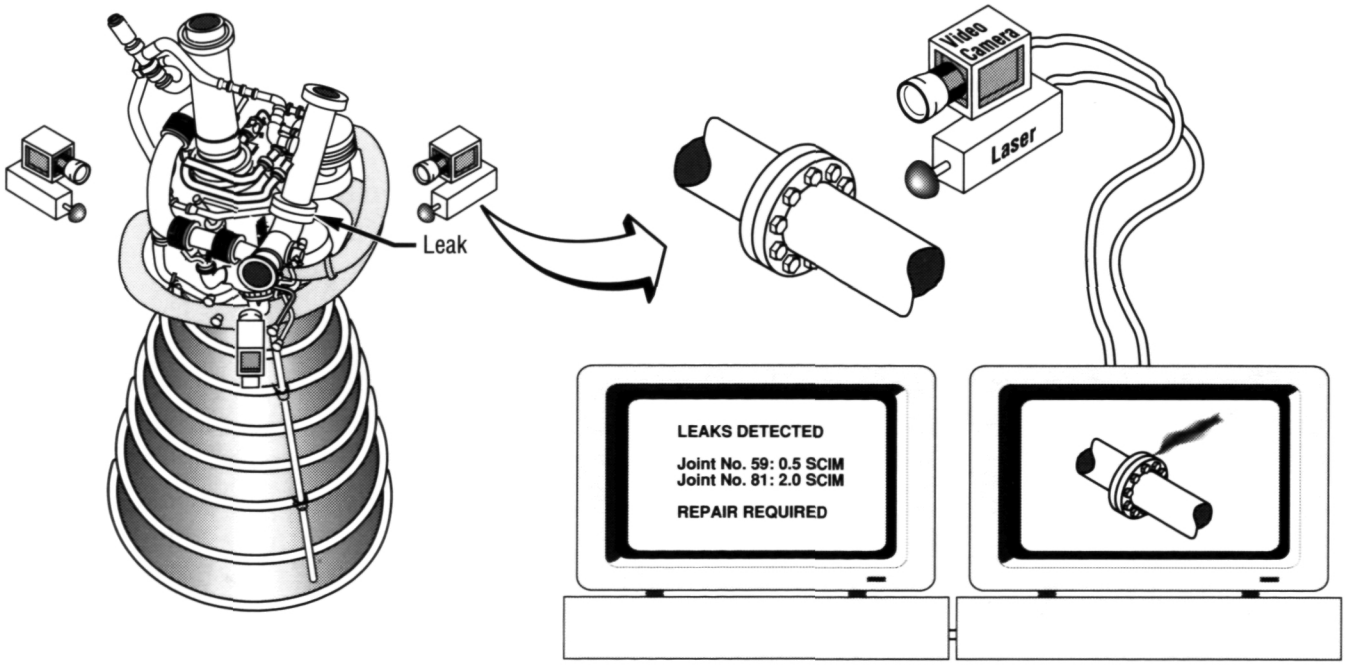

Figure 90. Optical Absorption Leak Detection

The advantage in the optical system lies in its ability to remotely examine large portions of complex hardware, such as on an SSME powerhead assembly, and to pinpoint and quantify leaks. The alternative is to manually inspect each individual joint with soap solution and a mass spectrometer. To aid in locating and quantifying leaks, a computerized vision-processor is required to analyze the images produced by the infrared camera. The vision-processor used here consists of an IBM 286-compatible computer utilizing a video frame-grabber plug-in module. By using image subtraction techniques, the vision processor can distinguish a leaking gas cloud from normal background objects. The "difference" image is an actual map of the gas distribution and concentration, and can be used to pinpoint the source of the leak. Automated processing methods can also be added to quantify the leak rate.

Optical absorption leak detection will allow leak testing of an entire engine in a matter of minutes, remotely and automatically. This can be done with as few as four stationary camera systems on an SSME-class engine. Optical methods will greatly improve the accuracy and reliability of rocket engine inspections, while drastically reducing the inspection time currently required by the present soap solution and spectrometric analysis method.

M.L. Johnson/EB22
(205) 544–5519
Sponsor: Office of Aeronautics Exploration and Technology

In-Flight Optical Leak Detection

Presently, there is no real-time propellant leak-detection capability that exists for implementing closed-loop control during flight. Neither is there a ground-based propellant leak-detection capability for flight readiness firings (FRF) with a leak-location ability for the space shuttle main engine (SSME).

Current leak-test procedures of the SSME are limited to ground-based, low-pressure inspections, post-flight analysis of sampling bottles mounted in the shuttle engine compartment, and mass spectrometer readings taken during FRF. In-flight parameters such as pressure, temperature, and residual gas concentrations were obtained from data collected during shuttle flights using the gas bottle technique for leak detection. The gases in the aft fuselage are sampled at designated intervals during shuttle lift-off. This method has the obvious disadvantages of being single point, nonperformable in real time, and not continuous.

Studies of literature from more than 70 leak-detection companies were made to determine what types of hydrogen, oxygen, and water vapor detection systems are commercially available for flight-practical leak-detection capability. Of the 13 different technologies found in the study, 11 could identify and quantify hydrogen, oxygen, or water vapor. The remaining two technologies were unable to distinguish the species of gas they were sensing. Each technology was reviewed for compatibility with in-flight environmental conditions and additional requirements, such as real-time data analysis capabilities and flight-weight practicality.

Optical absorption employs a camera for imaging a leaking gas and a light source which emits radiation at wavelengths that are strongly absorbed by the leaking gas. The beam of the light source is spread to illuminate the entire test area. A camera views the illuminated inspection area for any leaking gas, as shown in figure 91. Any leaking gas absorbs the light energy and appears as a black cloud to the camera. An advantage of an optical absorption

system lies with its ability to remotely examine large areas and to pinpoint and quantify leaks in real time. The only light sources identified for this technique would add impractical weight to the flight. This optical absorption method was abandoned for the Raman scattering technique. This was determined to be the most promising in-flight leak-detection method.

This optical technique is based upon inelastic collisions between photons and the leaking gas molecules, from which the Raman-scattered photon wavelength is shifted by an amount dependent upon the cross-section of the gas molecule with which they collide. The intensity of the Raman-scattered light provides a measure of gas concentration. It has the advantages of providing real-time scanning or imaging capabilities. Although the Raman-scattered signal is very small in comparison to the intensity of the excitation source, appropriate filtering and signal processing can be employed to discriminate the Raman signal from any background light.

The test setup for the Raman-scattering leak-detection test is shown in figure 92. A Nd: YAG laser is frequency doubled using an angle-tuned potassium dihydrogen phosphate (KDP) crystal. A harmonic beam splitter reflects the 1,064-nm beam into a beamstop and passes the 532-nm beam into the test cell. A large lens collects the Raman-scattered light at a 90° angle to the incident beam. The scattered light is then isolated with longwave and narrow bandpass filters, selected for the particular gas under test, before entering a **photomultiplier tube (PMT)**. Output of the **PMT** is measured with a high-speed oscilloscope, which is externally triggered by the advanced **Q-switch** synchronized output from the laser power supply.

Connected to the test cell is a vacuum pump, a vacuum pressure gauge, and gas lines for hydrogen or oxygen. The test cell could be pumped down to a moderate vacuum of 2 torr or filled with up to 2 atmospheres. The incident beam was passed into the test cell by two 1-in diameter quartz windows, and two 3-in diameter windows to the detectors. The

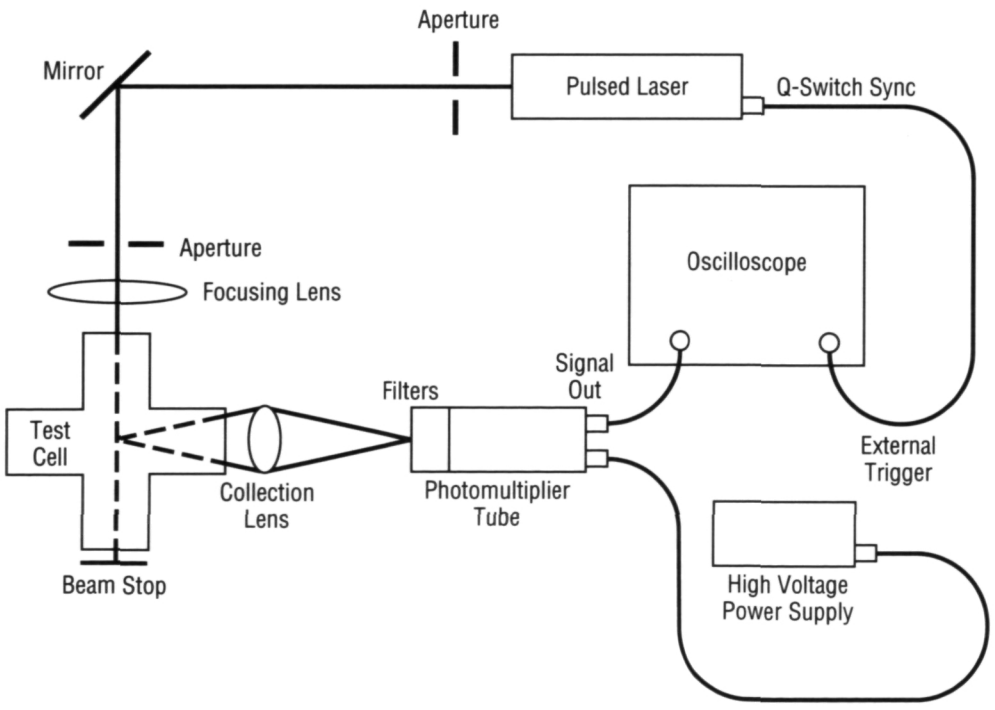

Figure 91. Raman Scattering Leak-Detection Test Setup

Rayleigh-scattered light intensity at the incident wavelength is six orders of magnitude larger than the Raman-scattered light intensity, so longwave and narrow bandpass filters, one for hydrogen and one for oxygen, were used to isolate the Raman-scattered light.

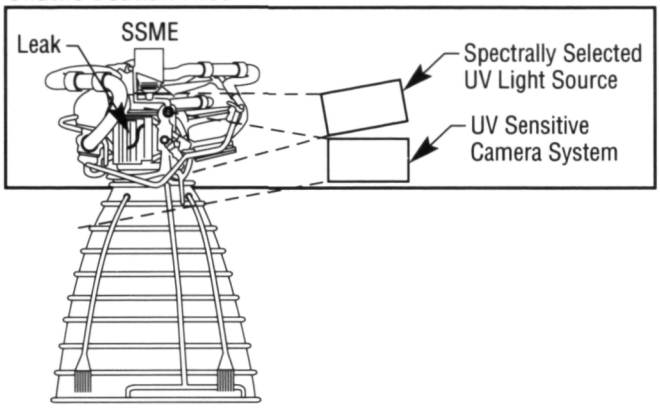

Figure 92. Propellant Leak-Imaging System

The test cell was initially evacuated. The signal from the **PMT** was monitored with the oscilloscope as the test cell was gradually filled up to one atmosphere of hydrogen or oxygen gas. The Raman-scattered intensity increased linearly with the gas partial pressure for hydrogen and oxygen. These results demonstrate the visibility of Raman scattering as a promising and practical technique for in-flight monitoring of hydrogen and oxygen propellant leaks.

With the development of remote, optical leak-measurement technologies such as optical absorption and Raman scattering, these techniques can provide high-speed, accurate, and reliable automated leak-detection systems which can achieve dramatic reductions in inspection times and drastically improve the reliability of in-flight leak-monitoring of liquid propellants to ensure a more reliable leak-detection system for launch readiness, in-flight monitoring, and documentation of space transportation system hardware.

M.L. Johnson/EB22
(205) 544–5519
Sponsor: Office of Aeronautics Exploration and Technology

Solid Rocket Motor Propellant and Polymer Materials Structural Test Program

Current structural analysis of solid **propellant grains** employs linear viscoelastic theory. It has been assumed in the past that since most strains induced in a solid rocket motor (SRM) during storage and operation were less than 20 percent, linear analysis was adequate to predict the response of the **propellant grain**. **Nonlinear analysis codes** have been developed, but material property measurement techniques which provide inputs to the codes have been slow in developing. Recently, questions have arisen as to the validity of the assumption of linearity of propellants below 20-percent strain. A small body of evidence indicates that nonlinear behavior in propellants may begin as early as 1- to 2-percent strain. If so, the Boltzmann superposition principle employed throughout the propellant industry to characterize propellant behavior may be in error. It is the goal of this 3-year study to determine the validity of the Boltzmann superposition principle and to establish as complete a characterization of the current and advanced SRM propellant as possible in order to facilitate structural analyses and determinations of factors of safety for the system.

The Propulsion Directorate of the U.S. Army Missile Command is currently designing, developing, analyzing, and testing specimens and constituent materials to support analyses and investigations of the space shuttle SRM and components. As needed, the Propulsion Directorate is also conducting structural analyses of the test articles and assisting in developing mathematical models applicable to the analysis of the SRM propellant and polymer materials.

The following is a summary of the structural testing series that has been achieved at the Propulsion Directorate U.S. Army Missile Command (MICOM) as of March 1, 1990:

- Post-Cure Testing
- Time-Temperature Characterization (JANNAF class C) (Joint Army, Navy, NASA, and Air Force)
- Linear Coefficient of Thermal Expansion
- Crosslink Density Determination
- Time-Temperature Characterization (JANNAF class A)
- Fatigue and Cyclic Thermomechanical Testing.

Further work to be completed by the MICOM Propulsion Laboratory includes the following:

- Stress Relaxation Modulus Followed by Recovery Measurements at Isothermal Conditions
- Creep Compliance Determination
- Stress-Free Temperature Shift; Permanent Set Determination.

Little, R.R., "Determination of Crosslink Density by the Equilibrium Volume Swell Method," internal letter report, October 1989.

Little, R.R., "SRM Propellant and Polymer Materials Structural Test Program," quarterly status report, June 1990.

V. Richard/ED24
(205) 544–7200
Sponsor: Solid Propulsion Integrity Program

Analysis of Static and Dynamic Nonlinear Viscoelastic Response

By performing **biaxial propellant testing**, the Jet Propulsion Laboratory has provided NASA with a more accurate understanding of space shuttle solid rocket booster propellant behavior. This type of testing will build a more complete data base for structural integrity analyses of current and next generation booster rockets.

The Jet Propulsion Laboratory is currently involved in four primary areas of propellant biaxial testing: (1) finite element code modifications to carry out multiaxial, **nonlinear (large deformation) viscoelastic response** of polybutadiene acrylonitrile (PBAN) propellant; (2) cutting/machining test specimens; (3) refurbishing test equipment, including data collection software, and test hardware; and (4) labor required for testing, data reduction, and documentation of results.

The following is a summary of the biaxial structural testing series that has been achieved at the Jet Propulsion Laboratory as of April 30, 1990:

- Biaxial Stress Relaxation Testing (multiple steps)
- Biaxial Constant Strain Rate Testing (different temperatures).

Further work to be completed by the Jet Propulsion Laboratory includes the following:

- Biaxial Creep Tests (multiple steps at different temperatures)
- Develop a model of **nonlinear (large deformation)** viscoelastic behavior which shall take into account dewetting and volume change response
- Determine stress and strain failure criteria which are compatible with nonlinear mechanical constitutive laws.

Landel, R.F., "Analysis of Statics and Dynamic Nonlinear Viscoelastic Response," quarterly status report, January 1990.

Landel, R.F., "Analysis of Statics and Dynamic Nonlinear Viscoelastic Response," quarterly status report, May 1990.

V. Richard/ED24
(205) 544–7200
Sponsor: Solid Propulsion Integrity Program

Formed Platelet Combustor Liner Construction Feasibility

Cooling liners for high-pressure combustion chamber operation such as that found in the space shuttle main engine (SSME) require designs which allow a high heat-transfer rate. These designs employ high thermoconductivity materials, high heat-transfer surface areas through high values of coolant channel height-to-width ratio and thin cross-section hot gas walls. The current fabrication approach employs milling and electroforming operations of forged and spun copper billets. This imposes a limit on the thinness of the hot wall to about 0.071cm (0.028 in) and on the height-to-width ratio of the cooling channels (about 5:1).

An alternate fabrication approach is being investigated which holds promise of achieving thinner hot walls and higher values of channel height-to-width ratio. This alternate approach is based on the use of thin copper plates (platelets) on which are chemically etched coolant channels. These platelets are then stacked and diffusion-bonded to form a closed cooling passage structure. The **cooling liner** is then formed by press-forming the panels into the combustor contour and welding the panels together to form the complete **cooling liner**. This approach allows the use of very thin plates to form the hot wall and is capable of forming high channel height-to-width ratios. The relationship of hot wall thickness to wall temperature in shown in figure 93. In the case of the SSME design, a wall temperature reduction of 60 percent may be achieved by reducing the hot wall thickness by 60–70 percent while increasing the number of cooling channels by a factor of 3.7. This reduction in hot wall thickness and the increase in the number of cooling channels is easily accommodated by the **platelet fabrication** approach.

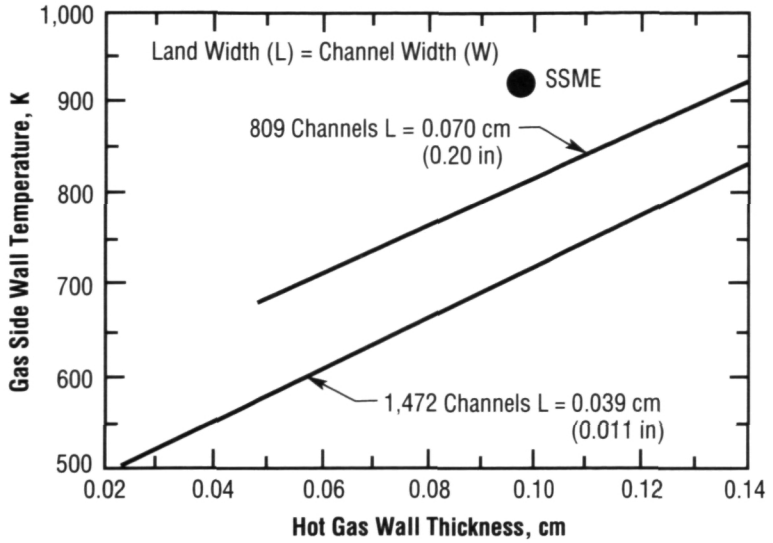

Figure 93. Hot Gas Wall Thickness

ORIGINAL PAGE
BLACK AND WHITE PHOTOGRAPH

Figure 94. Typical Formed Panel

The investigation of the **platelet fabrication** approach has progressed to the demonstration of formed platelet panels having very thin hot walls of 0.020 cm (0.008 in) and in channel height-to-width ratios of 10–15. A typical formed panel is shown in figure 94.

The welding of the panels has been demonstrated on the coupon scale. Future work is directed to fabrication and test of a complete subscale 178-kN (40-klb) thrust chamber **cooling liner** and a larger scale 2,581-kN (580-klb) thrust chamber **cooling liner**.

F. Braam/EP52
(205) 544–7055
Sponsor: Office of Aeronautics, Exploration, and Technology

Turbine Blade-Tip Seal Force Interaction—"Alford" Forces

The only known published test results on **turbine blade**-tip clearance forces, sometimes referred to as **"Alford" forces** or clearance excitation forces, are those obtained from the test program conducted at the Technical University of Munich (TU of M). The test facility is depicted, in front and side views, in figure 95. The tests results indicate that the measured forces are significantly larger than the predicted values. Direct correlation of the test results with the predicted destabilizing forces in the space shuttle main engine (SSME) turbine, however, is difficult to ascertain because of the difference between the operating conditions and geometry of the test and the SSME hardware. The SSME **turbopumps** appear to be more stable than predicted by the TU of M test results. This may be due to the presence of direct damping which theoretical and experimental results do not substantiate. It is imperative that a comprehensive investigation be initiated to better define the forces generated at the **turbine blade**-tip seal interface.

The overall objective of this effort is to generate the necessary data base from which a reasonably accurate model for predicting the **turbine blade**-tip seal clearance excitation forces in the SSME **turbopumps** may be obtained. The first step taken to initiate this investigation was the work required under the original contract NAS8-35018. Included in this effort was a thorough review of literature on **turbine blade**-tip seal clearance excitation forces, the development of an analytical model for predicting these forces for both shrouded and unshrouded **turbine blades**, and the definition of a test program for measuring stiffness and damping coefficients. The next step was to design, fabricate, and check-out

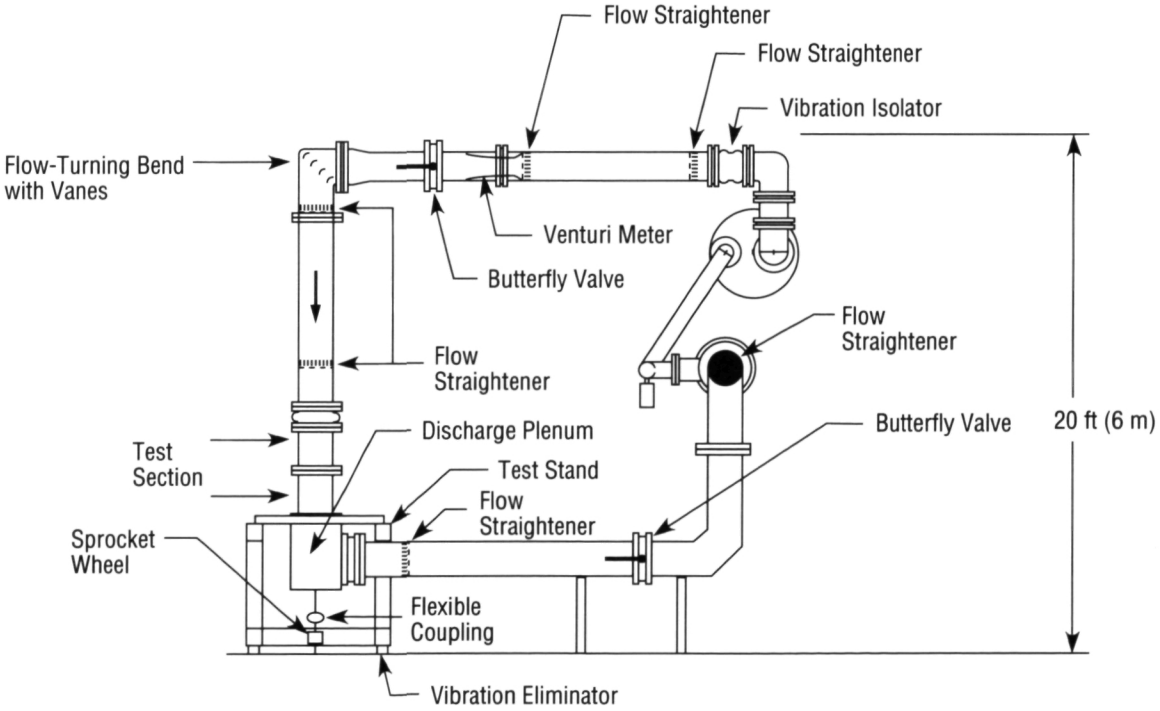

Figure 95a. Front View of the Test Facility

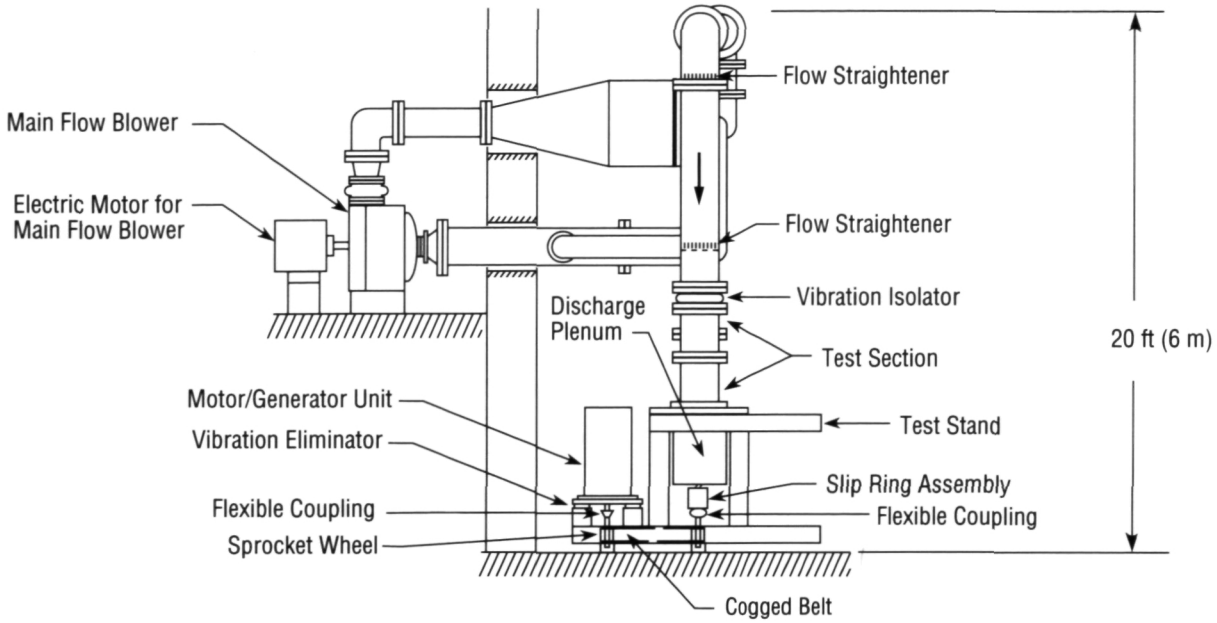

Figure 95b. Side View of the Test Facility

a test article and facility to measure the **turbine blade**-tip seal force interactions. This was accomplished by an extension to the original contract (phase II). The third and final phase is the actual empirical investigation of **Alford forces**.

Phases I and II have been completed. Phase II completion occurred in September 1989 with presentation of the results of the **Alford force** and seal facilities demonstration test to NASA personnel at the Massachusetts Institute of Technology (MIT). The final report for all the work accomplished in phase II was submitted in February 1990. The actual **Alford force** investigation began shortly after completion of the demonstration test review. Completion of the phase III empirical investigation and theory refinement is scheduled for June 1991. Initial results of the empirical investigation were presented at Texas A&M University in May 1990.

G.E. Wilmer/EP62
(205) 544–7115
Sponsor: Office of Aeronautics and Space Technology

Bipropellant Two-Phase Flow Simulation in a Rocket Thrust Chamber

The **Variable Thrust Engine (VTE)**, under development by TRW for NASA, is intended to serve during operations of the orbit maneuvering vehicle (OMV). To satisfy mission requirements, continuous thrust variations from 10 to 100 lb were selected with corresponding chamber pressures from 10 to 100 (psia) and a fuel to oxidizer propellant mixture ratio of Mr = 1.65. Hypergolic propellants (N_2O_4) and monomethylhydrazine (MMH) are pressure-fed into the combustion chamber through a single-pintle injection element. This injection element must efficiently atomize the liquid jets and distribute the **droplets** to hold the radiation-cooled wall below a temperature of 1,400 K while simultaneously producing a high specific impulse.

The analytical performance predictions, conducted with the joint Army, Navy, NASA, and Air Force (JANNAF) recommended two-dimensional kinetics (TDK) computer program, were closely confirmed with test results. However, the solutions have been based on a two concentric mixture ratio zones assumption with reaction products in chemical equilibrium at the end of the cylindrical combustion chamber. The near-wall mixture ratio was determined from the wall temperature measurements, while the core flow mixture ratio and the mass flow in each striation zone were established from an iterative process matching predicted C* values with the measured one. The combustion products were then expanded through a large area ratio nozzle (E = 125) to produce thrust. Although TDK predicted reliable performance values, the program did not provide any information of the real fluid-flow behavior in the subsonic domain of the combustion chamber downstream of the injection element.

To better understand the internal processes, steps have been taken to improve an existing **computational fluid dynamics (CFD)** computer program and simulate this complex **two-phase** spray region in detail. After preparation of the computational grid (see fig. 96a) for the chamber geometry with pintle details, several computations were made which are different from a fluid phase and chemistry aspect. Program solutions of the combustion chamber are presented and discussed below showing only the associated variations in static temperature for the 100-percent power level operation.

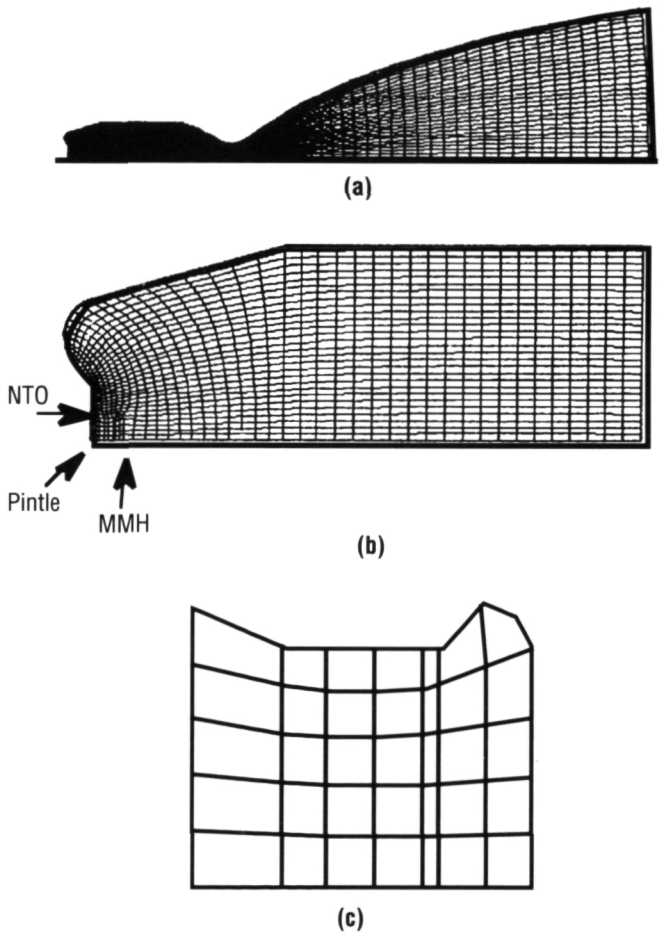

Figure 96. Computational Grid for the VTE Engine; (a). Computational Grid for the VTE Combustor and Nozzle, (b). Magnified View of the Combustor, (c). Magnified View of the Pintle

Injection of the propellants, both in gaseous form, produces a streamline pattern, shown in figure 97, with two recirculation zones when an instantaneous reaction process (chemical equilibrium) for the mixed gas portions is assumed. The respective static temperature, imaged with color fields, is provided in figure 98a and reflects one large recirculation bubble behind the pintle region and a smaller one in the recessed portion just above the N_2O_4 inlet. In figure 98b, the static temperature solutions are shown for the same conditions, except that a finite rate chemistry model was employed utilizing the global reaction equation:

$$CH_3NHNH_2 + 1.25\ N_2O_4 \rightarrow CO_2 + 3.0\ H_2O + 2.25\ N_2.$$

Figure 98c again displays the temperature distribution, but in this case the propellants are injected in the liquid state. At the injection ports the liquids were assumed to consist of **droplets** with an average drop size of 25 μm moving in the directions of the gas from the previous study cases. **Droplet** tracking with the Lagrangian scheme, coupled with an evaporation and mixing model provided the information for the finite rate reaction simulation. To examine the unknown hypergolic nature (experienced spontaneous ignition on contact) of the propellants, the activation energy in the Arrhenius rate equation was set to zero. This effect is reflected in Figure 98d, where the static temperature regions are identified.

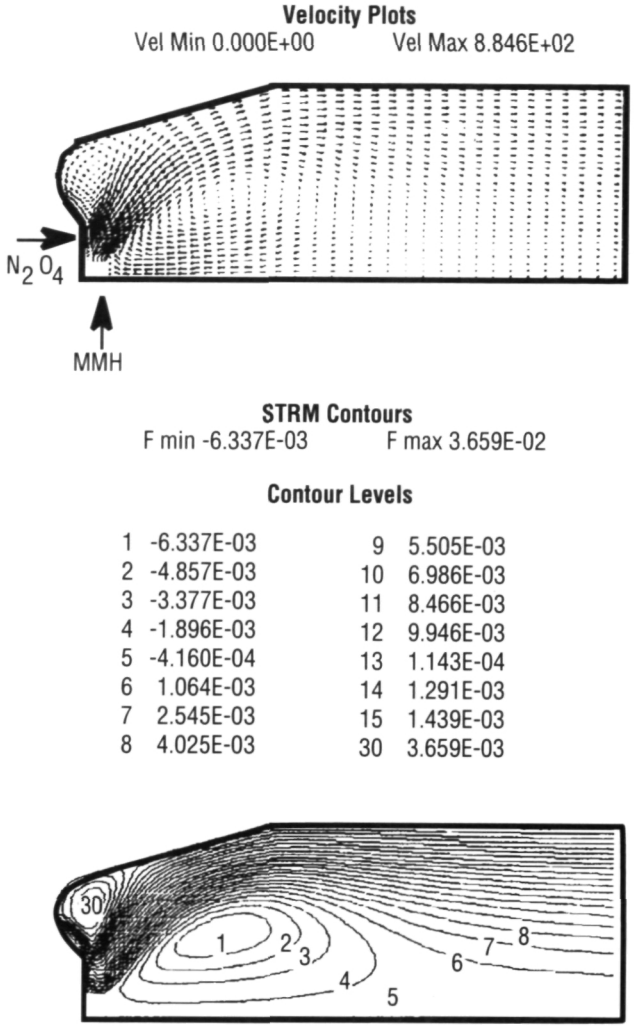

Figure 97. VTE Combustor: Velocities and Streamlines

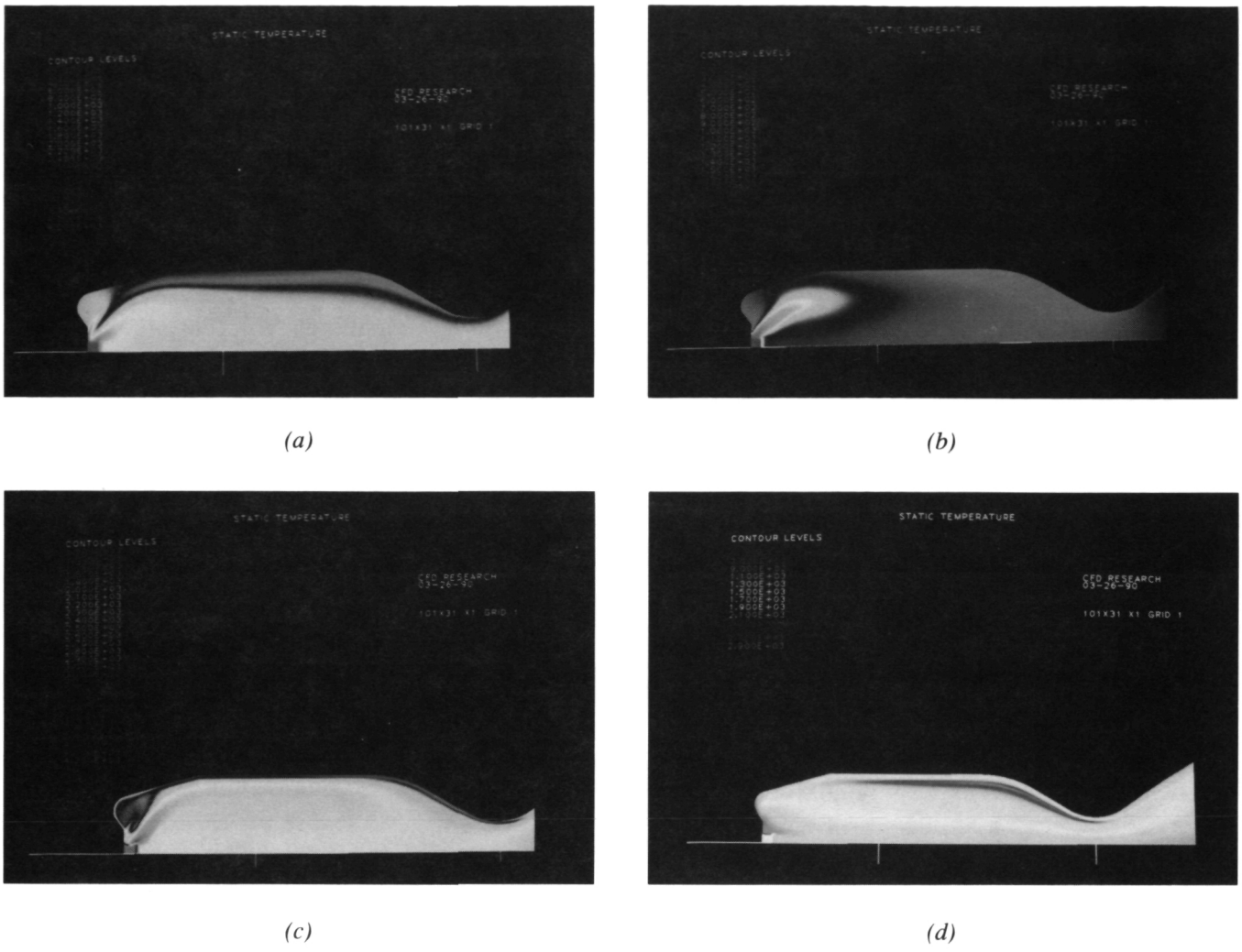

Figure 98. Combustion Chamber Variations During Bipropellant Flow Simulations: (a) Respective Static Temperatures, Imaged With Color Fields, (b) Employing Finite Rate Chemistry Model, (c) Propellants Rejected in Liquid State, (d) With Arrhenius Rate Equation Set to Zero

In comparing figures 98a to 98d, the significant temperature differences are evident, resulting from the simulation of gaseous or liquid-propellant injection, equilibrium or finite rate chemistry, and change of the activation energy. Changing the drop sizes and their direction of initial movement, as well as modifications of the vaporization and turbulence model, will further introduce variations in the analytical results. At this stage, the program predictions can only be utilized for relative sensitivity assessments and qualitative parametric information. In general, the **CFD** solutions indicate that an extensive amount of information can be provided beyond the present performance-oriented only JANNAF codes. The sensitivity and uncertainty of the solutions to various parameters can be narrowed by replacement of current assumptions with advanced concepts, such as an atomization model. However, calibration and verification of the program must occur by comparison with appropriate test data.

Continuation of this activity is in progress at the CFD Research Corporation in Huntsville, Alabama, under contract NAS8-37196.

K.W. Gross/EP55
(205) 544–2262
Sponsor: Office of Aeronautics and Space Technology

C-3

ORIGINAL PAGE IS
OF POOR QUALITY

Propellant Atomization Simulation of Coaxial and Impinging Injection Elements

Liquid **propellant atomization** plays a dominant role in performance efficiency and stable operation of rocket thrust chambers. At present, the atomization is accomplished with either **coaxial** or **impinging injection** elements for gas-liquid (fig. 99) and liquid-liquid (fig. 100) propellant jets, respectively. An analytical activity is in progress for the prediction of the average drop size, its breakaway location, and the droplet production rate to provide essential information for the optimization of injector plate designs.

From observations, it is evident that surface instabilities lead to wave formations, and their growth seems to be the major source of the primary breakup. A nonlinear atomization model has been formulated, characterizing low- and high-speed jets, coupled with the REFLEQS computer program to simulate the primary disintegration of the liquid jet. Solutions are obtained by solving the time-dependent Navier-Stokes equations, which use the nonlinear wave dynamics model and the Eulerian-Lagrangian two-phase flow approach.

Successful solutions have been obtained for low-speed jet breakup, showing the evolution of a main drop and its associated satellite (fig. 101). Also, the variation of their radii, R, as a function of the wave number ka (fig. 102) indicates the excellent agreement and reveals that both can be of equal size. Droplet deformation and breakup can occur in various patterns including ligaments, bags, and sheets. A specific drop shape-time history is portrayed in figure 103, and again, a good agreement

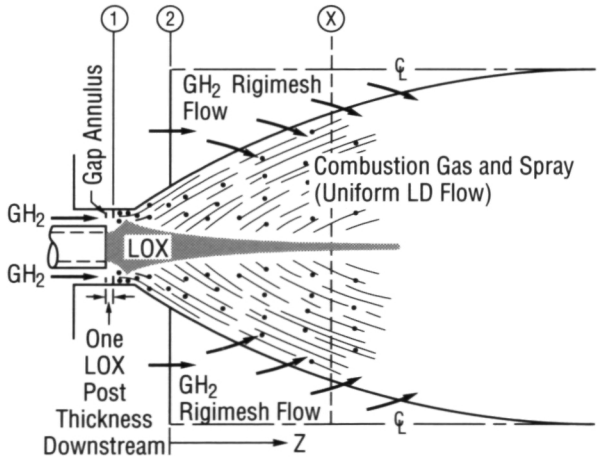

Figure 99. Conceptual Model of Uniformly Flowing Coaxial Injector Element

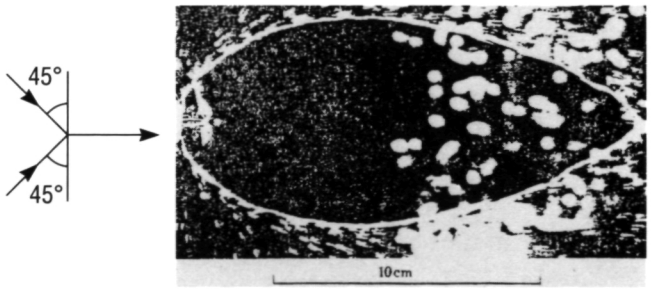

Figure 100. Sheet Produced by Impact of Cylindrical Jets $a = 45°$, $We = 200$; After G.I. Taylor (1960)

ORIGINAL PAGE IS
OF POOR QUALITY

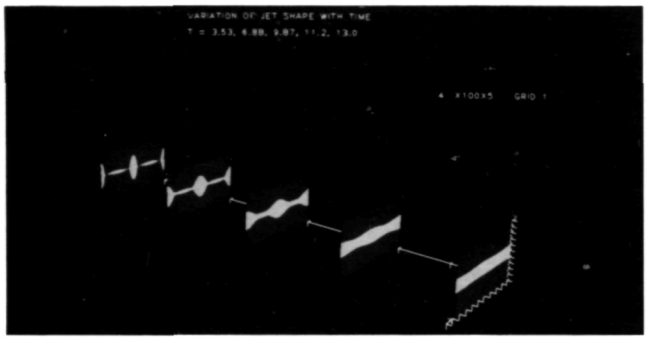

Figure 101. Evolution of a Main Drop and Its Satellite.

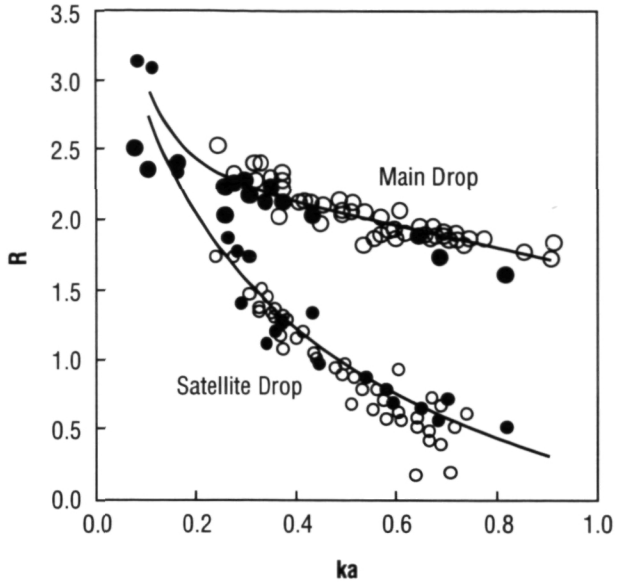

Figure 102. Variations of Dimensionless Drop Radii With Wave Number

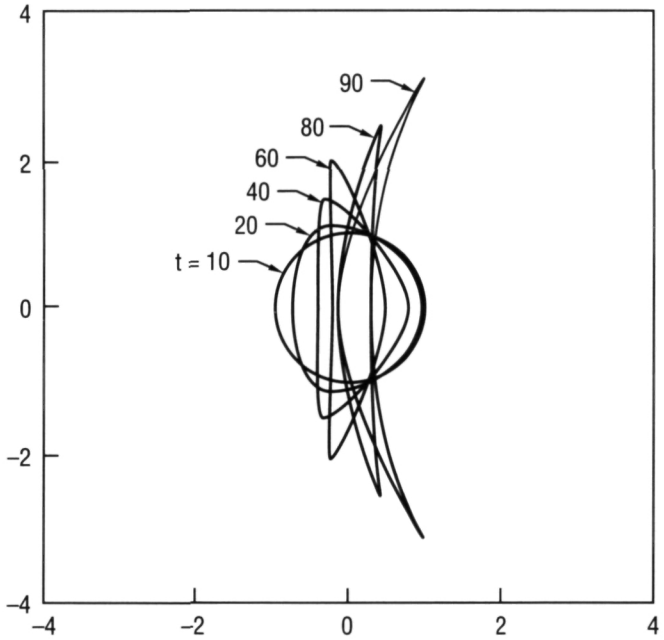

Figure 103. Spherical Drop Deformation at We = 10

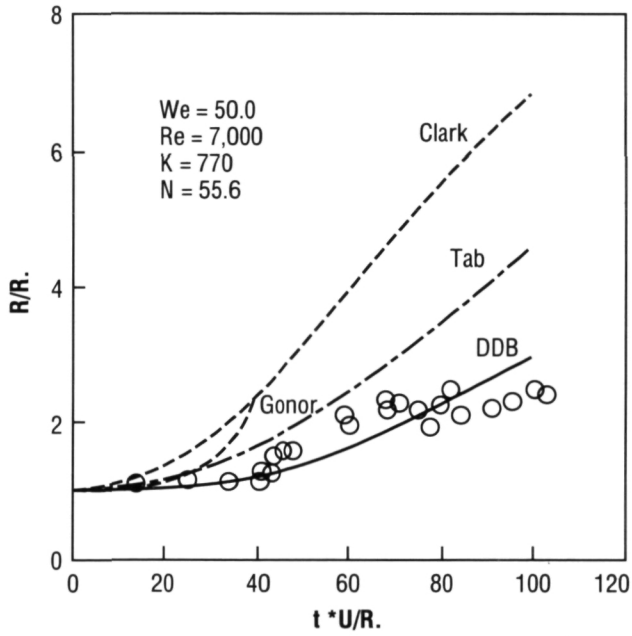

Figure 104. Comparison of Theoretical Predictions of Droplet Deformation and Breakup With Experimental Data of S.A. Krzeczkowski (1980)

between the analytical droplet deformation and breakup (DDB) method and experimental data is evident from figure 104. Initial steps have been taken to simulate the behavior of impinging jets analytically to support the development of rocket engines using hydrocarbon fuels and hypergolic propellants which perform most effectively with such injection mechanisms.

The analytical development effort is conducted by CFD Research Corporation in Huntsville, Alabama, under a Small Business Innovation Research contract NAS8-38425.

K.W. Gross/EP55
(205) 544–2262
Sponsor: Office of Aeronautics and Space Technology

Materials and Processes

Weld Process Modeling

Modeling of the **variable polarity plasma arc (VPPA) welding** process, which plays a major role in fabrication of the space shuttle external tank, was continued.

A computation relating weld-bead crown width and height, root width and height, and basic **VPPA welding** machine settings and material properties is in preliminary draft stage. Work has begun to incorporate this computation into a computer simulation. It is intended to incorporate a revised and verified version of this computation into a **VPPA** weld control system.

Work is continuing to relate workpiece geometry changes to equivalent **welding** heat source power changes and to determine equivalent power effects for different fixtures and workpieces.

A study on the effects of O_2, H_2, N_2 and CH_4 contaminants in weld gases at the 100- to 500-ppm level has been completed. A follow-up effort to develop a spectroscopic sensor for monitoring **welding**-arc contamination is beginning. A theoretical study evaluating a mechanism by which oxygen contamination may produce undercuts at the edges of a weld is almost completed; preliminary computations confirm the model. These studies will impact **VPPA** weld-process specifications and provide diagnostic support.

A theoretical effort to model the physics of the **welding** arc in sufficient detail to understand arc voltage changes encountered during polarity reversal in the **VPPA welding** system and to better understand the operation of low-pressure arcs supports studies of potential space **welding** processes.

An experimental study to evaluate a general model synthesizing the effects of a number of weld geometric and metallurgical parameters upon the tensile strength of a butt weld has been planned for the coming year. This study has potential for reducing weld-strength variability and thereby increasing allowable working stresses.

A.C. Nunes/EH42
(205) 544–2699
Sponsor: Office of Space Flight

Feasibility of Atomic Oxygen Interactions Accelerated Testing

Spacecraft which will be in **low Earth orbit (LEO)** will be subjected to reactive **atomic oxygen** atoms with an energy near 5 eV relative to the spacecraft. It is known that most materials will react with the oxygen, with some materials being very degraded in a short time in **LEO**. Because of the wide range of materials on spacecraft and the limited flight data, ground testing of materials to an **atomic oxygen** environment is necessary. However, it is very difficult to reproduce the **LEO** conditions in the laboratory. A study has been undertaken to quantify the difference in reactions between materials and **atomic oxygen** ions and neutrals at various energies in order to understand reaction mechanisms and establish relative rates of reactions. If accelerated testing in the laboratory can be performed reliably using 30-eV ions or neutrals instead of 5-eV ground-state neutrals, then laboratory testing for long exposure will be more practical. In order to accomplish this, the interaction mechanisms must be understood and the effects of ionization state and energy must be determined.

An **ion-beam** system with a grazing incidence neutralization process has been developed by Vanderbilt University for this study. Beams of ions and neutrals with variable energy from low energy to high energy are now routinely produced with this system. **Ion-beam** energies of only a few eV and neutral beams of just under 100 eV are now being produced. Most of the work to date has been performed using nitrogen or other gases due to the lifetime limits resulting from the use of oxygen exclusively during development and checkout.

Optical emissions of the surface exposed to the incoming beam, as well as the emissions of desorbed atoms, are examined in order to obtain data on the surface reactions. Laser-induced fluorescence is also used to determine the energy and temperature of the atoms which have left the surface. Some of the studies performed to date have shown that the optical spectra from surfaces show marked differences when exposed to **ion beams** or neutral beams. Detailed studies with **atomic oxygen** will only begin following complete operation and checkout of the system and studies with other gases of interest.

R. Carruth/EH12
(205) 544–7647
Sponsor: Office of Space Station

Long Duration Exposure Facility Experiments and Orbital Materials Interaction Studies

Materials selection for future space missions will be significantly influenced by the results of experiments exposed on the retrieved **Long Duration Exposure Facility (LDEF)**. Three **LDEF** experiments currently being subjected to intensive analysis in the Materials and Processes Laboratory of MSFC are providing results which are significantly extending the data base regarding environmentally sensitive materials for spacecraft thermal control, photovoltaic, and general purpose applications.

These three experiments include AO171, the Solar Array Materials **LDEF** Experiment; S0069, the Thermal Control Surfaces Experiment; and A0034, Atomic Oxygen Stimulated Outgassing. All three of these experiments were mounted on or adjacent to the leading edge of the **LDEF** for maximum exposure to the RAM-impacting **atomic oxygen** and orbital debris.

LDEF experiment AO171 includes a range of candidate solar-array materials, including solar cells, cover glasses with various antireflectance (AR) coatings, adhesives, encapsulants, reflector materials, substrate strength materials, mast and harness materials, structural composites, and thermal control treatments. The effects of the space environment on the specimens are being evaluated by comparison of preflight and postflight measurements of mechanical, electrical, and optical properties.

The battery-powered, active **LDEF** experiment S0069 measured the spectral hemispherical reflectance of selected thermal control specimens, providing (with calorimetric sensors) in-flight recorded values of solar absorptance and infrared thermal emittance. The active data is being analyzed, and the results compared to passively exposed specimens to differentiate environmental damage mechanisms, to separate the effects of

contamination from natural environment degradation, and for comparison, include selected thermal control coatings and optical materials in a configuration designed to provide more understanding of the role of **atomic oxygen** in the outgassing of molecular species from thermal control coatings.

Continuing analyses of the hardware, specimens, and sensors are providing the long-awaited extensions of material property degradation rates to long-term integrated exposure. Synergistic effects of **contamination** and the natural environment evidenced by unanticipated deposition and shadowing patterns may provide significant new information for analytical modeling of spacecraft molecular flow. The extensive range of phenomena observed and currently being analyzed on these **LDEF** experiments has broadened the scope of investigation to keep pace with the wider range of significant technical issues addressable.

A. Whitaker/EH11
(205) 544–1508
Sponsor: Research and Technology Office

In Situ Contamination Effects Study

The objectives of research with the in situ Contamination Effects Facility at MSFC are to experimentally relate the observed optical effects to **molecular contamination** growth kinetics for correlation with analytical modeling. Results of testing candidate materials for space application indicate that the useful range of acceptability for some materials can be extended by defining the critical temperature of an optical surface at which molecular deposition begins.

This in situ testing has been used to measure the time dependence of the bidirectional reflectance distribution function (BRDF) from molecularly contaminated optical surfaces at vacuum ultraviolet wavelengths. The specularly reflected and scattered light measurements have been accomplished in situ on optical surfaces in real time during the deposition of **molecular contaminants** generated by the heating of candidate materials. A microwave-excited krypton source has been used to provide noncoherent vacuum ultraviolet light, with the principal emission at 123.6 nm. Forward- and back-scattered light measurements are accomplished using an array of three solar-blind vacuum-ultraviolet-sensitive photomultipliers mounted in a plane in front of the exposed optical reflecting element.

The contamination study with the in situ facility is a joint endeavor by The University of Alabama in Huntsville and MSFC.

R. Linton/EH12
(205) 544–2526
Sponsor: Space Station Projects Office

Atomic Oxygen Ion Beam Neutralizer

Development of a low-energy neutral **atomic oxygen** beam source to screen materials for use in the low Earth orbit **atomic oxygen** environment has long been a priority for MSFC's Materials and Process Laboratory. Presently, MSFC has in operation a low-energy **atomic oxygen ion-beam** system, the **atomic oxygen simulation system (AOSS)**, used to study the effects of an **atomic oxygen ion beam** on materials. Because the effects of neutral **atomic oxygen** atoms impinging on materials may be different from those observed for ionic species, a method for neutralizing the atomic **ion beam** produced by the **AOSS** is being developed under contract by Vanderbilt University.

The neutralizer developed by Vanderbilt decreases the energy of the **AOSS ion beam** from 3 keV to 5 eV and reflects the **ion beam** from a metallic neutralizer plate. Because the **ion beam** strikes the neutralizer plate at a grazing incidence angle, the ions once neutralized will retain most, if not all, of their energy. A conceptual design of the neutralizer to be integrated into the **AOSS** is shown in figure 105. The screen at the front of the unit is used to reduce the energy of the incoming **ion beam** to the desired energy. The decel screen must be mounted near, and perpendicular to, the neutralizer plates to prevent the beam from expanding due to space charge effects before it reaches the plates. Because the trajectory of the ions is nearly parallel to the neutralizer plates, it causes the probability of the ions colliding with the neutralizer and being neutralized to be small. To overcome this problem, a row of neutralizer plates will be used to increase the neutralizing probability. Two grids are placed near the end of the neutralizer to keep charged particles produced during the ion/neutralizer plate interaction from impinging on the sample.

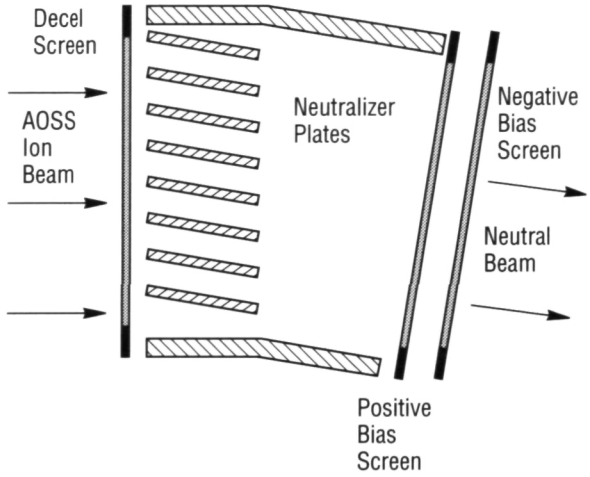

Figure 105. AOSS Neutralizer Conceptual Design

Preliminary tests during the past year, using a 20-eV nitrogen beam impinging on a molybdenum grazing incidence neutralizer at Vanderbilt demonstrated that the neutralizer does neutralize the beam without affecting the energy of the incoming ions. Furthermore, the tests indicate that the neutralization efficiency of incoming ions may be as high as 70 percent (i.e., 70 percent of the incoming ions are reflected as neutral atoms). A short test with oxygen was run and the results were similar to nitrogen. The integration of the neutralizer into the **AOSS** will be done at the start of FY91.

J.M. Reynolds/EH12
(205) 544–7651
Sponsor: Office of Space Station

Advanced Low Earth Orbit Atomic Oxygen Simulation System

The impingement of **atomic oxygen** atoms on materials in **low Earth orbit (LEO)** causes degradation of many materials, some severely. Because of the high cost of flying passive materials experiments aboard the space shuttle when a question of a new material's susceptibility to **atomic oxygen** degradation arises, a need for a ground-based system capable of simulating **LEO atomic oxygen** conditions exists. The development of an **Advanced Atomic Oxygen Simulation System (AAOSS)** with the purpose of simulating the **LEO atomic oxygen** environment has been underway during the past year at Princeton Plasma Physics Laboratory (PPPL) in cooperation with MSFC. The work completed during the past year included the initiation of neutral-beam energy testing, detection of low-energy **atomic oxygen** flux, and material testing.

The **AAOSS**, shown in figure 106, produces its low-energy beam by placing a metallic neutralizer plate in contact with a magnetically (3-4 kG) confined **plasma**. The oxygen **plasma** in the **AAOSS** is produced by a lower hybrid coaxial **plasma** source[1] which uses a 2.45-GHz radio frequency (RF) supplied at 1 kW to break down molecular oxygen gas. The neutralizer plate is biased negative of **plasma** potential to accelerate ions from the **plasma** toward its surface. Ions striking the surface of the neutralizer plate pick up an electron from the metallic plate and are neutralized. The energy of the neutral atoms reflected from the plate is determined by the difference in the voltage bias applied to the plate and **plasma** potential and the amount of energy lost during the elastic collision with the plate.

The flux of the **atomic oxygen** atoms in the **AAOSS** sample exposure region was measured using **atomic oxygen**-sensitive materials and a catalytic probe. These measurements verified the **AAOSS**'s ability to produce the flux levels in the range of $1x10^{15}$ to $1x10^{16}$ atoms/cm^2/s. Also, the flux measurements indicated a decrease of 11 percent in flux over a 12-cm (5-in) diameter beam.

Initial neutral beam energy measurements using argon and krypton plasmas produced an energy range of 4 to 20 eV depending on the bias voltage applied to the neutralizer plate. The energy measurements of the argon and krypton beams agreed with energy predictions from TRIM[2] which is a Monte Carlo code used to calculate the interaction of a particle with a surface. Attempts to measure low-energy neutral atoms produced from molecular gas species like nitrogen and oxygen have been unsuccessful to date. However, the TRIM code predicts that the **AAOSS** is producing low-energy (approximately 5 to 10 eV) **atomic oxygen** atoms. The emphasis of future work will be to produce experimental test data to verify these calculations.

Numerous materials have been tested to demonstrate the ability of the **AAOSS** to simulate the **LEO atomic oxygen** environment. A comparison of the reaction efficiency of materials exposed to **atomic oxygen** in **LEO** aboard STS-8 and STS-41G[3] agree with the reaction efficiencies of the same materials exposed in the **AAOSS**. Furthermore, the surface morphology of materials exposed to **atomic oxygen** in **LEO** is similar to the surface morphology of materials exposed in the **AAOSS**.

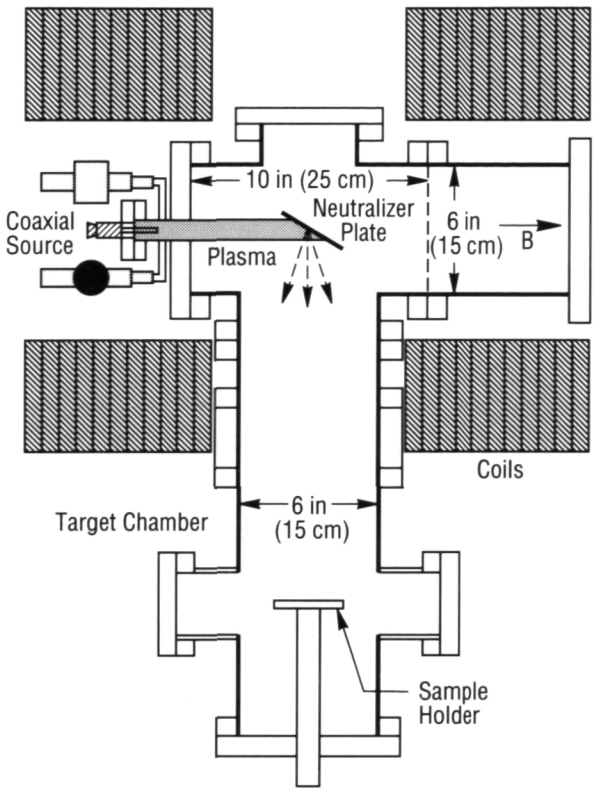

Figure 106. The Advanced Atomic Oxygen Simulation System (AAOSS)

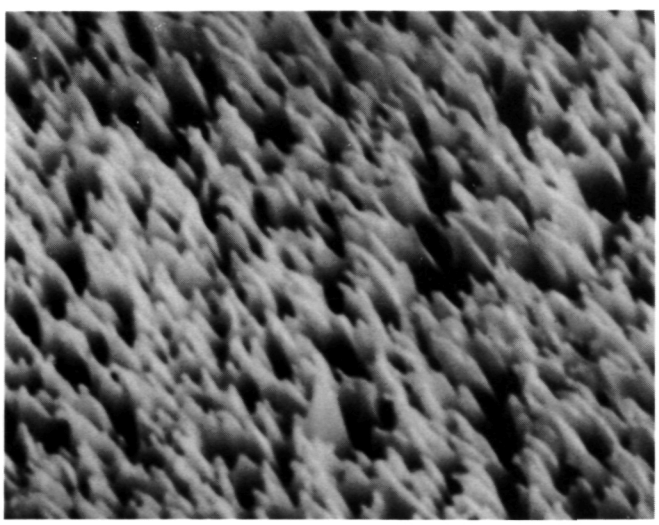

Figure 107a. Sample exposed to AO in the AAOSS

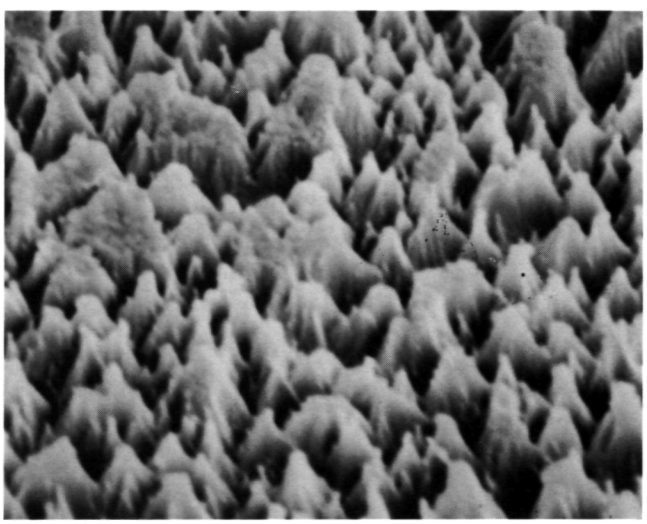

Figure 107b. Sample Exposed to AO Aboard Long Duration Exposure Facility (LDEF)

ORIGINAL PAGE
BLACK AND WHITE PHOTOGRAPH

Figure 107 is a comparison of the surface morphology of two separate samples of silver covered with 5 mils of FEP Teflon (Ag/FEP). Figure 107a is a sample of Ag/FEP exposed in the **AAOSS** and figure 107b is a sample of Ag/FEP which covered the Transverse, Flat-Plate Heat Pipe Experiment (S1005) aboard the Long Duration Exposure Facility (LDEF). The two photos show the same peaked surface morphology which has not been observed on samples of Ag/FEP test in ground-based **plasma** asher tests.

The results of the testing done to date indicated the **AAOSS** produces an accurate simulation of the **LEO atomic oxygen** conditions. Future work will concentrate on experiments to verify the energy of the neutral **atomic oxygen** beam.

[1]Motley, R.W., Bernabei, S., and Hooke, W.M., "Coaxial Lower Hybrid Plasma Source," *Review of Scientific Inst.*, 50 (1979) 1586.

[2]Biersack, J.P., and Haggmark, L.G., "A Monte Carlo Computer Program for the Transport of Energetic Ions in Amorphous Targets," *Nuclear Instrumental Methods*, 174 (1980) 257.

[3]Visentine, J.T., ed., "Atomic Oxygen Effects Measurements for Shuttle Missions STS-8 and -41G," NASA Tech. Memo 100459, 1988.

J.A. Vaughn/EH12
(205) 544–9347
Sponsor: Office of Space Station

Portable Spectroreflectometer

Increasingly complex and long-lifetime space missions require greater demands upon the performance of spacecraft materials. The spectral reflectance properties of materials used on space and ground systems are critically important to their design and operation; thus, there is a need to control manufacturing processes and to assess the effects of exposure of materials to ground handling and the space environment.

Current instruments for measuring spectral reflectance properties of materials do not offer the portability or the accessibility required for such operations on space systems and other extant or proposed assemblies while retaining the necessary high resolution. Therefore, research is underway to develop a portable integrating sphere **spectroreflectometer** to measure the spectral reflectance of extended surfaces and assemblies. This instrument will be usable as a **hand-held** device for ground and space application and will also be adaptable for remote use via a **remote manipulator system (RMS)**.

Figure 108. Space Application of a Portable Hand-Held Spectroreflectometer

Following research to develop the conceptual and functional design of a portable **spectroreflectometer**, the development of prototype instruments will ensue. The two **hand-held** prototype instruments will be field-tested to determine the suitability of the design for routine use by NASA and commercial users. The flight designs will be based on the ground prototype units, but will require alternate packaging to facilitate astronaut use and **RMS** interfacing. Such space-qualified flight versions of the portable **spectroreflectometer** will be required for future NASA long-term missions (such as Space Station *Freedom*), where astronauts must survey the condition of external spacecraft surfaces, like thermal radiators, solar arrays, and thermal insulation, to determine when on-orbit servicing of critical surfaces is needed (fig. 108).

J.K. Norwood/EH12
(205) 544–8281
Sponsor: Office of Aeronautics, Exploration, and Technology

Optically Stimulated Electron Emission for Bonding Surface Cleanliness Inspection

Optically stimulated electron emission (OSEE) is a nondestructive, noncontact surface **contamination detection** system capable of detecting thin-layer contamination down to the angstrom level. **OSEE** equipment has been used to inspect solid rocket motor (SRM) critical-bonding surfaces for contamination. The **OSEE** phenomenon, which uses photoelectron emission, is caused when **ultraviolet (UV)** light is incident on the specimen surface. Photoelectrons released from the surface are detected with a biased collector close to the surface. This signal from the surface may increase or decrease depending on the type and thickness of contaminant. Substrate materials must be photoemitting at the **UV** energies used.

An extensive **OSEE** equipment characterization effort has been underway since 1988. Characterization work completed includes determination of temperature and humidity effects on equipment and substrates; magnetic/electrostatic effects on substrate response; variations in equipment set-up parameters including sensor gain, surface to sensor gap, controller balance setting, and line voltage; and effects due to substrate variations in steel, aluminum, and composites.

A prototype end-effector to demonstrate the feasibility of automatic surface quality inspection was developed. The three-axis end-effector allowed the **OSEE** sensor to maintain the proper distance from and orientation to a flat or curved surface. Special supporting software was written for data acquisition and real-time display.

H. D. Burns/EH12
(205) 544–2529
Sponsor: Joint support from Redesigned Solid Rocket Motor and External Tank Programs

Impact Damage Tolerance of Composite Laminates

Foreign object impact damage to carbon fiber laminates is a very important issue concerning the use of these high-strength/high-modulus, lightweight materials. Poor impact resistance can exclude an otherwise very attractive material for use in many applications. A continuing mission of the Polymers and Composites Branch at MSFC has been to identify and characterize **carbon-fiber** composite systems with enhanced impact resistance. The most recent phase of this mission has been concentrated on studying toughened epoxy-matrix systems.

During the past year, instrumented drop-weight **impact testing** has been performed on a variety of carbon/epoxy systems. The typical testing procedure consists of laying up 16-ply $[0,+45,-45,90]_{s2}$ laminated plates with prepreg material made of the carbon/epoxy system to be tested and impacted with a Dynatup 8200 instrumented drop-weight apparatus. The drop height ranges from 8.9 cm (3.5 in) to 122 cm (48 in) with a drop weight ranging from 1.2 to 1.8 kg (2.6 to 4.0 lb). This enables a range of impact energies from 1.0 to 21.0 J (0.7 to 15.5 ft•lb) to be used. The impactor consists of a semi-spherically ended steel rod 1.27 cm (.5 in) in diameter and the specimens are clamped over a 7.6-cm (3-in) diameter hole. After impact, the maximum load during the impact event and total absorbed energy are recorded. The specimens are then cross-sectioned with a diamond wafering blade through the point of impact to be examined and photographed with a stereo-optical microscope to determine the extent and modes of damage.

The superiority of the new, toughened carbon/epoxy systems can be seen in figure 109. The standard T300/934 (untoughened) system sustained severe delaminations and fiber breakage at 7.1 J (5.2 ft•lb) of impact energy, whereas the other three systems shown fared much better. Examination of cross-sectioned specimens has proven to be a simple, inexpensive method of characterizing the damage

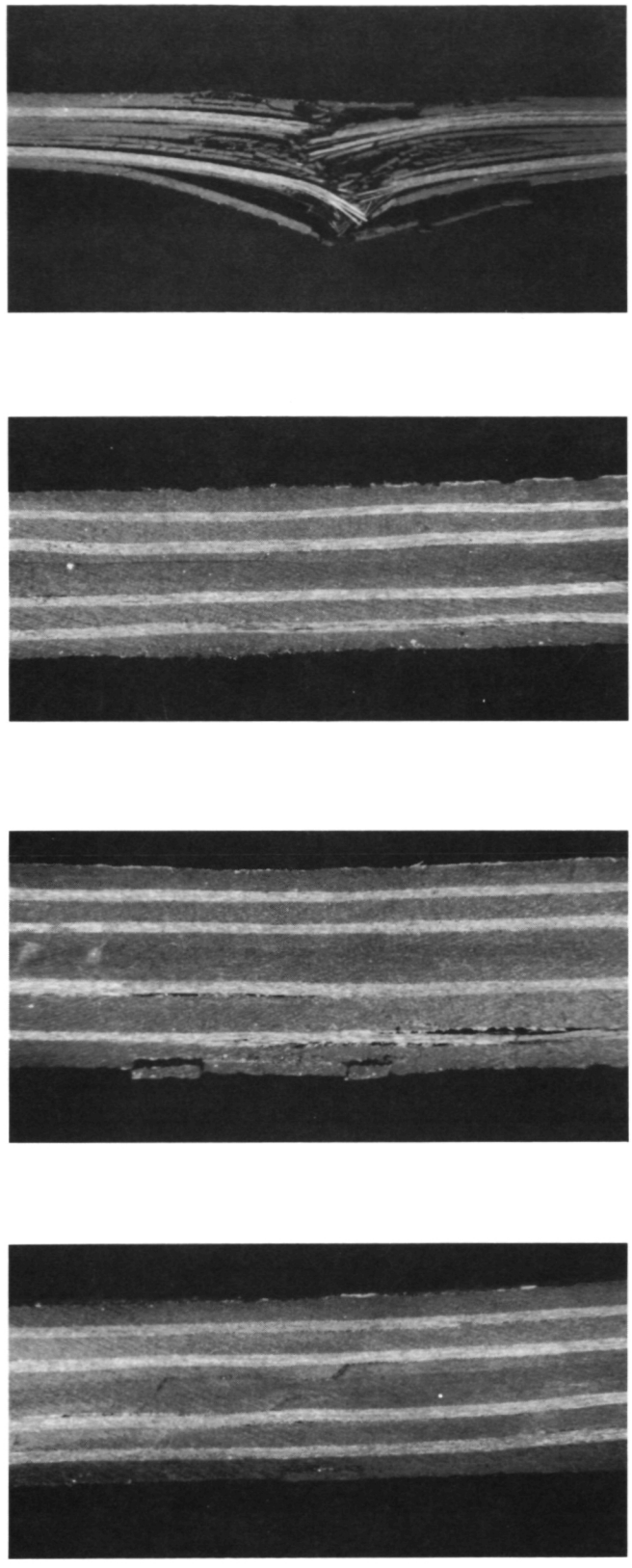

Figure 109. Cross-Sectional Views of 16-Ply Quasi-Isotropic Carbon/Epoxy Composite Laminated Impacted at 7.1 J (5.2 ft•lb.)

ORIGINAL PAGE
BLACK AND WHITE PHOTOGRAPH

in an impacted composite material, thus giving a good idea as to which materials will perform best after an impact event of a given energy level.

The instrumented impact data that is output after each impact event can also be used to help determine a material's impact resistance. A plot of maximum load of impact versus impact energy can determine the maximum load the material can withstand before fiber breakage occurs. Typically, this plot follows a linear relationship until a critical impact energy level is reached, at which point the maximum load values remain fairly constant as impact energy is further increased thus indicating fiber breakage. A maximum load-impact energy plot of five different material systems is shown in figure 110. Here again, the superiority of the new toughened systems over the T300/934 can be clearly seen. The untoughened T300/934 material can only withstand about 2,500 N (560 lb) of force whereas the other systems can withstand between 4,000 N (900 lb) (IM7/1939-3) up to 6,000 N (1,350 lb) (IM7/1962).

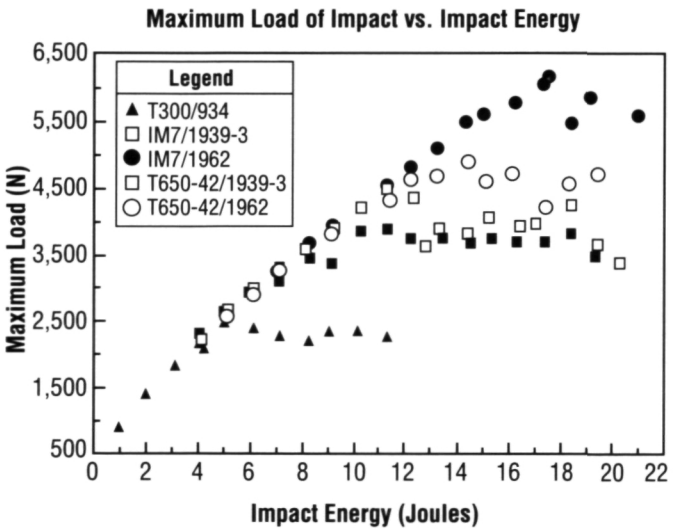

Figure 110. Maximum Load of Impact vs. Impact Energy

Using instrumented impact data and cross-sectional examination techniques to aid in determining a material's impact resistance is a quick, inexpensive, and relatively simple way of supplementing residual property data. These techniques can be used on any material, and, as this task has progressed, some thermoplastic matrix and hybrid **composite materials** have also been examined. The development of a complete data base on impact damage tolerance capabilities of many **composite materials** is being pursued by the Polymers and Composites Branch at MSFC.

A. Nettles/EH33
(205) 544–2677
Sponsor: Space Station Projects Office

Development of Low Thermal Conductivity PAN-Based Carbon Fibers For Solid Rocket Motor Nozzle Applications

Continuous filament viscose rayon has been the primary precursor for **carbon fibers** utilized in solid rocket motor (SRM) **nozzles** and heat shield materials. Due to the instability of the rayon industry, and also due to the desire for improved performance from **ablative materials**, various investigations have been initiated during the previous 15 years to evaluate alternate precursors, principally **peroxyacetyl nitrate (PAN)** fibers. The critical disadvantage for SRM applications, inherent in the current **PAN** fibers, is a thermal conductivity significantly higher than that of rayon-based fibers. This property results in deeper char, requiring increased liner thickness to maintain thermal margins of safety. Further, **PAN**-based ablatives have higher densities than comparable rayon-based ablatives, thus resulting in increased **nozzle** weight. Because of this disadvantage, attempts have been made to produce a low-thermal conductivity **PAN**-based **carbon fiber**. The program plan and early fiber characterization results for the on-going development are described in this report.

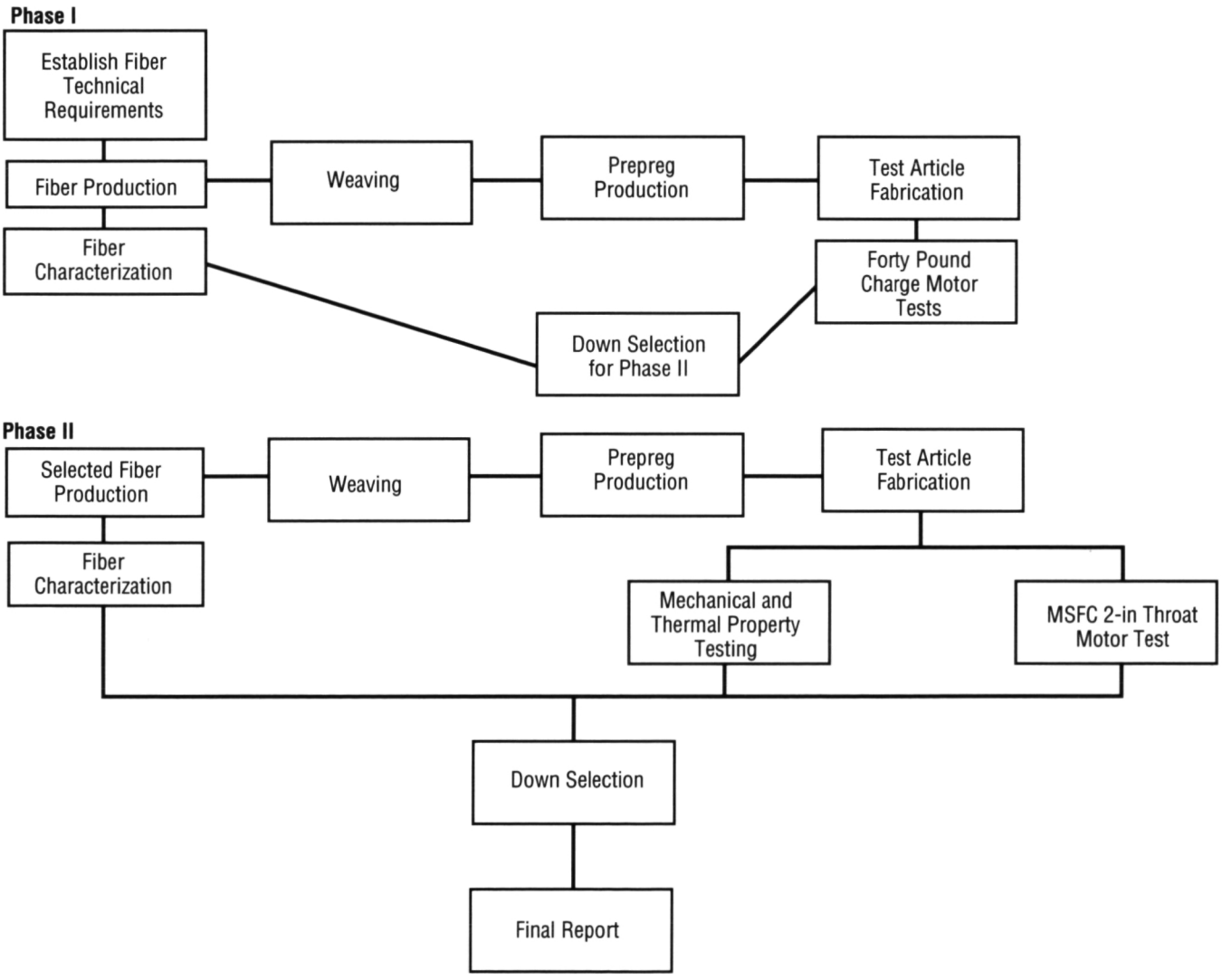

Figure 111. Low Thermal Conductivity PAN Fiber Development

A two-phased approach for development and evaluation of the **PAN**-based **carbon fibers** has been defined as shown schematically in figure 111. Technical requirements were defined by a multidisciplinary team comprised of **nozzle** designers, analysts, and material engineers representing both industry and government agencies. These properties, with the desired level and minimum values, are presented in table 6. Thermal conductivity is the highest priority requirement. Electrical resistivity is used as a quantifier for fiber thermal conductivity as it is a much simpler property to obtain. The remaining properties were not prioritized. Instead, emphasis was placed on understanding the goals, rationale, and trades by the team and all participating carbonizers. A more thorough discussion of the issues associated with each property is provided by Clinton and Pinoli.[1]

Four carbonizers elected to participate in the development program—Amoco, Textron Speciality Materials, BASF/Celanese, and Hercules. Each produced 20 lb (9 kg) of two candidate fibers. The fibers were then woven into a five-harness satin fabric by Textile Products Division of Ketema, and impregnated with SC 1008 phenolic resin and high-purity carbon filler by Fiberite. Sufficient quantities of the prepreg materials have been provided to Thiokol Corporation/Wasatch Division for fabrication of 40-lb-(18-kg-) charge (FPC) motor **nozzle** test sections. These subscale motor tests were scheduled for the summer of 1990.

Characterization of each of the eight candidate fibers is nearing completion. Preliminary results presented by Pinoli[2] are summarized as follows. Electrical resistivity values varied from approximately 60 micro-ohm meters to values exceeding 60,000 micro-ohm meters. Carbon assay ranged from 75–85 percent, and moisture absorption capacities were measured from 3.5–9 percent. Fiber densities were in the range from 1.75 grams/cubic centimeter (g/cc) to 1.80 g/cc, as expected, with the exception of the Textron Avcarb G candidate (1.65 g/cm^3). Strength and modulus values were in excess of 300 ksi and 21 Msi, respectively, again with exception of Avcarb G which exhibited a strength of 190 ksi and modulus of 10.5 Msi.

Table 6. MSFC M&P Laboratory Alternate Ablative Materials Descriptions

Priority	Fiber Property	Desired Level	Minimum Properties
	Electrical Resistivity	>70 μohm-m	50 μohm-m
Identified Significant Characteristics			
	Oxidation Rate	≤Rayon	Measure Response, Ea&A
	Alkalai Metal Content	Ultrapure Precursor	1,000 ppm of Na Equivalents
	Moisture Adsorption Capacity	Low	<6 w Percent
	Density	<1.50 g/cm^3	<1.80 g/cm^3
	Thermal Shrinkage (to 2,500 °C)	Low	Measure Response
	Carbon Assay (C, N, H)	High	80 w Percent
	Tensile Strength	High	>200 ksi
	Tensile Modulus	Low	<30 msi

In concluding this status report, it is noteworthy that one candidate (Hercules R879-02) is presently under evaluation by Hercules as a rayon replacement in the development of the Titan IV SRMU **nozzle** for the Air Force. It is also emphasized that the reductions in conductivity have been achieved primarily through decreasing the temperature in the fiber carbonization process. No attempt has been made to improve properties for ablative applications through innovations in earlier fiber processing steps or at the precursor level. Research at these levels is being proposed for a long-term development program.

[1]Clinton, R.G., and Pinoli, P.C., "Development of Low Thermal Conductivity PAN-Based Carbon Fibers for Solid Rocket Motor Nozzle Application." Ann. Rept., NASA Contract NAS8-37801, November 1989.

[2]Pinoli, P.C., "SPIP Low Thermal Conductivity PAN Fiber Program-Preliminary Fiber Assessment and Review," presented at SPIP Quarterly Review, MSFC, Alabama, February 1990.

R.G. Clinton/EH34
(205) 544–2682
Sponsor: Office of Space Flight

Alternate Ablative Material Development for Solid Rocket Motor Nozzle Applications

During the phase B pre-proposal activities for the advanced solid rocket motor (ASRM), the Materials and Processes Laboratory initiated an advanced development program to evaluate candidate ablative material systems for the ASRM **nozzle**. Initially, technical interchange meetings were held with **carbon fiber** and fabric producers, **carbon phenolic** prepreg suppliers, **solid rocket motor (SRM) nozzle** analysts and fabricators, and materials engineers. Recommendations were also requested and received from industry prime contractors participating in the ASRM phase B effort. After evaluation of available information, the most promising material systems were selected for evaluation. Both rayon-based and peroxyacetyl nitrate- (**PAN-**)based carbon fabrics were evaluated, and these are listed and described in table 7 (materials 3–10). Materials 1 and 2 are the obvious redesigned solid rocket motor (RSRM) baseline prepregs. Materials 11–13 were subsequently added to the program to support the Solid Propulsion Integrity Program (SPIP) **PAN**-based **ablative materials** development.

Several of the rayon-based materials represent advancements in the state-of-the-art for prepreg materials. The MX4996 and MXG275 prepregs were constructed from "post-woven" carbon fabrics produced by weaving carbonized yarns. This approach differs from the standard carbonized fabric manufacturing in which rayon yarns are first woven into a fabric and the entire fabric is carbonized. The post-weaving process eliminates many variabilities inherent in carbonized fabrics such as weave distortion, nonuniform areal weight, and bag. The other advanced material is MX4989. Although a carbonized fabric, the production process incorporates statistical process control as well as other improvements made by Amoco to enhance the quality and uniformity of the fabric. Further, the fabric is impregnated with phenolic resin using film-on-fiber technology for improved control of resin content and advancement.

Table 7. MSFC M&P Labortory Alternate Ablative Materials Descriptions

	Product	Fiber	Heat Treat[1]	Weave	Resin	Filler	Weave/Prepreg
1.	MX4926	Rayon-CSA	1,350 °C	8HS	SC1008	Carbon	Fiberite
2.	FM5055	Rayon-CCA-3	1,350 °C	8HS	9ILD	USP28	US Polymeric
3.	MX4926VCK	Rayon-VCK	1,600 °C	5HS	SC1008	Carbon	Fiberite
4.	MX4989[2]	Rayon-VCX-13	1,650 °C	5HS	SC1008	High Purity Carbon	Fiberite
5.	MX4996[3]	Rayon-W2526	1,700 °C	5HS	SC1008	High Purity Carbon	Fiberite
6.	MXG275[4]	Rayon-W2508	2,600 °C	5HS	SC1008	High Purity Carbon	Fiberite
7.	FM5014	Rayon-WCA	2,600 °C	PLAIN	9ILD	USP28	US Polymeric
8.	FM5879D	PAN-Hitex 6 k	1,650 °C	5HS	9ILD	USP28	US Polymeric
9.	FM5834B	PAN-Hitex 12 k Heltra Spun Yarn	1,650 °C	8HS	9ILD	USP28	US Polymeric
10.	MX134LDC	PAN-T300/3 K	1,250 °C	PLAIN	SC1008	Carbon Microballoons	Fiberite
11.	MX4922	PAN-AS4	1,250 °C	5HS	SC1008	High Purity Carbon	Fiberite
12.	MX4952	PAN-T350/35XLD Heltra Spun Yarn	1,650 °C	5HS	SC1008	High Purity Carbon	Fiberite
13.	MX4963	PAN-T350/35XLD Heltra Spun Yarn	1,650 °C	5HS	FF26	High Purity Carbon	Fiberite

Footnotes

(1) Carbonization temperatures for the rayon-based materials are approximate. Exact tempertures are proprietary

(2) This product is impregnated using film on fiber technology. The fabric is claimed by Amoco to be their highest quality carbonized fabric.

(3) The fabic used in the product is woven from carbonized rayon yarns (5 plies of 1,650 denier yarn). It is commonly referred to as post-woven fabric.

(4) This fabric is also post-woven. Yarns are 5-plied 1,100-denier yarns.

The evaluation program consisted of three phases: (1) prepreg material characterization, (2) processing assessment, and (3) mechanical and thermal property generation. Standard RSRM acceptance tests, resin flow, constituent and volatile contents, and alkali metal content, were performed on material at specific intervals throughout the rolls of prepreg. Additional characterization tests were conducted on sections from the head of each roll. Objectives of the second phase were to assess the processability of each material in terms of handleability, thermal response during cure, and tag-end acceptance data. Thermocouples were embedded in a simulated ring section to provide data for correlation with analytical predictions made using the thermochemical cure model and to enable refinements to the model for constituent effects (fabric conductivity) on the thermal profile. Screening-type (level 1 data base) mechanical and thermal properties are being generated by Southern Research Institute on all materials. Properties sufficient to comprise a data input set for comparative level thermostructural analysis (level 2 data base) are being developed for MX4996, FM5879D, and FM5834B.

Results from the prepreg evaluation indicate that the MX4989 exhibited the greatest uniformity of all materials tested. The MX4926VCK also was quite consistent. Postweaving of the carbonized rayon yarns yielded improved reproducibility and uniformity when compared to the baseline prepregs; however, roll-to-roll variability was higher than expected. Results from the remaining phases of the investigation will be reported in 1991.

Benefits from this program have been and will continue to be most significant for the NASA SPIP and ASRM programs. The postwoven materials and VCX-13 fabric characterized in this effort figure prominently in the ASRM material development plan. The data base for preliminary ASRM **nozzle** design is also being provided by this program. All **PAN**-based materials are currently under evaluation in the SPIP task and either have been or are scheduled to be fired in the MSFC 2-inch throat solid rocket test motor. Further, results of this work are contributing to the evaluation and downselection of a **PAN**-based ablative material for the Air Force Titan IV SRMU **nozzle** being developed by Hercules.

R.G. Clinton/EH34
(205) 544–2682
Sponsor: Office of Space Flight

Diamond Film Production Using an Oxyacetylene Torch

Continuous films of **diamond** offer a number of outstanding materials properties each with practical application in aerospace systems. **Diamond** boasts the highest hardness and the highest room temperature thermal conductivity of any known material. **Diamond** also possesses a small coefficient of thermal expansion and a low coefficient of friction.

Frequently, the dimensions obtained with plasma deposition systems are too small to be of practical use in aerospace applications. Recently, a number of laboratories have demonstrated the ability to deposit thin **films** of **diamond** using an oxyacetylene torch. This technique holds the promise of allowing deposition of continuous large-area coatings. Large-area **films** have not yet been produced, even on a laboratory scale. Our research is directed toward understanding the processes underlying the nucleation and growth of these **films** and using the results to produce large-area continuous **films**.

The schematic shown in figure 112 illustrates the intended setup for baseline production of continuous **diamond** films. **Films** are produced by obtaining the necessary gas mixture ratio with the mass flow controllers and then maintaining the sample in the narrow temperature region by use of the chill block, the optical pyrometer, and the relative distance from the torch tip to the sample surface. Only a narrow range of positions is allowable for the torch-to-sample distance, further limiting the system. Concurrent with obtaining and setting up the system, we hope to produce small-area **films** under conditions which will allow increases in quality and types of available substrates for deposition. We are setting up a microcomputer-controlled deposition system to permit processed feedback signals to control the deposition of the **films**.

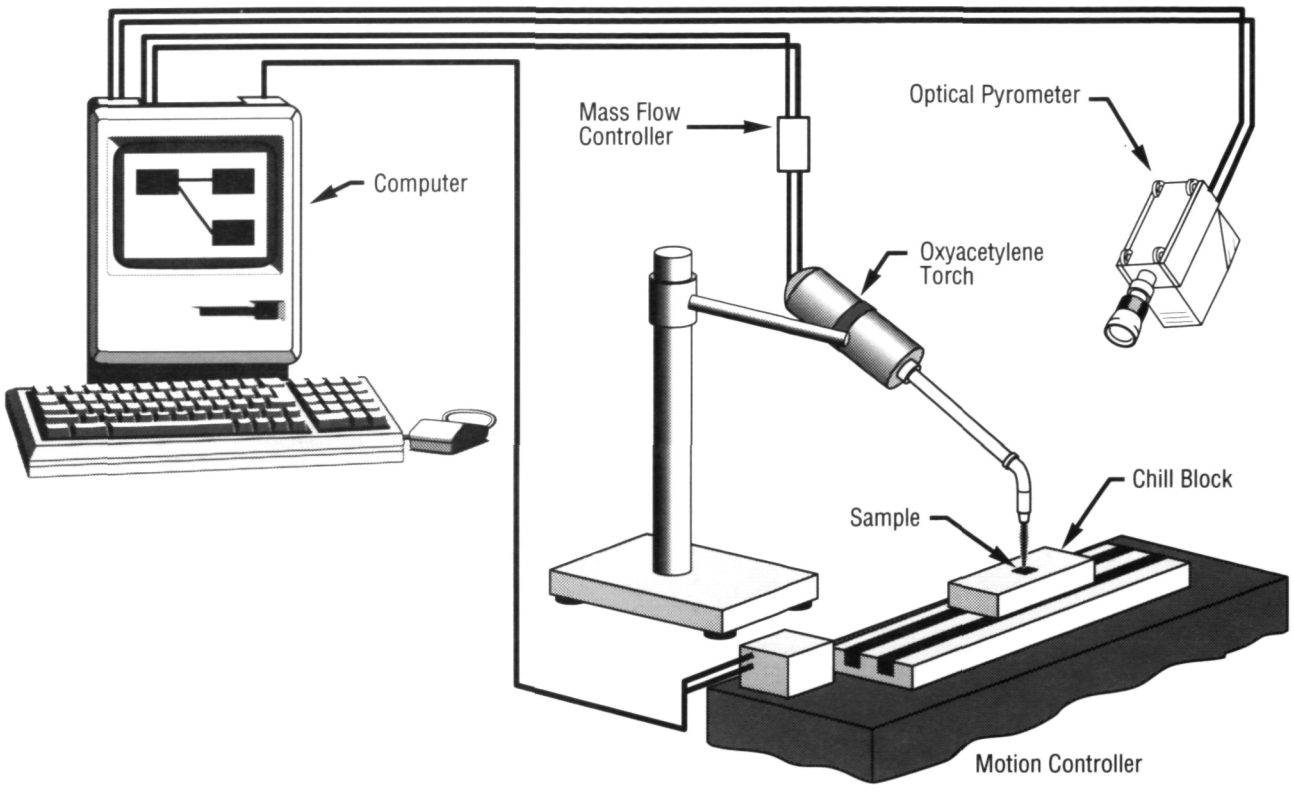

Figure 112. Continuous Diamond Film Production Schematic

Using a preliminary setup, comprised of simply the mass flow controllers and a thermocouple, we have reproduced some of the encouraging torch work reported in the literature. We have produced small islands of pure **diamond** crystals. During the next 6-month period we hope to produce small-area continuous **films** on a variety of substrates.

Large area **diamond films** have applications in such diverse applications as micrometeriod impact resistant windows, turbine blade edge coatings, cooling tube coatings, and nozzle and reentry surface coatings.

F. Roberts/EH34
(205) 544–1967
Sponsor: Office of Space Flight

Industry Advisory Committee Established for Carbon Phenolic Constituent Test Methodology and Specifications

There have been several failures and/or anomalies in past firings of solid rocket motors (SRM's) utilized in space efforts. These problems were mainly in the nozzle area. Postflight failure analysis of the nozzles revealed large variability in the finished product due to lack of strict standards for the materials and processes utilized in this technology. This led to a review of the state-of-the-art design, manufacturing, testing, and acceptance criteria for SRM's and nozzles. This review revealed that although some improvements in the technology base have been made over the past few years, too much of the technology is empirically based.

In order to improve the reproducibility, reliability, and uniformity of **SRM nozzles**, an industry advisory committee has been established to review and refine the specifications and test methodology of **carbon-phenolic composite** materials utilized in the manufacture of the **SRM nozzles**.

The committee meets twice a year, and is chaired by Dr. William B. Hall, professor at Mississippi State University (MSU), currently under a research grant with MSFC entitled, "Standardization of the Carbon-Carbon and Carbon-Phenolic Materials." Committee members are persons under current NASA contracts who provide carbon-phenolic constituents up through and including the carbon phenolic **prepreg**. The objectives of this committee are as follows:

- Assess current constituent testing methodology for relevancy, test accuracy, and precision
- Identify and prioritize study tasks
- Perform analytical studies in support of tasks under advisement
- Coordinate round-robin testing
- Provide specification and test methodology recommendations to the domestic solid rocket propulsion industry
- Publish study results in biannual reports.

An executive Committee has also been established to ensure that the objectives listed above are met. This committee consists of the following individuals: Dr. William B. Hall, Chairman (MSU); Pat C. Pinoli, independent laboratory support (Lockheed, Palo Alto Research Lab); and Lou Ann Fikes, NASA/MSFC focal point.

One task undertaken by the industry advisory committee was to study the processing parameter effects on the oxidation mass loss for carbon fabrics. The results shown in figure 113 clearly indicate that the rate of mass loss at a specified temperature is a function of the fabric carbonization process.

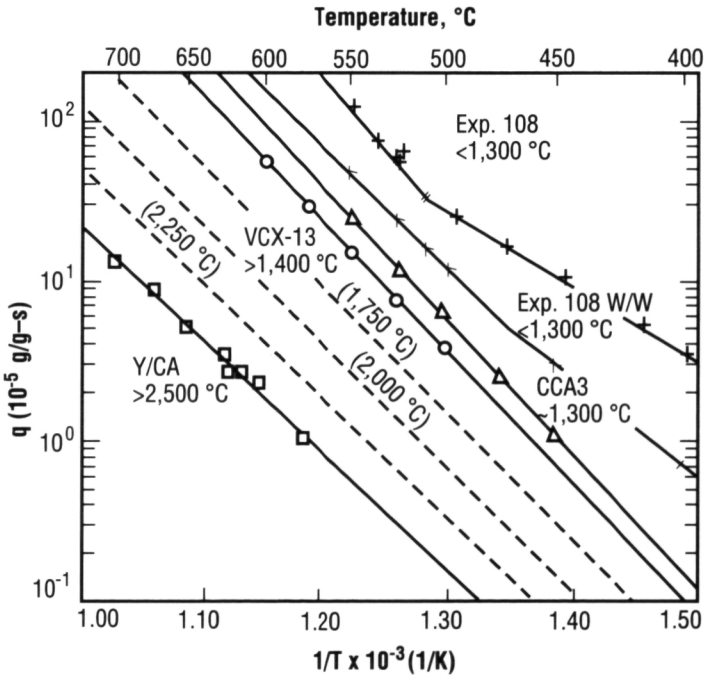

Figure 113. Testing Carbon Fabric for Oxidation Mass Loss

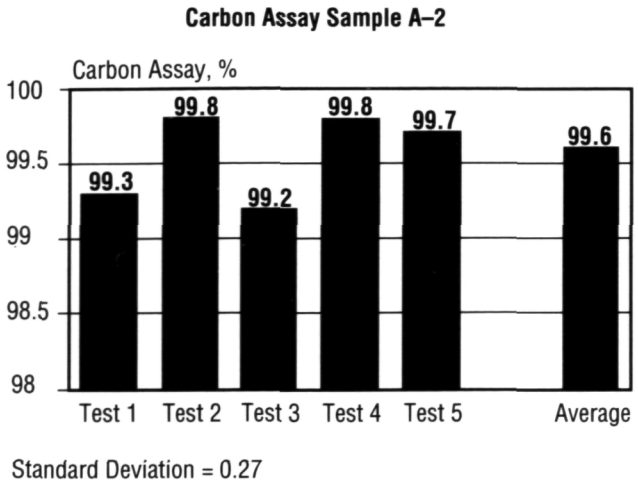

Figure 114. Carbon Assay Results

Another task undertaken by the committee was to evaluate the current test method for carbon content of the carbon fabric. It was found with round-robin testing that reproducibility was excellent within laboratories, but unacceptable between laboratories. The results of the carbon assay of one carbon fabric in one laboratory is shown in figure 114.

The difficulty between laboratories was found to be in the standards used to calibrate the carbon assay equipment. Work is underway to find an acceptable standard to be used in all laboratories to calibrate their equipment.

Other studies underway include:

- Phenolic resin advancement
- Carbon assay
- Rayon yarn specifications
- Sodium level test procedures
- Product identification code procedure for **prepregs**

L.A. Fikes/EH34
(205) 544–2599
Sponsor: Office of Space Flight

Prepreg Properties and Process Relationships to Microstructure in Carbon-Phenolic Laminates

A significant result of a prior investigation[1] of the effects of process parameters on the mechanical and thermal properties of **carbon-phenolic** materials was that materials which had been cured (final hold temperature) in the range of 168–174 °C (335–345 °F) exhibited microcracks within the yarn bundles. Those materials cured at the standard final hold temperature of 154 °C (310 °F) did not exhibit microcracks. The microcracking resulted in a decrease in the across-ply tensile strength, but did not affect the modulus, indicating reduced strain capability.

Subsequent investigations of **microstructure** (by Southern Research Institute) for other **carbon-phenolic** materials cured in excess of 174 °C (345 °F) have indicated that factors other than final cure temperature may influence microcracking. It was postulated that prepreg properties might be coupled with cure temperature in governing material response with respect to propensity to microcrack during cure. An investigation of the microcracking phenomenon was initiated in the Materials and Processes Laboratory. The objective of the investigation was to evaluate the effect of selected levels of advancement of prepreg resin and selected final cure temperatures on the propensity of **carbon-phenolic** laminates to form microcracks during cure, and to access the subsequent effect on physical and mechanical properties of the test articles.

Standard shuttle redesigned solid rocket motor (RSRM)-grade **carbon-phenolic** prepreg material (FM 5055B) was selected for evaluation, as it had been studied in the earlier program. A total of nine flat panels of dimensions 22.9×22.9×2.5 cm (9×9×1 in) were fabricated. The panels were constructed from prepreg material which had been staged at 77 °C (170 °F) to obtain three different levels of advancement, as measured by flow tests. The as-received material had a nominal resin flow of 18 percent. This material was staged to achieve

nominal 12- and 6-percent resin flow levels. Three panels were constructed from material at each flow level. Resulting panels were cured at three temperatures, 154, 166, and 177 °C (310, 330, and 350 °F) for a full factorial matrix of two variables at three levels. All panels were cured in a hydroclave following the standard RSRM throat ring cycle, with exception of final cure temperature. Panels to be cured at the same final temperature were cured simultaneously using the trilateral fixture to minimize variations.

Resulting cured laminates were nondestructively inspected using digital ultrasonics. No clear differences among the panels were apparent. However, some subtle distinctions were observed. The data is being further evaluated in an attempt to quantify the results. The panels have been provided to Southern Research Institute where the first phase of a two-phased characterization program is in progress. In the initial phase, additional **nondestructive evaluation** is being performed, and results will be correlated with a comprehensive **microstructural** evaluation. In the second phase, mechanical, physical, and thermal property tests will be performed to assess the effect of **microstructure** on these properties. The results of the characterization will be reported in 1991.

Clinton, R.G., "Carbon Phenolic Material for Solid Rocket Motor Nozzles," MSFC Research and Technology, 1987.

R.G. Clinton/EH34
(205) 544–2682
Sponsor: Office of Space Flight

Mechanical Property Testing of Tag Ends

Routine acceptance testing is a necessary part of flight qualification. Acceptance tests must be relatively quick, reproducible, and yield consistent results. Data obtained from the acceptance tests are used to verify component compliance to established limits and are added to the historical data base of the process and materials.

During the solid rocket motor (SRM) redesign effort, a research program was initiated to investigate acceptance test methodology in order to standardize existing test procedures and to develop improved test methods. Potential improvements to the existing compressing strength acceptance test were identified in two of the **mechanical property tests**. These two tests, **across-ply tensile (APT)** and **double-notch shear (DNS)**, are being developed and evaluated.

Initial test method development has identified problem areas in conducting **APT** and **DNS** tests. One problem area identified was test specimen design. Because the test specimens are machined from **tag-end** material, the test specimen design is restrained by the component **tag-end** configuration. The industry standard **DNS** specimen design used by Southern Research Institute (SRI) is easily adapted to **tag ends** (fig. 115). Therefore, the specimen and test fixture designs utilized by SRI were selected for further development. However, SRI's standard **APT** specimen design was too large for the available **tag-end** sections. The available **tag-end** sections limited the **APT** specimens to approximately 1.9 cm (0.75 in). The size restriction on the **APT**

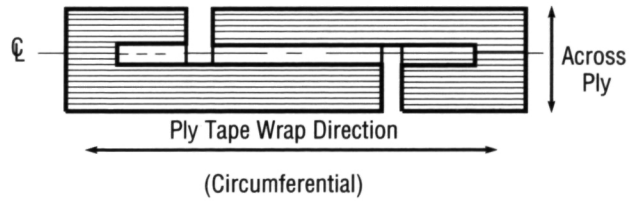

Figure 115. Double-Notch Shear Test Specimen

specimens created an additional concern: maintaining a representative cell size in the specimen gauge section. Significant stress concentrations in the transition region can develop, and this can lead to poor results. Design iterations using the finite element method (ANAYS) were used to develop the optimal specimen configuration, which minimized the stress concentration area. Along with the optimal specimen configuration, an improved test fixture was designed to ensure uniaxial loading. The fixture was improved by modifying a chain and clevis setup. This modification minimized off-axis loading.

Initial **APT** tests yielded results that were in reasonable agreement with test data generated by SRI. However, during further testing, the specimens began to debond from the steel sample rod holders before breaking in the test gauge section (fig. 116). A review of the bonding, machining, nondestructive evaluation (NDE), and handling procedures has begun to determine possible causes for the debonding. Also, aluminum and graphite pull rods are being fabricated and tested as possible replacement material for the steel.

Initial **DNS** tests of carbon phenolic material yielded results that were approximately 40 percent higher than accepted SRI properties. The identified problem was that the clearance between the test sample and the test fixture was below the recommended tolerance used by SRI. The test fixture has been modified and shims have been implemented to reduce friction. Results using the modified fixture and shims have been in reasonable agreement with data generated by SRI. Additional development and qualification tests are in progress.

Evaluation efforts for both mechanical tests include time span and cost analysis, data quality assessment, and data base generation on redesigned solid rocket motor (RSRM) nozzle component **tag ends**.

Clinton, R.G., "Redesigned Solid Rocket Motor Composite Material Testing." Research and Technology, 1989.

S.W. Tillery/EH34
(205) 544–8651
Sponsor: Office of Space Flight

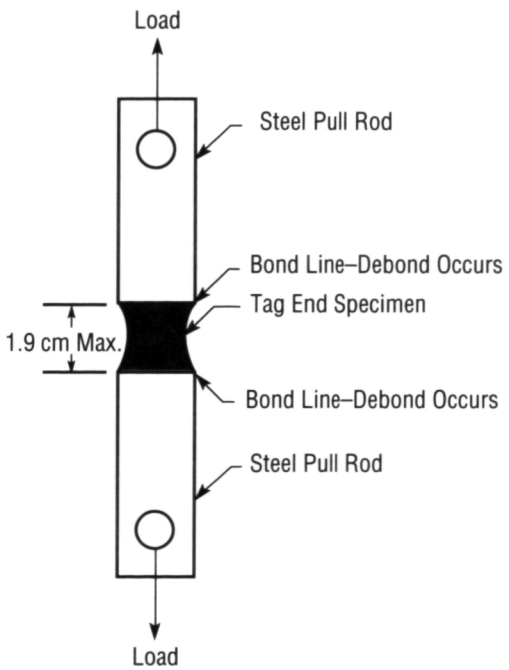

Figure 116. Debond of Test Specimen From Pull Rod

High Heat-Flux Testing Using the Plasma Torch Test Bed

The **Plasma Torch Test Bed (PTTB)** is a low-cost laboratory-scale means of performing **high heat-flux** material evaluation. The system (fig. 117) is made up of a Metco plasma arc spray gun and a load application system. The load system consists of a hydraulic jack, load cell, and steel frame. A standard test calls for a 2.54×2.54×5.08 cm (1×1×2 in) sample to be placed in the load frame and the desired load (from 0 to 6,895 kPa) applied. The torch is started and brought up to the proper power level and then moved onto the sample for the desired test duration (usually 10 s). The tests are typically performed at heat fluxes of 17.0×10^6 to 22.7×10^6 J/m^{2}s (1,500 to 2,000 Btu/ft^{2}s).

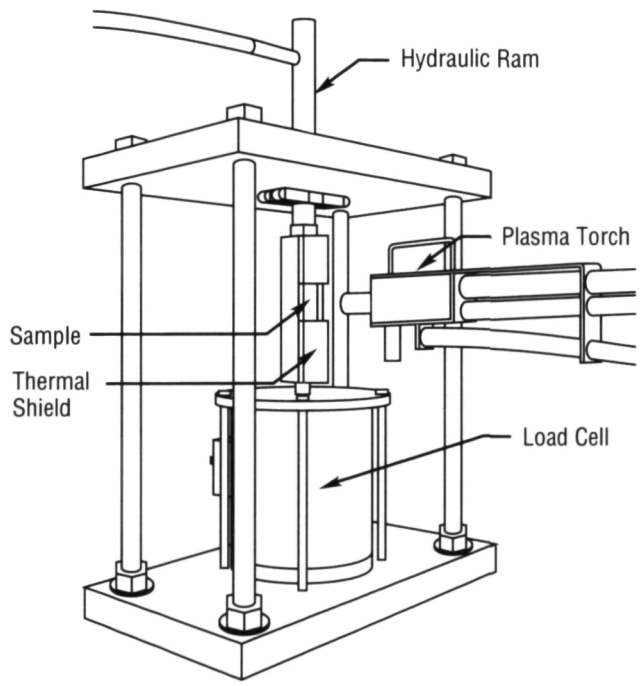

Figure 117. Plasma Torch Test Bed

The purpose of the **PTTB** is to provide a screening mechanism for ablative insulator materials and for high-temperature instrumentation. A series of tests can be performed in the **PTTB** for a fraction of the cost of a subscale motor, and in a much shorter amount of time. Carbon phenolic used in the nozzle of solid rocket motors has been the bulk of the testing, but, with the development of the test bed, other ablative insulators are being tested. In this report, results of the evaluation of Avtex rayon-based carbon-phenolic materials using the **PTTB** are discussed.

In the manufacture of the ablative liner material for the space shuttle redesigned solid rocket motor (RSRM) nozzle, rayon yarn is woven into a cloth, carbonized, and prepregged. Avtex, the manufacturer of the base rayon yarn, shut down and subsequently restarted the production facility. A test program to determine whether the material had changed due to the shutdown and restart was developed. **Plasma torch** testing was performed as a first-order screening to determine if there were any gross changes in the performance behavior.

The **prepreg** material is supplied by two sources (U.S. Polymeric and Fiberite) and material from each supplier was tested. The samples were machined from flat panels with the plies oriented perpendicular to the direction of the load. A total of 57 tests was run on materials from both suppliers, comparing preshutdown material to restart material. All material was processed using the same cure cycle parameters.

There were 26 tests of Fiberite material, 17 restart, and 9 preshutdown, with no variance noted in the performance of any of the samples. For U.S. Polymeric, there were 31 tests, 18 restarts and 13 preshutdowns, with 6 additional preshutdown data points included from a previous program to enlarge the data base. All of the U.S. Polymeric restart material pocketed. Of the preshutdown specimens,

8 pocketed and 11 did not. The increase in pocketing of the U.S. Polymeric restart material coincides with a slightly lower fill-tensile strength exhibited by the restart composite laminates.

The configuration tested, ply angles perpendicular to flame front, represented a worst-case environment with respect to promoting pocketing. The U.S. Polymeric material has always fluctuated between pocketing and not pocketing in this configuration. The drop in tensile strength was apparently sufficient to significantly increase the propensity for pocketing. It is emphasized that perpendicular-to-flame front ply angles were eliminated in the RSRM nozzle during the redesign effort.

As a result of the increased pocketing in the **plasma torch** tests, a closer evaluation of the composite microstructure was performed. Differences in the warp and fill yarns, resulting from the carbonization processes of the two vendors, were discovered. These differences had existed for years. The observed differences correlated with the materials, responses, in the **PTTB**. The complete verification program, with properties testing, subscale motor testing, and a full-scale firing, proved the restart material to be acceptable for flight.

The results of the **plasma torch** testing proved the **PTTB** to be a viable means of screening ablative materials used in solid rocket motor nozzles. The **PTTB** has also been used to evaluate the effects of moisture on nozzle ablative materials performance and carbon inclusions in case insulation materials. Some high-temperature instrumentation tests have also been performed to demonstrate their viability before testing in an actual motor. The system is being upgraded, and testing expanded, to develop its full capabilities. It promises to be a valuable tool to perform quick, inexpensive evaluations on systems requiring a **high heat-flux** environment.

T. Lawrence/EH34
(205) 544–2660
Sponsor: Office of Space Flight

The Temperature Variation of Hydrogen Diffusion Coefficients

The determination of **hydrogen diffusion** coefficients in metals by the timelag technique is a permeation method which has often yielded diffusion coefficients too small, by some orders of magnitude, compared with more recent data obtained by other techniques, such as the evolution methods. These differences have been attributed to the effects of surface layers, such as oxide films, which coat the metal surface. In the timelag technique, an evacuated system is filled with hydrogen gas on one side of a metal membrane, and the buildup of pressure on the other side, as the hydrogen diffuses through the membrane, is measured as a function of time. From these data, the delay in pressure response due to diffusing hydrogen is obtained, and the resulting **hydrogen diffusion** coefficient is calculated.

In an attempt to understand differences in results for **hydrogen diffusion** coefficients obtained with the timelag method and electrochemically measured results obtained by evolution methods, Inconel 718, Waspaloy, Incoloy 903, and pure nickel (270), which have also been studied by the timelag technique,[1,2,3] were studied electrochemically using an evolution technique. The amount of hydrogen diffusing to a metal surface is measured as a function of time, and the **hydrogen diffusion** coefficient is obtained, as well as the amount of mobile hydrogen initially contained in the sample. In order to accomplish this, it was necessary to employ an autoclave system that contains liquids (0.1 NNaOH, in this case) under pressure at higher temperatures. Samples were studied at 25, 75, and 125 °C (77, 167, and 257 °F). The **temperature variation of the diffusion coefficients** was determined by fitting to the Arrhenius equation, $D = D_o \exp(-E/RT)$, the parameters being D_o(cm^2/s) and E(cal/mole).

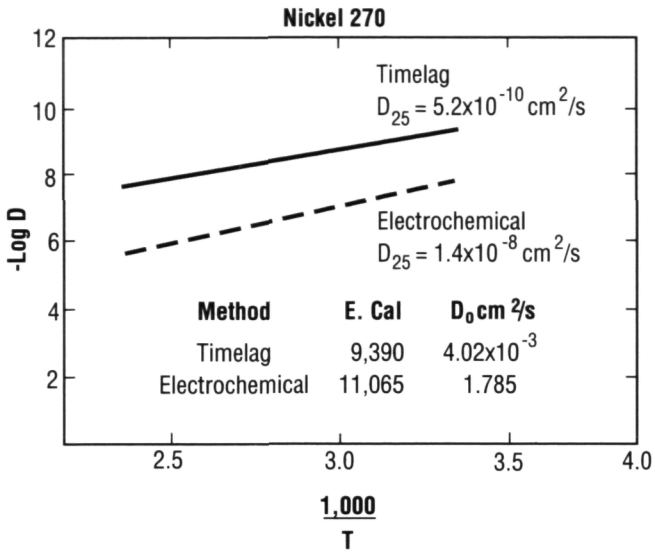

Figure 118. Electrochemical and Timelag Curves for Nickel 270

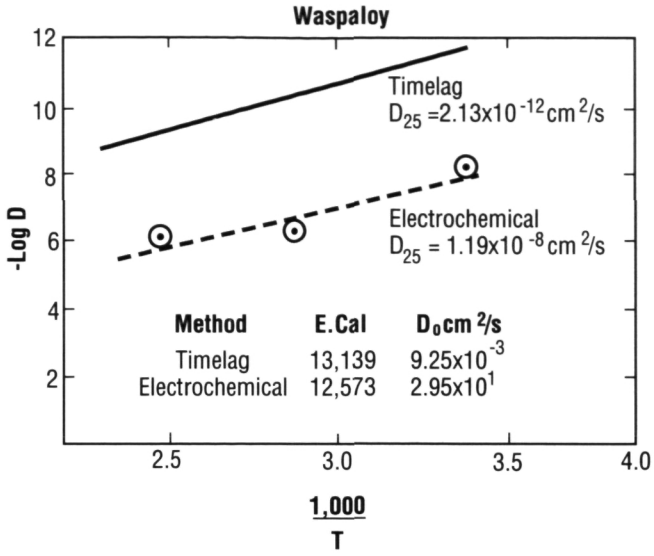

Figure 119. Electrochemical and Timelag Curves for Waspaloy

Electrochemically measured results for Ni 270 and Waspaloy, shown in figures 118 and 119, respectively, are compared to those for the **timelag method**. The slopes of the logarithmic straight lines are the same as those for the **timelag method** within the experimental error. However, the values of the diffusion coefficients are much smaller for the **timelag method**, and this is true for all cases studied. The ratios of the diffusion coefficients by the evolution method compared to those by the **timelag method** at 25 °C (77 °F) were 5,590 for Waspaloy, but only 27 for Ni 270. Waspaloy traps hydrogen much more strongly than does Ni 270, and the major difference in results by the two methods is therefore attributed to hydrogen trapping. Also, the amount of mobile hydrogen in the samples increases with increasing temperature, and this is attributed to the fact that hydrides become less stable at higher temperatures.

[1]Perng, T.P., Johnson, M.J., and Alstetter, C.J., *Metallurgical Transactions*, Vol. 19A, May, 1988.

[2]Robertson, W.M., *Metallurgical Transactions*, Vol. 8a, November, 1977, p. 1709.

[3]Robertson, W.M., *Zeiten Metallkde*, Vol. 64, 1973, p. 218.

M.D. Danford/EH24
(205) 544–2612
Sponsor: Office of Space Flight

Structures and Dynamics

Adaptive Computational Methods for High Reynolds Number Internal Flows

The accurate numerical simulation of fluid flows in complex geometries, such as exist in the space shuttle main engine (SSME), requires the construction of well-designed grids upon which to obtain solutions to the governing partial differential equations. This is never a trivial task, and in fact requires considerable ingenuity, as well as understanding of the basic physics of the flow involved.

However, the flow solution is not, in general, known a priori, so the computational grid may be far from optimal and can induce significant errors. This is the impetus for the development of **adaptive grid** generation techniques in computational fluid dynamics (CFD). **Adaptive grids** are those which adjust to the evolving CFD solution, usually in response to estimated error or to gradients in the solution. The idea is that grid points will be moved into regions of large error or gradients and away from smooth regions where the points are not needed. For example, grid points would become concentrated in boundary layers or around shock waves. Some adaptive strategies rely upon the addition of points to the grid rather than the redistribution of existing points.

A generalized adaptive version of the EAGLE grid-generation system has been developed, with particular application to incompressible, high Reynolds number flows such as occur in the SSME power head. EAGLE, originally developed at Mississippi State University under U.S. Air Force sponsorship, is a set of two grid-generation codes. One code is for the construction of grid-boundary surfaces. The second is an algebraic and elliptic grid-generation code. The adaptive version will adjust the grid in response to user-specified weight

functions. Examples of these weight functions are vorticity and velocity magnitude gradients. Figure 120 shows a simple algebraic grid for flow over a back-facing step and the streamwise velocity contours of the solution obtained on the grid. Figure 121 is the grid after adaptation of the velocity.

Additional difficulties in numerical grid generation arise from the geometric complexity of arbitrary flow fields, and from the memory limitations of even the largest supercomputers. These difficulties are overcome by the construction of composite **block grids**. EAGLE itself is based upon this concept and provides for complete grid continuity across block interfaces. During both the grid-generation process and the CFD solution, only one block of the grid will reside in the computer at a time.

The decomposition of the domain in this way not only solves the problem of memory limitations, but also makes possible the construction of smooth, continuous grids around complex shapes. For example, even the simple geometry of the back-facing step in figure 120 does not lend itself to a single-**block grid**. The boundaries of the three blocks used are clearly visible, and the solution is seen to be continuous there.

The adaptive version of EAGLE can, in principle, be coupled directly with any CFD code. However, there are few generalized multiblock flow solvers in the public domain. Most codes require ad hoc changes to conform to specific geometries. Therefore, the widely used INS3D incompressible Navier-Stokes solver, developed at Ames Research Center, has been significantly modified so that boundary conditions and block-to-block connectivity are specified by user input.

P.K. McConnaughey/ED32
(205) 544–1599
Sponsor: Structures and Dynamics Laboratory

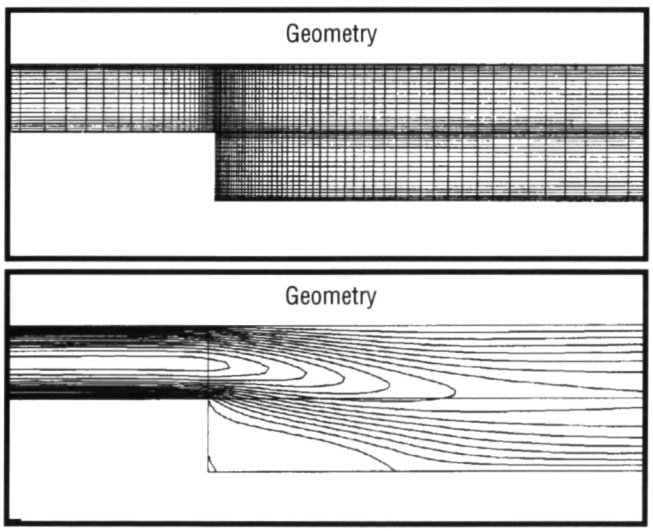

Figure 120. Algebraic Grid and Stream-Wise Velocity Contours for Flow Over Back-Facing Step at Reynolds Number of 100

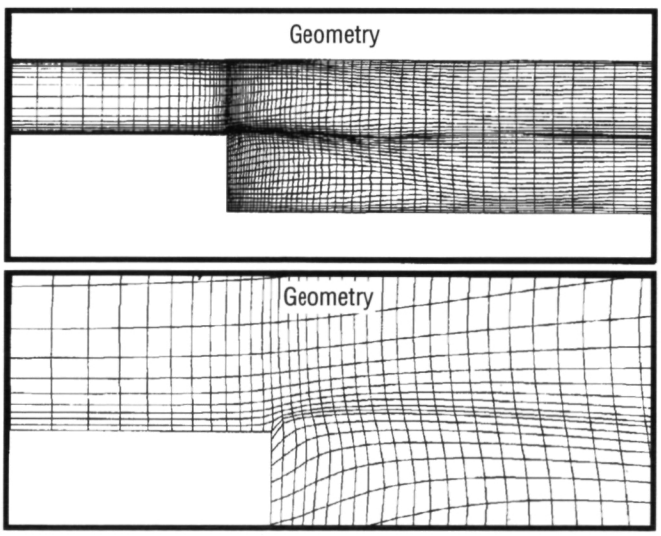

Figure 121. Grid for Backward-Facing Step Following Adaptations to Stream-Wise Velocity Magnitude

An Algorithm for Periodic Waveform Recovery from Space Shuttle Main Engine Vibration Measurements

The frequency content in dynamic measurements from rotating machinery contains much subtle information concerning equipment operating condition and component degradation. For this reason, the power spectral density (PSD) has long been employed to assess the relative magnitude of fault-related spectral contributions. Measurements on high-performance rocket engine turbomachinery suffer from severe noise contamination, from numerous extraneous sources, which impedes rotating element diagnostic evaluation. Thus, it is difficult to determine whether an apparent high-level harmonic contribution is indeed related to the fundamental rotational frequency, f_r, or possibly due to an independent source. In an effort to correlate synchronous frequency characteristics with an arbitrary harmonic component, a unique coherence spectrum was devised which we call the **"hypercoherence" function**. The **hypercoherence function**, $\Gamma(n;f)$, defines the nonlinear correlation between waves at a reference frequency, f, and harmonics at nf, $n = 1, 2,.....$

Application of the **hypercoherence functions** to SSME turbomachinery diagnostic data assessment was summarized in the 1986 R&T Report (NASA TM 86567). This frequency-domain analysis has since been extended to a time-domain filtering algorithm for the extraction of periodic signals in noisy data. Assume we have two turbopump vibration measurements located (approximately) 90° apart radially about the casing, say $X(t)$ and $Y(t)$. If the shaft (and inner bearing race) motion is sensed by these transducers, a plot of $X(t)$ versus $Y(t)$ should indicate the orbital motion of the shaft end measured. Each of these "signals" will clearly be corrupted with undesired noise (both random and periodic) during practice. The analytical basis for the techniques can be summarized briefly. Assume $X(t)$ and $Y(t)$ jointly periodic, with additive uncorrelated noise and (possibly coincident) period components.

Let

$$X'(t) = F^{-1}\left[\sqrt{S_{xx}(nf)_1}\,\Gamma_x(n;f_1)\right]$$
$$Y'(t) = F^{-1}\left[\sqrt{S_{yy}(nf)_1}\,\Gamma_y(n;f_1)\right]$$

where

$n = 1, 2, 3.....$

S = Ordinary power spectrum

G = **Hypercoherence function**

F^{-1} = Inverse Fourier transform

Now X' and Y' represent filtered time histories, and include only harmonics (nonlinearly) correlated with the common fundamental frequency. To generate an orbit plot, or phase-plane representation of the two quantities, let

$$Y''(t) = Y(t-\tau)$$

$$\tau = \phi/2\pi f_1$$

$$f = Tan^{-1}\left[Q_{xy}(f_1)/C_{xy}(f_1)\right]$$

Q_{xy} = QUADRATURE SPECTRUM

C_{xy} = COSPECTRUM

The time delay, τ, serves as a "key phasor," to initiate the relative phase angle between the two vectors. A phase-plane diagram of the filtered signals is thus obtained by plotting X' versus Y''. The procedure is best illustrated by example. Figure 122a illustrates the orbit plot for two jointly periodic signals, each containing three harmonic components. Figure 122b represents the same plot when uncorrelated noise and independent, coincident pe-

riodic components have been added to each signal. This chaotic pattern is highly representative of hot firing data. Figures 122c and 122d are the recovered orbital diagrams by **hypercoherence filtering** and comb filtering, respectively. The superior performance of **hypercoherence filtering** is clearly indicated.

When compared with available noise cancellation methods, such as time domain averaging (TDA), comb filtering, and adaptive line enhancement, the **hypercoherence filter** has the following two advantages: (1) only the **hypercoherence filter** can reject independent components at the same frequency (while the other noise cancellation methods will pass all data in the pass-band including both true harmonics and independent components); (2) a slight phase drift would be fatal for techniques, such as the TDA method, which require precise phase lock-in. For the **hypercoherence filter**, on the other hand, since only relative phase information is required, slight phase drifting is not as critical. This is significant when considering the small speed variations inherent in turbopump operation, even at a constant power level.

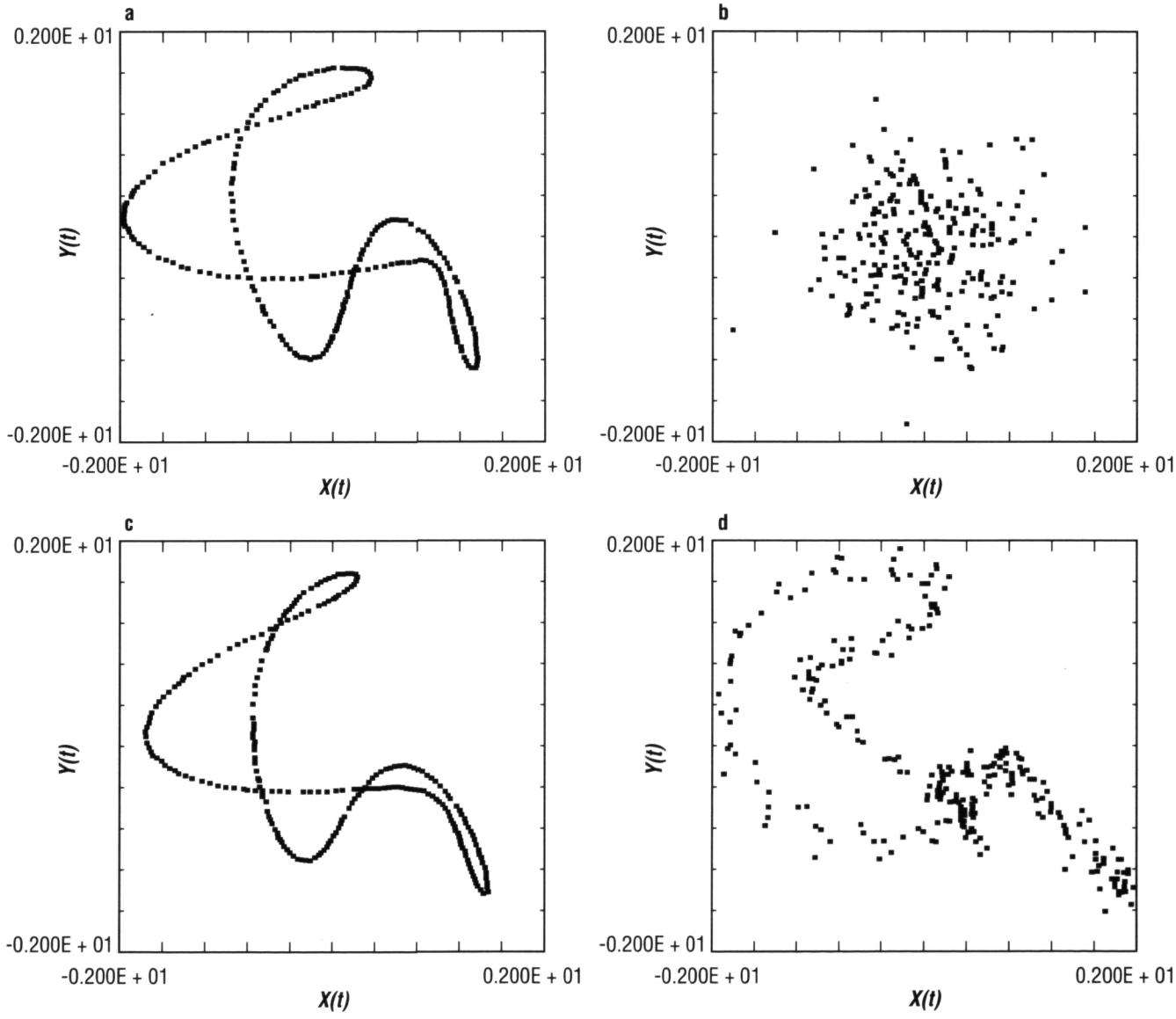

Figure 122. (a) Orbital Diagram of Noise-Free Simulation, (b). Orbital Diagram of Simulation With Additive Gassian White Noise, (c). Recovered Orbital Diagram by Using Hypercoherence Filtering, (d). Recovered Orbital Diagram by Using Comb Filtering

Figures 123a and 123b represent the filtered orbits from measurements at HPFP rad-90° and rad-170° during SSME tests 901-471 and 901-436, respectively. Figure 123a has a smooth orbital motion which represents a well behaved rotational system. Figure 123b, however, indicates a potential rubbing problem. The two locations with sharp cusps appear to indicate possible impact between stationary and rotating system components.

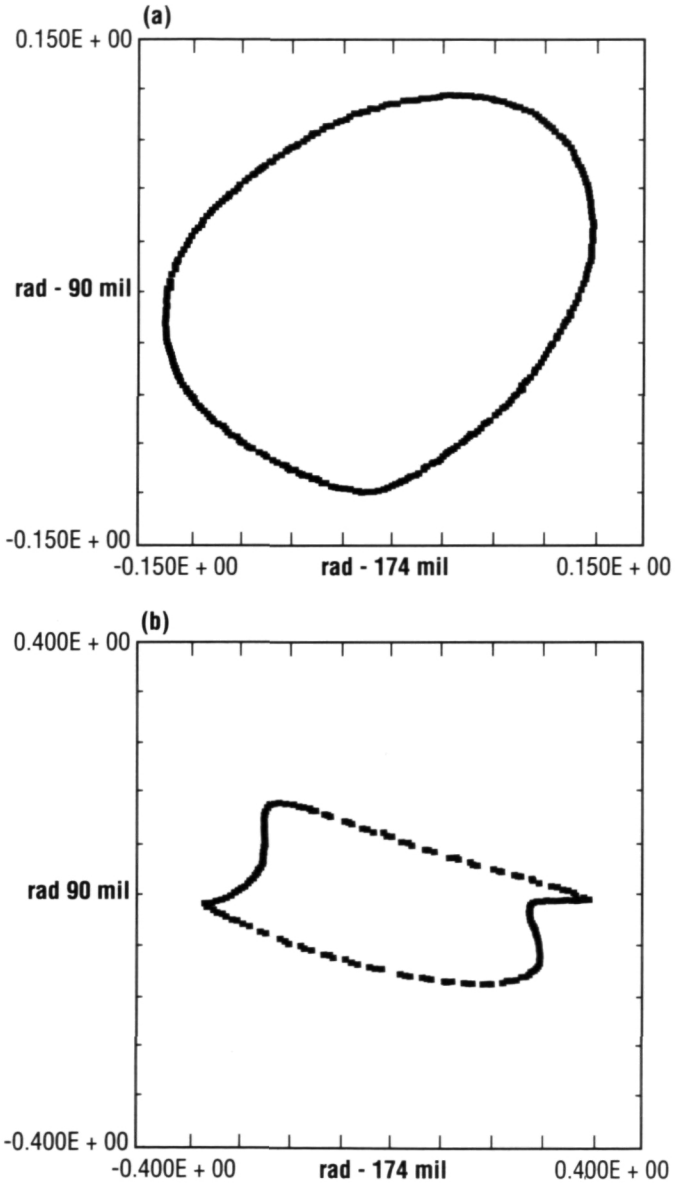

Figure 123. Orbital Plot From Test 901-4T1 by Hypercoherence Filtering, b. Orbital Diagram of 901-436 by Hypercoherence Filtering

The above algorithm is presently operational and has been integrated into the SSME Diagnostic Analysis Package developed by Structures and Dynamics Laboratory.

Coffin, T., and Jong, J.Y., "A Nonlinear Coherence Function and Its Application to Machines Diagnostics," *Journal of the Acoustical Society of America*, Supplement 1, Vol. 78, Fall, 1985.

Jong, J.Y., and Coffin, T., "Diagnostic Assessment of Turbomachinery by the Hypercoherence Method," NASA Conference on Advanced Earth-to-Orbit Propulsion Technology, Marshall Space Flight Center, May, 1986.

Coffin, T., and Jong J.Y., "Some Nonlinear Methods and Their Application To Rocket Engine Diagnostic Evaluation," 1st International Machinery Monitoring and Diagnostic Conference, September, 1989.

J.E. McBride/ED23
(205) 544–1523
Sponsor: Structures and Dynamics Laboratory

Deployable Aerobrake Structural Development

A variety of proposed space missions involve the transfer of a spacecraft from a high-velocity interplanetary trajectory or geosynchronous orbit to a low-velocity low Earth orbit. This transfer requires significant deceleration which can be accomplished either by propulsive means or by aerobraking. An aerobrake is a blunt structure on the front of a vehicle that allows the use of aerodynamic drag to slow the spacecraft during a controlled trajectory (aeropass) through a planetary atmosphere.

The **deployable aerobrake** designs currently being studied consist of a rigid-tile circular central section surrounded by a deployable umbrella-like structure, as shown in figure 124. To protect the spacecraft from the thermal environment encountered during aeropass, the deployable portion of the aerobrake will likely be constructed of a flexible insulation material developed by NASA Ames Research Center. This new material, called **tailorable advanced blanket insulation (TABI)**, is a challenge to characterize both experimentally and theoretically due to its high flexibility. As shown in the inset of figure 125, **TABI** consists of two parallel sheets of woven ceramic fabric connected by triangular cores. The cores are filled with fibrous ceramic insulation.

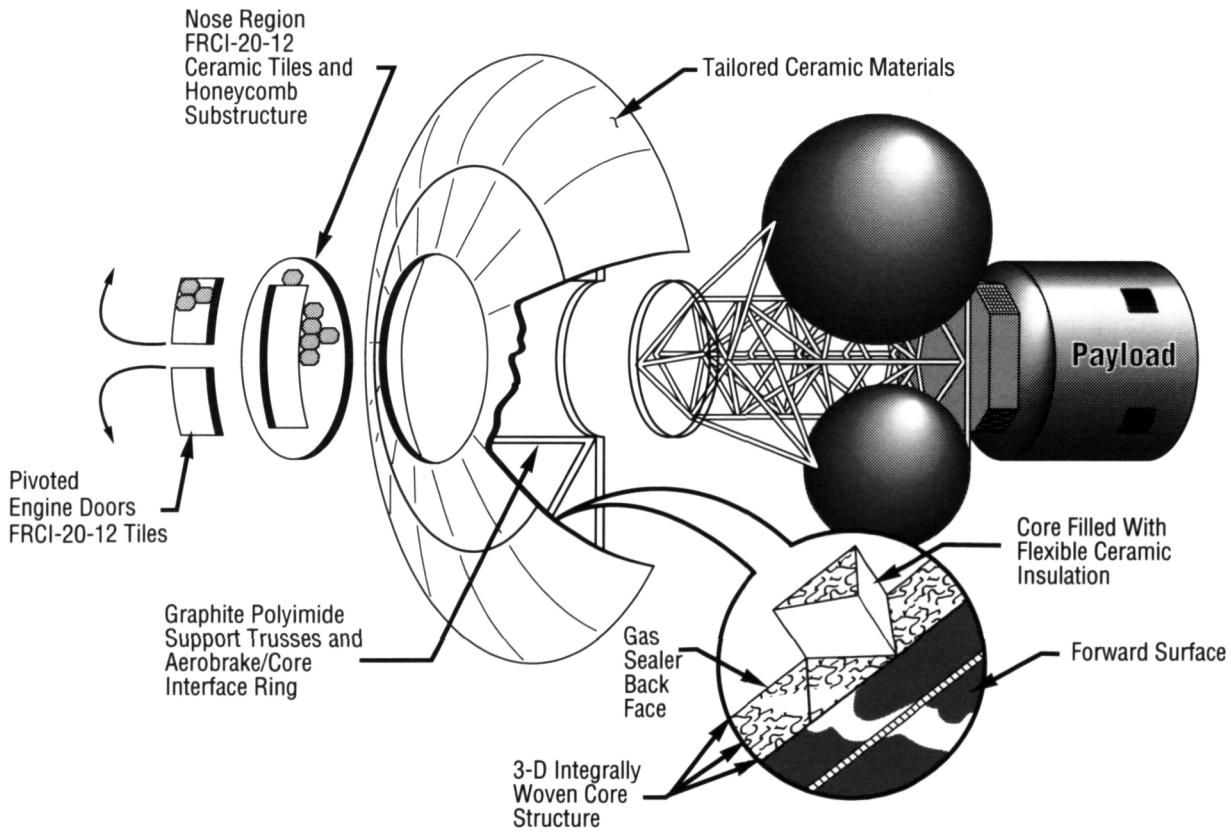

Figure 124. Spacecraft With Deployable Aerobrake Structure

The first phase of a program to design, construct, and test **deployable aerobrake** test articles was completed in FY90. The main purpose of this research program is to develop the capability to model the blanket insulation material (**TABI**) and then to incorporate that capability into the analysis of the aerobrake structure, fully accounting for the aerothermal environment in which the vehicle will operate. The purpose is not to formulate a rigorous aerobrake design, but rather to develop and verify finite element modeling techniques for this technology, which can then be used for future aerobrake design and analysis.

Goals of the initial phase of the study were the following: (1) to summarize existing research on the properties of **TABI**; (2) to perform **TABI** modulus of elasticity and damping tests; (3) to plan a series of aerobrake subsystem tests in an effort to build a structural/thermal database; and (4) to develop a finite element methodology for analysis of flexible aerobrake structures. Since the existing data base of **TABI** structural properties is incomplete, a test program was initiated at MSFC. In figure 125, representative results are shown. Both the stiffness and damping curves illustrate the nonlinear nature of the material. Subsystem tests are planned which will provide the variation of structural properties due to changes in temperature, heat rate, and boundary support conditions. Finite element analyses of the aerobrake response to pressure loads indicate that due to the requirements of loading normal to membrane elements, a stress-stiffening option is required.

The second phase of the **deployable aerobrake** study will begin near the end of FY90 and continue through FY92. Objectives of continued research include the following: (1) analysis of aeropass loads acting on the aerobrake; (2) definition of legitimate failure criteria and determination of "hot" break strength and elastic modulus for TABI; (3) development of a thermal/structural data base and establishment of a dynamic/thermal trend through a series of subsystem tests; (4) design, modeling, construction, and modal testing of a 10-ft diameter large-scale aerobrake test article; and (5) analysis of the aerobrake response to the aeropass environmental loads.

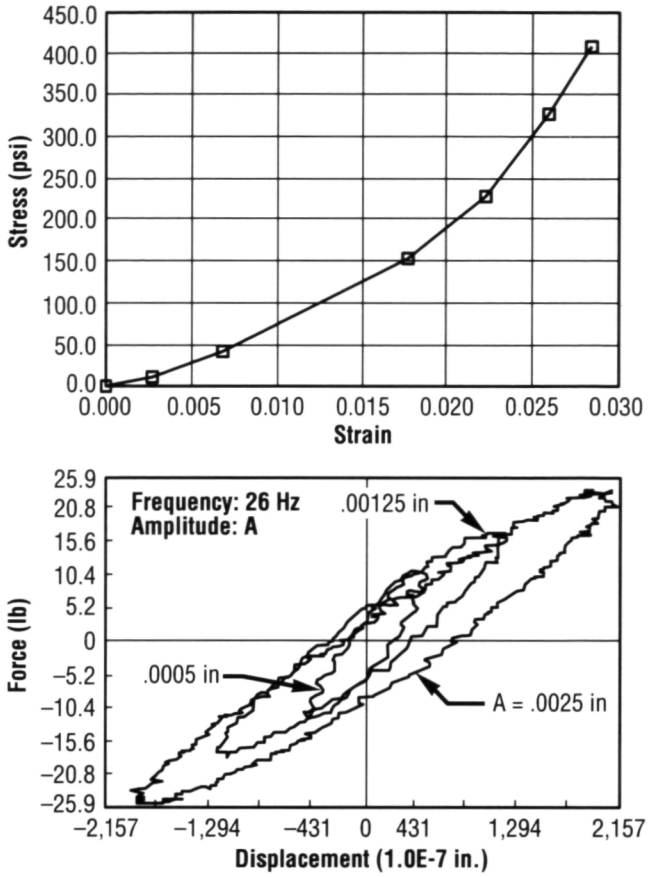

Figure 125. Stiffness Curve (Top) and Hysteresis Damping Curves (Bottom) for Aerobrake Blanket Insulation Material

Sawko, P.M., "Tailorable Advanced Blanket Insulation (TABI)," Joint NASA/Clemson University Conference on Advanced Engineering Fibers and Textile Structures for Composites, Greenville, SC, November 3–6, 1987.

Calamito, D.P., "Development of Tailorable Advanced Blanket Insulation for Advanced Space Transportation Systems," NASA CR 177444, April 1987.

Pitts, W.C., and Murbach, M.S., "Thermal Design of Aeroassisted Orbital Transfer Vehicle Heat Shields for a Conical Drag Brake," Journal of Spacecraft and Rockets, Vol. 23, No. 4, July/August 1986.

M.L. Tinker/ED22
(205) 544–4973
Sponsor: Office of Aeronautics and Space Technology

Novel Composites for Protection Against Orbital Debris

The manmade **orbital-debris** environment poses a threat to all orbiting spacecraft. To demonstrate the ability of a unique combination of bumper materials to counter this threat, this effort includes fabrication and tests of z-direction reinforced composite bumper specimens. An additional objective of this effort is to evaluate a novel bumper attachment method for its applicability to NASA requirements.

The process used to introduce the z-direction fibers is company proprietary; however, previous programs have shown that the z-direction fibers cause an increase of up to four times the resistance to composite delamination with negligible effects on in-plane properties. Several z-direction fiber materials, diameters, and volume fractions will be examined to determine the most effective in fragmenting a hypervelocity **orbital debris** particle. It has been theorized, for this reason, that the bumper should have a high shock impedance, but fragmented to the maximum extent possible so that large bumper fragments do not become projectiles impacting the item to be protected. Several specimens will be tested in a **hypervelocity impact** facility, and compared with similar tests of aluminum bumpers and kevlar-epoxy bumpers to determine the effectiveness of the z-direction fibers.

Finally, a metallic hook-and-loop scheme of attachment of bumpers to a space vehicle will be evaluated, and recommendations for use will be made, considering NASA structural and operational requirements.

J.R. Horn/ED52
(205) 544–7013
Sponsor: Small Business Innovation and Research

Slit Digital Radiography for Analysis of Bondline Defects in Solid Rocket Motors

Bio-Imaging Research of Chicago, Illnois, has teamed with Marshall Space Flight Center under a Small Business Innovation Research task to look at the feasibility of using a radiographics nondestructive evaluation method, known as **slit digital radiography** to potentially inspect the first bondline between case and insulation in typical large **solid rocket motors (SRM's)**. In past **SRM** motor programs, the first bondline has been nondestructively inspected by ultrasonic pulse-echo methods and by conventional film radiography techniques. This method of **slit digital radiography** has the potential to improve on the resolution of this bondline and the probability of detection of common anomalies such as unbonds.

Discrete-element x-ray detectors developed from medical computed tomography (CT) are being applied to industrial x-ray digital radiography (DR) and CT imaging. **Slit digital radiography** is a technique which may be applied to mapping density variations within rocket motor walls. This could replace the use of traditional film tangential radiography for inspecting the case-to-insulation bondline. The standard x-ray technique used today to image **bondline defects** in **SRM's** has an x-ray beam passing through the edge of the motor tangent to the bondline circumference and detected by an area detector such as film or an x-ray image intensifier. While more effective than traditional radial x-ray techniques, this method has a difficult time imaging subtle defects because the area detector is exposed to a range of thicknesses, causing a wide range of background attenuating. In the **slit radiography** method, the rocket motor would be rotated as an x-ray beam passes through the bondline tangent to the detector array, creating a two-dimensional mapping of the bondline circumference. The small size of the detectors means this new technique can receive x rays through an essentially constant attenuation path and map bondline features against a constant contrast level. Thus, small features will

stand out and be easily identified. Line profiles are first taken at multiple angular positions as the test object is rotated, and the data is formatted into a two-dimensional image. The image will provide a circumferential mapping of the rocket motor bondline taken at the optimum x-ray exposure angle, with accurate information about the density and position of features within the bond.

The detectors that make this a potential **SRM** inspection tool were originally developed for medical computed tomography. In this discrete-element system, each detector has its own scintillator and photodiode, and an attenuating septum separates adjacent detectors. This significantly reduces both light and radiation crosstalk, which can cause defocusing in areas of excessive brightness or poor edge definition in traditional techniques that use film or image intensifiers. The detectors are instrument-grade elements that have a 16-bit, or roughly 65,000-gray-level accuracy. After the necessary data correction processes, this accuracy generally results in a dynamic range of 10,000 to 1. Traditional systems, such as fluoroscopic screens, have a contrast of 20 to 1. Even film, the standard in the radiography industry, has only a 100 to 1 dynamic range.

The **slit digital radiography** technique, using a slit for a collimator, will initially be used to inspect smaller motors (less than 20-in (51-cm) diameter) to see if scaling up the inspection tool to test large solid rocket motors (shuttle class) is feasible .

M.W. Suits/EH13
(205) 544–8336
Sponsor: Office of Commercial Programs

An Analytical Formulation for a Design Technology for Multiphase Structures

Thermosetting polymer matrix composites are used as sacrificial, thermal insulators in solid rocket motor (SRM) nozzles. During motor operation, the inside surface of the nozzle insulation is exposed to extreme temperatures. As a result, the inside surface of the nozzle insulation undergoes **thermochemical decomposition** and is reduced to a char layer (carbon residue) and a variety of pyrolysis gases. These gases, in turn, diffuse through the char layer and escape to the motor exhaust.

Recently, there has been evidence of anomalous **charring and erosion** in the space shuttle's SRM nozzle. It is believed that the accumulation of the pyrolysis gases inside the char layer leads to excessive pore pressures and possibly to structural failure of the char layer.

The present research effort is an attempt to develop an analytical tool to model the generation and subsequent diffusion of the pyrolysis gases through the insulation and to model the effect of these gases on the solid skeleton deformations and stresses.

In the past year, the foundations of the theoretical formulation have been reviewed, and various forms of the constitutive relations for fluid-filled, porelastic materials have been developed. Forms for both **anisotropic** and **isotropic** thermoelastic behavior have been developed. It has been found that the elementary mixture theory given by Biot is adequate to simulate the problem, but that determination of stress in the solid material is speculative and must be coupled to experimental observations.

Salamon, N.J., First Year Report and Proposal for Further Work on: An Analytical Formulation for a Design Technology for Multiphase Structures, Department of Engineering Science and Mechanics, The Pennsylvania State University, May 1990.

R.M. Sullivan/ED24
(205) 544–7240
Sponsor: Structures and Dynamics Laboratory

Generalized Failure Criteria for 2-D Carbon-Carbon

Over the past several years, many tactical **solid rocket motors (SRM's)** have been constructed with **2-D carbon-carbon** exit cones. The properties of **2-D carbon-carbon** make it a logical choice for such applications. For example, **2-D carbon-carbon** exit cones are strong, durable, and considerably lighter than ablative exit cones. More importantly, **2-D carbon-carbon** does not erode in a nozzle environment, so the same exit cone profile is maintained throughout motor operation.

Unfortunately, the failures of the WESTAR and PALAPA spacecrafts have identified certain shortcomings associated with determining the margins of safety for **2-D carbon-carbon** exit cones. The present effort is an attempt to improve the **failure criteria** for **2-D carbon-carbon** material by expanding the present data base. The effort can be loosely classified by tasks as:

- Review the mathematics of the present **failure criteria** for **2-D carbon-carbon**
- Collect strength data obtained from previous programs
- Examine test specimens from previous programs and determine the modes of failure (i.e., microscopic inspection of the failure surface)
- Perform finite element analysis on the test specimens and determine the stress state at failure
- Develop improved mathematical models to determine failure
- Identify the strength data which is needed for the improved models
- Conduct tests to obtain this strength data
- Verify model.

Over the past year, the test specimens and the measured strength data have been collected from the previous programs. The test specimens have been examined and classified by their modes of failure, and finite element analysis has been conducted to determine the stress at each failure. Presently, improved failure models are being explored.

Marx, D.A., "Generalized Failure Criteria for 2-D Carbon-Carbon": Phase I Results and Proposal for Phase II, PDA Engineering, Costa Mesa, CA, 1990.

R.M. Sullivan/ED24
(205) 544–7240
Sponsor: Structures and Dynamics Laboratory

Thermal Degradation Tests of Damaged Multilayer Insulation From Hypervelocity Impacts

The objective of this test program is to measure the degradation of the insulating capabilities of **multilayer insulation (MLI)** subjected to effects of **hypervelocity impact** in a configuration similar to that anticipated for Space Station *Freedom*. This configuration entails placing a thin aluminum "bumper" plate between the **MLI** and the aluminum projectile which is traveling at speeds in excess of 5 km/s (3.1 mi/s). The impact test setup is intended to simulate the effects of impacts to the space station from orbital debris. Quantifying the damage to the **MLI** from such impacts is necessary to predict local heating and cooling in the pressure wall of *Freedom*. Local cooling is of the most concern, as it could result in the formation of condensate inside the space station, which could, in turn, lead to electrical and fungus growth problems.

A series of approximately 20 thermal tests has been planned using a test fixture, designed by Boeing Aerospace Corporation, which simulates the current baselined wall design for S.S. *Freedom* modules. **Hypervelocity impact**-damaged **MLI** specimens (provided by Boeing using MSFC's light gas gun facilities) will be attached to the test fixture and subjected to a simulated space environment using MSFC's thermal vacuum chamber facilities. Measurements will be made to determine the change in the insulating capabilities of the **MLI** in the vicinity of the impact damage.

The data obtained from this thermal test program will be made readily available to the space station designers in the form of a microcomputer program currently being developed by Dr. William K. Rule of the University of Alabama in Tuscaloosa. The program will predict damage to the insulating capabilities of the **MLI** for debris impact conditions specified by the designer. It will then perform a transient heat transfer analysis to determine the local temperature profile in the space station's pressure wall. The **MLI** damage predictions will be based on interpolations/extrapolations of the results from the thermal test program. The amount of condensate formed will also be predicted by the program. This program will be completed by September 1991.

P.E. Thompson/ED52
(205) 544–7017
Sponsor: Space Station *Freedom* Program

Probabilistic Model for Fracture Mechanics Service Life Analysis

Advanced high-pressure oxygen/hydrogen propulsion components such as the space shuttle main engine (SSME) employ the concept of system reusability in an effort to reduce payload-to-orbit costs. This requires critical components to be designed for extended operational periods in a myriad of environments and stress fields. Extensive operational experience has shown that **crack**-like defects are detected from manufacturing processes and operational environments greater than originally anticipated. Fracture mechanics is an engineering discipline that quantifies the conditions under which a structure can fail due to the growth of a **crack** contained in that body.

Fracture mechanics analyses for SSME-critical components often underestimate life by assuming worst-case conditions for fracture properties, initial flaw size, stress levels, and operating environments, even though all of those variables are subject to statistical variations and the probability of occurrence for any worst-case conditions is very low. These deterministic assumptions are required due to the limited ability to adequately inspect complex structures, the uncertainty of operational environments during the entire engine cycle, and the absence of material properties specific to the environmental and geometric conditions being analyzed. The probabilistic approach to fracture mechanics analysis is ideally suited to the treatment of variables that are statistically distributed, and the data are usually in a form that is amenable to statistical analysis.

A probabilistically modeled computer code, the **space shuttle probabilistic optimization code (SSPOC)**, for fracture mechanics service life analysis was developed. **SSPOC** uses statistical distributions of life-controlling parameters to compute occurrence rates for significant events such as part removals, initiated **cracks**, and in-service failure.

The **SSPOC** simulator is composed of the following elements:

- Initial material quality
- **Crack** initiation behavior
- **Crack** size behavior—propagation life (a vs. n)
- **Crack** propagation variability
- Stress analysis variability
- Mission severity, and
- Nondestructive evaluation (NDE) variability.

The initiation life system is composed of the initial material quality system, mission severity system, stress variability system, the stress (s)-cycle (N) system, and the transition system (initial material quality through initiation to propagation phase). The initial material quality system determines the size of an existing microstructural anomaly. The stress the part sees during the inspection interval is accounted for by the stress variability system. Actual initiation life is then fixed by the s-N system using results from the above systems. The mission severity system fixes the service interval length, in terms of the damage accumulated, based on analysis of actual missions and the required service interval. The transition system tracks the part from zero time through the end of the initiation period determined by the s-N system; the anomaly size increases during this period and this increasing size influences the NDE detectability.

There are four NDE models available in **SSPOC**; perfect NDE, logodds model, lognormal model, and the bivariate normal model. Figure 126 compares perfect and realistic NDE using the conventional probability of detection (POD) versus cracksize plot. All **cracks** smaller than the inspection size will be passed by the system (i.e., zero probability of detection when $a < a_o$, and **cracks** larger than inspection size will be subjected to POD = 100 percent).

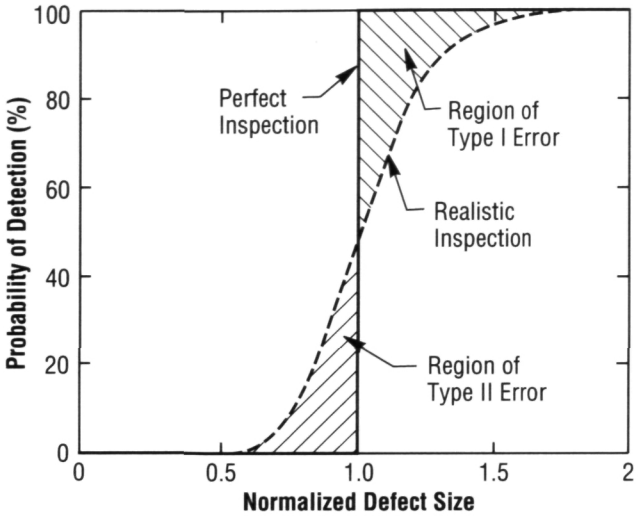

Figure 126. NDE-Realistic vs. Perfect Inspection

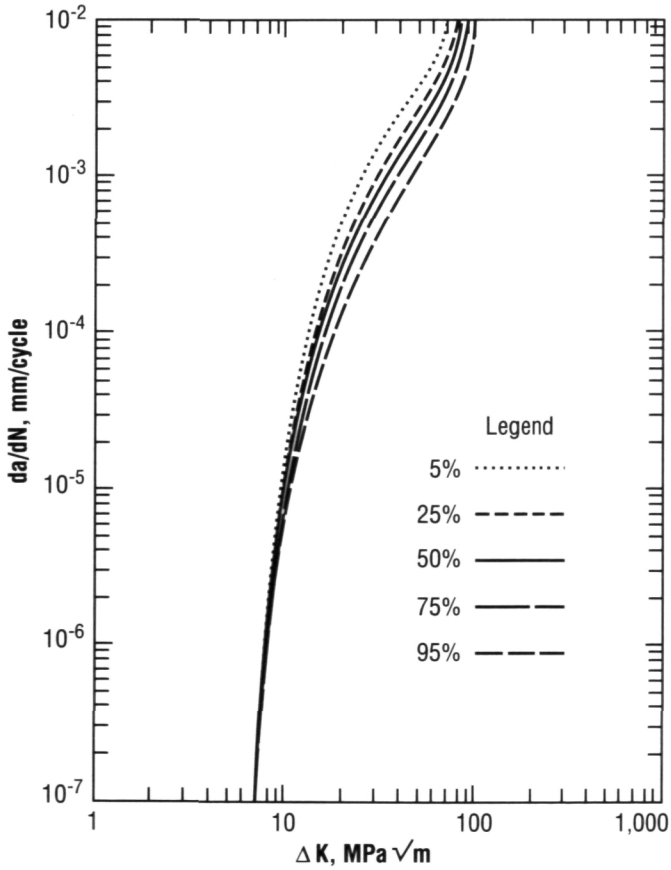

Figure 127. Percentiles of Log Crack Growth Rate as a Function of Log Stress Intensity

The **crack** propagation system is divided into three parts: stress variability system, mission severity system, and the life prediction system. As shown in figure 127, scatter in *da/dN* introduces variability in the ratio of actual to predicted lives. The analysis of the local stress field can also introduce a bias error or additional scatter in actual to predicted lives. The *a-N* system contained in the code consists of three different models: Pseudo-Paris; inverse polynomial in *a, N*; and the polynominal in *a, N*.

SSPOC uses the normal, lognormal, Weibull, and beta probability distributions. Low cycle fatigue life is adequately described by the Weibull model.

[1]Probabilistic Model for Fracture Mechanics Service Life Analysis, Final Report, October 1989, NAS8-36901

[2]Probabilistic Model for Fracture Mechanics Service Life Analysis, User's Manual, November 1989, NAS8-36901

R. Stallworth/ED25
(205) 544–7189
Sponsor: Office of Aeronautics, Exploration, and Technology

Automated Systems

WELDSMART: A Vision-Based Weld Quality Assurance System

WELDSMART is a system under development to apply **computer vision** technology to the problem of **weld inspection**. A large number of inspection techniques involve the visual inspection of the weldment or images thereof. These image data are evaluated by human experts and, as such, the results may be subjective. Training of individuals qualified to perform **weld inspection** is also primarily through on-the-job experience. The objective of this project is the coupling of an image-processing development system with an **expert-system**-based user interface. The **expert system** is provided with knowledge of the vision system's image processing library and an interactive user interface. Through an interactive dialogue, the human weld inspector will identify the criteria upon which an assessment of the weld's quality can be made. Additionally, text data documenting the conditions are linked to the identified feature set. When fully operational, WELDSMART may be utilized to perform or assist in the performance of **weld inspection**. A training mode will also allow the use of WELDSMART as a tutor in training weld inspectors. The accompanying photograph (fig. 128) depicts both conventional inspection and the baseline WELDSMART system, and a computer-enhanced image of weldment under inspection. In the first year of this 3-year project, the image processor has been applied to a number of weld specimens of known quality. An expert system has been used as an interface to the image processing library, and the system has been used successfully to determine quality on a number of unknown specimens exhibiting fault-types similar to the set used in training. In cooperation with the appropriate quality and materials organizations, future activities will include further testing, development, and evaluation.

K. Fernandez/EB44
(205) 544–3825
Sponsor: NASA Technology Utilization Office

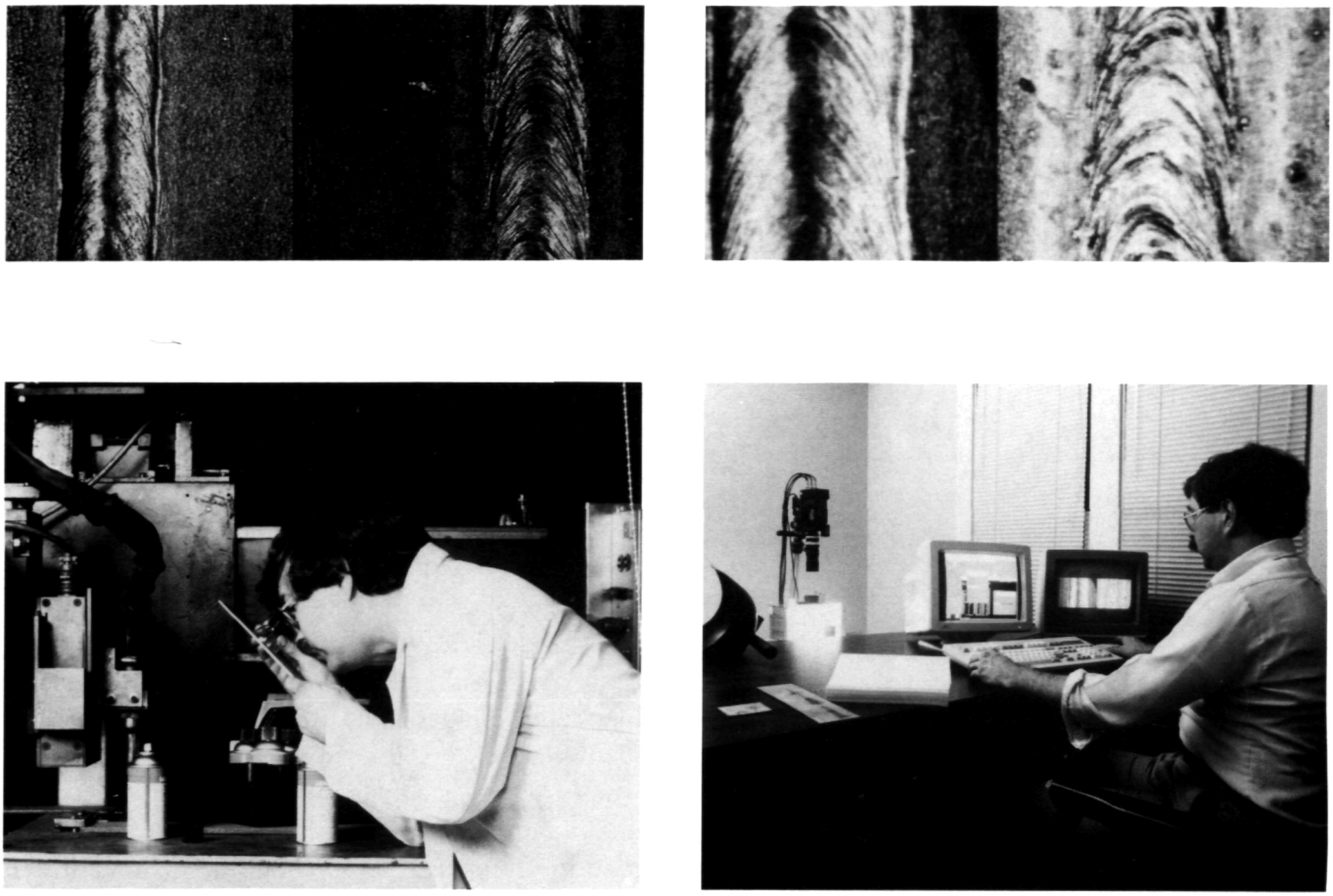

Figure 128. WELDSMART: A Vision-Based Weld Quality Assurance System

ORIGINAL PAGE
BLACK AND WHITE PHOTOGRAPH

Development of ROBOSIM for Academic/Industrial Use

ROBOSIM is a NASA-developed, **graphics**-based **robotics simulation** software package for support of both industrial and aerospace design applications. The package has been used as a cost-effective tool for the development of **robotic** concepts for both on-orbit and Earth-based manufacturing systems. The accompanying photographs depict ROBOSIM in use in the classroom to study **robotics** for aerospace and industrial applications. During the past year, a number of milestones have been accomplished on this project, including the implementation of an X-Windows/Unix version; porting to a variety of common commercial workstations; the implementation of real-time collision detection; dynamic modeling; and integration with an artificial intelligence (A.I.) **path planner** allowing automatic, collision-free task programming. ROBOSIM has been in use both at NASA and in the university environment supporting **robotics** research and education (fig. 129). ROBOSIM was used to develop industrial **robotic** applications for a variety of shuttle systems, **robotic** algorithms for optimal **control** of **robotic** welding systems, and modeling of **robotic** systems concepts for use on Space Station *Freedom*. The objective of this project is the further development and transfer of ROBOSIM technology for distribution within the Agency, government, industry, and academia.

K. Fernandez/EB44
(205) 544–3825
Sponsor: NASA Technology Utilization Office

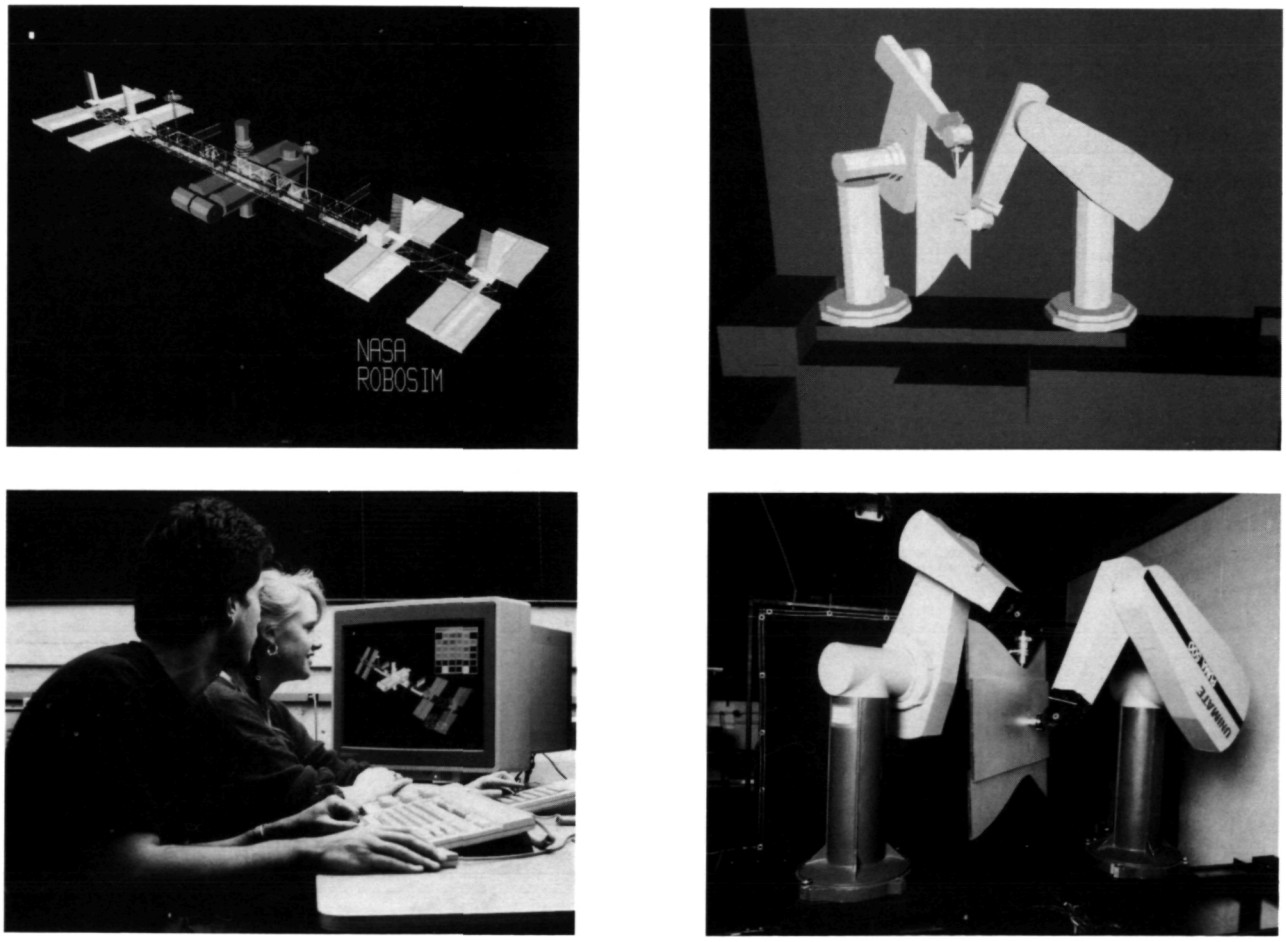

Figure 129. Application of ROBOSIM for Academic and Industrial Use

ORIGINAL PAGE
BLACK AND WHITE PHOTOGRAPH

Robotic Eddy Current Inspection System

With the increased use of carbon-carbon and graphite-epoxy materials in the aerospace industry also comes a demand for more sophisticated methods of nondestructive evaluation (NDE) of these types of materials. The integration of computers into NDE equipment, coupled with automated methods of scanning hardware, allows both inspection and interpretation of results to be performed on-line in real time. The development of these types of "smart" systems also results in shorter inspection times and a more accurate interpretation of results.

Under the direction of MSFC, The University of Alabama in Huntsville (UAH) has developed a "smart" system for eddy current inspection of both carbon-carbon and graphite-epoxy materials and hardware. The system, which is nearing the fully-operational stage, consists of a robotic manipulator arm that holds an inspection probe, a turntable that allows automated rotation of cylindrical hardware, and an eddy current instrument for test signal generation and display of results, all linked together by a supervisory computer, which, when fully operational, will store and interpret all of the test results. A new contract has been awarded to UAH for completion of this effort, at which time the system will be turned over to the NDE branch at MSFC.

Preliminary laboratory tests have shown that digital eddy current testing may be a viable method for in-process monitoring of composite components. Once fully-operational, the **robotic eddy current inspection** system will be used to perform analyses of graphite-epoxy and carbon-phenolic raw materials, in-process parts, and finished parts to identify general trends in processed materials, as well as localized changes in conductivity which might indicate changed mechanical or thermal properties. This information will be correlated with NDE data from other sources, such as computed tomography and ultrasonics through the Integrated NDE Data Evaluation and Reduction System (INDERS).

A further contribution of digital eddy current testing is expected to be the extrapolation of ply-orientation from three-dimensional readings of directional conductivity. This technique provides critical orientation information in a quantitative format, which can then be used to support thermostructural analyses of as-built components. Preliminary testing with carbon-carbon indicates this information is critical in predicting the failure load of composite rings and cylinders. Efforts to extract ply-orientation effects in wrinkled carbon-carbon cylinders have shown promise, but further development is required.

The information gained from this program will contribute to an increased understanding of the effects of processing on composite material properties and of the way composite materials fail.

C.C. Bryson/EH13
(205) 544–2553
Sponsor: Office of Space Transportation

Artificial Intelligence as Applied to Flight Mechanics

It is apparent that the initial generation of NASA that literally developed most space technology is approaching retirement age. For this reason, it is critical to attempt to capture as much knowledge from current employees as possible. In particular, the present research is attempting to capture the knowledge of **flight mechanics** engineers. The assignment can be summarized as follows:

Problem: Write a computer program which answers all possible well-formulated analytical questions which may be posed in an equation-based discipline.

The scope of the above problem is so great that a special technique had to be developed to cope with it. This technique proceeds in somewhat the same way that a person would proceed when faced with an orbital mechanics problem. The person first collects the known information then writes those equations which are needed to obtain the desired answer. From this point onward, it becomes a question of engineering experience to bridge the gap between the known data and the required data.

In the case of a machine operation, we cannot be this selective, but we can be just as successful. The first step is to collect all equations which apply to the discipline (i.e., **flight mechanics**). We now solve every equation for every variable. This is not a simple procedure, but it can be done even if we must rely upon iterations, numerical integration, etc.

The program now has a huge set of information at its disposal. And it is readily possible, especially if one uses an **artificial intelligence (AI)** language such as list processing (LISP), to examine all of the quantities which are needed on the right-hand side of some equation in order to calculate the left-hand side. If all of the elements on the right-hand side are known—and if the left-hand side is not known—then we proceed to calculate the left-hand side of the equation. This new information now becomes available to the "known" set of information and can often trigger additional variable isolations.

The above technique appears to be inefficient (it is) but that is really of no consequence. Modern machines are so fast and their storage capacity is so large that we are looking at only a few tenths of a second to squeeze out all the results which are implicit in a given data set. The growth of information is so rapid that only a few inputs by the user can sometimes solve seemingly intractable problems.

In addition to the basic concept, above, various other tricks, such as self-correcting menus, etc., make the entire program very user friendly. Additionally, the program contains "look-ahead" features which preclude the user from making any requests which could not be fulfilled in the future. This is done by setting the technology parameters to their extreme values and checking whether or not input requests could be fulfilled. If the users inputs are out of bounds, the machine informs the user of extreme values which can be accepted at each input.

It is also a simple matter to record the order in which the equations "fired" and then produce this listing for the user when the problem is complete. In this way, the computer not only solves arbitrary problems, but also reiterates the derivation which was used to obtain the solution.

It is worthwhile to note that the above techniques can be applied to any equation-driven discipline. It could outline, for example, organic synthesis techniques that might not occur to the human mind. Additionally, if a textbook were to be programmed with such a technique, any problem that could be assigned from that text could be immediately solved.

R. Burns/EL58
(205) 544–2284
Sponsor: System Analysis and Integration Laboratory

Fully Automated Variable Polarity Plasma Arc Welding

Computer-controlled variable polarity plasma arc (VPPA) welding has been used in the production of the space shuttle external tank since 1983. This welding system provides control of the critical welding parameters in addition to providing historical documentation of programmed and actual welding parameters for all welds. The welding operator, however, is still responsible for providing real-time adjustment to weld current, seam tracking, wire-feed entry, and plasma jet orientation. Therefore, the quality and repeatability of VPPA welds is still dependent on human judgement and skill.

MSFC has undertaken the design and development of the Marshall **automated** weld system (MAWS), independent of human intervention, to eliminate the possibility of weld defect caused by human error. The overall system architecture is shown in figure 130. The system integrates multiple **sensors** (providing real-time information on weld-bead geometry, weld-joint location, and wire-feed entry) with a weld model (describing weld geometry in relation to critical parameters) and computer-**controller** VPPA equipment. This system will provide real-time, closed-loop control of the weld as it is

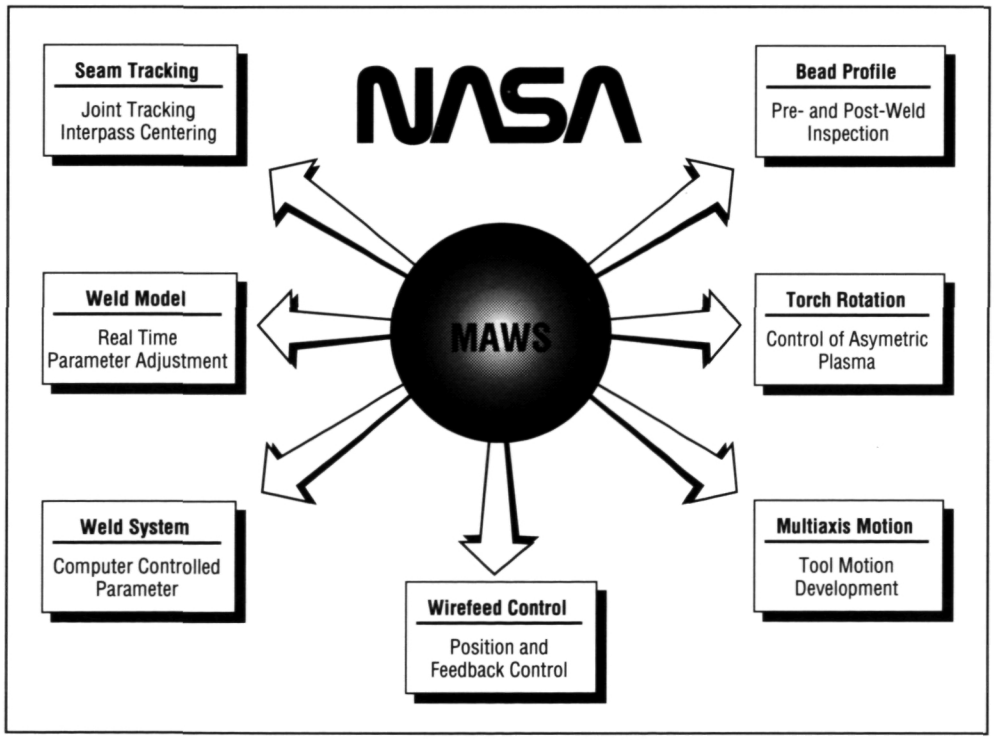

Figure 130. Automatic Weld System

being made. A secondary benefit of this system is the potential for **automated** weld visual inspection, either during or after welding, of the weld dimensions, peaking, and mismatch for quality assurance requirements.

Presently, design and development of each component of the overall system is in work. The welding control computer has been defined to a "real-time," UNIX-based **controller** able to integrate processing from up to 17 **sensors** and 12 axes of coordinated motion. Second- and third-generation **sensors** based on stereo imaging and multiple light sources are being developed for seam tracking. The second-generation seam tracker is an industrially packaged, scaled-down version with improved lighting over the previous design. The third-generation seam tracker now under a research contract processes information taken directly from the weld pool. A second-generation optical laser **sensor** has been fabricated for weld-bead profiling and torch rotation. This smaller packaged **sensor** will eliminate some of the time delays in VPPA torch rotation by taking vision data closer to the arc. The wire-feed control **sensor** is in a preliminary phase of development. The weld-model theoretical relations have been identified, and a computer simulation of the VPPA process is nearing completion. NASA personnel, in addition to multiple contractors, are involved, as the complexity of the system requires a team approach utilizing multiple engineering disciplines.

K. Lawless/EH42
(205) 544–2705
Sponsor: Office of Space Flight

Autonomous Rendezvous and Docking

As more and more vehicle systems are put into space, and greater numbers of missions must be performed, **autonomous rendezvous and docking (AR&D)** has become a required technology. It is especially necessary for the upcoming lunar transfer vehicles, orbital transfer vehicle, and the Mars rover sample return. This work has centered on the development of a video-based **sensor** using laser diodes to illuminate a passive (reflective) target (fig. 131). The **sensor** computes and outputs the positions and attitudes of the **sensor** relative to the target. The **sensor** consists of several components. The video portion uses a charge-coupled device-based camera for the actual optical input. Two sets of laser diodes at two different frequencies are placed around the camera lens to illuminate the target. The camera feeds into a frame grabber that captures the video input on command. The digitized image is processed by an Intel 80386-based personal computer, and the attitudes and positions are calculated from the processed image. The data can be fed internally into a guidance algorithm or output through a serial port into an external guidance routine or data gathering algorithm. The target being tracked consists of a modified remote manipulator system grapple fixture target; the modifications consist of the placement of narrow-bandpass-filter-covered retroreflective material at the outer ends of the target and on the top of the center post. Figure 132 depicts the OMV mockup.

R. Howard/EB24
(205) 544–3536
Sponsor: Office of Aeronautics, Exploration, and Technology

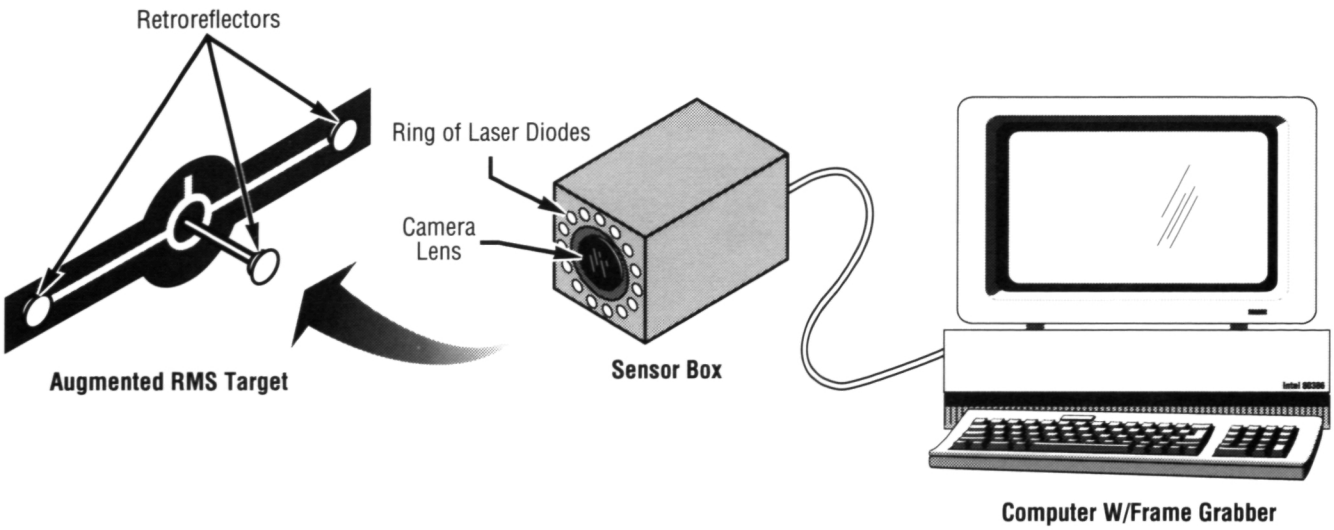

Figure 131. Passive Target and Sensor System

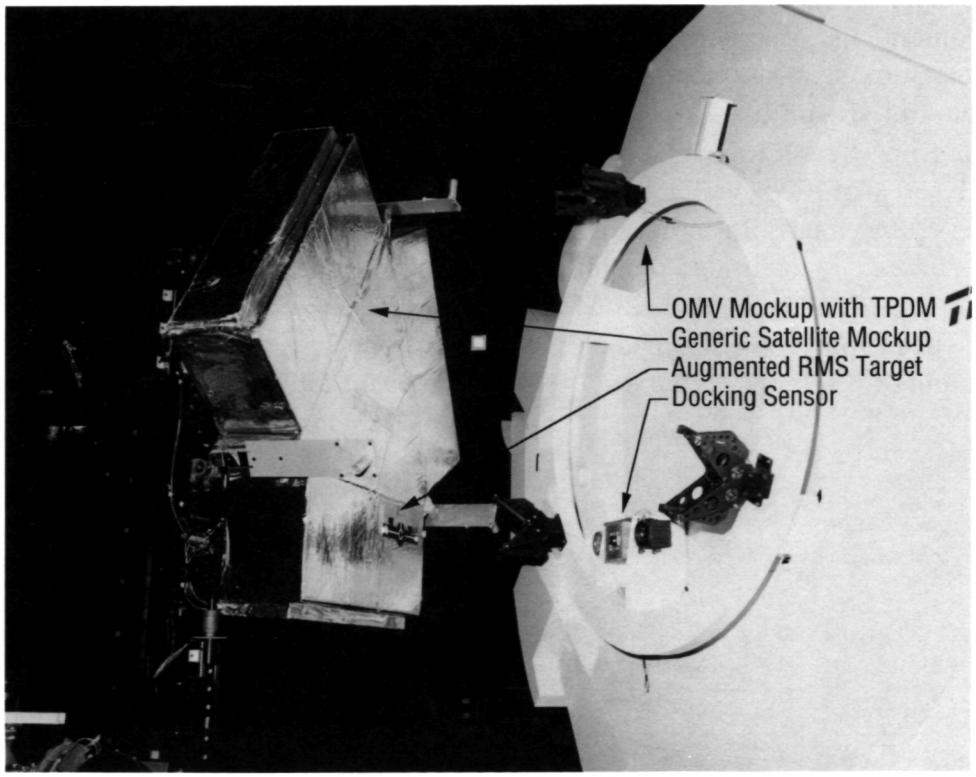

Figure 132. OMV Mockup With Three-Point Docking Mechanism and Sensor Docking With Satellite Mockup

ORIGINAL PAGE
BLACK AND WHITE PHOTOGRAPH

Advanced Telerobotic Concepts Using Neural Networks

A phase I Small Business Innovation Research study was completed which demonstrated the feasibility of using **neural networks** for **telerobotics**. Areas that were studied include neurocontrol, movement training, sensor data association, task improvement, and interaction of **neural networks** working with multiple joints. These neural network concepts and designs can be applied to **telerobotics**, such as the space shuttle remote manipulator system (RMS). Neurocontrol of three joints was accomplished using multiple, interacting feedforward **neural networks**.

Testing of neurocontrol for a simulated **telerobotic** arm that has the same number of joints, directions, and proportions as the space shuttle RMS was accomplished. Training of the neurocontrol concepts was developed, and an innovative way for performing automated training was programmed and tested.

An innovative, three-tier, **decentralized controller** was designed and its feasibility investigated. The usual implementation of such a controller is computationally intensive due to the nonlinearities involved. The modular neural network approach solves this problem. It also allows implementation and testing of the various subsystems in an ordinary, sequential procedure in which subsystems may be included or omitted as monetary or other practical considerations warrant. The proposed three-tier, **decentralized controller** can be implemented in a way which is, at once, both robust and stable. The first tier is the planning neural network that feeds information to the optimization network which then controls the joint controller networks.

The proposed neural network concept holds great promise for improving control of the space shuttle RMS. It is directly applicable to the assembly of the space station and is also applicable to other robotic applications such as the flight **telerobotic** servicer.

Pap, R.M., Harston, C.T., Maren, A.J., Parten, C.R., Rich, M.L., and Thomas, C.R., "Advanced Telerobotic Concepts Using Neural Networks." Contract NAS8-38443, Final Report.

R.R. Kissel/EB24
(205) 544–3510
Sponsor: Office of Commercial Programs

A Perception System for Object Recognition, Acquisition, and Tracking in Cluttered Environments

A phase I Small Business Innovation Research study was completed which developed a **perception** system for use in space applications such as the Mars rover sample return mission. Preliminary systems requirements were established along with a specification for a **perception** system that will meet NASA's objectives. A data base of 3-D imagery was generated and served as the basis for testing each element of the **perception** system in simulation.

The **perception** system consists of: (1) a special-purpose preprocessor that is optimized to detect objects in the field of view; (2) a unique 3-D object recognizer which utilizes a **neural network** for classification; (3) a multiple target **tracker**; and (4) a **perception** control system. Preliminary tests on the object recognizer indicate that this approach can recognize 97 percent of the test image data base. In addition, the multiple-target tracking system based on a Kalman-filter approach was tested against dynamic sequences of imagery consisting of target and clutter. The **perception** control system was designed to synergistically integrate the functions of the recognizer and **tracker** to achieve greater track tenacity in cluttered environments.

The end-to-end performance of the **perception** system was successfully demonstrated against the dynamic image sequences, including the capability of reacquiring objects after loss of track. Finally, an advanced concept for estimating the orientation of the NASA remote manipulator system docking target was developed and tested in simulation. Orientation was determined to within a few degrees.

Burman, J.A., and Brykman, J.A., "A Perception System for Object Recognition, Acquisition, and Tracking in Cluttered Environments." Contract NAS8-38047, Final Report.

R.R. Kissel/EB24
(205) 544–3510
Sponsor: Office of Commercial Programs

Active Detection and Tracking Sensor for Passive Targets

This Small Business Innovation Research (SBIR) from Computer Algorithm Development (CAD) of Austin, Texas, is in the development of algorithms to perform real-time, model-based computer vision for **detecting** and **tracking** targets. The target has one or more high-contrast markers on it, and each marker can have a **bit pattern** embedded in it for marker identification. The target is viewed by a video camera connected to a frame grabber in a Mac II computer. Figure 133 shows what a marker might look like.

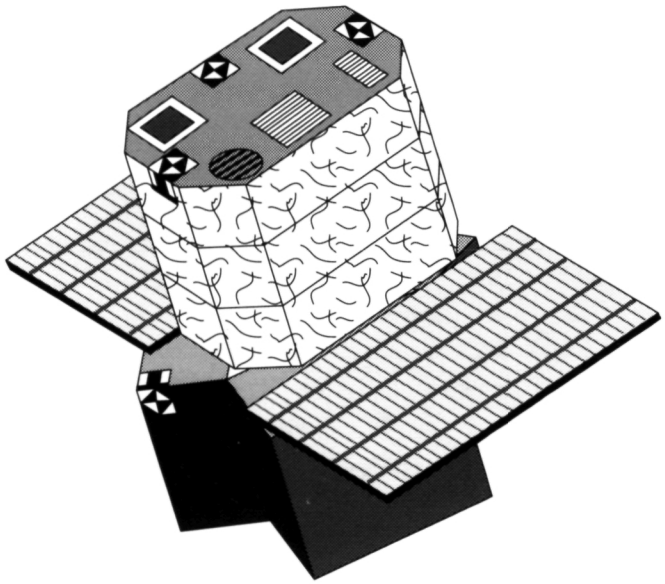

Marker at Single Scale, on Single Face, and With Bit Pattern for Marker Identification.

Figure 133. Passive Markers as They Might Appear Attached to a Satellite

One major slowdown in real-time image-processing is in the scanning of the entire frame for the high-contrast areas in which the edge-**detection** algorithms must be performed. CAD first uses algorithms which break the image down into areas which are individually searched for high-contrasts. This reduces the area to be processed to only 10–20 percent of the full image. The next step in the target **detection** algorithm is the fast edge detector. It finds all of the edges in the high contrast areas, and then passes this information in to the line detector, which first finds short lines and then long lines. From the information found from the lines, the marker and target can be identified and, later on, **tracked**.

Another research area under this SBIR is the capability to control a robot using a computer that can take the information about the target and thereby direct the movements of the robot.

Further work to be investigated includes accurate determination of relative positions and attitudes from the camera to the target. Also, angular ambiguity must be able to be resolved, camera and lens distortion effects will be examined, as will the ability to read a **bit pattern** embedded in the marker and the ability to track the mark(s), and thus the target. Finally, implementation of a full real-time **detection** and **tracking** system on a microprocessor such as the Intel 80860 will be examined. These items will be performed under phase II of the SBIR, if it is awarded.

R. Howard/EB24
(205) 544–3525
Sponsor: Office of Commercial Programs

The Environmental Control and Life Support System Advanced Automation Project

The **Environmental Control and Life Support System (ECLSS)** Advanced Automation Project is an ongoing R&T activity at MSFC which is intended to develop and demonstrate an integrated automated monitoring and fault-diagnosis capability for regenerative **ECLSS** systems. A prototype **ECLSS potable water processing assembly (PWPA)** computer simulation and fault-detection system has been developed. Continuing efforts include an advanced monitoring system with automatic complex fault-detection and model-based diagnosis capability for the test bed and flight **ECLSS**.

The **ECLSS** advanced automation project (**ECLSS** AAP) began with an overall analysis of the baselined Space Station *Freedom* **ECLSS** to determine candidate applications for advanced automation software. The real-time subsystem fault-detection and off-line fault-diagnosis tasks were determined to be the favored applications for emerging software technology. The real-time **PWPA** fault-detection algorithm was then prototyped using C-language production system (CLIPS) on an Apple Macintosh computer with a Hypercard user interface.

The first prototype showed that quick faults could be effectively detected using a rule-based methodology, but that the **ECLSS**, as a physiochemical process control system, has latency times which would allow for a deeper, and more time-consuming, model-based diagnosis methodology. The **ECLSS** AAP is developing both types of algorithms. Rule-based fault detection may quickly narrow the candidate components on-orbit, while model-based fault diagnosis, a less mature methodology, may automate ground analysis.

Diagnosis (isolate what caused the break, not what is broken) using models entails development of object-oriented models of the physical components

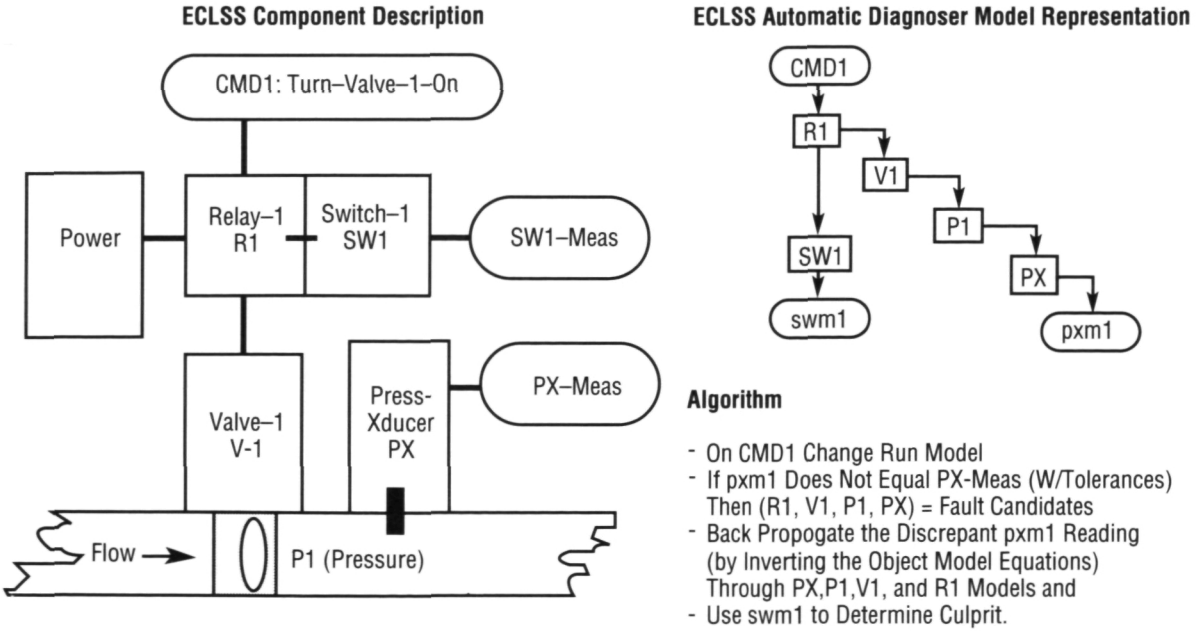

Figure 134. ECLSS Advanced Automation Project

in the **ECLSS**. As shown in figure 134, a change in the commands to the **ECLSS** subassembly also instructs the diagnoser to activate. The measurements, or sensor values, from the subassembly are then compared with the resultant modeled value, and a difference (plus or minus a tolerance) causes further processing. The object-oriented model is traced backwards from the sensor in order to list the candidate faulty components. Various techniques, including accounting-valid sister sensors, equation inversion, and rules of thumb, are used to narrow the search to the component.

Automated diagnosis of this type will detect any abnormal condition and attempt to determine the cause or possible causes, while traditional heuristic rule-based methods will detect only faults which have been previously programmed into the system.

Dewberry, B.S., The Environmental Control and Life Support System (ECLSS) Advanced Automation Project, Proceedings of the Third Annual Workshop on Space Operations Automation and Robotics (SOAR 89) July 25–27, 1989.

Dewberry, B.S., and Carnes, J. Ray, The ECLSS Advanced Automation Project-Domain Overview and Application Evaluation. Proceedings of the Space Station Evolution Conference, February 6–8, 1990.

Lukefar, B.D., et al., ECLSS Advanced Automation Preliminary Requirements-Final Report, UAH Research Report Number 823, The University of Alabama in Huntsville, Johnson Research Center, November 1989.

B.S. Dewberry/EB42
(205) 544–4247
Sponsor: Information and Electronic Systems Laboratory

Space Systems

Welding in Space

Welding can be a valuable process for fabrication and repair of metal structures in the space environment. A workshop on Welding in Space Technology was conducted at MSFC in 1989. This workshop identified applications for welding in space, technical issues to be addressed, and current research efforts on welding development for space. The Space Station *Freedom* will potentially be the first application for **welding** to repair structural damage or make plumbing repairs. The Moon/Mars mission will also require joining of structural components. Technical issues identified during the workshop include: safety, contamination, zero-g, **vacuum**, severe operator constraints, limited available power, difficulty in dumping waste heat, weld-joint design considerations, quality assurance, and automation. Currently, five joining methods are being investigated for possible space applications: stud **welding**, **gas tungsten arc**, laser beam, electron beam, and plasma arc **welding**. The latter four have been proposed for evaluation onboard a shuttle flight experiment.

The effects of zero-g are under study through the use of the NASA KC-135 aircraft. At present, no significant effects of gravity upon weld quality have been identified. Evaluation of weld-joint design is ongoing.

Vacuum welding experiments are being conducted in a **vacuum** chamber with high gas-load capability (six 81-cm (32-in) diffusion pumps) belonging to MSFC's Low-Density Flow Facility. Various weld processes will be evaluated to determine their effectiveness in **vacuum**. The first process being evaluated is the **gas tungsten arc welding (GTAW)** process. A hollowed tungsten electrode is used with small gas flows to transfer the arc to the work piece. The process has potential for space applications, but further development of the tungsten electrode and weld torch are mandatory for this process to be used in the space environment.

C. Kurgan/EH42
(205) 544–2705
Sponsor: Office of Aeronautics and Space Technology

CO_2 Laser Research and Development

Effort is continuing in the investigation of candidate **lasers** for use in the space-based coherent Doppler lidar known as the **Laser Atmospheric Wind Sounder (LAWS)**. Although the **LAWS** is a facility instrument under the Office of Space Science and Application's Earth Observing System, this effort is funded under the Office of Aeronautics and Space Technology's Civil Space Technology Initiative. The effort consists of both theoretical and experimental investigations of **lasers** and **laser** subsystems to determine the optimum technology for **LAWS**.

The FY90 work encompassed investigations at MSFC, Langley Research Center (LaRC), Jet Propulsion Laboratory (JPL), National Oceanic and Atmospheric Administration's (NOAA's) Wave Propagation Laboratory, and Spectra Technology, Inc. A phase I Small Business Innovation Research (SBIR) was completed by Qsource, Inc., investigating pulsed radio frequency (RF) discharge systems. A phase II SBIR was awarded to Qsource for continuation of this work. Two new phase I SBIR's were awarded, one to Science Research Lab, Inc., involving advanced CO_2 amplifier concepts, and one to Electro-optics Technology, Inc., involving a solid-state ring resonator.

Investigations at Spectra Technology, Inc., involving **laser** operation employing the rare isotope $^{12}C^{18}O_2$ were completed and a final report released. This study was cofunded with the Air Force Geophysics Laboratory.

Investigations to characterize the NOAA injection-locked TEA were completed by the NOAA Wave Propagation Laboratory and the results submitted for publication.

LaRC investigations in catalysis were restructured to focus on high-efficiency operation at room temperature for the $1^2C^{18}O_2$ isotope. A workshop was held on catalysts, and preparations for isotopic operation in chemical reactors began.

In-house investigations have focused on theoretical and experimental investigations involving sympathetic discharge **laser** and a hybrid-TEA-based master oscillator power amplifier **laser**. The sympathetic discharge **laser** was satisfactorily stabilized by extending the cavity length. Work is proceeding to incorporate this **laser** into a lidar system. A series of experimental investigations of **laser** system components has been identified and refurbishment of the hybrid-TEA-**laser** undertaken.

Plans for the coming year include the development of two breadboard **lasers** to be incorporated into the **LAWS** phase II study. Component and subsystem investigations will continue on a reduced scale.

Fisher, C.H., Hamilton, C.E., Mead, R.D., and Pindroh, A.L., "Kinetic and Extraction Measurements on $^{12}C^{18}O_2$," Final Report GL-TR-89-0292, October 31, 1989.

Post, M.J., and Cupp, R.E., "Optimizing a Pulsed Doppler Lidar," Submitted to Applied Optics, January, 1990.

Schryer, D.R., "CO Oxidation Catalysts for Long-Life CO_2 Lasers," NASA Conference Publication 10037, October, 1989.

J.W. Bilbro/EB23
(205) 544–3467
Sponsor: Office of Aeronautics and Space Technology

Coherent Doppler Lidar Research and Development

Research and development into **coherent Doppler lidars** (laser radars) covered a broad spectrum during FY90. Technical support was provided to program development on the two parallel studies for the laser atmospheric wind sounder (LAWS). These parallel studies are being conducted by GE and Lockheed. Phase I of the study was completed, and phase II was initiated. Work continues in the upgrade of the ground-based lidar facility, incorporating the capability to capture and record raw data, and to integrate large numbers of pulse returns. The 9.11-μm atmospheric **backscatter** system was completed and flown along with the 10.6-μm **backscatter** system on board the NASA Ames DC-8 aircraft as part of the **Global Backscatter Experiment (GLOBE)** mission, an experiment to measure atmospheric **backscatter** in the free troposphere. Additional theoretical and experimental investigations were performed in signal processing and in assessing atmospheric effects.

Software capabilities for display and processing of lidar data are continuing to be enhanced. Programs are being put in place which allow the collection and processing of data for wind profiling, **backscatter**, absorption profiling, and investigating atmospheric decorrelation effects. Efforts in the measurement of **backscatter** have been concentrated in the completion of the 9.11-μm systems and the detailed

calibration of both the 9.11-μm and 10.6-μm system in preparation for the flight tests. Both systems were flown aboard Ames Research Center's DC-8 during the fall of 1989 and the spring of 1990 as part of **GLOBE**. Data from this experiment will allow performance of the proposed LAWS instrument to be assessed, and the final design to be optimized.

In-house work is continuing in support of LAWS. Programs are being developed which will provide capability of simulating the LAWS system from a variety of orbital and atmospheric conditions.

J.W. Bilbro/EB23
(205) 544–3479
Sponsor: Office of Space Science and Application

Advanced X-Ray Astrophysics Facility's Technology Mirror Assembly

The technology **mirror** assembly (TMA) consists of two mirrors which are approximately two-thirds the size of the innermost pair of **mirrors** of the **Advanced X-Ray Astrophysics Facility (AXAF)**. The TMA program was designed to demonstrate the ability to fabricate optics to the level of precision required for the **AXAF**. Following **x-ray** testing of the **mirrors** in the spring of 1989, a program was undertaken to ascertain the level of particulate contamination on the **mirrors** and to determine the cause of alignment instabilities discovered during testing.

Investigations into the measurement of contamination levels were brought about by the desire to determine the effect of particulate contamination on **x-ray** performance. The investigation involved photographing the surface of the TMA mirrors through access holes in the inner protective cylinder. A unique piece of equipment, similar to a periscope, was designed to operate in the restrictive environment available within the TMA. The test setup is shown in figure 135. The photographic system was capable of resolving particles as small as 3 μm in diameter.

A plot showing the results of the data analysis is given in figure 136. This plot shows the areal coverage of contaminants observed through the access holes as a function of particle size.

At the completion of the contamination measurements, testing of the TMA optics for instability will be carried out.

J.W. Bilbro/EB23
(205) 544–3488
Sponsor: Office of Space Science and Applications

ORIGINAL PAGE
BLACK AND WHITE PHOTOGRAPH

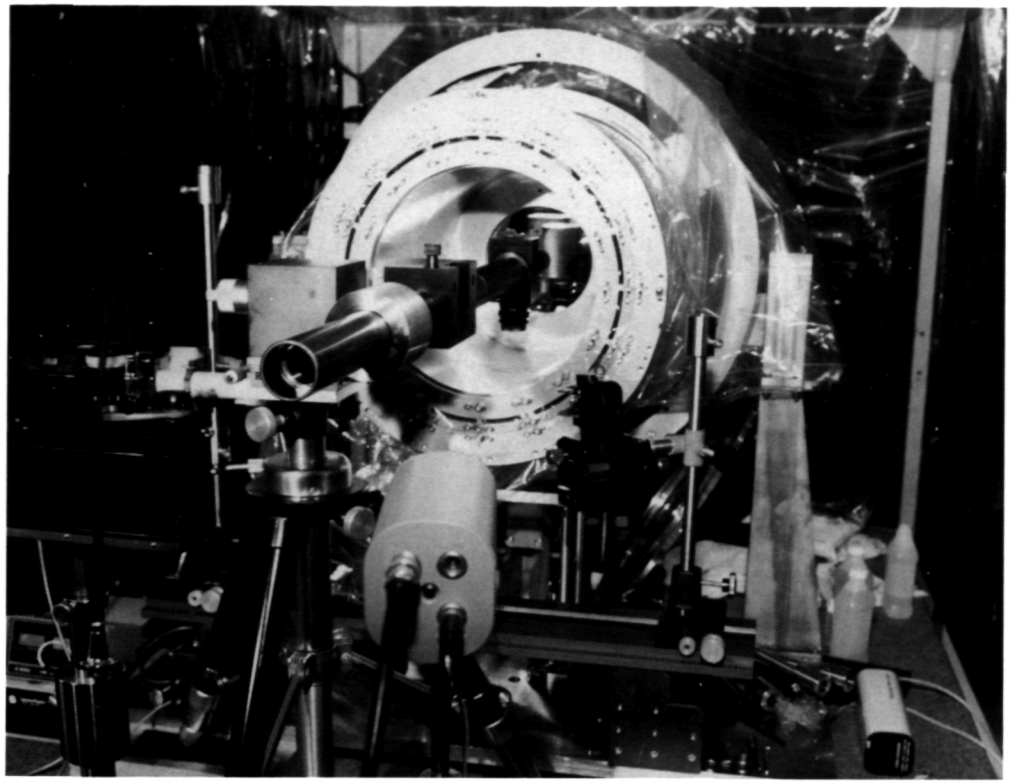

Figure 135. Test Setup for Photographing the Surface of TMA's to Determine the Effect of Particulate Contamination on X-Ray Performance

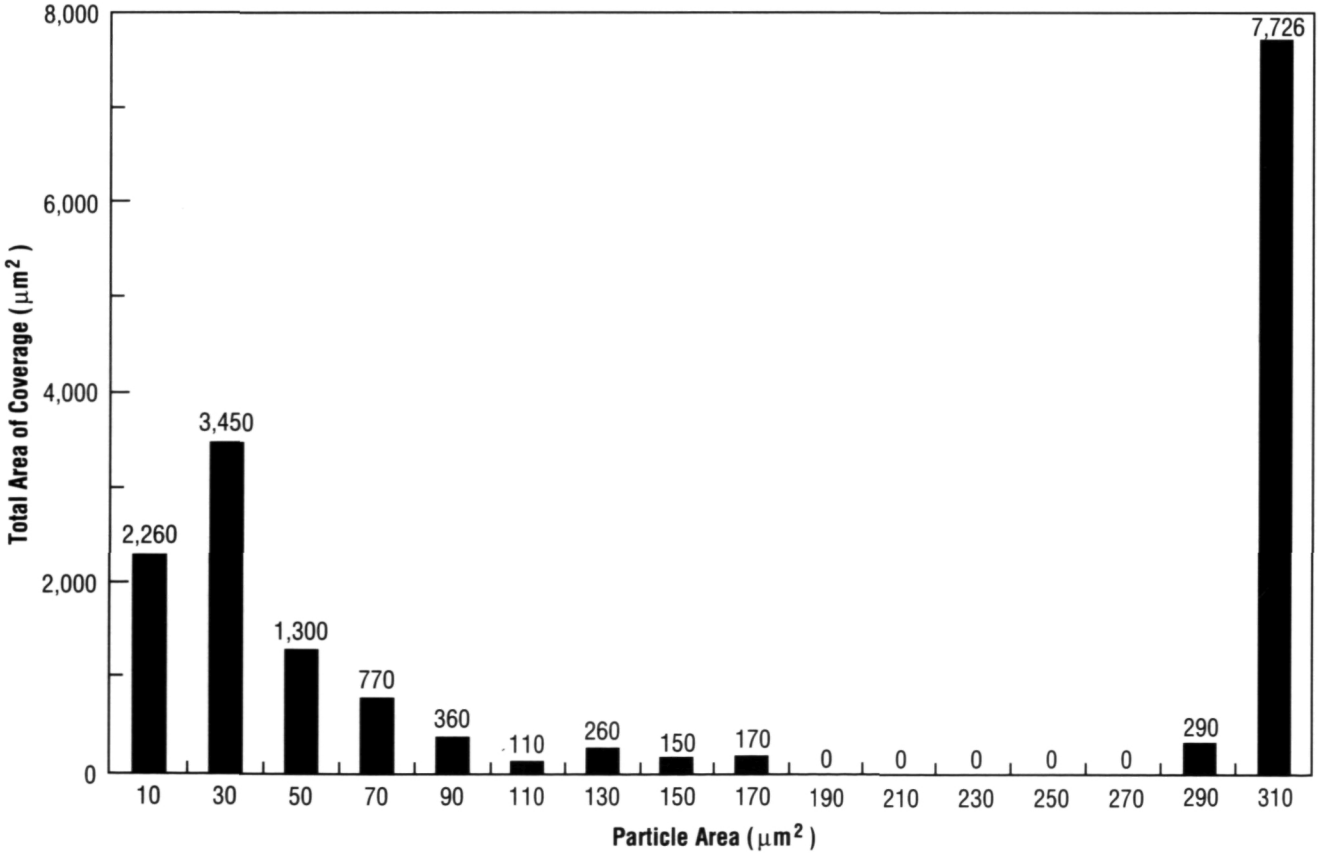

Figure 136. Total Particulate Coverage as a Function of Particle Area for the TMA Parabolic and Hyperbolic Mirrors

Expendable Lightweight Composite Intertank

The advent of larger, heavier payloads requires an inexpensive heavy-lift launch vehicle. The Advanced Launch System (ALS) offers large payload capacity for future missions. A lightweight **composite intertank** is an integral part of the expendable ALS vehicle (fig. 137).

The objective of the **intertank** study is to prove the application of research with a cylindrical structural test article (STA). The STA will not only be used to exhibit the strength of the structure, but will also be used to verify the design and analysis, automated fabrication process, and cost estimates for production. The study contract is divided into three phases. Phase I covers the design, analysis, and component tests of the **intertank**. Phase II covers the fabrication of the cylindrical STA. Phase III encompasses the testing of the STA.

Currently, phase I activities continue to improve the robustness of the design. Since the **intertank** is positioned between the liquid oxygen and liquid hydrogen propellant tanks and supports all the mass above it, the **intertank** is a highly loaded structure with cryogenic interfaces. The **composite intertank** design is more efficient and can be manufactured at a lower cost than an advanced metallic structure. The **intertank** is a honeycomb sandwich construction with graphite/epoxy skins. The resin system selection is based upon good compaction and flow characteristics. The **composite** lay-up is tailored to handle high loads under cryogenic conditions. The interface-joint design is being refined to develop a configuration that is insensitive to variations in fabrication processes. Automated manufacturing techniques can be employed to produce high-quality **intertanks**. Component tests have been performed to determine areas of improvement and verify the analysis. **Damage tolerance** tests have been performed to characterize the residual strength of the sandwich structure. Both destructive and nondestructive evaluation were incorporated to determine the extent of the **damage**. This lightweight structure allows either more payload capacity or a smaller vehicle for delivery of required payloads into orbit.

D.B. Ford/ED42
(205) 544–2454
Sponsor: Office of Aeronautics and Space Technology

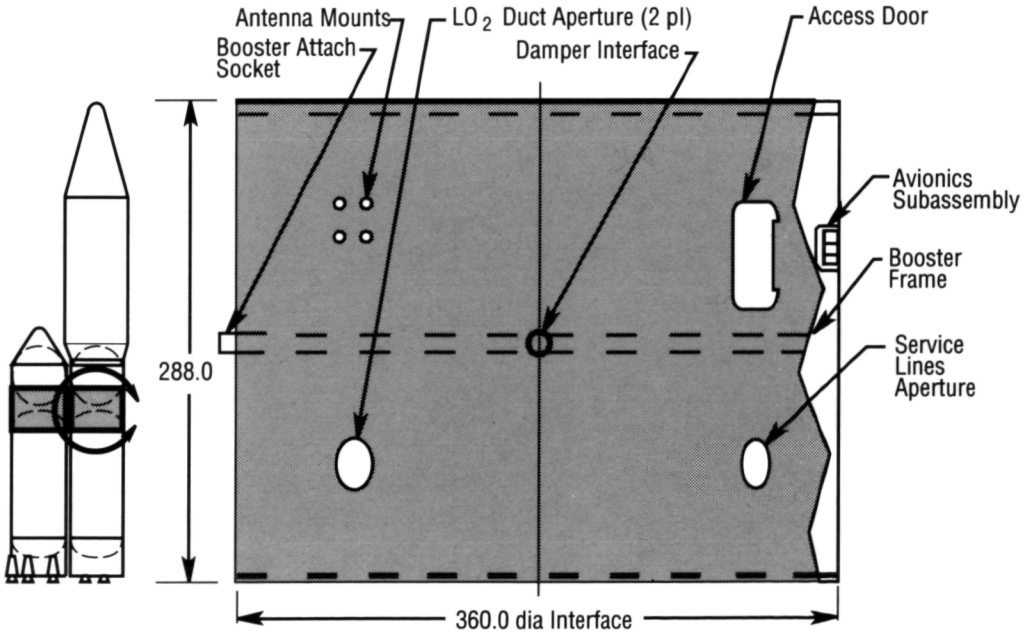

Figure 137. Expendable Lightweight Composite Intertank

Pathfinder Mechanical Joints for In-Space Assembly and Construction

The objective of the Pathfinder In-Space Assembly and Construction project is to develop the technology required to assemble and construct space vehicle components on orbit. A goal of this project is to minimize extravehicular activity (EVA) and maximize automation methods. The requirements to meet these objectives are:

- Develop methods for constructing large vehicle components in space
- Develop joint concepts for constructing and assembling components in space
- Develop the ability to manipulate, position, and assemble large, massive components in space
- Define the infrastructure to accomplish the construction, joining, and assembly of vehicles in space.

MSFC has identified the assembly and construction of a 37-m (120-ft) diameter tetrahedral **aerobrake** truss as a focus problem. The intent is to use the **aerobrake** structure to determine requirements for developing joining methods and assembly concept technologies. MSFC has determined that over 90 percent of the axial loads of the tetrahedral truss would be approximately 444.8 kN (100,000 lbf) or less in tension or compression for a 3-g deceleration of 3,780.8 kN (850,000 lbf) space vehicle. MSFC has also identified various typical large components, such as cylindrical and spherical vessels, that might be required for a Lunar/Mars mission that would need to be attached to the **aerobrake**.

A personal computer version of NASTRAN was used to model a 3.94-m (12.91-ft) diameter, 357.43-kN (80,356 lb) spherical liquid oxygen (LOX) tank and a 12.8 m (42 ft) long by 4.42 m (14.5 ft) wide, 286.13 kN (64,328-lbf) Space Station *Freedom* laboratory module connected to the 37-m (120-ft) diameter tetrahedral truss. A 3-g deceleration in the vertical direction and a 1-g deceleration of each of the transverse directions was applied to the sphere and the cylinder. The resulting loads in the members connecting the sphere and cylinder to the tetrahedral truss for selected configurations with the lowest magnitude of load ranged from –315.81 kN (–71,000 lbf) to 711.6 kN (160,000 lbf), and –151.23 kN (–34,000 lbf) to 155.068 kN (35,000 lbf), respectively. Preliminary concepts for the joining of large components to the **aerobrake** truss followed.

Several ideas for joint concepts were initiated that would support the ±444.8-kN (±100,000-lbf) load requirement of the **aerobrake** and allow for assembly, thermal, and tolerance misalignment totaling ±0.0508 cm (±0.020 in). A **robot-compatible mechanical joint** concept, called the grip joint, which could be misaligned by more than ±0.0508 cm (±0.020 in) and support the ±444.8 kN (±100,000 lbf) load was designed and fabricated and is shown in figure 138.

To verify the strength of the joint for various materials, three 2219-T6 aluminum joints were fabricated for the tetrahedral truss members for ±444.8 kN (±100,000 lbf) and less. Two 6AL-4V

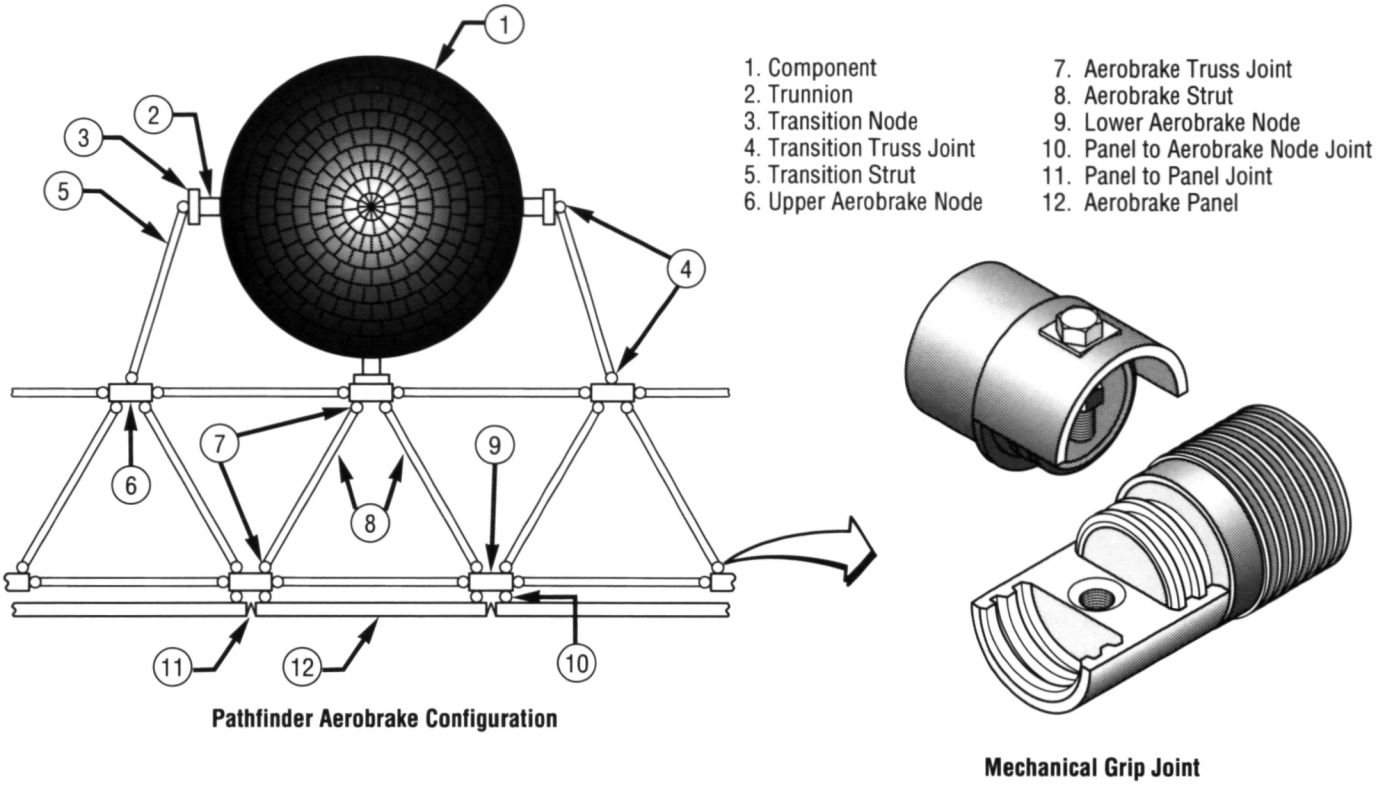

Figure 138. Pathfinder In-Space Assembly and Construction

titanium joints were fabricated for the truss members supporting truss struts over ±444.8 kN (±100,000 lbf) because of its high strength and its low coefficient of thermal expansion characteristics. Two silicon carbide 6061 aluminum metal-matrix composite joints are being fabricated to help reduce the weight and provide a lower coefficient of thermal expansion. Three tests are to be performed on one of the joints of each different material. The first test will be a ramp loading test. The joint will be loaded to ±88.96 kN (±20,000 lbf) and to ±222.4 kN (±50,000 lbf) in 44.48-kN (10,000-lbf) increments. The second test will determine the coefficient of torque friction used to calculate the torque needed to obtain the required preload on the joint. The third test will load the joint to failure in 88.96-kN (20,000-lbf) increments. One of the aluminum joints has been delivered to Langley Research Center to be used in a test bed for robotic assembly.

Once these tests have been completed and the data analyzed, the grip joint will be modified and optimized for weight. An alternate joint concept, the slip joint, is being designed. Results of the slip-joint testing will be used to identify strong and weak points between both joint concepts. Also, a node that will be the point of connection for up to nine struts will be designed and fabricated this year.

F.P. Thomas/ED52
(205) 544–4936
Sponsor: Office of Aeronautics and Space Technology

Space Station Low-Temperature Portable Cooler for Biological Samples

Biological experiments on the **Space Station *Freedom*** will require the **storage** and transport of biological samples from space to Earth. To prevent biological growth, the samples must be maintained below –70 °C (–94 °F). Periodic removal, transfer from station to shuttle, and transport to Earth of these biological samples will require a **portable**, controllable **storage** container. Under this NASA Small Business Innovation Research program, a **portable**, self-contained **storage cooler** was developed. The **cooler** can maintain the contents below –70 °C for at least 125 hours without any power from the station orbiter. This period of autonomous thermal control is based on mission timelines for an orbit-to-Earth profile, including landing. While mounted in a double rack on the **Space Station *Freedom***, the **cooler** will use station power for monitoring temperatures within the **storage** volume and maintaining the low temperature via mechanical refrigeration. During transport, no electrical power is required, with only a self-contained battery pack used to monitor temperature.

The **cooler** is designed to minimize thermal losses through design details incorporating high-performance multilayer insulation (MLI), low-conductance fiberglass, and low-temperature phase-change material (PCM). Because of the low-temperature requirement, the thermal losses can become substantial. To minimize these losses, a design was selected that eliminates structural protrusions through the MLI. The resulting design, shown in figure 139, indicates that the **cooler** is supported only at the neck and lower support pin. Because the neck at the access port carries a substantial amount of the launch and landing loads, it represents a major source of heat loss. To minimize this impact, low-temperature phase-change material is localized in this region. The phase-change material is enclosed in a toroidal tank, is noncorrosive and nontoxic, and provides an effective specific heat of 1.42 kJ/kg- °C (0.34 Btu/lb- °F).

The design of the phase-change material container is such that insertion and removal of phase-change material is quick and easy. An integral cooling passage is designed into the base of the container to facilitate cooling while in orbit. A high-performance neck plug is used to seal the **cooler** and provide easy access. The neck plug utilizes MLI in an evacuated cavity to minimize heat losses. The designs of the **storage** containers rang from small 20-cc ampoules to 1-L bottles. The **storage** system is designed to minimize removal of existing samples while in orbit by allowing racks to be rotated and translated for access to a desired rack. The commercial potential of this development is excellent. Storage and transport of biological tissue, samples, and organs on Earth often require a rapid and mobile response. This can be achieved with a minimum of support equipment, thereby reducing cost and saving time.

C. Horan/ED63
(205) 544–7201
Sponsor: Small Business Innovative Research Program

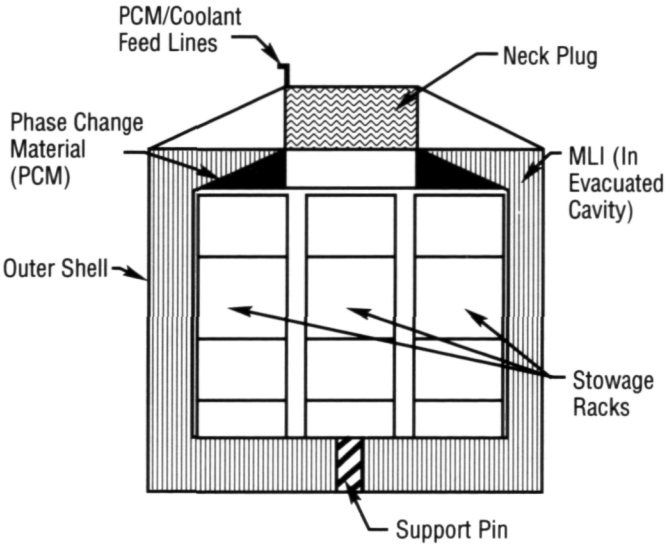

Figure 139. Space Station Portable Storage Cooler

Assessment of Materials in Solid Rocket Motors by Near Real-Time Computed Tomography

At MSFC, there is the need to determine the effects of heat and stress on materials used in **solid rocket motors (SRM's)**. An immediate need in the area of SRM subscale test bed technology is the characterization of peroxyacetyl nitrate (PAN) and rayon ablative materials used in **nozzle assemblies**. The nondestructive method known as **computed tomography (CT)** is an ideal and well-established method for examining the properties of materials. Over the last 15 to 20 years, **CT** has evolved from being used exclusively as a medical diagnostic tool, to finding applications in the industrial world. With this evolution has come more efficient types of scan methods, better image processing, and more dependable **x-ray** sources. Consequently, speed of imaging has increased dramatically, and given us what is now recognized as a new generation of high-speed **CT** scanners. These **CT** scanners are capable of rates of 50 ms per **x-ray** scan. One of these scanners is produced by Imatron, Inc., of San Francisco, California. Imatron, Inc., and MSFC have teamed up to look at the feasibility of initially using the fast **CT** scanner to evaluate carbon-phenolic and glass-phenolic ablative materials under stress and heat in an environmental oven. By having **CT** images of the part at near real time, we can visually detect failure modes of these materials.

The Imatron C-100 scanner is a fifth-generation scanner. First- and second-generation **CT** scanners require translation and rotation of the test object and/or **x-ray** source. The third- and fourth-generation require rotation only. These mechanical constraints limit the speed in which a scan can be taken. This problem has been overcome by Imatron's electron-beam C-100 scanner. The C-100 replaces mechanical motion with an electromagnetically deflected electron beam, thus allowing for its rapid scan rates. The slice, or image cross section, ranges from 3 mm to 10 mm depending on which image resolution is chosen. The lower resolution is a multislice mode with a scan time of 50 ms, while in the high-resolution or single-slice mode, a scan time of 100 ms is achieved.

Under a current Small Business Innovation Research (SBIR) phase I task, Imatron and MSFC will perform compression and heat tests on two material ablatives used commonly in rocket nozzles. They are carbon and glass phenolics. The images will be visually inspected first to look at possible failure modes within the specimens. Then subsequent analysis will potentially correlate density changes to heat and stress measurements. The impact of this successful SBIR phase I task in the **SRM** community is that a diagnostic **CT** tool may potentially be able to evaluate material in a plasma-spray chamber under a realistic plume environment. The scale-up of such a device to actual **SRM** hardware testing is the long-range objective of this program.

M.W. Suits/EH13
(205) 544–8336
Sponsor: Office of Commercial Programs

Space Station Module Power Management and Distribution

The **Space Station Module Power Management and Distribution (SSM/PMAD)** breadboard models the power distribution within a Space Station *Freedom* habitation or laboratory module. Besides power hardware, the system includes computer control through a hierarchy of processors. At the lowest level is a fast, simple (from a computer standpoint) switch gear, capable of quickly "safing" the system. At the next level are local load-center processors, called **lowest level processors (LLP's)**, which execute scheduling, perform redundant switching, and shed loads which draw more than scheduled power. Above the **LLP's** is a communication and algorithmic controller which coordinates communications with the highest level of control. At this highest level are three cooperating artificial intelligence (AI) systems which handle load prioritization, scheduling, load shedding, and fault recovery and management. The system, working together, provides an excellent venue for developing and examining advanced automation techniques.

The work which led to the **SSM/PMAD** breadboard began in 1984. The present test bed which models the Space Station *Freedom* power subsystem consists of three load centers powered by two power distribution control units in a 120-Vdc star-bus configuration shown in figure 140. The **LLP's** are 80386-based microcomputers with an Ethernet communications board. The three AI systems are

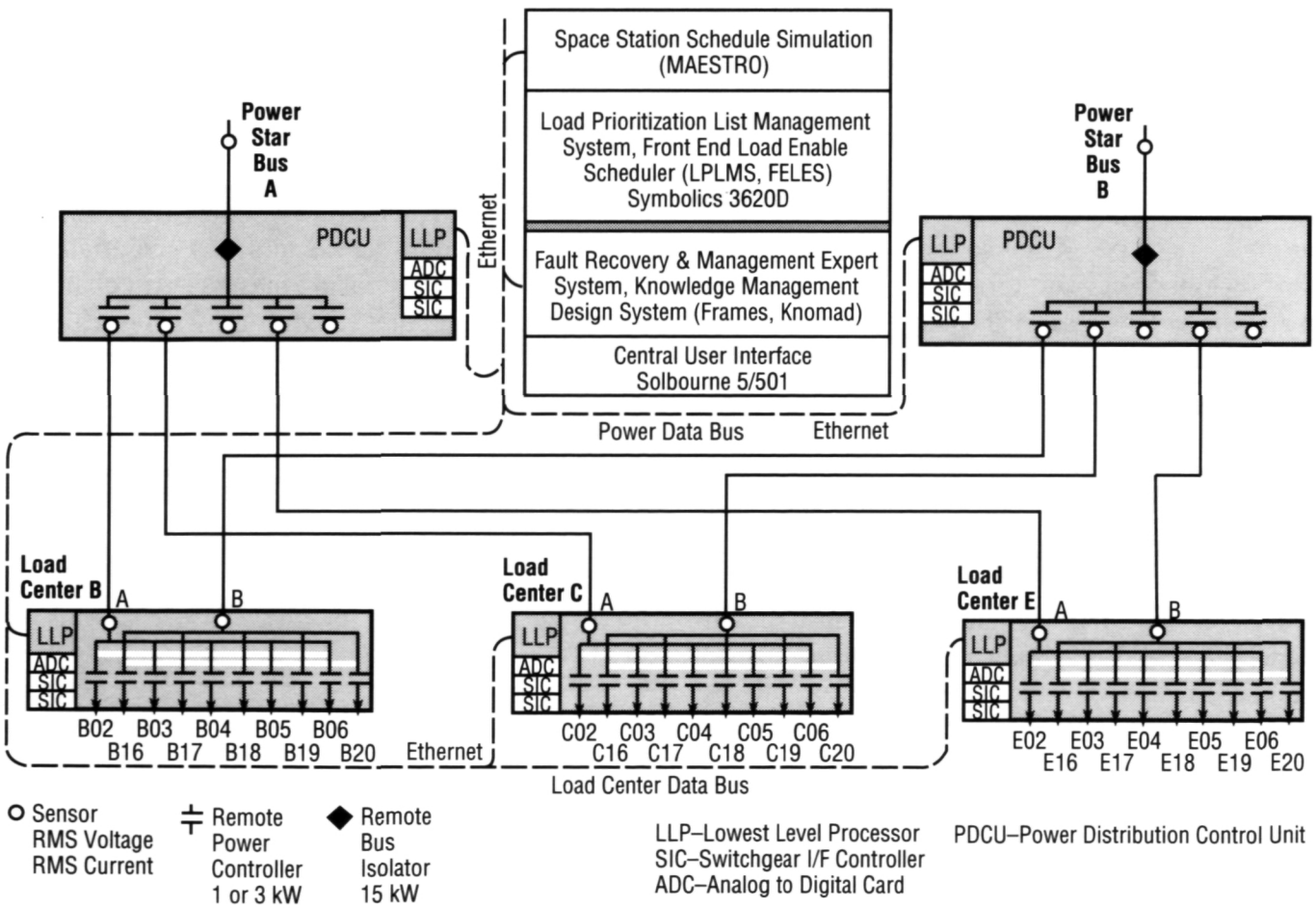

Figure 140. Space Station Module/Power Management and Distribution System

installed on a Solbourne 5/501 workstation and a Symbolics 3620-D AI workstation. The user interface and the communications gateway are installed on the Solbourne workstation with all high-level communications being performed on an Ethernet local area network. One of the three AI systems has been ported into a new **knowledge-based management system (KBMS)** with a second to be ported soon. The **KBMS** makes the knowledge in the system more explicit and groups the knowledge into modular groups of rules. It will also serve as an overall framework to expedite improvement of the cooperation between the three AI systems in the breadboard.

As the breadboard matures, several efforts are underway to make the breadboard more robust. The first effort involves enhancing the man-machine interface to be more graphic and user-friendly. The next effort involves adding intermediate levels of autonomy in order for the system operator to be "in the loop." This will allow an override capability without requiring the operator to take complete control of the breadboard. Another effort will involve evaluating the system in order to push as many functions as possible down the levels of hierarchy. This could help reduce some of the data management requirements for an autonomous system such as the **SSM/PMAD**. Finally, a link to the Lewis Research Center Autonomous Power System is being implemented.

Miller, W., et al., "Space Station Automation of Common Module Power Management and Distribution." NASA Contractor Report 4260, November, 1989.

Lollar, L.F., and Walls, B., "Automating Large Electrical Power Systems for Spacecraft." *Applied Intelligence Journal.* (In review for the January 1991 journal.)

Riedesel, J.D., "Knowledge Management: An Abstraction of Knowledge Base and Data Base Management Systems." NASA Contractor Report 4273. January, 1990.

L.F. Lollar/EB12
(205) 544–3306
Sponsor: Office of Aeronautics, Exploration and Technology

Avionics

Nickel-Cadmium Battery Expert System-2

The Electrical Division at NASA/Marshall Space Flight Center is heavily involved in the testing of **batteries** for use in space flight. There is a continuing effort to reduce the amount of data retrieved from these **battery** tests to more usable data that can be manipulated to evaluate each **battery's** status, and provide decision support as to whether or not a change in the operation of the **battery(ies)** is needed (i.e., reconditioning, a charging scheme change, or a load adjustment).

The use of **expert systems** to reduce data and evaluate **batteries** has been the approach taken in performing the task of providing decision support and **battery** status. Expert systems have played an important role in the testing of **batteries** at MSFC. The use of **expert systems** began with the nickel-cadmium **battery expert system** (NICBES) in 1986. It was developed by Martin Marietta Corporation, Aerospace Division, Denver, Colorado, and was used with the Hubble Space Telescope (HST) electrical power system (EPS) nickel-cadmium six-**battery** test bed at MSFC. NICBES successfully predicted certain anomalies in the test bed. The involvement with **expert systems** has continually progressed to include an updated version of NICBES which greatly enhances the previous system. Dr. Alex Bykat of the University of Tennessee at Chattanooga was successful in adding an online rule editor to NICBES to make necessary changes to parameters of rules much quicker and more efficiently. Next, he upgraded the system so that it would be multitasking, capable of storing more orbits for more accurate trend analysis, and have better graphics resolution and faster computation capability. This upgrade was entitled NICBES-2 (fig. 141). It was developed through a grant to the University of Tennessee at Chattanooga. NICBES-2 greatly enhanced the operation of the original NICBES and is still being utilized by the test bed.

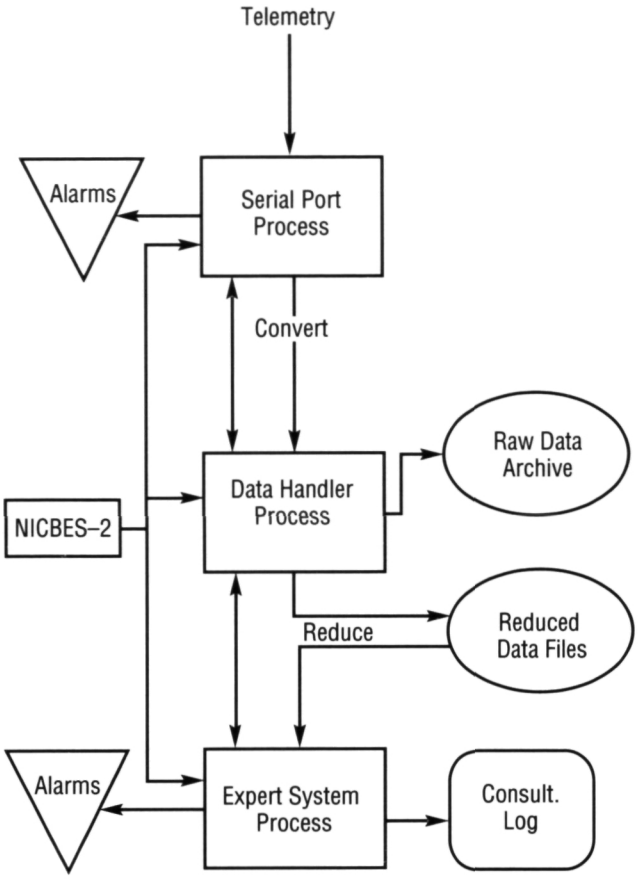

Figure 141. NICBES-2 Top Level Structure

NICBES-2 resides on a Sun 386i/150x with a 4-MB RAM expansion, 60-MB tape drive, development toolkit, Quintus Prolog, and Quintus ProWindows. A DEC LSI-11 sends telemetry to the Sun from the EPS test bed. By using the SunOS variant of the Unix operating system, NICBES-2 is capable of performing concurrent tasks. It performs orbit data gathering, data evaluation, alarm diagnosis and action advice, and status and history display on each **battery**. The decision-support capabilities of the original NICBES were enhanced in NICBES-2. The graphics were enhanced, and the causes of alarms are now explained in more detail. The data handler portion of NICBES-2 is written in BSD C. The data is gathered from an RS-232 connection which is controlled by a serial port process. The data handler receives raw data from the EPS test bed digital data acquisition system (DDAS), reduces the data, stores the data in corresponding files, and transmits the data to the **expert system**. The **expert system** program is written in Quintus Prolog. It is started by the **expert system** process and uses the data files from the data handler process to generate status and advice information.

Due to needed changes of rules at certain times, NICBES-2 has the capability to display and edit rules in its knowledge base. A simple interactive rule editor (SIRE) provides this capability. SIRE allows a user, who may have no knowledge of PROLOG or any other programming language, to modify the existing rule base of NICBES-2. Upon exiting SIRE, the rule base is automatically updated and transformed into PROLOG clauses. New rule-base files are created only when the rule base has been changed.

Bykat, A., "Expansion of Nickel-Cadmium Battery Expert System's Capabilities," Final Report On MSFC/NASA Grant NAG8-105.

Y.B. Johnson/EB12
(205) 544–3310
Sponsor: Office of Space Flight

Optical Plume Anomaly Detector

Over the past 4 years, a system that would monitor the health of the space shuttle main engine (SSME) during ground-test operation has been under development. The approach taken was to use the principle of exhaust-**plume** spectroscopy as the method to monitor the condition of the SSME during testing. Thus, by spectrally examining the exhaust for metallic emission, the state of propulsion system can be determined on a real-time basis. Pretest evaluation of engine status was not addressed during this undertaking.

The **optical plume anomaly detector (OPAD)** system (fig. 142) evolved into a 16-channel **polychromator** of high spectral and temporal resolution which monitors preselected elements compounds in the exhaust **plume**. The **polychromator** has a 3-ms response time. The second instrument is a moderately high-resolution **spectrometer** with an OMA-type detector covering a spectral range from 280 to 740 nm. A more comprehensive description of the **OPAD** hardware is reported in the below-referenced publications.

The **OPAD** instrumentation at MSFC has, to date, monitored 18 ground-level test firings of the SSME on the Technology Test Bed. Since the SSME performed nominally during many of the recent tests, most of the acquired data are being used to support the data based for normal **plume** emissions. Efforts along these lines include a complete analysis of these data to spectrally characterize (1) engine startup and shutdown phases of all tests (periods of great dynamic change); (2) steady-state operation of the engine including programmed changes in power levels; (3) specific timed events (e.g., the

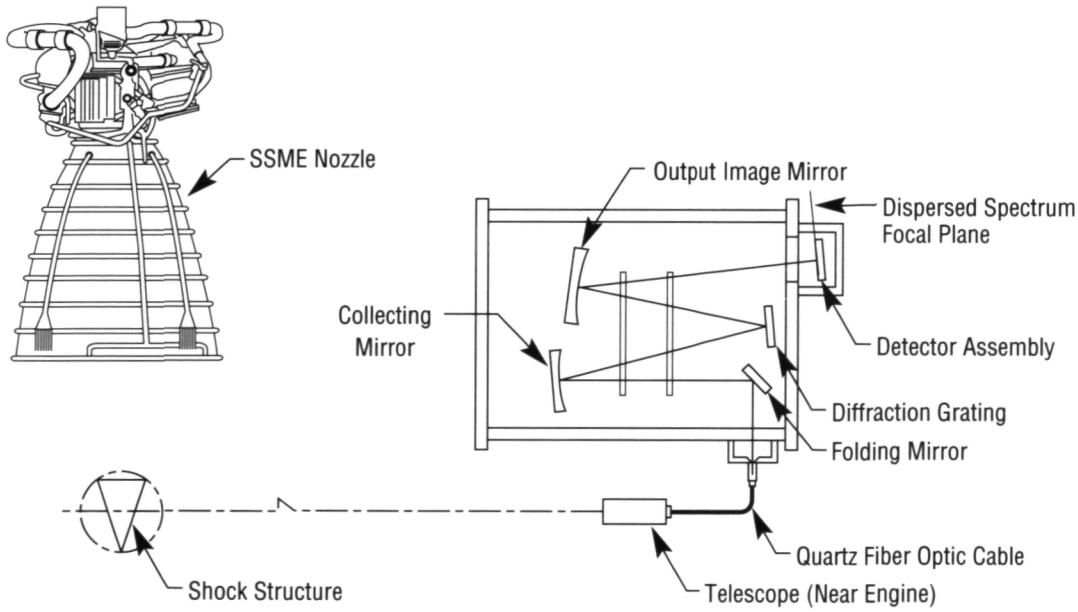

Figure 142. Optical Plume Anomaly Detector Configuration

induction of a controlled microinstability into the rocket combustion system); and (4) malfunctions in engine operation. For example, during TTB-016, a weld failure in an exhaust duct of the SSME occurred at approximately 3.5 s into a 165-s test. The **OPAD** system noted a marked spectral intensity increase in chromium at this time. Chromium is an element found in the welding material.

To date, all investigation has been affected by post-firing analysis; that is, the data are scrutinized for anomalous artifacts during the days after a test, and some items are identified through conversations with the engine hardware engineers. In the interest of speeding up the analysis, new computer hardware and software is being brought on line in the near future. To yield real-time number-crunching and transfer data to high-resolution display screens and printer units, 33-MHz 386-based machines were employed. Continuously updated full spectra are displayed in "waterfall" format, and the 16 channels of **polychromator** data are displayed in X vs. T format. Enough computing power is available to allow decisions to be made even if several simultaneous inputs are employed. This program is still considered to be experimental, although certain features of it are utilized now.

Powers, W.T., Zaccardi, V.A., "Status of OPAD Instrumentation Conference, on Advanced Earth-to-Orbit Technology," MSFC, AL: May 17, 1990.

Wallace, T.L., and Cooper, A.E., "Summary of Data from OPAD Program; Conference, on Advanced Earth-to-Orbit Technology," MSFC, AL; May 17, 1990.

W.T Powers/EB22
(205) 544–3452
Sponsor: Office of Aeronautics, Exploration, and Technology

Nonintrusive Flowmeters for Rocket Engines

Flow measurements are essential to rocket-engine control and condition monitoring, providing more reliable engine operation. **Nonintrusive flowmeters** do not disturb the propellant flow, which could create potential hazards. Commercial, **nonintrusive**, ultrasonic **flowmeters** have typically been used to measure flow rates up to 30 ft/s for noncryogenic liquids.

During this program, water flow rates up to 100 ft/s have been obtained using this technique. In addition, cryogenic transducers have been developed, demonstrating survivability at liquid-nitrogen temperature, while providing good acoustic coupling. The cryogenic transducer survivability and high-flow measurements demonstrate that a **nonintrusive**, ultrasonic **flowmeter** has the potential of providing cryogenic high-flow measurements for more reliable liquid-propellant rocket engine operation.

Ultrasonic **flowmeters** do not require a sensor to intrude into the flow path. Figure 143 shows a diagram of a transit-time ultrasonic **flowmeter**. **Piezoelectric** transducer pairs are attached to opposite sides of a duct, one upstream and one downstream. Each transducer pair transmits and receives ultrasonic pulses through the duct wall and the liquid. Flow velocity is measured by subtracting the upstream (T_u) and the downstream (T_d) transit times of the ultrasonic pulses which travel a distance, L, through duct diameter, D, according to the equation: $V = 2L^2 (T_u - T_d)/D(T_u + T_d)^2$. This flowrate measurement technique has the advantage of depending only upon the duct diameter and the separation of the transducer pairs, while being completely independent of the density, viscosity, pressure, temperature, and speed of sound of the liquid.

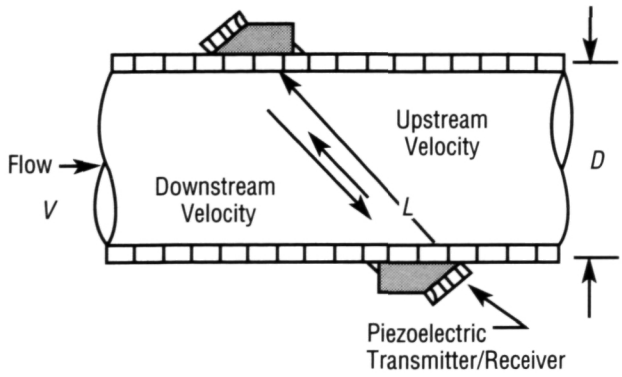

$$(T_U - T_D)/T^2 = 2VD/L^2$$

Where:
D = Duct Diameter
L = Path Length
V = Flow Velocity
T = Average Transit Time
T_U = Upstream Transit Time
T_D = Downstream Transit Time

Figure 143. Transit-Time Ultrasonic Flowmeter

Commercially available **nonintrusive**, ultrasonic **flowmeters** have typically been used to measure flow rates up to 30 ft/s, ten-fold lower than is required for high-power rocket-engine turbopumps. Furthermore, at cryogenic temperature, acoustic coupling is poor due to freezing and cracking of the conventional ultrasonic couplets. At present, no **nonintrusive**, ultrasonic **flowmeter** capable of measuring high flow rates of cryogenic liquids is available commercially.

The flow in the duct of the SSME high-pressure liquid-oxygen turbopump discharge has been used as the baseline for this program. Early development of an ultrasonic **flowmeter** for this application had two major limitations: (1) cavitation and flow detachment due to an inadvertent abrupt diameter enlargement from the pump exit port (10 cm (4 in)) to the inlet of the duct (10.8 cm (4.24 in)), blocking the reception of ultrasonic signals during high-speed flow, and (2) failure of the **piezoelectric** transducers due to the soft solder detachment during high-vibration engine firings.

This program was to demonstrate that cavitation and flow detachment, caused by an abrupt duct diameter change, prevented high-speed flow measurements. To this end, 4-in (10-cm) matched, 4-in (10-cm) to 4.25-in (10.8-cm) mismatched, and 2-in (5-cm) matched ducting configurations were installed into the water test facility at NASA/MSFC, which provided water flows of up to 3,000 gal/min at 70 psi. A plexiglass viewing port was fabricated and inserted downstream of the matched and mismatched ducts to visually monitor for cavitation. A commercial transit-time ultrasonic **flowmeter** employing 1-MHz clamp-on Rayleigh transducers was used to measure the water flow rates and referenced to a facility 8-in (20-cm) turbine **flowmeter**.

With the 4-in (10-cm) matched configuration, a maximum flow rate of 3000 gal/min (limited by overheating of the facility pump), corresponding to 75 ft/s, was obtained. Similar results were obtained for the 2-in (5-cm) matched configuration to a maximum flow rate of 100 ft/s (1,000 gal/min). This flow rate was limited by pump cavitation caused by the low facility pressure of 70 psi. This was characterized by decreasing upstream pressure, causing cavitation at lower flow rates. The data obtained for the 4- to 4.25-in (10- to 10.8-cm) mismatched configuration was unreliable, grossly inaccurate, and showed the reduction and disappearance of the ultrasonic signal at 2,500 gal/min due to cavitation. Furthermore, the duct mismatch prevented ultrasonic measurements below 50 gal/min, due to flow detachment.

The second phase of this program focuses on the development of transducers which will operate and survive in cryogenic environments. Seventeen combinations of **piezoelectric** crystals and bonding materials, including solders and epoxies, were tested after attachment to Inconel 718 wedges. Low-melting-point solders fail due to poor bonding

with the Inconel 718 wedges. High-melting-point solders and brazes could not be used since the **piezoelectric** crystals would be permanently damaged as their Curie temperature was reached. When cured, most of the epoxy bonds were several mils thick and frothy, the air bubbles extinguishing the ultrasonic signals. One particular epoxy provided excellent acoustic coupling with a very thin (less than 1 mil) bonding layer, and further tests were performed with these transducers.

The transducer wedges were attached with the epoxy to an Inconel 718 duct which was capped at one end. The duct was filled first with water, then with LN_2. Comparison of the water and LN_2 signal amplitudes agreed to within 10 percent of the theoretical value, demonstrating that the epoxy bond did not crack or fail at cryogenic temperatures. Furthermore, the transducer bonds survived twelve thermal cycles from LN_2 to ambient temperature, and 25-g vibrations for 30 minutes with no apparent loss in bond integrity.

The combination of high-speed water flow measurements and the development of cryogenically survivable transducers demonstrate the potential of providing real-time, **nonintrusive**, high-speed flow measurements of rocket engine cryogenic liquid propellants.

W.T. Powers/EB22
(205) 544–3452
Sponsor: Office of Aeronautics, Exploration, and Technology

Nonintrusive Hot Gas Temperature Sensor

A program was performed to evaluate the potential of an infrared detector system for determining the temperature of the **hot gas** (hydrogen-rich water vapor) in the high pressure turbopump discharge ducts of the space shuttle main engine. Figure 144 depicts the basic sensor layout, and figure 145 is an enlargement. The sensor concept under evaluation utilizes the 2.6-μm water-band emission as the measuring standard in this application. This effort established potential sensor locations in the **hot gas** manifold, analyzed the environmental constraints on the sensor design, and designed, fabricated, and laboratory-tested breadboard, **nonintrusive, hot gas** temperature sensor hardware. Figure 146 shows the **nonintrusive hot gas** temperature sensor cylindrical design. The data analysis from these evaluations demonstrated the feasibility of this optical approach and showed a high degree of accuracy in temperature determinations of a laboratory flame. A preliminary design analysis effort was performed to recommend material candidates for housing and window substrates, and both thermodynamic and aerothermodynamic analyses of the proposed sensor were performed.

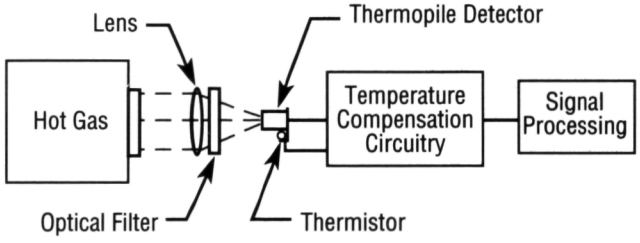

Figure 144. Basic Sensor Layout

Subsystem laboratory evaluations addressed the issue of the effects of varying mixture ratios in the flat-flame burner on the breadboard sensor performance with the result that this 2.6-μm water-band temperature-sensing technique was found to be quite independent of flame mixture ratio. Detailed design focused upon the design specification issues with regard to the detector, its optical window, the sensor housing, and the sensor electronics.

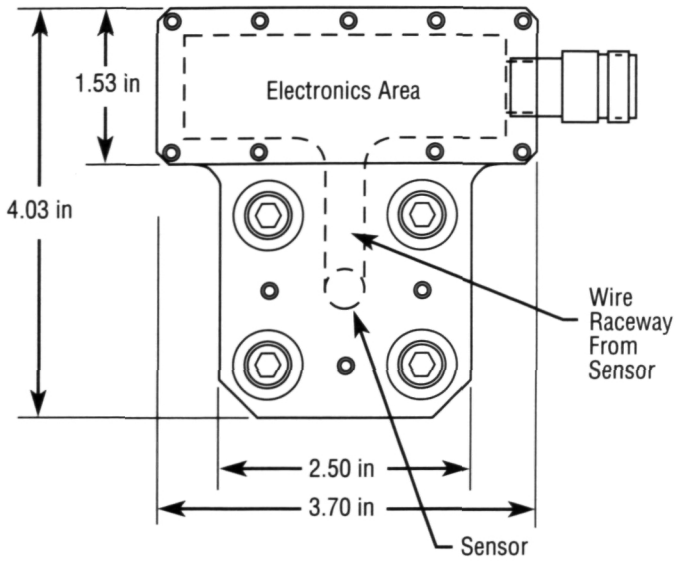

Figure 145. Basic Sensor Enlarged

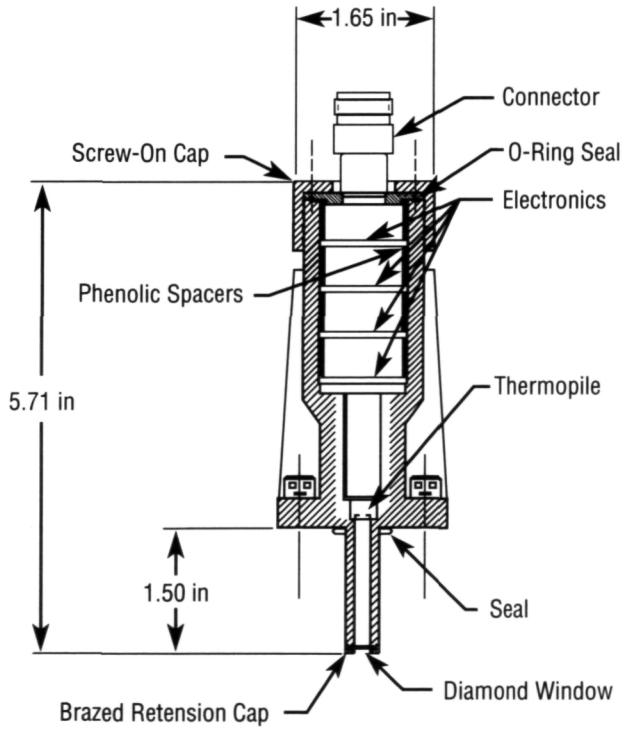

Figure 146. Nonintrusive Hot Gas Temperature Sensor Cylindrical Design (Screw-On Cap)

Functional and environmental constraints placed upon this sensor effectively limit the choice to two candidates: thermopile and indium arsenide detectors. The **thermopile detector** is a miniature, multijunctional collection of evaporated bismuth and antimony elements, whose active areas are covered with a black, energy-absorbing layer. This detector is a voltage-generating device, and no voltage or current biasing is needed for operation. It provides an extremely wide spectral response which must be narrowed by an appropriate choice of optical filter and/or window coatings. The thermopile has a typical response frequency of 10 Hz. Indium arsenide detectors are current-generating, photovoltaic infrared diodes sensitive to 1.0–3.6-μm wavelength radiation. This detector has a typical response frequency of dc to 10 MHz, an inherently faster response time than that of the **thermopile detector** or the resistance temperature device (RTD) **hot gas** temperature sensor presently in use in the SSME, and may allow more accurate thermal tracking of transient conditions in the turbopump discharge ducts.

Diamond remains the window material of choice for this application. Its relatively large thermal conductivity coupled with its relatively small thermal expansion coefficient results in a negligible temperature gradient and an acceptably low shear stress across the window. A series of design analyses of proposed diamond windows have been performed, and all indicate that acceptable window thicknesses result from calculations utilizing typical SSME mainstage and transient conditions. The 20,000-psi burst-pressure requirement and 10,000-psi proof-pressure requirements for the current RTD **hot-gas** temperature sensor were included in these calculations.

The electronics required for signal conditioning of the detector output differ according to the detector selected for implementation. In the **thermopile detector** case, the supporting electronic circuit would consist of 3 integrated circuits and approximately 20 discrete components. Provision is made for the thermopile ambient temperature sensor (thermistor) and its feedback into the temperature-compensation circuitry. The indium arsenide detector would be supported by different electronic circuitry, and may include the provision for a thermoelectric cooler for detector-temperature regulation. In either case, the electronics should be capable of operating under conditions of 70 °C (158 °F) ambient temperature and vibration levels of 30 g_{rms}.

The completed system will permit fast temperature measurement (1 kHz or better) and high accuracy so that dynamic reactions may be monitored and closed-loop control may be effectively enhanced.

W.T. Powers/EB22
(205) 544–3452
Sponsor: Office of Aeronautics, Exploration, and Technology

Index of Contacts

Abbas, M.M.	Infrared Spectroscopy of the Stratosphere	85
Bilbro, J.W.	Advanced X-Ray Astrophysics Facility's Technology Mirror Assembly	223
	CO_2 Laser Research and Development	221
	Coherent Doppler Lidar Research and Development	222
Blakeslee, R.J.	Atmospheric Electricity Research	99
	Lightning/Rainfall Relationships	104
Bordelon, W.J., Jr.	Cold Flow Aerodynamic Turbine Testing	135
Braam, F.	Formed Platelet Combustor Liner Construction Feasibility	161
Bryson, C.C.	Robotic Eddy Current Inspection System	210
Burns, H.D.	Optically Stimulated Electron Emission for Bonding Surface Cleanliness Inspection	178
Burns, R.	Artificial Intelligence as Applied to Flight Mechanics	211
	Completion of Forbidden Orbit Transfer Study	149
Butler, J.M.	Geostationary Earth Observatory Programs	21
	Space Station Advanced Programs	20
Carlson-Lapenta, C.	Doppler Radar Wind Profiler	109
Carruth, R.	Feasibility of Atomic Oxygen Interactions Accelerated Testing	171
Carter, D.C.	Protein Crystal Growth	55
Chandler, M.O.	Interplanetary Magnetic Field Influences on the Polar Wind	81
Cikanek, H.A.	Space Transportation Main Engine	14
Clinton, R.G.	Alternate Ablative Material Development for Solid Rocket Motor Nozzle Applications	183
	Development of Low Thermal Conductivity PAN-Based Carbon Fibers for Solid Rocket Motor Nozzle Applications	181
	Prepreg Properties and Process Relationships to Microstructure in Carbon Phenolic Laminates	188
Coffey, V.N.	Superthermal Ion Composition Spectrometer Double-Focusing Electrostatic Analyzer	76
Craven, P.D.	The Statistical Behavior of Hydrogen Ion Temperatures From Dynamics Explorer 1/Retarding Ion Mass Spectrometer	77
Dabbs, J.R.	Controls, Astrophysics, and Structures Experiment in Space	23
	Pinhole Occulter Facility	23
Danford, M.D.	The Temperature Variation of Hydrogen Diffusion Coefficients	192
Deaton, A.W.	Aeroassisted Orbital Transfers	31
Dewberry, B.S.	The Environmental Control and Life Support System Advanced Automation Project	218
Dugal-Whitehead, N.R.	Electrical Power System Fault Study	24
	Intelligent Protection System for Space Power Applications	88
Edwards, D.L.	Electron Irradiation of GaAs Solar Cells	67
Eskridge, R.H.	Injector Diagnostics Development	147
	Plume Temperature Measurements	146
Fernandez, K.	Development of ROBOSIM for Academic/Industrial Use	209
	WELDSMART: A Vision-Based Weld Quality Assurance System	207
Fikes, L.A.	Industry Advisory Committee Established for Carbon Phenolic Constituent Test Methodology and Specifications	187
Fishman, G.J.	Gamma-Ray Burst Studies	57
	Induced Radioactivity Analysis of the Long Duration Exposure Facility	59

Ford, D.B.	Expendable Lightweight Composite Intertank	225
Frazier, D.O.	Model Immiscible Systems	51
Gallagher, D.L.	Plasma Waves and Ion Heating at the Earth's Magnetic Equator	74
Goodman, H.M.	WetNet: An Interdisciplinary Information and Research Data System	37
Goodman, S.J.	Interannual Variations of Thunderstorms and Lightning Activity at Global and Regional Scales	38
Gross, K.W.	Imaging of the Atomization Process	125
	Bipropellant Two-Phase Flow Simulation in a Rocket Thrust Chamber	165
	Propellant Atomization Simulation of Coaxial and Impinging Injection Elements	168
Hafner, A.	Habitable Atmosphere Contaminant Monitoring	90
	Trace Atmospheric Carbon Monoxide Sensor	90
Hagyard, M.J.	Solar Magnetic Fields	70
Harrison, J.K.	Tether Applications in Space	26
Heaman, J.P.	Velocimetry with Refractive Index Matching	133
Higgins, G.	Compiling Knowledge Bases	42
	Computer Accessibility for the Visually Impaired	41
Horan, C.	Space Station Low-Temperature Portable Cooler for Biological Samples	228
Horn, J.R.	Novel Composites for Protection Against Orbital Debris	201
Howard, R.	Active Detection and Tracking Sensor for Passive Targets	217
	Autonomous Rendezvous and Docking	213
Hueter, U.	Integrated Earth-To-Orbit Transportation	5
Ise, R.	Gravity Probe-B	16
James, B.F.	Mars-Global Reference Atmosphere Model	94
James, M.W.	Lightning Simulator and Sensor Calibration	100
	Quick View System for Aircraft Data	102
	Space Applications of Sensor Development	110
Jedlovec, G.J.	Aircraft Data Evaluation Workstation Development	120
	Geophysical Parameter Retrieval from Multispectral Aircraft Measurements for Geostationary Earth Observatory Science Applications	122
	Investigations of Atmospheric Moisture Variability	124
	Satellite Sensor Simulations	123
Johnson, C.L.	Future Lunar Science Missions	30
	Superconductivity Gravity Gradiometer	32
Johnson, G.W.	Advanced Recovery Systems	2
Johnson, M.L.	In-Flight Optical Leak Detection	157
	Optical Leak Detection for Ground-Based Operations	156
	Space Shuttle Main Engine Propellant Path Leak Detection, Real-Time	155
Johnson, Y.B.	Nickel-Cadmium Battery Expert System-2	232
Kiefling, L.	Optimization of Measurement to Determine Crystal Strain State	46
Kissell, R.R.	Advanced Telerobotic Concepts Using Neural Networks	215
	A Perception System for Object Recognition, Acquisition, and Tracking in Cluttered Environments	216
Kroes, R.L.	Solution Crystal Growth	54
Kurgan, C.	Welding in Space	220

Lawless, K.	Fully Automated Variable Polarity Plasma Arc Welding	212
Lawrence, T.	High Heat-Flux Testing Using the Plasma Torch Test Bed	191
Leslie, F.W.	The Geophysical Fluid Flow Cell	91
Linton, R.	In Situ Contamination Effects Study	173
Lollar, L.F.	Space Station Module Power Management and Distribution	230
McBride, J.E.	An Algorithm for Periodic Waveform Recovery from Space Shuttle Main Engine Vibration Measurements	196
	The Topo Plot: A Data Reduction/Graphics Routine for Tracking Spectral Trends in Vibration Data	34
McConnaughey, P.K.	Adaptive Computational Methods for High Reynolds Number Internal Flows	194
	Adaptive High-Order *h-p* Finite Element Method for Complex 3-D Flows	137
Meyer, P.J.	Four-Dimensional Man-Computer Interactive Data Access System Technology	43
Miller, T.L.	Atmospheric Laboratory for Applications and Science	113
	Numerical Modeling of Nonlinear Baroclinic Fluid Systems	115
Nein, M.E.	Gamma-Ray Imaging Telescope	17
Nettles, A.	Impact Damage Tolerance of Composite Laminates	179
Norwood, J.K.	Portable Spectroreflectometer	177
Nunes, A.C.	Weld Process Modeling	170
Peters, P.	Superconducting Magnetic Suspension Systems and Bearings	61
Pollock, C.J.	Development of Microchannel Plate-Based Low-Energy Electron Spectrometer	83
Powers, W.T.	Nonintrusive Flowmeters for Rocket Engines	235
	Nonintrusive Hot Gas Temperature Sensor	237
	Optical Plume Anomaly Detector	234
	Space Shuttle Main Engine Exit Diagnostics	152
	Space Shuttle Main Engine Preburner Temperature Profiler	149
	Vortex-Shedding Flowmeter for Space Shuttle Main Engine	153
Reynolds, J.M.	Atomic Oxygen Ion Beam Neutralizer	174
Richard, V.	Analysis of Static and Dynamic Nonlinear Viscoelastic Response	160
	Solid Rocket Motor Propellant and Polymer Materials Structural Test Program	159
Roberts, F.	Diamond Film Production Using an Oxyacetylene Torch	185
Roberts, W.T.	Neutral Environment with Plasma Interactions Monitoring System	73
Robertson, F.R.	Global Atmospheric Modeling	119
	Organization of Cloud and Precipitation Patterns Within Extratropical Baroclinic Waves	111
	Remote Sensing Perspectives on the Global Hydrologic Cycle	117
Rothermel, J.	Aerosol Optical Properties Laboratory	98
	Aerosol Physiocochemistry and Backscatter Modeling	96
	Global Backscatter Experiment	97
Selig, W.J.	Expert System Reasoning	64
Smith, S.	Revised Gust Model for Space Vehicle Performance Assessments	93
Spencer, R.W.	Global Atmospheric Temperature Monitoring From Satellites	105
	The Advanced Microwave Precipitation Radiometer	107
	The High-Resolution Microwave Spectrometer Sounder	108

Stallworth, R.	Probabilistic Model for Fracture Mechanics Service Life Analysis	205
Stone, J.F.	Microgravity Activities	47
Suess, S.T.	Coronal and Interplanetary Physics	69
Suggs, R.J.	Thermosphere Model Verification Studies With the Long Duration Exposure Facility	92
Suits, M.W.	Assessment of Materials in Solid Rocket Motors by Near Real-Time Computed Technology	229
	Slit Digital Radiography for Analysis of Bondline Defects in Solid Rocket Motors	201
Sullivan, R.M.	An Analytical Formulation for a Design Technology for Multiphase Structures	202
	Generalized Failure Criteria for 2-D Carbon-Carbon	203
Sumrall J.P.	Space Exploration Initiative	8
Taylor, J.L., Jr.	Advanced Launch System Propulsion Advanced Development	11
Telesco, C.M.	Infrared Astronomy and Cometary Research	65
Thomas, F.P.	Pathfinder Mechanical Joints for In-Space Assembly and Construction	226
Thompson, P.E.	Thermal Degradation Tests of Damaged Multilayer Insulation From Hypervelocity Impacts	204
Tillery, S.W.	Mechanical Property Testing of Tag Ends	189
Tinker, M.L.	Deployable Aerobrake Structural Development	199
Torr, M.R.	Imaging of Magnetospheric Energy in the Vacuum Ultraviolet	79
Turner, J.R.	Tumbling Satellite Retrieval	27
Vaughan, O.H.	MSFC Shuttle Lightning Research	103
Vaughn, J.A.	Advanced Low Earth Orbit Atomic Oxygen Simulation System	175
Vlasse, M.	Advanced Technology Materials	52
Watts, J.W.	Long Duration Exposure Facility Dose Predictions and Measurement	28
Weisskopf, M.C.	X-Ray Astronomy Research	62
Whitaker, A.	Long Duration Exposure Facility Experiments and Orbital Materials Interaction Studies	172
Wilhold, G.A.	Computational Fluid Dynamics Flow Analysis of the Bearing, Seals, and Material Tester	130
	Computational Fluid Dynamics Methodology for Fast Transients	132
	Combustion Chamber Analysis Code	134
	Development of Unsteady Aero/Heat Transfer Experimental Data Base for Axial Turbines	139
	Three-Dimensional Turbopump Flowfield Analysis	142
	Turbine Stage Computational Fluid Dynamics Analysis and Data Base for Unsteady Aero/Heat Transfer	144
	Verification of Internal Flow Analysis in 3-D Geometries	138
Wilmer, G.E.	Turbine Blade-Tip Seal Force Interaction — "Alford" Forces	163
Watkins, J.T.	Advanced Launch System	10

NASA

National Aeronautics and
Space Administration

George C. Marshall Space Flight Center
Marshall Space Flight Center, Alabama 35812

MSFC Cover 42 (Rev. Dec. 1990)